THE HONG KONG POLYTECHNIC UNIVERSITY

Department of Electrical Engineering

ANALYSIS, MODELLING AND ROBUST CONTROL OF AUTOMOTIVE HID HEADLIGHT SYSTEMS

Ping DONG

A thesis submitted in partial fulfilment of the requirements for the Degree of Doctor of Philosophy

Aug. 2008

CERTIFICATE OF ORIGINALITY

I hereby declare that this thesis is my own work and that, to the best of my knowledge and belief, it reproduces no material previously published or written nor material which has been accepted for the award of any other degree or diploma, except where due acknowledgement has been made in the text.

_______________(Signed)

__Ping Dong____(Name of student)

DEDICATION

To my husband, Bangxin SUN

my parents, Jixin DONG and Zhe NING

for their endless love

ABSTRACT

Automotive high intensity discharge (HID) lamps have received attention recently because of its significant improvement in vision and high luminous efficacy. The automotive headlight system usually consists of Xenon lamp and HID ballast. The modelling of Xenon type lamp requires programming of complex physical characteristic. The characteristic is nonlinear and highly dependent on temperature. Ageing study of the lamp allows the improvement in ballast design and illumination compensation. An ageing model is therefore necessary, but it requires the detailed study under the long term time-monitoring of the lamp. Another issue is the dimming control as it provides a flexible control of the lighting output. This thesis is focused on these two aspects: development of the electronic ballast circuit, and the new control methods to optimize the performance of the system.

The study first begins with the comparison of a commerical available controller UCC2305 for the electronic ballast and a microprocessor controlled electronic ballast. The design method, theoretical analysis and experimental results are presented. A unified controller is then developed based on a flexible control platform dSPACE and it is realized by adaptive control method and PI control method. The adaptive control parameter is then examined and compared with the conventional PI control method. Simulation and experimental results show that the system is stable and the nonlinear adaptive control is more robust to system parameter variation.

A 2-D spline interpolation model has been developed to present the characteristics of lamp. The model can then accurately represent the transient and steady states under various

temperature control schemes. It provides a platform using the spline method to develop other HID lamp models with limited data.

In order to further examine various control methods, especially under constant power control for the lamp, Passivity-based Control (PBC) controller of HID electronic ballast is examined. This controller uses the nonlinear equations of the system to avoid the nonlinearity of plant, and to guarantee the global stability and the asymptotic convergence of all state errors. Using a power function, this indirect PBC controller is realized by reshaping the energy of the system and injecting the required damping. The load estimator is derived to insure that the controller is effective in large load disturbance. The simulation and experimental results are then used to verify the model and the nonlinear controller.

The dimming control for the HID lamp ballast is further investigated to include the relationship between the lamp power and various control parameters. A power-dependent lamp model is first established. Two dimming control methods, namely variable duty-ratio control and variable bus voltage control, are then compared and developed. The summation method and multiplier method versions of variable bus voltage dimming control are compared for theoretical calculation and simulaion. It is found that the summation method has a higher performance in constant power control under lamp voltage variation. The variable duty-ratio control is then examined. Three different duty-ratio dimming control methods, power tracking method, constant voltage power tracking method and constant current power tracking method, are compared. The simulation results show the power tracking method is better and more applicable to a practical lamp. The experimental results are used to verify the power tracking method and summation method.

Lastly, the lamp ageing measurement including voltage, current and lumen were made. Two groups of lamp each consisting of 5 lamps have been used. The results provide useful data for the understanding of the ageing. The lamp resistance and life time study are provided. A compensation has been proposed for the aged lamp in order to provide a consistent lumen output. The result forms a useful application for practical lamp implementation.

PUBLICATIONS ARISING FROM THE THESIS

Journal Papers:

[1] P. Dong, K.W.E. Cheng and S. L. Ho, "Interpolation Simulation Model of Steady-State and Dynamic Characteristics for Car Automotive System", *IET Proceedings-Electrical Power Applications* –accepted for publication, Jun. 2007.

[2] P. Dong, K. W. E. Cheng, D. H. Wang and B. P. Divakar, "Investigation on the Modelling and Ageing Characteristics of the HID Car Headlight automotive System", *Journal of Key Engineering Materials* (KEM), Trans Tech Publications, Switzerland, Vol. 364, pp. 1280-1284.

[3] P. Dong, K. W. E. Cheng and S. L. Ho, "Development and DSP Implementation of electronic Ballast for HID lamps Based on Unified Controller, *IEEE Trans. on Power Electronics*, (Submitted: TPEL-Reg-2008-09-0474)

[4] P. Dong, K. W. E. Cheng and S. L. Ho, "Power Tracking and Voltage Multiplier Dimming Control for Automotive HID Headlight Electronic Ballast", *IET Proceedings - Power Electronics*, (Submitted: PEL-2008-0182)

[5] P. Dong, K. W. E. Cheng and S. L. Ho, "Constant Power Controller based on Indirect Robust Passivity used in Electronic Ballast of Automotive HID Headlight system", *IEEE Trans. on Power Electronics*(Submitted: TPEL-Reg-2008-09-0446)

Conference Papers:

[1] P. Dong, K. W. E. Cheng, S. L. Ho and D. H. Wang, "Comparison and Design Analysis of Pulse Transformer for HID Ballast", In 12th Biennial IEEE Conference on Electromagnetic Field Computation (CEFC), Vol. 1, pp. 156–156, April-May, 2006, Miami, U. S. A.

[2] P. Dong, K. W. E. Cheng, S. L. Ho and D. H. Wang, "Study of Distributing Parameters in High Voltage Transformer for HID Ballast", In IEEE International Magnetics Conference- InterMag2006, 8-12 May 2006, pp.128 – 128, San Diego, California, U.S.A.

[3] P. Dong, K. W. E. Cheng, "Simplified Model and Simulation Validation in Xenon Automotive Lamps", In 7th IEE International Conference on Advanced Power System Control, Operation and Management, Oct. 31 –Nov. 2, 2006, Hong Kong, P. R. China, published in CD.

[4] P. Dong, K. W. E. Cheng, Ho, S. L.; Wang, D. H.; Divakar, B. P.; Ding, K. "General Discussion of Dimming Control Methods used in Discharge Lamps", In 2nd Conference on Power Electronics System Application - PESA2006, 12-14 Nov., pp. 178–181, Hong Kong.

[5] P. Dong, K. W.E. Cheng and S. L. Ho, "Research on the Modelling and Ageing Characteristics of the HID automotive Headlight system", In Asia Pacific Conference on Optics Manufacture - APCOM 2007, January 11-13, Hong Kong, published in CD.

[6] P. Dong, K.W.E. Cheng and S. L. Ho, "Research on Dimming Control Method of Electronic Ballast for the Automotive HID Headlight", In 13th International Power Electronics and Motion Control Conference - EPE-PESM 2008, September 1-3, Poznan, Poland, published in CD.

ACKNOWLEDGEMENT

I am greatly indebted to my chief supervisor, Professor, K. W. Eric Cheng, of the Department of Electrical Engineering, the Hong Kong Polytechnic University, for his guidance and advice, his support and confidence throughout the course of this research project.

I would like to express my gratitude to Professor, S. L. Ho, my co-supervisor, for his valuable suggestions, and to Dr. Norbert Cheung, for his continuous advice.

My extended thanks go to technical staff, Mr. K.Y.Tse, and project fellow Mr. Jones Chan, in the Department who facilitated my experimentation and other related works. Distinguished thank to my colleagues, Dr. B. P. Divakar, Dr. Y. Lu, Dr. X. D. Xue, Dr. S. W. Zhao and Mr. D. H. Wang, in the Power Electronics and Utilisation Group who gave me help from different aspects.

I gratefully acknowledge the financial support from the Innovation and Technology Commission under the Project Guangdong - Hong Kong technology Cooperation funding scheme (Project No: ITF/073/04) and the Research Committee of the Hong Kong Polytechnic University.

TABLE OF CONTENTS

LISTS OF FIGURES, TABLES AND ABBREVIATIONS

List of Figures

List of Tables

List of Abbreviations

AC	Alternate Current
APFC	Active Power Factor Correction
CCC	Constant Current Control
CCM	Continuous Conduction Mode
CCT	Correlated Color Temperature
CPC	Constant Power Control
CVC	Constant Voltage Control
DCM	Discontinuous Conduction Mode
DSP	Digital Signal Processing
DPC	Decrease Power Control
DPR	Direct Power Regulation
EB	Electronic Ballast
EL	Euler-Lagrange
HID	High Intensity Discharge
HPS	High Pressure Sodium
IC	Integrated Circuit
LUT	Look-up Table
MH	Metal halide
PBC	Passivity-based Control
PCH	Port-controlled Hamiltonian
PFC	Power Factor Correction
PLL	Phase-locked Loop
PR	Power Regulation
R&D	Research & Development
RTW	Real Time Workshop
SAE	Society of Automotive Engineers
SG	Spark Gap
SSA	State-Space Averaging
THD	Total Harmonic Distortion
2D	Two-dimensional
VDRDM	Variable Duty Ratio Dimming Method
VBVDM	Variable Bus Voltage Dimming Method

Chapter 1

Introduction

1.1 Background

The carbon arc is the first commercially available high intensity light source powered by electricity. Different discharge lamps are currently being manufactured. In general, they can be classified into two categories: low-pressure and high-pressure/high-intensity discharge (HID) lamps. Compared to the low pressure discharge lamps, HID lamps have short arcs and operate under more stringent conditions. They are generally characterized by high luminous efficacy and/or high point brightness. HID lamps such as mercury HID and high pressure sodium lamps are widely used for industrial, public area and street lighting.

With the development of car technology, the safety of night driving becomes a concern. At present, the car bulbs used in the market are halogen lamps whose output power is 60W. The radiation principle of those lamps is using the hot filament. The efficacy of halogen lamp is around 12-25*lm*/W. Lamp life is between 800 hours and 1000 hours. Low light intensity will reduce the vision distance and increase driving fatigue. With the increasing population of elderly drivers, the illumination level and the quality of the light need to be further improved appropriate for the aged person. The spectrum is needed to be in the sky light or white light region in order to provide good rendering factor. Car manufacturers and the Society of Automotive Engineers (SAE) agree that HID lighting is an improved method of illumination [1]. Today Xenon headlight lamps are commonly used in the market to provide the above shortcomings.

Xenon lamps have a very short arc length and a near continuous spectrum which are used as car headlights or projector lamps. Nowadays, Xenon HID lights have been offered by Acura, Audi, BMW, GMC, Honda, Infiniti, Lexus, Lincoln, Mercedes-Benz and Porsche [2]. The automotive HID headlight lamps are often referred to as Xenon lamps but they are more of a specialized metal halide lamp than anything else. Unlike a halogen bulb, the Xenon bulbs have no filament. The light arc is created between two electrodes.

The Xenon bulbs have two main merits: (1) the light is daylight balanced, blue-white light (colour temperature close to daylight) is to provide optimal illumination for driving, and enable the driver to see more clearly. (2) the bulbs produce more lumens per watt; Less power consumption is to facilitate higher overall efficiency or more efficient car design.

The output power of car headlight is 35W. There are different HID bulbs used in the car lighting. The main part numbers are:

D2S –is the most widely used HID bulb

D2R - like D2S but with heat-resistant black paint on spots to control the light output pattern

D1S - like D2S, but with integral igniter

D1R - like D2R but with integral igniter

Fig. 1.1 shows the difference of D2 type lamps and D1 type lamps [3].

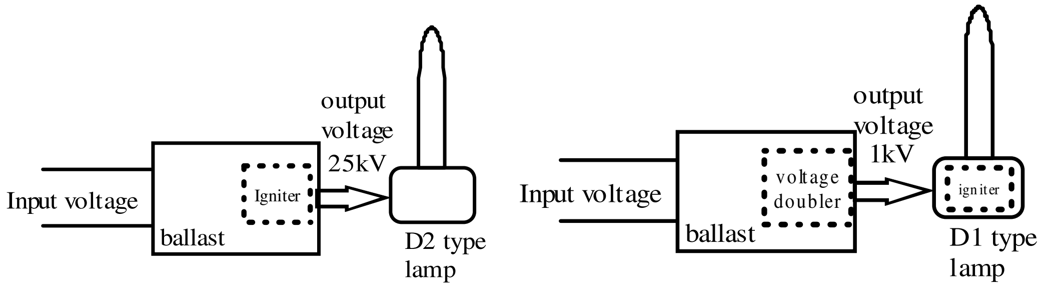

Fig. 1.1 The comparison of D2 type lamp and D1 type lamp

35W D2S and D1S types nominally produce 3200 lumens of light and the D2R and D1R types nominally produce 2800 lumens of light. Table 1.1 gives the characteristics of two different brands of D2S lamps [4, 5].

Table 1.1 Characteristics of different D2S lamps

Type	OSRAM (D2S)	Philips (D2S)
Rated operating power	35W	35W
Rated operating voltage	85V	85V
Rated maximum current	2.5A	2.5A
Rated operating current	400mA	400mA
Maximum start voltage	23kV	23kV
Light efficiency	91 *lm*/W	91 *lm*/W
Average life	3000 hours	3000 hours
Lumen	3200 *lm*	3200 *lm*
Colour temperature	4300K	4100K

In addition, H_1, H_3, H_4, H_7, 9005, 9006 are all the different types of lamp style used in car headlight system. Table 1.2 shows the comparison of different types of the HID lamp used in the automotive headlight.

Table 1.2 Comparison of different types of the HID lamp

Lamp Style	Power (W)	Lumen (*lm*)	Colour Temperature (*K*)	Lamp Life (hr)
HID	35	3200	4000	3000
9006	55	1000	3000	1000
9005	65	1700	3200	320
H_1	55	1500	3200	320
H_7	55	1500	3350	400

1.2 Research Objectives

In this thesis, the main objective is the study on car automotive headlight system which includes Xenon lamp and the HID ballast.

For the Xenon lamp, due to the complex physical characteristics, it is difficult to establish the detailed physical model. The nonlinear time-variant characteristic is hard to formulate and it strongly depends on the ambient temperature. In addition, an ageing model of the lamp is important for the analysis and understanding the circuit and operation of the lamp ballast. So, how to establish a precise lamp model and the ageing model is the focus in this project.

Classically, for the HID ballast, the HID lamps use magnetic ballast and their cost, size and weight are not acceptable. The electronic ballast circuit for the HID lamp is also complicated as it has to handle large amount of current. As the HID lamp ages, the characteristic also changes and the performance of HID lamp also deteriorates.

In order to provide an energy saving scheme, the dimming control is proposed to use in the headlight automotive system. HID lamps are operated at 75W during start up transient to meet the SAE J2009 standard and the power is reduced to 35W at steady state. HID lamps are being fitted in both high beam, low beam, and each operates at the same rated power of 35W. The total illumination level is high when both high and low beams are on simultaneously. Dimming control therefore can be applied for such case to provide energy saving and the light output control.

In conclusion, the research objectives in this project are as follows:

- Establish a new model of HID lamp
- Develop a new HID ballast used in car headlight automotive system
- Research the constant power control strategy
- Develop the dimming control strategy
- Analyze the ageing process of the lamp

1.3 Review of Models of HID Lamps

In view of the methods to establish HID lamp models, models of HID lamps can be classified into two kinds. One is the theoretical physical model; the other is the *V-I* behavior model.

1.3.1 Theoretical Physical model

This model is based on basic physical processes inside the lamps. The energy balance model is firstly developed by considering the energy conservation inside a lamp. Balance equations based on physical phenomenon for the electron density, electron temperature, axial electric field and current density were formulated in reference [6]. A graphical approach with the assumed averaged values of the radial distribution function was used to solve the equations. A general differential equation derived by Francis [7] is used to describe the dynamic characteristics of any discharge tube. The data of electron excitation cross section was obtained in references [8] [9] as it is important to calculate the rate of excitation and ionization of the gas. In references [10, 11], the finite-difference methods were used to solve the physical equations. In addition, Cifuentes [12], Lowke [13], Stromberg [14], Lister [15], Benilov [16] and Fischer [17] applied this method to model the HID lamp. In general, the behavior of any arc column may be determined by solving the conservation equations with appropriate boundary conditions, providing that the thermodynamic state of the plasma and the transport coefficients are known [18].

Considerable advances in understanding the interaction of high-pressure plasmas with thermionic cathodes have been achieved during the last decade [19, 20]. The modeling of complex 3D geometries is possible [21-24]. However, the energy balance equations require information on lamp parameters and complex procedures for evaluation functions of the plasma composition, the temperature profile, and the arc volume. Moreover, the construction of the energy balance equation is highly dependent on the geometry of the lamp and electrode. The parameters in the model are complicated and difficult to be obtained and be used. Wei [25] improved this method by using the typical electrical terminal measurement of the HID lamps and genetic algorithm (GA) method [26] and the difficult obtained parameters were avoided to use.

1.3.2 *V-I* Terminal Behaviour model

The *V-I* terminal behaviour is used in some empirical model of the HID lamp. Janos [27] and Rasch [28] assumed the lamp as a constant resistance in the ballast circuit design and it is a linear pure dynamic resistance model. Laskowski [29] had done some research work about the terminal *V-I* behaviour of the lamp. In order to express the nonlinear property of the lamp, a piecewise linear model is used by staged function to fit the *V-I* curve [30]. A simple *V-I* curve, linearly or nonlinearly, cannot accommodate for the characteristics of the lamp.

In addition, models used in the computer-aided design of lamp ballast have been reported. Circuit simulation software, such as Saber, Matlab and Spice, to modelling lamp has been reported and it is based on physical models and *V-I* terminal behaviour models. In software PSpice, Tseng [31] developed the model based on the Cassie differential equations and a good agreement with experimental data was obtained. Sun [32] used a different function to fit the experimental data and Wu [33] treated the lamp as linear resistance and this was early verified by Gulko [34]. Loo used the Matlab to develop the model of mercury-argon discharge lamp [35] and fluorescent lamp [36] and a good agreement was obtained.

In short, models of HID lamps could be established to facilitate the HID research in this project and is also one of the research objectives.

1.4 Review of HID Ballast

The negative impedance characteristics require a current controlling or limiting device that is integrated in the electronic ballast of the lamp. Conventionally, the magnetic ballast is used in the lighting system. This type of ballast is called starter and has the merits, such as simple structure, high reliability and long life. But the bulky, high power loss and large audible noise are its disadvantages. At present, the magnetic ballast is used in metal halide lamp. But in Xenon headlight system, due to high startup requirement, it is difficult to use magnetic ballast and the electronic ballast is therefore used. The rapid increase for iron in the last few years also triggers the need to use electronic ballast. Fig. 1.2 gives some topologies of magnetic ballast used in USA and Europe.

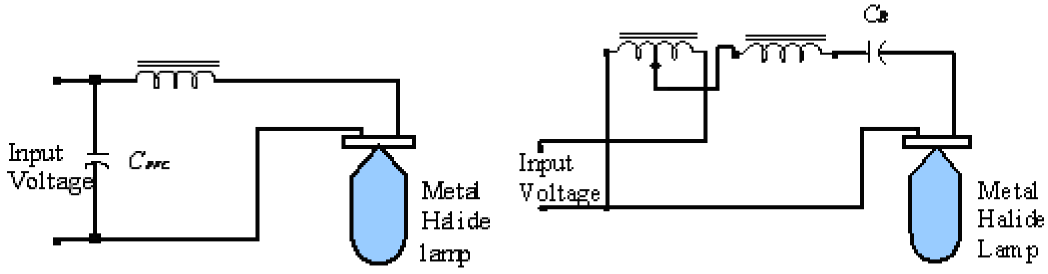

(a) (b)

Fig. 1.2 (a) The standard reactor circuit used in USA and Europe (b) The most popular CWA (Constant Wattage Autotransformer) circuit

1.4.1 Origin and Development of Electronic Ballast

At the end of 1970's, Philips and other companies developed the AC electronic ballast for fluorescent lamp and after the 1990's, the development and research contribute to the electronic ballast used in the field of HID lamps became popular. Due to the development of modern control theory, power electronics and microelectronics, the research and exploitation of electronic ballast can be divided into three stages:

1. The first stage was from the middle of 1980's to the beginning of 1990's. In this period, the Active Power Factor Correction (APFC) just emerged and based on the high frequency switching techniques. During this time, the electronic ballast had two main characteristics: (1) uncontrolled rectifier and large value capacitor were used at the input terminal as a filter, so a low power factor was obtained. (2) Passive filter technique was used in the ballast and power factor was more than 0.9 [37]. THD was less than 30%. That

same period, Alling [45, 46] and Verderber [47] developed the electronic ballasts for fluorescent lamps.

2. The second stage comes from the beginning of 1990's to the middle of 1990's. With the development of APFC, some special IC appeared. The control chip [38], UC2/3305, was developed by Unitrode and was used to control the switches of boost-PFC converter. Two-stage (boost-APFC and DC/AC Inverter) power converter was used in the ballast [39-41]. The power factor was high which can reach up to 0.99 but the efficiency was slightly low (80%-90%) due to two stages connected in series. The current-fed push-pull electronic ballasts became an interesting research topic in the fluorescent lamp and automotive HID lamps [48-52].

3. The third stage comes from the middle of the 1990's. The circuit used a single-stage, multifunction topology [42-44]. By reducing the components of the circuit, the integrated rectifier and the ballast inverter was realised. Overall circuit is reduced in size. Cost-effective modified class E electronic ballast was also reported for cold cathode fluorescent lamp applications [53].

The non-resonant electronic ballasts based on PWM technique were reported [54, 55]. Boost-type [56] and Buck-type [57] in which a voltage-doubler was used to ignite the lamp versions were discussed.

1.4.2 The main topologies used in Electronic Ballast

Many efforts have been made to establish cost-effective electronic ballasts. The main topologies of electronic ballast used in Xenon automotive headlight system are given below. Fig. 1.3 shows two main topologies:

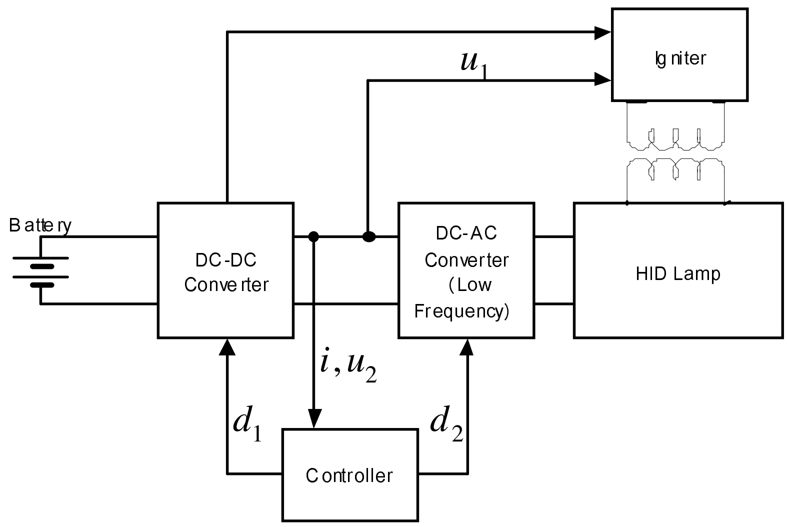

(a)

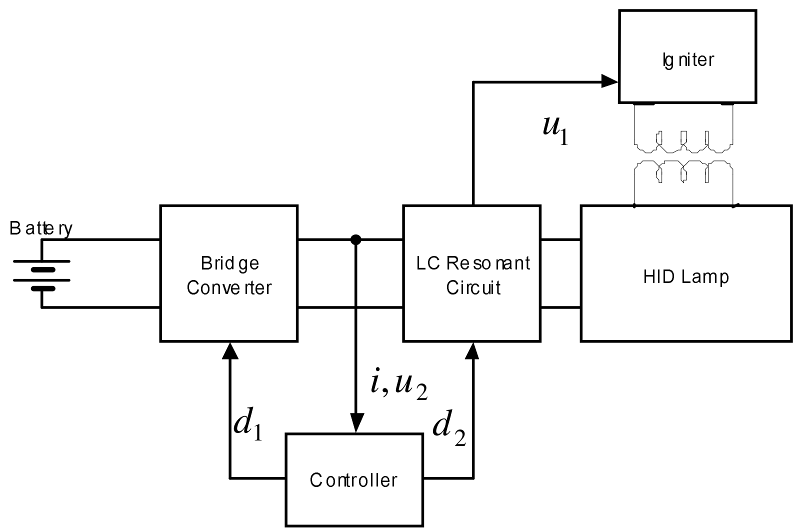

(b)

Fig. 1.3 (a) Structure of traditional HID ballast (b) Asymmetry half-bridge structure of HID ballast (*d* is duty ratio, *u* is the voltage and *i* is the current)

For the first topology (shown in Fig. 1.3 (a)), it consists of the DC-DC converter, DC-AC inverter, Igniter, Controller, battery and HID lamp. In this structure, a low frequency is used in the DC-AC inverter in order to avoid the acoustic resonance. In addition, the controller is easy to be realized. In this project, the first topology is used and will be given in detail in the following chapters.

For the second topology (Fig. 1.3(b)), the resonant voltage is used to ignite the HID lamp. The LC resonant circuit is used. If the bridge converter is the full bridge, there are three different arrangements of igniters. The lamp voltage can be obtained from the capacitor or inductor and Fig. 1.4 shows three different topologies of the lamp connection [58].

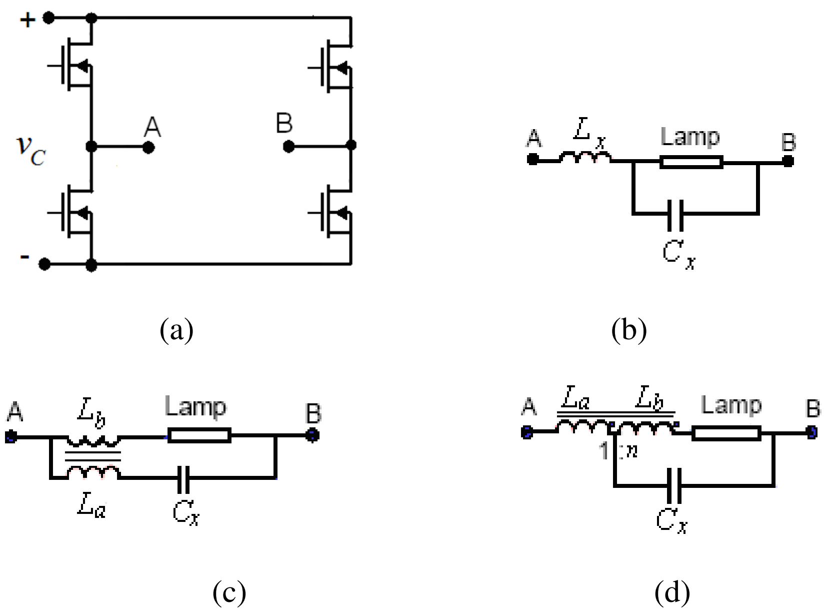

Fig. 1.4 (a) Full-bridge inverter (b) LC resonant tank (c) Transformer configuration (d) Autotransformer configuration

The resonant voltage across C_x provides the required high voltage to the lamp. To obtain voltage higher than the resonant voltage, an additional winding is applied. As shown in Fig. 1.4 (c), the two inductors L_a and L_b are magnetically coupled and operate as a coupled inductor. When the inductor L_a and capacitor C_x operate close to the resonant frequency, the lamp voltage is equal to the voltage across the inductor L_b. To exploit the voltage across the inductor L_a as well, the configuration of autotransformer was proposed, as shown in Fig. 1.4 (d). However this kind of circuit is just suitable for low power ballast.

For the half-bridge inverter, the high lamp voltage is obtained by resonance. If the resonant voltage is not high enough, an igniter circuit is added [59].

1.4.3 The Key Problems to be solved

(1) The hot restrike

A hot lamp needs much higher voltage to ignite, due to the requirement of high amplitude and enough time width time in hot restrike, starting voltage of HID lamp is one of the major problems in ballast design. Normally, the ballast has to use a very large turn ratio transformer (called high voltage step-up transformer), therefore large series inductance is resulted with the lamp when the lamp is ignited. The large inductance would generate a large voltage spike in dc bus capacitor.

In addition, the windings in high voltage transformer are subjected to high electric stress. Inadequate insulation can result in serious problem due to insulation breakdown. Therefore, the insulation in high voltage transformer is important.

(2) The scheduling control

In the operation of the lamp, the timing control of the operation of igniting the lamp and running the full-bridge inverter is a consideration. The controller must generate suitable signals to the DC/DC converter and to the DC/AC inverter and also judge the lamp state, in order to give constant power control to the lamp. So, the timing control is very important.

(3) The efficiency

The electronic ballast used in automotive headlight system is also applied in high temperature and atrocious environment. The power loss of the ballast is often released as heat. Low efficiency means hot ballast. To save energy, high efficiency is needed. The efficiency of the electronic ballast used in the market today is between 60%-85%. How to improve the efficiency is another important point in the future.

1.5 Organization of the thesis

This research project is to investigate the present HID automotive headlight system and to develop an improved solution by means of DSP controller - DS1104. The thesis is structured with individual chapters and each focuses on a specific goal. Each chapter includes its own review of previous work, implications of the proposed work, simulation, experimental implementation and is followed by a summary. In the whole, the two parts are included in this thesis, that is, the development and the optimization (or improvement).

The initial stage of this thesis states the background of the research. Following the description of research objectives, the state of the art is given in the review of the HID ballast.

The purpose of chapter 2 is to compare the traditional HID ballasts and the design method of the electronic ballast used in the automotive system. The design specifications of HID ballast are firstly described. A comparison of two traditional ballasts is presented. The ballast circuit design, the theoretical computation and the experimental results are then presented. Finally, a concise practical design consideration is analyzed.

Chapter 3 establishes a transient lamp model based on the bicubic interpolation method. This model establishes the relationship among terminal behavior (current, voltage) of the lamps and its characteristics of temperature variation. The lamp characteristics were measured and the experimental results were used to confirm the accuracy of the model.

Chapter 4 introduces the design and construction of new electronic ballast based on DS1104. A nonlinear robust controller with a better performance is developed for this ballast. The simulation results and experimental results demonstrate the merits of the robust controller.

Chapter 5 focuses on investigation of an indirect passivity-based controller of the constant power control. Both simulation and experimental results show that the controller is effective and robust to disturbances.

Chapter 6 discusses the dimming characterization of the HID lamp. Experiment for dimming model establishment is conducted to explore the power-dependent lamp model. Two real dimming control methods are compared under the theoretical computation, simulation and experimental conditions.

Chapter 7 focuses on the ageing analysis of HID lamp. Detailed ageing results of different lamps are recorded and investigated. Compensation is proposed for the ageing effect. This chapter shows an application of illumination compensation of aged Xenon lamps to complete the work of HID lamp research. This chapter is not to aim for high level research analysis but as information for readers.

Chapter 8 summarizes the whole thesis. The main results and achievement of the thesis are highlighted. Further work on the possible improvement of the ballast and lamp technology is suggested.

Chapter 2

Development and Comparison of Two Traditional Electronic Ballasts

2.1 Introduction

Automotive high intensity discharge (HID) lamps are 35W high-pressure Xenon gas discharge lamps, designed for a horizontal position operation at a steady state rms voltage ranging from 70V to 100V. These lamps offer higher lighting emissions than 50W halogen lamps and have an expected 5000h operating life. Because the negative resistance characteristics in operating regions and the characteristic of their resistance variation with time, a current limiting device called ballast is necessary to ensure stable operation [60].

The topology used in this project has been shown in Fig. 1.3 (a), which is the conventional structure as redrawn in Fig. 2.1, and the ballast comprises of the DC-DC converter which can boost the battery voltage up to the HID lamp voltage, the DC-AC inverter, the controller and the igniter.

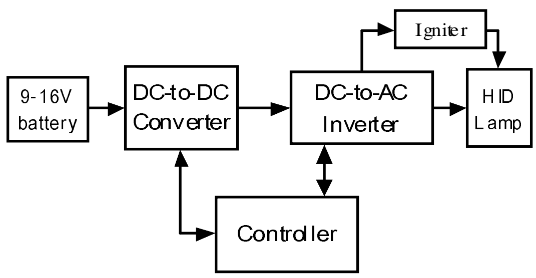

Fig. 2.1 Block diagram of traditional HID ballast

The operation process of the HID ballast to the lamp is that: At first, in order to start the lamp, the DC-DC converter must be able to raise the input voltage of the igniter to an operating voltage of the arc-gap. The starting voltage of general HID lamps is about 6kV when they at under cold-start, and is about 22-30kV when they at under hot-start. When the arc-gap is turned on, the induced high DC voltage of primary side of the lamp transformer causes breakdown of the lamp. And right after this, the DC-DC converter must supply enough current to make the lamp at glow-discharge state to be its arc discharge state. Therefore, separate and outer current path is needed to overcome slow response speed of the DC-DC converter. After the transient state of the start up, the controller of the ballast regulates the HID lamp power under stable operation. Balanced AC is excited to the lamp to ensure that each electrode consumes equally to the current. This function is achieved by the full-bridge inverter that operates under low frequency to avoid acoustic resonance [61] and cataphoretic effects. In addition, the improved performance of the HID lamp comes at the cost of added complexity in the design of its ballast which provides a series control profile from start up to steady state. HID lamps are operated at 75W during start up and 35W during steady state to meet the SAE J2009 standard.

The two traditional HID ballasts analyzed in this chapter have the same structure and the controllers are realized by microprocessor and special chip (UCC2305). The ballast circuits are based on a 100 kHz DC-DC converter, a voltage double igniter and a square-wave inverter with low frequency. The reason for selecting 100 kHz is a compromise between the switching loss and the power density. Higher switching frequency increases the loss in switching components and reactive components. Lower switching frequency increases the overall size.

This chapter is organized as follows: The design specifications of HID ballast are first described. The comparison of these two traditional ballasts is presented. The ballast circuit design, the theoretical computation and the experimental results are then presented. The purpose of this chapter is to compare the traditional HID ballasts and the design method of the electronic ballast used in the automotive system. Finally, a concise practical design consideration is analyzed. This chapter has presented an improved controller design and the distributed parameters in high voltage transformer that is verified by experiment.

2.2 Design Specifications of HID Ballast

The basic requirements or design specifications of an electronic ballast circuit for automotive headlight applications are briefly summarized as:

1) Steady-state Specifications

(a) Input voltage range: 9-16V DC.

(b) Nominal output power: 35W±3W.

(c) Nominal output current: 0.4A

(d) Nominal output voltage: 85V rms

(e) Operation frequency of DC-DC converter: 100 kHz

2) Transient Specifications

(a) Output current: 2A rms for 10s

(b) Output voltage: the transient ignition voltage is 22-30kV, which is obtained from a special voltage step-up circuit and a voltage doubler is used in many designs

(c) Output power: 70±5W for 10s.

Moreover, the ballast circuit must allow for

(a) Protection function: open circuit protection, short circuit protection, over-voltage/current protection, inverse input connection protection.

(b) A fast transient response because of variations of the load resistance. In addition, the HID lamp requires enough take-over current to sustain arc immediately upon ignition.

(c) Insulation problem: The high voltage generated under the hot re-strike condition could cause a short circuit between the windings of the high voltage transformer.

2.3 Development of two Different Electronic Ballasts

2.3.1 Electronic Ballast Based on Special chip- UCC2305

The block diagram of the electronic circuit is shown in Fig. 2.2. The periphery circuit of UCC2305 is omitted in order to show the whole structure. The complete circuit consists of two sub-circuits, namely: Power control circuit and the Commutator circuit.

The power control circuit is a sepic converter. It raises the battery voltage to higher input voltage for the commutator circuit.

The commutator circuit is a full bridge converter that commutates the DC current from the sepic converter into an AC current. Furthermore, it supplies the igniter to generate ignition pulses.

The full-bridge is used because of easy control and low cost. Generally, HID lamps cannot be operated on sinusoidal high-frequency currents between 1-300 kHz because of arc instability by acoustic resonance of high-temperature vaporized gases. Conventional wisdom recommends that the lamps could be operated less than 1000 Hz alternating rectangular current [62]. The control signals of two converters are all provided by the special chip-UCC2305.

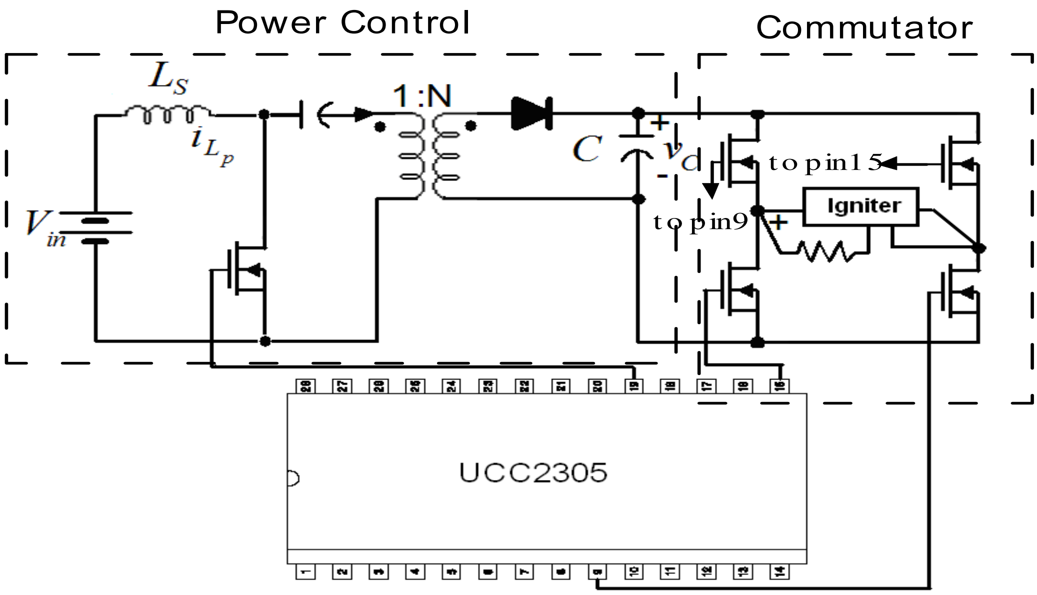

Fig. 2.2 Block diagram of the ballast based on UCC2305

The power control is achieved by a sepic converter at a relative high frequency of 100 kHz and 85V output voltage (lamp voltage). The lamp power is stabilized by UCC2305. This control IC is realized by analog circuit and the PI controller is used in the circuit for the constant power control. The commutation of the full bridge converter is driven by the IC-UCC2305 with a commutation frequency of 200Hz. The igniter is connected between the two mid-points of the full bridge and generates ignition pulses which can get the re-ignition signal from pin 6 of UCC2305. The breakdown device is a spark gap (SG) with a typical breakdown voltage of 600V.

2.3.1.1 Circuit Operation

From the ignition of the HID lamp to its steady state, three different stages happen. They are, before ignition state, transient state and steady state. The performance of the DC-DC converter dominates the performance of the whole ballast system, because the DC-AC inverter is an unregulated low frequency full-bridge converter without magnetic components. The circuit operation of this ballast can be analyzed by the following equivalent circuit shown in Fig.2.3.

If the lamp gas breaks down, the DC-DC converter operates like an open circuit (shown in Fig. 2.3 (a)) until the breakdown voltage of spark gap in the igniter circuit is reached, and this means the output voltage v_C of DC-DC converter is equal to the minimum break through voltage of spark gap. This stage just needs very short duration, a few tens of milliseconds. v_C is the output voltage of DC-DC converter, R is the equivalent resistance of HID lamp.

The igniter only works in this transient state and when the lamp ignites, the igniter will be disconnected from the circuit. The operation of the igniter will be analyzed in detail in the next section. When the HID lamp is ignited, the equivalent circuit of the whole system is the same in all different stages (shown in Fig. 2.3 (b)).

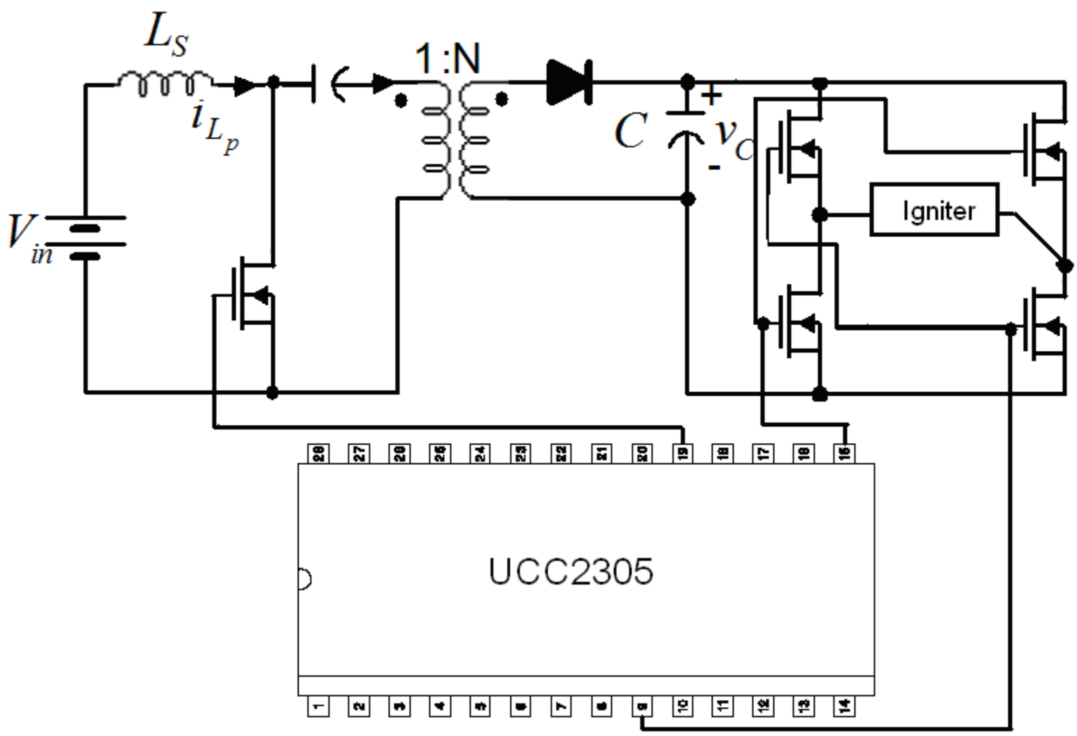

(a)

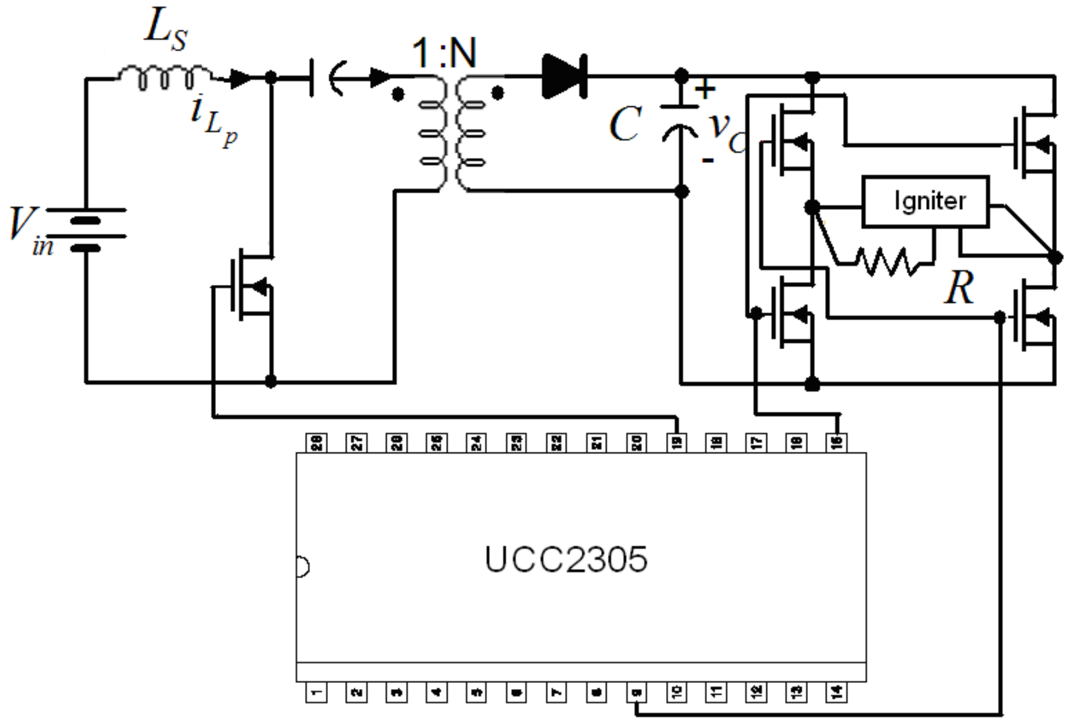

(b)

Fig. 2.3 Equivalent circuit of the whole system (a) before the lamp is ignited (b) after the lamp is ignited

2.3.1.2 Controller Design

The IC-UCC2305 based controller can provide many functions, such as voltage/current control, power control, lamp re-ignition and fault protection. The detailed instruction is given in the datasheet [63], and the main function can be shown in the block diagram Fig. 2.4.

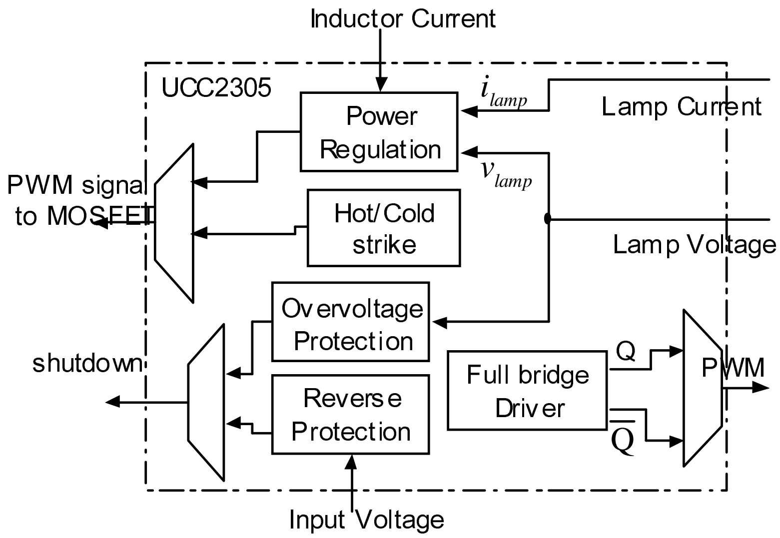

Fig. 2.4 Block diagram for UCC2305

Power Regulation (PR): This is the main control loop used in the IC based controller. There is an adder sub-circuit in the PR that provides the constant power control. The classical PI controller, in order to realize current-mode control, is used here. The current sensing block measures the inductor current and lamp current, in the meantime, the voltage sensing block measures the lamp voltage.

Hot/Cold Strike: The start voltages of cold and hot lamp are different and a lamp start-up voltage is needed. In this IC, the charge and discharge of capacitors connected between the WARMUPC (pin 3) and GND (pin 20) are used. The voltage of capacitors can be used as a signal appropriately for driving.

Over-voltage and Reverse Protection: These protection functions are used to make the electronic ballast safe to operate and they are easy to be realized by a comparator.

Full bridge driver: This IC can give a PWM signal with fixed frequency and duty ratio to drive the full bridge inverter.

2.3.2 Electronic Ballast Based on Microprocessor

The block diagram of the electronic circuit is shown in Fig. 2.5.

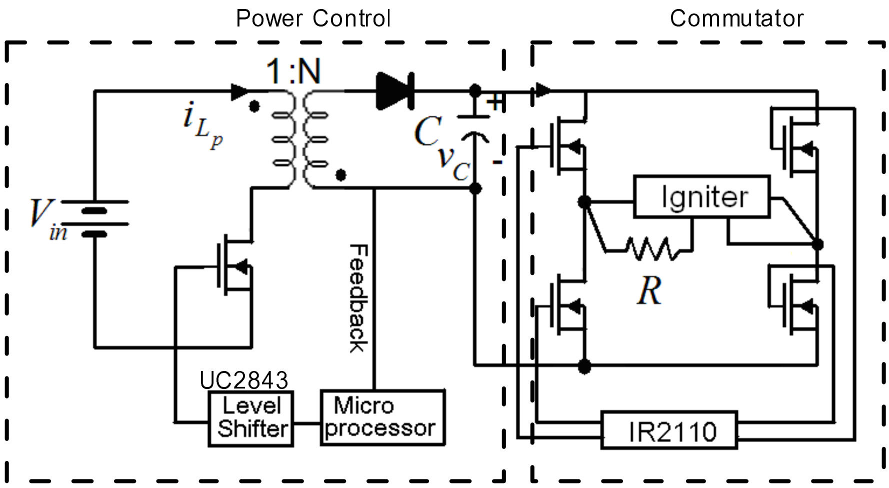

Fig. 2.5 Block diagram of the ballast based on microprocessor

The circuit is similar with the IC based electronic ballast. But the flyback converter is used which also runs at high frequency of 100 kHz and 85 V output voltage (lamp voltage). The microprocessor is used to do the lamp control and a level-shift IC- UC2843 is used to drive the power MOSFET of flyback converter. The control signal of full bridge is produced by IC-IR2110 and the frequency is 400 Hz.

2.3.2.1 Circuit Operation

The whole circuit operation is the same to the IC based electronic ballast said in section 2.3.1. Now the equivalent circuits of the whole system in two stages of operation are given in Fig. 2.6.

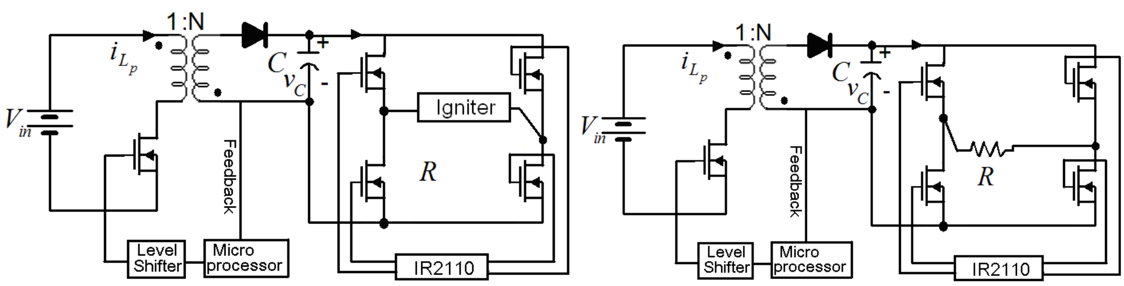

(a) (b)

Fig. 2.6 Equivalent circuits of the whole system (a) before the lamp is ignited (b) after the lamp is ignited

2.3.2.2 Controller Design

The control functions described in section 2.3.1.2 can be realized in the microprocessor. The block diagram for this digital ballast controller is shown in Fig. 2.7.

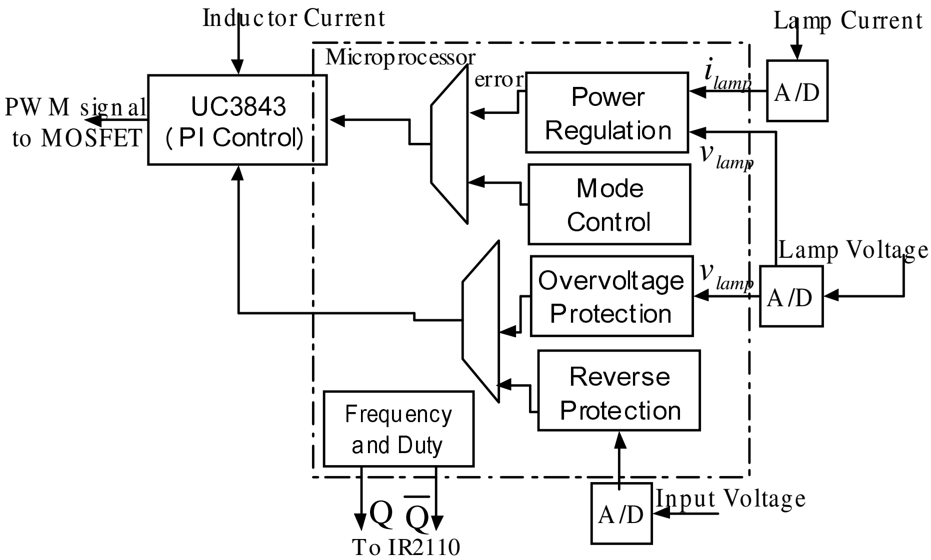

Fig. 2.7 Block diagram for microprocessor controller

The microprocessor has the same function as the IC based controller. But it is implemented in a mixed-signal manner. After the lamp current and lamp voltage are calculated and compared in the program of the microprocessor, the errors or other control signals (protection signals) are transferred to the IC-UC3843. A PI controller is contained in UC3843, so the PWM signal to the power MOSFET of flyback converter is developed. The power regulation is realized by C programming and the current-mode control is implemented. After sensing the lamp voltage and current, an A/D device is used to transfer the data to the microprocessor. In addition, the driver signal with fixed low frequency and duty ratio is derived in the microprocessor and transferred to the IC-IR2110.

2.3.3 Igniter

The inverter circuit can not provide the starting voltage and an igniter is needed. The igniter can give a voltage pulse with high amplitude and enough width time which contains a high voltage transformer. The high voltage transformer converts the low voltage from the DC converter into a high-voltage pulse of 10-30kV magnitude for initiating an arc across the lamp electrodes.

2.3.3.1 Voltage doubler circuit igniter in IC based EB

Resonant tank was used in the igniter to obtain the high starting voltage [64-66], but the high stresses in reactive elements lead to higher cost and volume. Two stages of step-up circuits with two step-up transformers were used in the igniter [61, 67], but the circuit reliability is decreased, and the power loss is increased due to the use of more transformers. In addition, voltage doubler circuit or some similar circuits were used in the igniter [68-69] that can provide a compromise of the low cost and complexity. In this project, the voltage doubler circuit igniter is used (shown in Fig. 2.8).

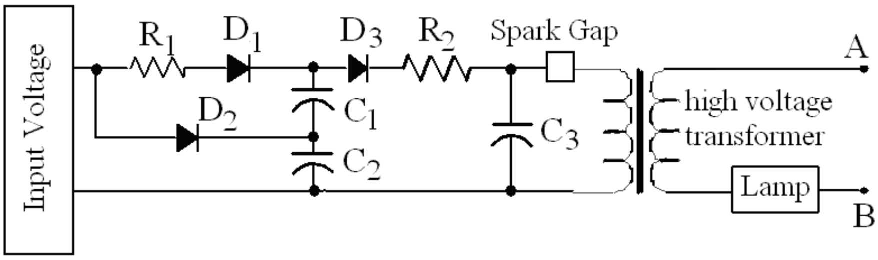

Fig. 2.8 The voltage doubler circuit igniter in IC based EB

This circuit is also called single-stage step-up igniter. Here, points A and B are connected to the full-bridge inverter. R_1 is used to limit the circuit current and the high voltage transformer is connected in series with the lamp. The resistances R_1 and R_2 are used to control the charge speed of the capacitor and hence the ignition speed of the lamp is controlled. The voltage of capacitor C_2 is the sum of capacitor C_1 and C_3. When the voltage exceeds the switching voltage, the spark gap (SG) breaks down and a voltage pulse is applied to the high voltage transformer.

2.3.3.2 Voltage doubler igniter in Microprocessor based EB

The igniter used in microprocessor based EB is shown in Fig. 2.9. Resistances R_1, …, R_6 and both capacitors C_1 and C_2 have the same values. In different half periods of the full bridge, the capacitors C_1 and C_2 are charged alternately. And the voltage in the spark gap is the sum of the voltage of two capacitors. When the voltage in the spark gap is more than the breakdown voltage, the high voltage transformer will be excited and the HID lamp will be ignited. The breakdown voltage of the SG is 600V.

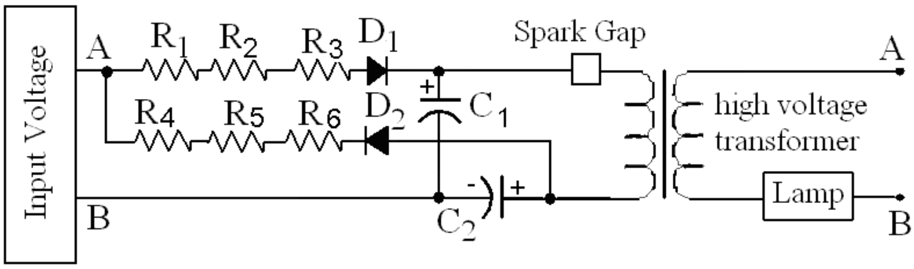

Fig. 2.9 Voltage doubler igniter in microprocessor based EB

2.3.3.3 Spark Gap (SG)

This spark gap is like a switch which is used to get a higher voltage pulse. The operation principle is shown in Fig. 2.10. The electrodes are made up of two metallic conductors like a ball whose radius is *r* and the distance between two balls is *d*. SG is used to control the energy transferred to the high voltage transformer. When the voltage between two electrodes is higher than the maximal value, the insulation between the two electrodes breaks down and the spark discharge occurs.

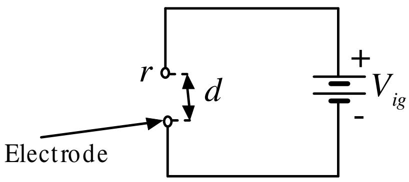

Fig. 2.10 Structure of SG

Assuming that the medium between two electrodes are air, and then the relationship between the discharge voltage of SG and the parameters of electrodes is [70]:

$$E = 0.9 * \frac{V_{ig}\left(r + d/2\right)}{dr} \tag{2.7}$$

where E is the electric field intensity between two electrodes and the common value is 3kV/mm. V_{ig} is the voltage of spark discharge.

2.4 Comparison of these two Electronic Ballasts

The two types of electronic ballasts are developed as proposed in section 2.3. In this section, a detailed comparison is given from a few aspects including the input, output, mechanical subsystem and the circuit components. Two electronic ballasts (EBs), one microprocessor based and one IC chip based, as specified in the requirements as shown in section 2.2 is analyzed below. The HID lamp is Philips 35W MH lamp (D2S) with a cylindrical arc tube and the operating condition is the same.

2.4.1 Performance and Parameters

The input and output performance are shown in Table 2.1. The components in the circuit are shown in Table 2.2. Fig. 2.11 gives the desired waveforms of lamp current and lamp voltage. From these results, it is easy to see that:

1) The chip UCC2305 has all the function suitable for the control of the lamp, but it is expensive and sensitive to noise.

2) The flyback converter used in microprocessor based EB has the minimum part count.

3) A lower frequency around 200Hz is used in full bridge converter in IC based EB, but the frequency range in microprocessor based EB is from 300 Hz to 400 Hz.

4) Most components used in these two EBs are the same.

Table 2.1 Input and Output Performance

<table>
<tr><td colspan="3">Type of Performance</td><td>IC based EB</td><td>Microprocessor based EB</td></tr>
<tr><td rowspan="4">Input</td><td colspan="2">Nominal input voltage</td><td>12V, DC battery</td><td>12V, DC battery</td></tr>
<tr><td colspan="2">Input current</td><td>3.72A (12V), DC</td><td>3.43A (12V), DC</td></tr>
<tr><td colspan="2">Inrush current</td><td>11.25A</td><td>16.87A</td></tr>
<tr><td colspan="2">Input voltage range</td><td>9-16V</td><td>9-16V</td></tr>
<tr><td rowspan="14">Output</td><td colspan="2" rowspan="4">Lamp current and voltage

Wanted wave shown in Fig. 2. 15</td><td>Experimental wave(see Fig. 2.12(a))</td><td>Experimental wave(see Fig. 2.12(b))</td></tr>
<tr><td>Current (RMS): 0.447A</td><td>Current (RMS): 0.413A</td></tr>
<tr><td>Voltage (RMS): 85.09V</td><td>Voltage (RMS): 82.32V</td></tr>
<tr><td>Frequency: 180.3Hz, scope: around 200Hz</td><td>Frequency: 349.7Hz, scope: [300Hz- 400Hz]</td></tr>
<tr><td rowspan="3">Power</td><td>Input Power</td><td>44.64W</td><td>41.16W</td></tr>
<tr><td>Output Power</td><td>38.03W</td><td>34W</td></tr>
<tr><td>Efficiency</td><td>85.2%</td><td>82.6%</td></tr>
<tr><td colspan="2">Flickering</td><td>None</td><td>None</td></tr>
<tr><td colspan="2">Acoustic resonance</td><td>None</td><td>None</td></tr>
<tr><td colspan="2">Short circuit</td><td>Automatic switch off</td><td>Automatic switch off</td></tr>
<tr><td colspan="2">No load condition</td><td>Automatic switch off after 3 times ignition</td><td>Automatic switch off after 4 times ignition</td></tr>
<tr><td colspan="2">Hot re-ignition time</td><td>1μs</td><td>1μs</td></tr>
<tr><td colspan="2">Successful probability of re-ignition (10 times /1s)</td><td>100%</td><td>100%</td></tr>
<tr><td colspan="2">Power control</td><td>±5%</td><td>±2% (±1% if required)</td></tr>
<tr><td>Mechanical</td><td colspan="2">Weight</td><td>188g</td><td>133g</td></tr>
</table>

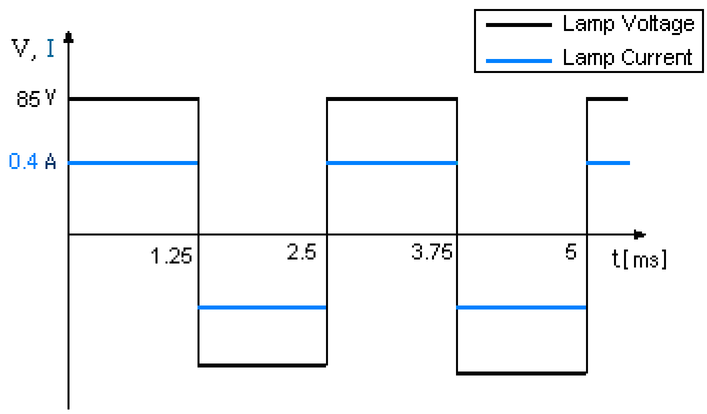

Fig.2.11 Desired waveform of lamp voltage and lamp current

Table 2.2 Components in the circuit

Parts	Components		IC based EB	Microprocessor based EB
DC-DC Converter	Switches		IRF3710	IRF3710
	Transformer	Turns ratio	7:56	7:70
		Core Type	EE core (RM10)	EE core (RM10)
	Capacitors		4.7μ/400V	4.7μ/400V
	Diodes		MUR860	MUR860
Full bridge	Switches		IRF840	IRF840
Igniter	Voltage Doubler	Resistance	300kΩ	300Ω/1W
		Capacitors	0.63μ/630V	0.68μ/400V
		Diodes	IN4007	US1J
	High Voltage Transformer	Turns ratio	2:200	2:200
		Core type	Rod Core	Rod Core
	SG		SG-600V	SG-600V
Controller	IC chips	Number	1	3
		Name	UCC2305	IR2110 ; UC3843
	Microprocessor		None	Atmega8

5) The expensive commercial available chips, IR2110, are replaced with discrete components in our commercial products. For information, the price of one single chip, UCC2305, is about HK$100; but the total price of the EB based on microprocessor is around HK$50.

2.4.2 Waveforms

In order to verify the comparison results, experimental waveforms of the two EBs are given. The lamp voltage and current in steady state, before ignition, and in transient state are given. The input current of the EBs, the output voltage of sepic converter and flyback converter are given as well. From the experimental results, the following conclusions are made:

1) The lamp voltage and current are all square wave as the desired waveform in Fig. 2.11. The experimental results are shown in Fig. 2.12. But the frequencies for the IC based EB

and the microprocessor based EB are not the same but still below the values to avoid the acoustic resonance. The voltage and current of the lamp have the same phase and shape, so the lamp could be seen as a pure resistive load.

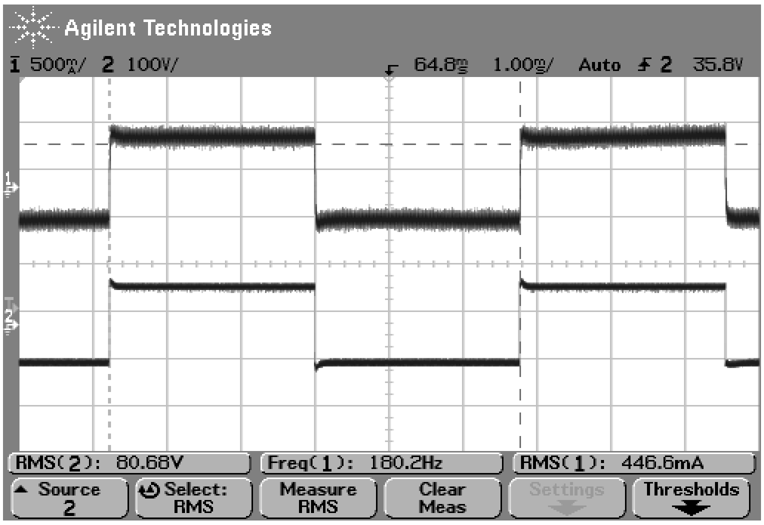

(a) IC based EB

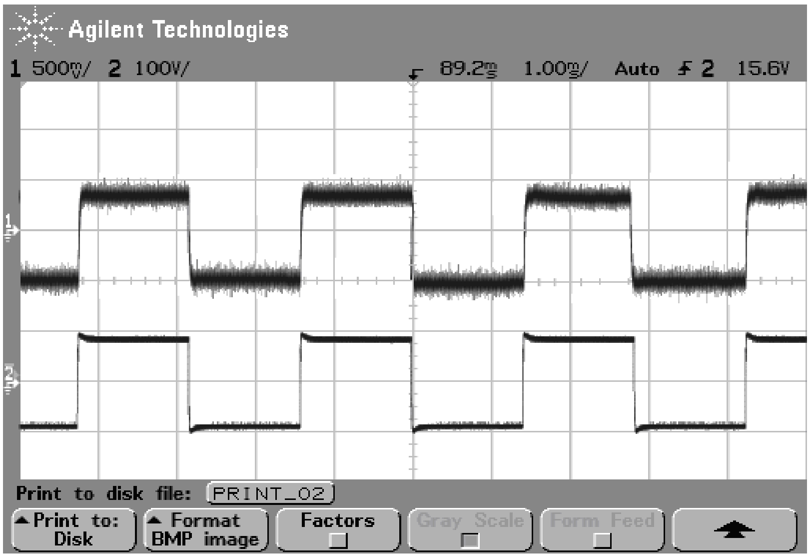

(b) Microprocessor based EB

Fig. 2.12 Lamp voltage and lamp current in steady state (ch1: 500mA/div, 1ms/div, lamp current; ch2: 100V/div, 1ms/div, lamp voltage)

2) The output voltage and the input current of DC-DC converter are all dc values. Fig. 2.13 gives the waveforms of output voltage of DC-DC converter and the lamp current in steady state. Fig. 2.14 gives the waveforms of the input current and lamp voltage in steady state.

The two figures show the input and output performance of the EBs.

3) The waveforms of the two EBs in start state are different (shown in Fig. 2.15). Different frequencies in full bridge and different ignition methods are used in two EBs.

In IC based EB, the frequency is around 200Hz. It is easy to ignite the lamp and it is not easy to extinguish when the input AC voltage changes its polarity. But in microprocessor based EB, the frequency is higher than that of IC based EB. In order to ignite the lamp successfully, the inverter must not change its polarity in a required predetermined time. If the polarity of the AC signal to the lamp is changed earlier than required, the lamp current will go through zero and the lamp will extinguish as there is no emission from another cold electrode. This failure to light up the lamp is rectified by preventing the inverter to change its polarity till the electrodes attain enough temperature to sustain the arc. This is achieved by freezing the gate signals to the switches of the inverter and in doing so, the lamp is driven on DC current for a predetermined time which is a function of the temperature of the lamp.

In Fig. 2.14 and Fig. 2.15, the amplitudes of lamp voltage are different and the reason is that the lamp voltage in steady state is about 85V (as shown in Fig. 2.14), but the lamp voltage changes from 600V to a few volts in the start state.

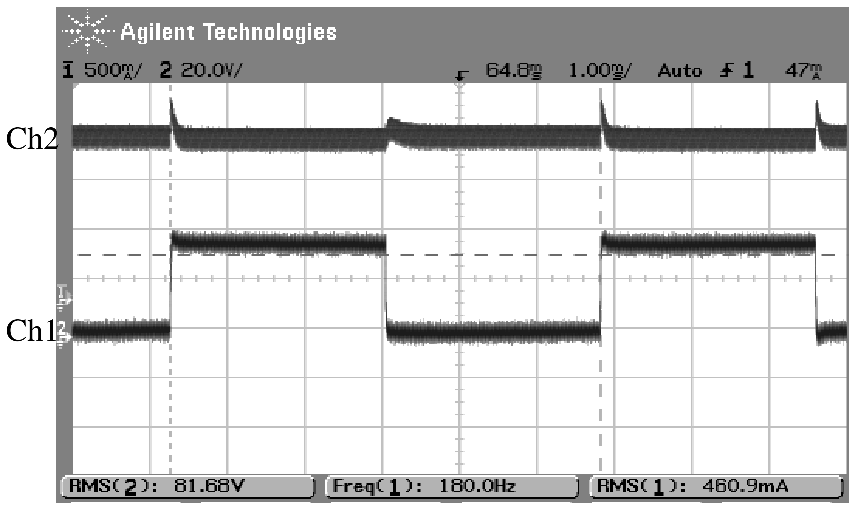

(a) IC based EB

Ch 2

Ch1

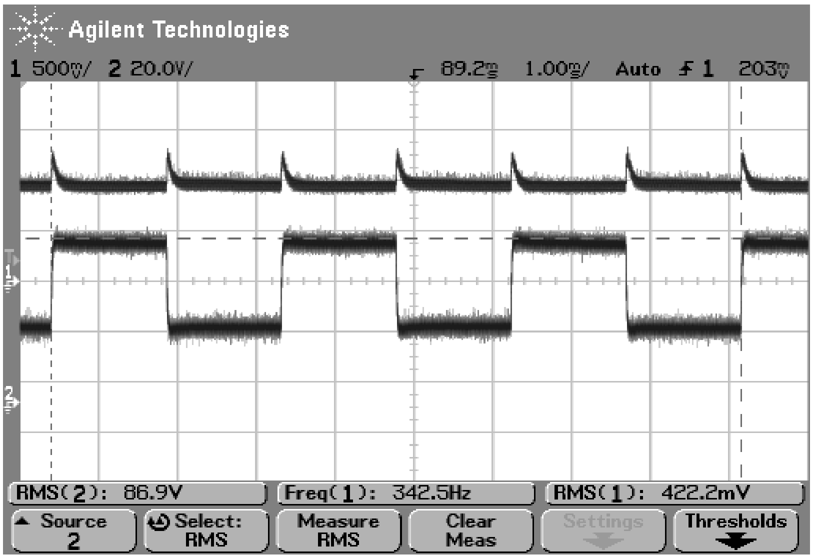

(b) Microprocessor based EB

Fig. 2.13 Output voltage of DC-DC converter and lamp current in steady state (ch1: 500mA/div, 1ms/div, lamp current; ch2: 20V/div, 1ms/div, output voltage of DC-DC converter)

Ch1

Ch 2

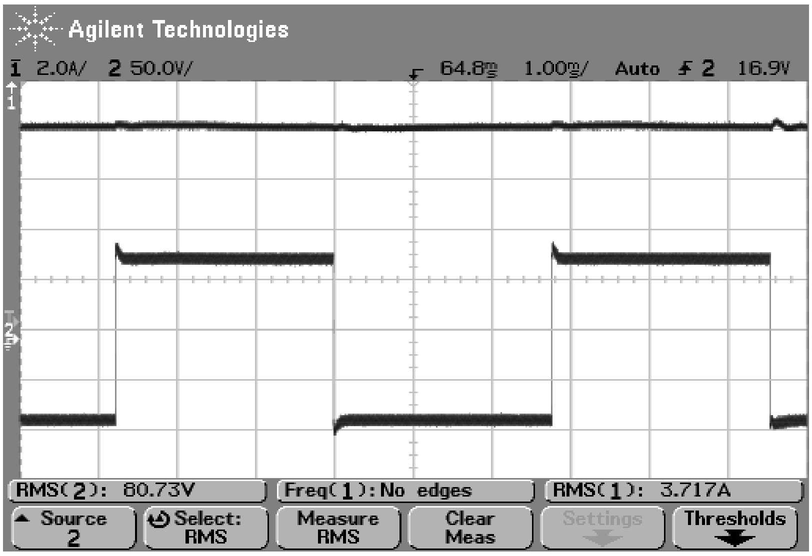

(a) IC based EB

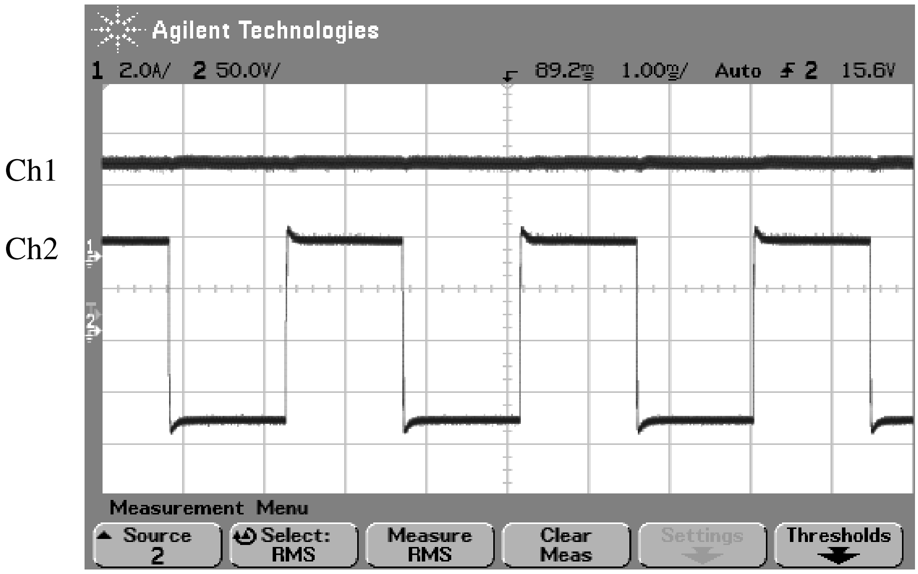

(b) Microprocessor based EB

Fig. 2.14 Input current and lamp voltage in steady state (ch1: 2A/div, 1ms/div, input current; ch2: 50V/div, 1ms/div, lamp voltage)

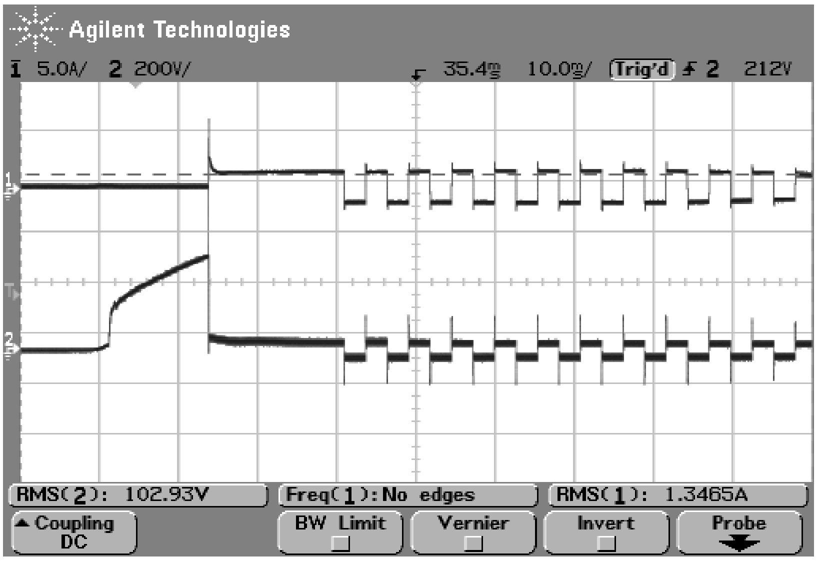

(a) IC based EB

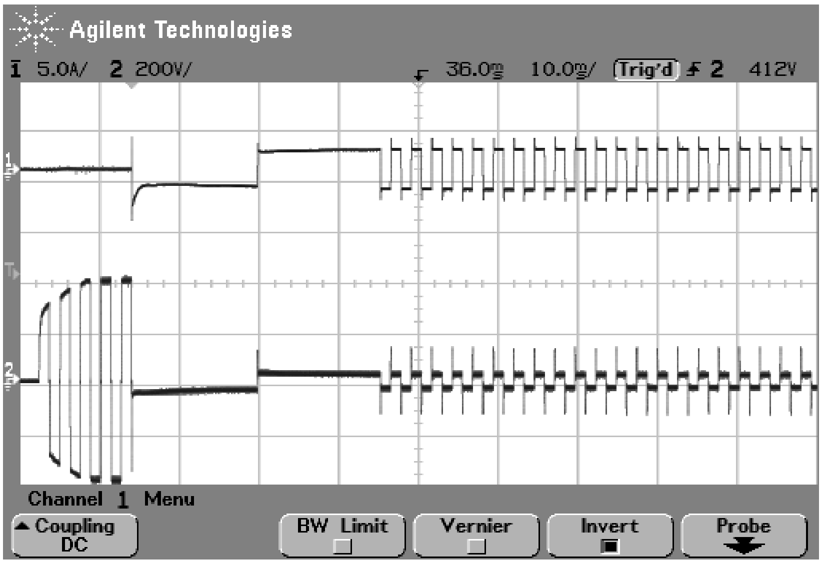

(b) Microprocessor based EB

Fig. 2.15 Lamp voltage and lamp current in start state (before ignition and transient state)

(ch1: 5A/div, 10ms/div, Lamp current; ch2: 200V/div, 10ms/div, lamp voltage)

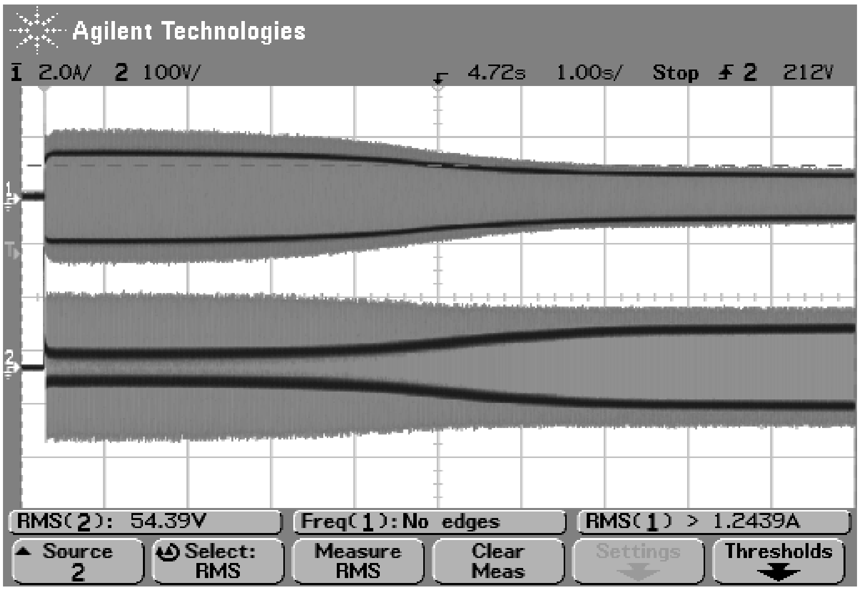

(a) IC based EB

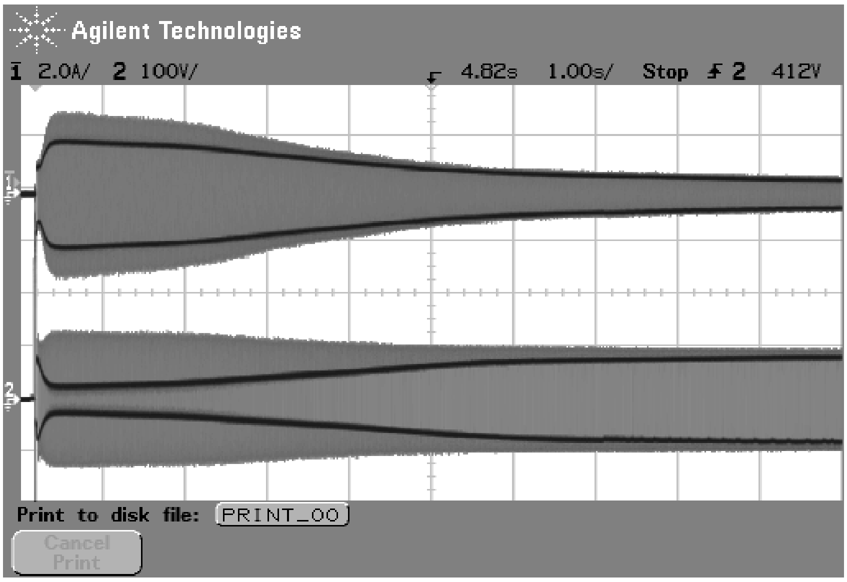

(b) Microprocessor based EB

Fig. 2.16 Lamp voltage and lamp current in whole state (ch1: 2A/div, 1s/div, lamp current; ch2: 100V/div, 1s/div, lamp voltage)

2.5 Practical Design Consideration

2.5.1 Analysis of the Magnetic Field of High Voltage Transformer

The igniter circuit used to this analysis is given as Fig.2.8. The novelty of this high voltage transformer is it has a rod type magnetic core. Length of this core is l and the diameter of cross section is d. According to anticipant output voltage of lamp, the number of turns in primary and secondary windings is fixed. Define the number of turns of primary winding to be N_1, and secondary winding to be N_2, and the method of winding is shown in Fig. 2.17.

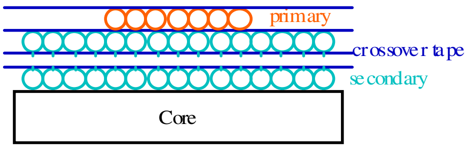

Fig. 2.17 (a) R core (b) Cross section of transformer

Considering distributed parameters, the equivalent circuit of this transformer is shown in

Fig. 2.18. R_p, R_s, L_p, L_s are the resistance and leakage inductance of primary and secondary windings, respectively. C_{pp} is the stray capacitance between layers of primary windings. C_{ss} is the capacitance between layers of secondary windings. C_{ps} is the capacitance between the layers of primary windings and secondary windings. L_m is the equivalent magnetizing inductance and R_{Fe} is the iron loss resistance. All the parameters are referred to the primary windings.

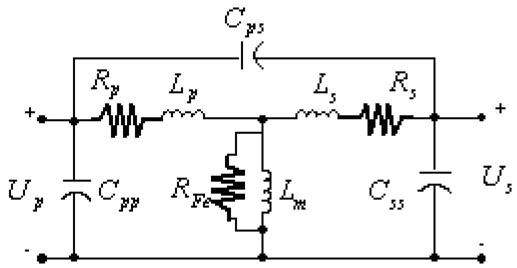

Fig. 2.18 The equivalent circuit of high voltage transformer

During the ignition process of the HID lamp, capacitance C_3 discharges through spark gap. Due to few turns of primary winding and small current value, the resistance of primary winding R_p, iron loss resistance R_{Fe}, leakage inductance L_s, and stray capacitance C_{pp}, C_{ps} can be ignored. The discharge circuit is shown as Fig. 2.19.

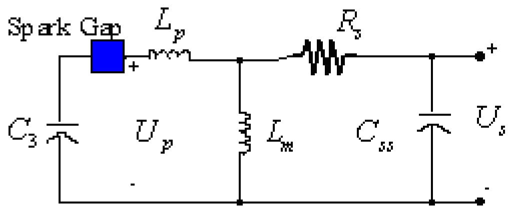

Fig. 2.19 Simplified circuit of high voltage transformer

The discharge process can be divided into two states. The first one is the spark gap turn on state; and the other one is the spark gap turn off state which can be called resonant state. When the spark gap turns on, the currents i_1 and i_2 flowing through the leakage inductance L_p and stray capacitance C_{ss} are:

$$\begin{aligned} i_1 &= \frac{-\omega^2 L_m C_{ss} U_s + U_p}{j\omega(L_p + L_m)} \\ i_2 &= j\omega C_{ss} U_s \end{aligned} \tag{2.8}$$

where ω is equal to $2\pi/T$. T is the delay such that the spark gap turns off after a delay time T. At this time, the circuit is a second order circuit:

$$-L_m C_{ss}\frac{d^2U_s}{dt^2} + R_s C_{ss}\frac{dU_s}{dt} + U_s = 0 \tag{2.9}$$

The method used here to calculate the parameters of inductance and capacitance is an extension method used in reference [122, 123]. R_s is the effective AC resistance of winding, which is given by

$$R_s = \mathrm{Re}\left\{\alpha h\left(\coth(\alpha h) + \frac{2}{3}(N^2 - 1)\tanh\frac{\alpha h}{2}\right)\right\}R_{dc} \tag{2.10}$$

where N is the number of winding layer, $\alpha = \sqrt{j\omega\mu_0 h / \rho W_s}$, h is the height of conductor which is equal to d, ρ is the resistivity, ω is the frequency and W_s is the turn pitch.

The stray capacitance and leakage inductance are the focus in this calculation. Due to high voltage in the secondary winding of the transformer, 5 (this is the minimum number to avoid the high voltage break down between winding layers) insulation tapes (called insulation band) are used in this transformer. The stray capacitance of each unit of the layer is the sum of the capacitance in the air gap C_a and the capacitance C_t in the insulation band (as shown in Fig. 2.20). Then

$$C_a = \int_{-\frac{\pi}{2}}^{\frac{\pi}{2}} \frac{\varepsilon_0 \cos\theta}{2(1-\cos\theta)}d\theta,\ C_t = \frac{(d + 2t_i)\varepsilon_0\varepsilon_k}{h_k} \tag{2.11}$$

where ε_0 and ε_k are the permittivity of the air and the insulation band respectively; t_i is the thickness of the insulation band. Then the stray capacitance C_{ss} is the series capacitance of C_a and C_t, that is,

$$C_{ss} = M_1 M_2 \frac{1}{\frac{1}{C_a} + \frac{1}{C_t}} \tag{2.12}$$

where M_1 is the number of turns of each layer of secondary windings, M_2 is the number of layers.

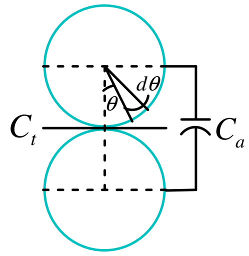

Fig. 2.20 Cross section of transformer windings

The magnetic flux is contributed by the conduction current and displacement current together, and the leakage inductance is calculated by Stokes' theorem

$$L = \frac{\psi}{I} = \oint_{C_i} A_j dl_i / I = \frac{\mu_0}{4\pi} \oint_{C_i} \oint_{C_j} \frac{dl_j dl_i}{R} \tag{2.13}$$

It is realized by using the finite element method. Define XY surface is the circle of diameter and Z direction is l direction (which is the direction of length). Fig. 2.21 shows the equi-flux distribution of B at Z direction. In order to obtain the leakage inductance, Fig. 2.22 gives the distribution of input and output magnetic flux density with position which is located in YZ surface. It is shown that the difference is the result of leakage inductance.

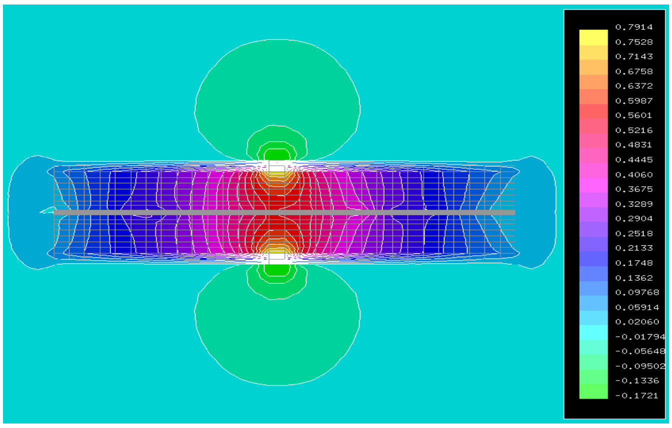

Fig. 2.21 The Equiflux distribution of B at Z direction (unit: T)

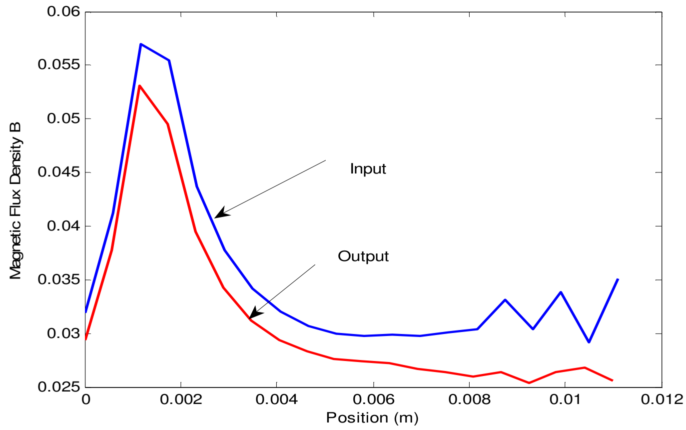

Fig. 2.22 Distribution of input and output magnetic flux density with position

2.5.1.1 Prototype and Experimental Results

An actual high-voltage transformer was designed for application in the 35W HID headlight system. The design specifications are listed in Table 2.3.

Table 2.3 Materials and parameters

Copper wire	AWG# 30
Magnetic core	R type
Number of turns in Primary winding	2
Number of turns in Secondary winding	200

It has the dimensions of 60mm (L)*8mm (D). Fig. 2.23 shows the photo of this transformer.

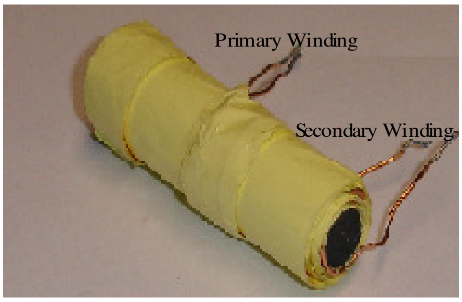

Fig. 2.23 Photo of high voltage transformer

A network analyzer was used to measure the values. The calculated values and measured values of these distributed parameters are given in Table 2.4.

Table 2.4 Distributed parameters

	Measured	Calculated
Stray capacitance C_{ss}	17.69pF	16.42pF
Leakage inductance L_p	518.04nH	517.92nH

The igniter circuit has been tested, and the breakdown voltage of spark gap is 600V. The measurement result of output voltage of high voltage transformer is shown in Fig. 2.24. The result shows that the discharge process can be divided into two states. The distributed parameters of high-voltage transformer cannot be ignored. This igniter was also tested in the ballast and successfully ignited the lamp.

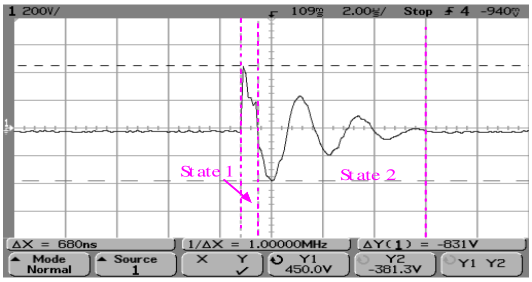

Fig. 2.24 Voltage of high-voltage transformer

2.5.1.2 Summary

The effect of distributed parameters in high-voltage transformer is studied. After calculated these parameters by finite element method, the values are obtained and have been validated by experimental results. Generally speaking, if the number of turns of primary winding and secondary winding are fixed, when the length l is increased, then the leakage inductance increases but the stray capacitance reduces; whereas when l is decreased, the leakage inductance reduces and the stray capacitance increases. When the length l varies, the coupling factor and other magnetic parameters vary, too.

Due to the presence of leakage inductance and stray capacitance, the resonance does have some electromagnetic interference to the circuit. Proper methods must be implemented to reduce the values of distributed parameters in the high-voltage transformer.

In addition, the high voltage pulse with low current is easy to handle. The insulation problem of this high-voltage transformer is another focus in the future.

2.5.2 Comparison of Different Magnetic Cores

2.5.2.1 Operation Principle

The igniter circuit which will generate a voltage pulse to the transformer is shown in Fig.2.8. The energy in one pulse must be high enough to cater for lamps having different individual characteristics, different operating thermal profile and spark gap response time. The charging time constant of capacitor C_3 and discharging time of C_2 are given as follows:

$$\tau_{c3} = (R_1 + R_2)C_3,\ \tau_{dc2} = R_2(C_1 // C_2 // C_3) \tag{2.14}$$

In order to ignite the lamp, two conditions must be met. The first one is that the inverter must be enabled to work before the lamp is ignited. The second one is that enough current must be supplied to make the lamp ignite.

The controller could enable the inverter before the lamp is ignited by timing control. But if the lamp ignites and the inverter could not supply enough current in a short time, other energy should be provided. Experimental results show that capacitor C_4 gives the energy.

2.5.2.2 Design Considerations

In order to design a high-voltage transformer, the following items would be considered:

(1) Effect of distributed parameters including the leakage inductance and stray capacitance of transformer:

The equivalent circuit of high voltage transformer is given in Fig. 2.18. The effect and calculating methods of distributed parameters were given in reference [73]. The existence of stray capacitance and leakage inductance will result in high frequency electro-magnetic interference and power loss. In this section, the distributed parameters with different magnetic cores are compared. The lower the value of the distributed parameters, the better is the performance of the high voltage transformer.

(2) The effect of the core type and the size upon the coupling factor and degree of flux saturation:

Coupling factor usually can be expressed as the ratio of actual mutual inductance to the maximum mutual inductance, that is,

$$k = L_m / L_{m-\max} = L_m / \sqrt{L_1 L_2} \tag{2.15}$$

where L_m is the mutual inductance, L_1 is the self inductance of primary winding when the secondary winding is on open circuit. And L_2 is the self inductance of secondary winding when the primary winding is on open circuit. A high coupling factor could minimize the turns ratio and reduce the volume of transformer.

When working at steady state, the lamp is supplied by the full-bridge inverter. The igniter is disabled but the secondary winding of the high voltage transformer is connected to the lamp. In this design, the turn ratio of high voltage transformer is 1:100, so the value of L_2 is very high. According to the B-H curve of soft magnetic material, careful design must be conducted to avoid saturation for large inductance.

(3) Size and cost of the optimal transformer:

The size and cost are important aspects to be considered in designing a transformer. Low cost and small size are preferred. High voltage generated by secondary winding is easy to breakdown the insulation layer of transformer and insulation bands with high withstand voltage should be used.

2.5.2.3 Comparison of Different High Voltage Transformers

After designing 4 different transformers, the coupling factor, distributed parameters (leakage inductance, stray capacitance), flux saturation, size and cost are compared in this section.

(1) Comparison using Different Magnetic Cores

One type is with EE magnetic core (ETD29), the other is R core (d=0.8cm, l=3cm). These two cores are all ferrite types. R core has good temperature stability. As, this type core could be seen as having large air gap or having open magnetic circuit, a high current could be carried of without being saturated.

The photos of different magnetic cores are shown in Fig. 2.25. Fig. 2.26 shows the distributed parameters of different cores. Fig. 2.27 shows the experimental results (input voltage, output voltage of the transformer and voltage of spark gap in a cold HID lamp).

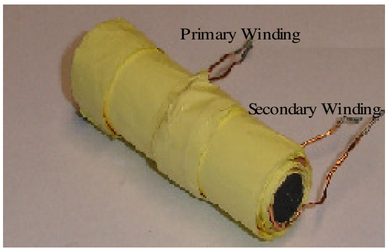

(a)

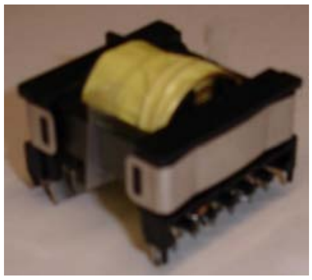

(b)

Fig. 2.25 The prototype of high voltage transformer (a) R core transformer (b) EE core transformer

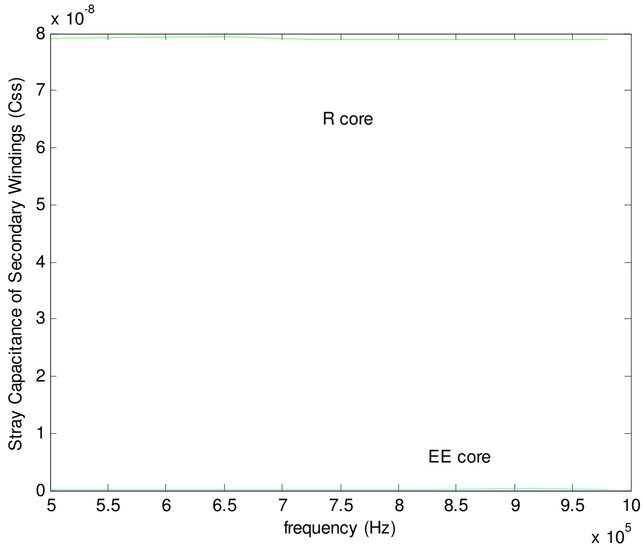

(a)

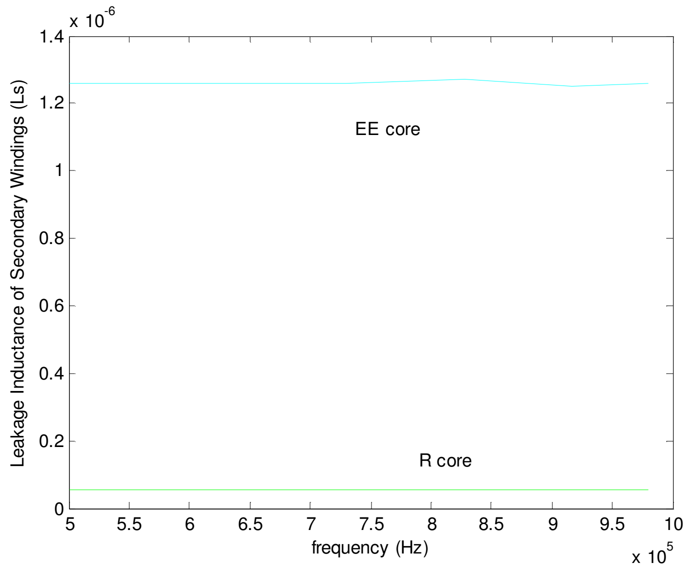

(b)

Fig. 2.26 Measured results (a) Stray capacitance vs frequency of different magnetic core

(b) Leakage inductance vs frequency of different magnetic core

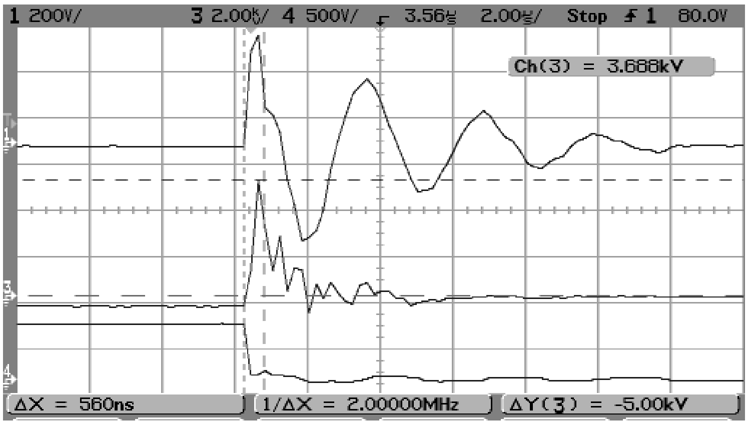

(a)

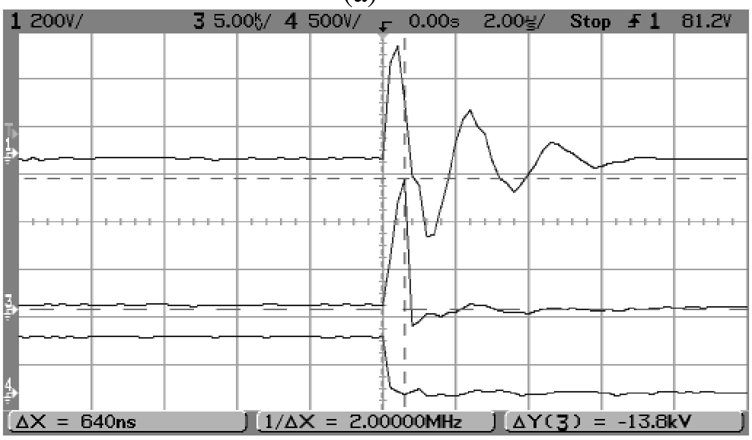

(b)

Fig. 2.27 (a) Voltage of EE core transformer(b) Voltage of R core transformer (ch1: input voltage of transformer, 200V/div; ch3: output voltage of transformer, 5kV/div; ch4: voltage of spark gap, 500V/div)

It can seen from the results that: (a) The transformer with EE core is bulky and R core is small. (b) The effect of distributed parameters on the transformer with EE core is high. (c) The transformer with EE core is easier to saturate and has noise problem. (d) The transformer fails in hot restrike at the step-up voltage is just around 5kV, but it is successful with R core. The winding window is smaller in EE core. So, the transformer with R core is used in this project.

(2) Comparison with Different Sizes

The R core is selected to make the transformer. In order to study on the effect of different lengths, three transformers based R core with different lengths are used. Fig. 2.28 gives the prototype of high voltage transformer with R core. Fig. 2.29 also shows the distributed parameters of different lengths and Fig. 2.30 shows the experimental results in hot restrike. In Fig. 2.30, the magnitude of input voltage of transformer (shown as ch1) is the same as the output voltage of the SG (shown as ch4). If the output voltage reaches the breakdown voltage of SG, the SG breaks down and discharges. In the meantime, the input voltage of transformer increases and the output voltage of the transformer (shown as ch3) could ignite the lamp.

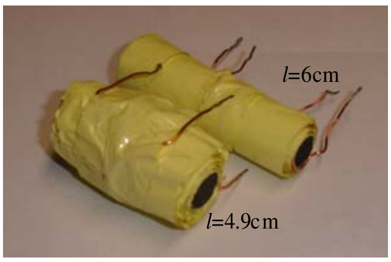

Fig. 2.28 The prototype of high voltage transformer

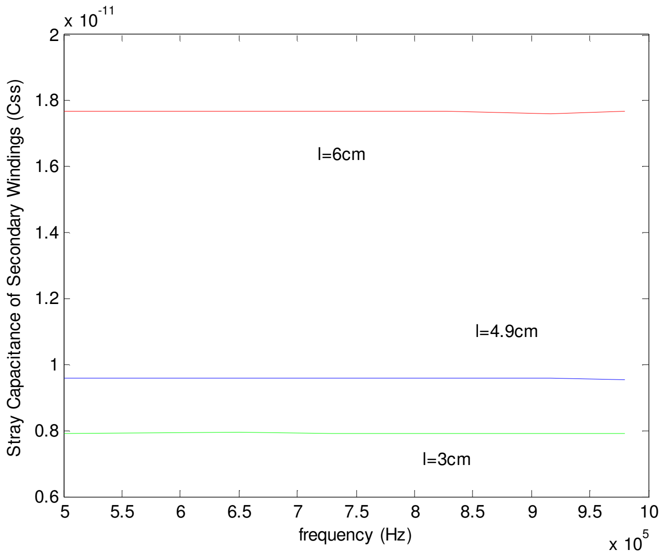

(a)

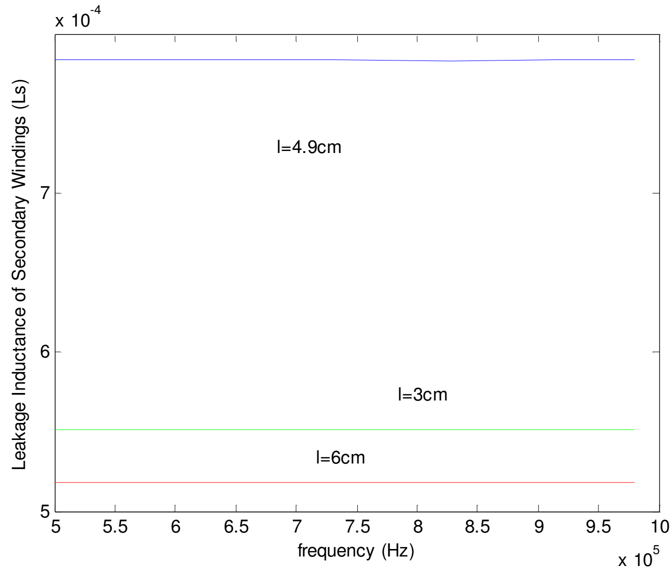

(b)

Fig. 2.29 Measured results (a) Stray capacitance vs frequency with different length (b) Leakage inductance vs frequency with different length

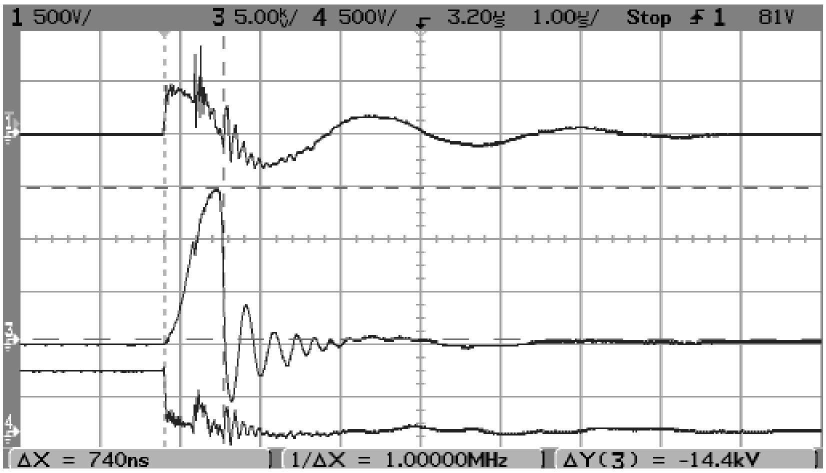

(a)

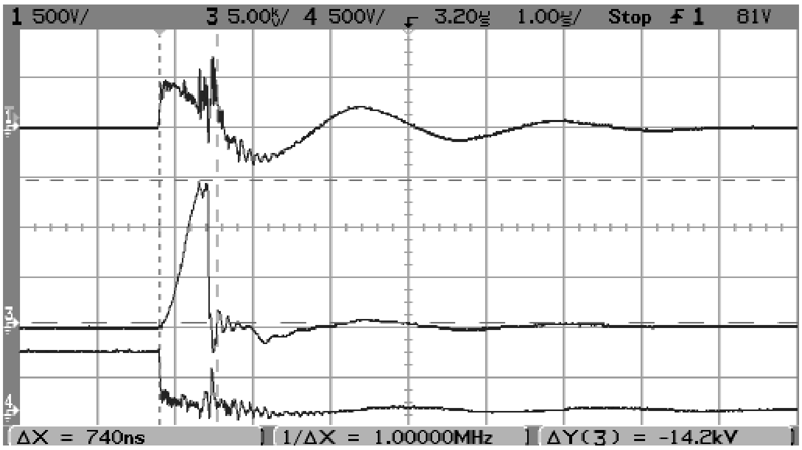

(b)

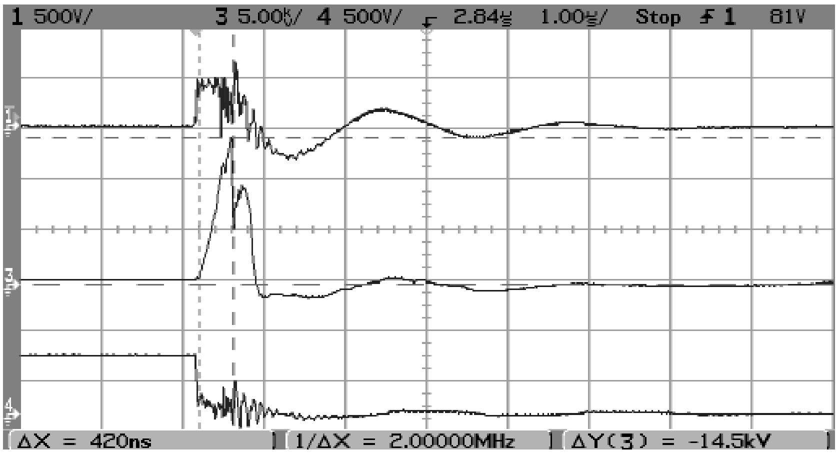

(c)

Fig. 2.30 (a) Voltage of R_1 core (d=0.8, *l*=3cm) (b) Voltage of R_2 core (d=0.8, *l*=4.9cm) (c) Voltage of R_3 core (d=0.8, *l*=6cm) (ch1: input volt. of transformer, 500V/div; ch3: output volt. of transformer, 5kV/div; ch4: volt. of spark gap, 500V/div)

These results show that the R core whose length is 3cm is optimal. It can meet the need of the cold strike and hot restrike. And it has a small size and lower cost.

2.5.2.4 Summary and Analysis

It is confirmed that a transformer with EE core is easy to saturate. The stray capacitance decreases and leakage inductance increase with the length for the R core. The output voltage is higher in the R core for the same number of turns. In the end, the R core whose length is 3cm is selected in this project. The experimental results show that this high voltage transformer could meet the requirement of HID ballast.

2.6 Summary

A comparison analysis and experimental verifications of two traditional electronic ballast circuits implemented by different circuit topologies and different control hardware for automotive HID lamp have been derived in this chapter. The components and the high voltage ignition transformer have also been examined. Precise design criteria and specification have been presented. After comparison, the following can be summarized:

1) The chip UCC2305 has all the functions suitable for the control of the lamp, but it is expensive and sensitive to noise.

2) The flyback converter used in microprocessor based EB has the less component count.

3) A low frequency around 200Hz is used in full bridge converter in IC based EB, but the frequency range in microprocessor based EB is from 300 Hz to 400 Hz.

4) Most components used in these two EBs are the same.

5) The lamp voltage and current are all square wave as the desired waveform (in Fig. 2.11).

6) Different ignition methods are used in two EBs. In microprocessor based EB, a DC operation time is needed to make sure that the HID lamp does not extinguish.

7) It is confirmed that transformer with EE core is easier to saturate. The stray capacitance decreases and leakage inductance increases with the length of the R core.

Chapter 3

Interpolation Simulation Model of Steady-State and Dynamic Characteristics for HID lamp

3.1 Introduction

In order to control accurately, to realize optimal design of electronic ballast and to analyze the characteristic of an automotive Xenon headlight system, it is important to establish the model of the Xenon lamp. In fact, Xenon lamps are extremely complex devices, which have many variables and parameters to be determined for optimum performance. From a plasma physics point of view, a complete model should include all physical processes and chemical species. Thus, a model must involve the simultaneous solutions of the chemical-equilibrium plasma-composition equations, the radiation transport equations, and the energy balance equations. The chemical composition equation must consider the transport of molecular, free radical, and atomic species by convection and by diffusion. Undoubtedly, this kind of model is useful for a lamp manufacturer to optimize their product design.

Much effort has been devoted to the development of sophisticated high intensity discharge lamp models. In 1978 Waymouth established the HID model based on the physical phenomenon [74]. But the parameters in the model are complicated and difficult to be obtained and be used. Deng used the small signal method in the fluorescent field [75]. Wei and Liu modulated the model of HID and fluorescent lamp into the software Pspice [26, 76].

However, for a ballast circuit designer, the most interesting characteristic of a lamp is its terminal characteristic as an electrical load. Therefore, a simplified lamp model is needed that can be described in the form of CAD representation. This model should be simple and user-friendly but can also reveal important physical trends in a lamp for a wide range of operating frequency. Laskowski [29] had done some research work about the terminal *V-I* behaviour of the lamp and others also used staged function to fit the *V-I* curve [30]. But the values of lamp voltage and current are affected by the temperature, a simple *V-I* curve cannot accommodate for the characteristics of the lamp, especially to the automotive headlight.

In this chapter, according to the terminal behavior of the lamp, the characteristics of temperature, voltage and current are presented. A novel automotive lamp model based on the bicubic interpolation method is developed. The simulation and experimental results are presented to validate the model.

3.2 Analysis of the Electrical Properties

The lamp ignition and steady-state excitation consists of basically three states. They are the preparation state or the before ignition state, the transient state and the steady-state. Before ignition, the lamp requires a spike voltage of tens of thousands volts in order to activate the ignition. The schematic diagram of the power supply and HID lamp is shown as Fig. 3.1(a). After the lamp is ignited, the equivalent circuit can be expressed as in Fig. 3.1(b). L_{s_h} is the inductance of secondary windings in the high voltage transformer used in the igniter.

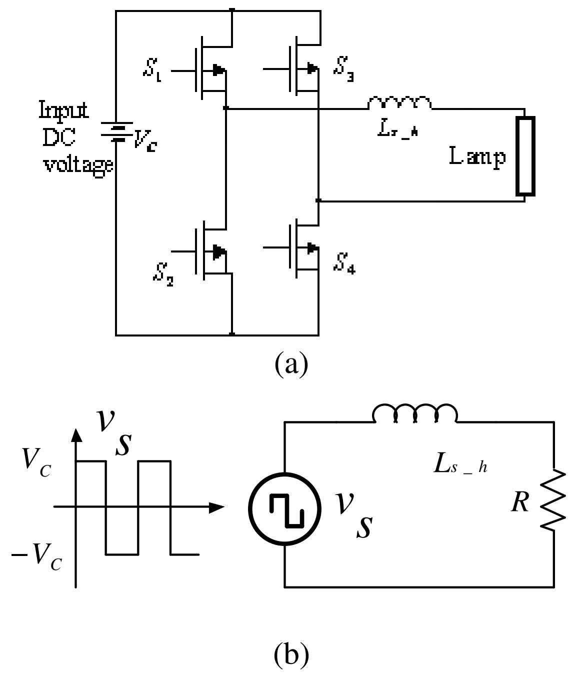

Fig. 3.1 (a) Drive circuit of HID lamp (b) Equivalent circuit of (a)

The characteristics of lamp voltage and current are shown in Fig. 3.2. In the transient state, three different states are included, that is, take-over state (shown in area (a)), warm-up state (also called constant current mode, shown in area (b)) and the run-up state (shown in area (c)).

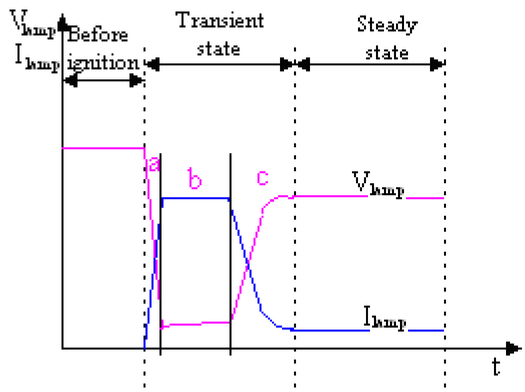

Fig. 3.2 The characteristic of Xenon lamp

The detailed analysis of operation modes is as follows:

(1) Before ignition

The ballast gives power input to the HID lamp. There is no current until the voltage is increased to 25kV.

(2) Transient state

This state can be divided into three different stages:

a. Take-over state: when the lamp is ignited, the lamp resistance is reduced to a few ohms and the current increases instantaneously. In this time, the voltage of the lamp drops.

b. Warm-up state: which is also called constant current state. In this state, a large current is supplied in order to ensure that the lamp is ignited and go to the steady state quickly.

c. Run-up state: before the lamp works in the steady state, the power supply of the ballast to the lamp is from low voltage high current to rated voltage and current. In this state, lamp current drops and the voltage rises.

(3) Steady state

This is the state of lamp to give a stable light output. In this time, the constant power is used to control the power supply of the lamp.

In reference [74], the resistance of the lamp in the steady state is considered as a constant value. In reference [30], the resistance of the lamp in the steady state is considered as a constant value and just three different values are used to replace the lamp model. But it is not very accurate. Actually, the lamp resistance is a nonlinear time-variant function. Due to the different requirements of cold start and hot re-strike of the lamp, the characteristic of lamp resistance depends on the lamp temperature. The relationships between lamp *I-T* (current, temperature) and time (*t*), lamp *V-T* (voltage, temperature) and time (*t*) are shown in Fig. 3.3 (a), (b). *T* is the lamp temperature in degrees.

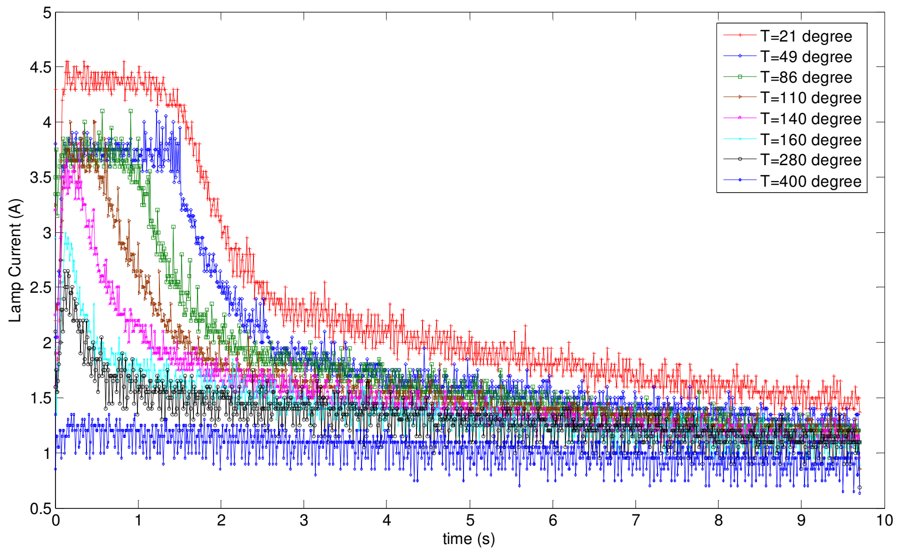

(a)

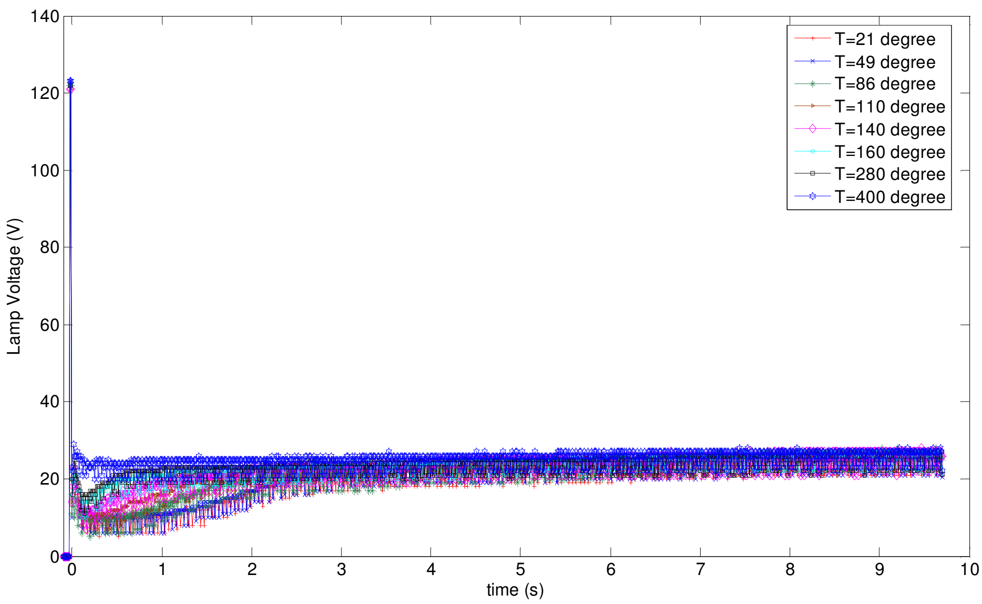

(b)

Fig. 3.3 (a) The current-temperature characteristics of the lamp (b) The voltage-temperature characteristics of the lamp

According to reference [74], the lamp temperature is increased until it comes to the full operating temperature. Nearing the full operating temperature, the ionizing and recombination state is a dynamic equivalent state and the temperature varies in a little scope. Different lamps with different color temperatures have the different values of full operating temperature (T_{ft}). A lamp model based on the bicubic spline interpolation method is presented in the following section.

3.3 Lamp Model Based on Bicubic Spline Interpolation

3.3.1 Lamp model

Before ignition, the lamp resistance is very large. When the lamp works in the transient state, the lamp resistance changes in a large scope and varies with time and initial temperature. After it goes into the steady state, the resistance could be thought as a constant value with little variation. So, the lamp resistance $R(t,T_{st})$ can be divided into three stages and is shown in (3.1), in which t is the time, T_{st} is the start temperature of the lamp; t_{stable} is the time when the lamp comes to the steady state and when t=0, the lamp is ignited. C_{ont} means a constant value.

$$R(t,T_{st}) = \begin{cases} \infty & t < 0 \\ \dfrac{U(t,T_{st})}{I(t,T_{st})} & 0 \le t \le t_{stable} \\ C_{ont} & t > t_{stable} \end{cases} \tag{3.1}$$

For t<0 and $t > t_{stable}$, the lamp resistance does not vary with the time and start temperature. When $0 \le t \le t_{stable}$, lamp resistance R can be expressed as the third dimensional quantity sitting on a 2-D plane comprising of time t and the start temperature T_{st} which is in the range [T_{rt}, T_{ft}]. T_{rt} means room temperature of the lamp. T_{ft} is the maximum operating temperature of the lamp. $U(t,T_{st})$ is the lamp voltage and $I(t,T_{st})$ is the lamp current.

3.3.2 Bicubic spline function and calculation

According to reference [25, 77], if t and T_{st} are discrete values and t is N ranks, T_{st} is M ranks, the proposed 2-D bicubic spline function can be written as follows:

$$R(t,T_{st}) = (g_{k1}(t), g_{k2}(t), g_{k3}(t), g_{k4}(t))A\begin{pmatrix} g_{j1}(T_{st}) \\ g_{j2}(T_{st}) \\ g_{j3}(T_{st}) \\ g_{j4}(T_{st}) \end{pmatrix} \tag{3.2}$$

where $1 \le k \le (N-1)$, $1 \le j \le (M-1)$. $t_k \le t \le t_{k+1}$, $T_{st\,j} \le T_{st} \le T_{st\,j+1}$. Also, the g_{kl} and g_{jl} are (l=1, 2, 3, 4):

$$\begin{cases} g_{k1} = 1 \\ g_{k2} = t - t_k \\ g_{k3} = (t-t_k)^2 \\ g_{k4} = (t-t_k)^3 \end{cases} \quad \begin{cases} g_{j1} = 1 \\ g_{j2} = T_{st} - T_{st\,j} \\ g_{j3} = (T_{st} - T_{st\,j})^2 \\ g_{j4} = (T_{st} - T_{st\,j})^3 \end{cases} \tag{3.3}$$

And the matrix A is:

$$A = \begin{pmatrix} a_{kj11} & a_{kj12} & a_{kj13} & a_{kj14} \\ a_{kj21} & a_{kj22} & a_{kj23} & a_{kj24} \\ a_{kj31} & a_{kj32} & a_{kj33} & a_{kj34} \\ a_{kj41} & a_{kj42} & a_{kj43} & a_{kj44} \end{pmatrix} \tag{3.4}$$

Any lamp resistance value can be obtained from (3.2) if the coefficients in the matrix A are known. For the whole region, the total of $16\times(N-1)\times(M-1)$ coefficients must be defined.

For each sub-rectangle, the bicubic spline interpolation gives four conditions, that is the four nodes of the sub-rectangle. As shown before, the four nodes of one sub-rectangle are as: (t_k, T_{stj}), (t_{k+1}, T_{stj}), $(t_{k+1}, T_{st(j+1)})$, (t_{k+1}, T_{stj}). In order to obtain the coefficients of the matrix A, a total of 12 temporary unknowns or parameters are introduced. Hence, the matrix C to determine matrix A is given in the following:

$$C = \begin{bmatrix} R_{kj} & q_{kj} & R_{k,j+1} & q_{k,j+1} \\ p_{kj} & r_{kj} & p_{k,j+1} & r_{k,j+1} \\ R_{k+1,j} & q_{k+1,j} & R_{k+1,j+1} & q_{k+1,j+1} \\ p_{k+1,j} & r_{k+1,j} & p_{k+1,j+1} & r_{k+1,j+1} \end{bmatrix} \tag{3.5}$$

From (3.2), if matrix $U(t_k)$ which is in relation with the time t is given as:

$$U(t_k) = \begin{bmatrix} g_{k1}(t_k) & g_{k2}(t_k) & g_{k3}(t_k) & g_{k4}(t_k) \\ g'_{k1}(t_k) & g'_{k2}(t_k) & g'_{k3}(t_k) & g'_{k4}(t_k) \\ g_{k1}(t_{k+1}) & g_{k2}(t_{k+1}) & g_{k3}(t_{k+1}) & g_{k4}(t_{k+1}) \\ g'_{k1}(t_{k+1}) & g'_{k2}(t_{k+1}) & g'_{k3}(t_{k+1}) & g'_{k4}(t_{k+1}) \end{bmatrix} = \begin{bmatrix} 1 & 0 & 0 & 0 \\ 0 & 1 & 0 & 0 \\ 1 & \Delta t_k & \Delta t_k^{\ 2} & \Delta t_k^{\ 3} \\ 0 & 1 & 2\Delta t_k & 3\Delta t_k \end{bmatrix} \tag{3.6}$$

where $\Delta t_k = t_{k+1} - t_k$.

Then the matrix $W(T_{stj})$ is the same as the matrix U,

$W(T_j) = \begin{bmatrix} 1 & 0 & 0 & 0 \\ 0 & 1 & 0 & 0 \\ 1 & \Delta T_{stj} & \Delta T_{stj}^{\ 2} & \Delta T_{stj}^{\ 3} \\ 0 & 1 & 2\Delta T_{stj} & 3\Delta T_{stj} \end{bmatrix}$, so the matrix A can be obtained as:

$$A = [U(t_k)]^{-1} C [W(T_{stj})]^{-t}$$

From the nodes of sub-rectangle, the parameters p_{kj}, q_{kj} are given by the following equations:

For j=1, …, M, one has

$$\frac{1}{\Delta t_{k-1}} p_{k-1,j} + 2\left[\frac{1}{\Delta t_{k-1}} + \frac{1}{\Delta t_k}\right] p_{kj} + \frac{1}{\Delta t_k} p_{k+1,j} = 3\left[\frac{R_{kj} - R_{k-1,j}}{\Delta t_{k-1}^{\ 2}} + \frac{R_{k+1,j} - R_{k,j}}{\Delta t_k^{\ 2}}\right], k = 2, \cdots, N-1 \tag{3.7}$$

For k=1, …, N, then

$$\frac{1}{\Delta T_{st(j-1)}} q_{k,j-1} + 2\left[\frac{1}{\Delta T_{st(j-1)}} + \frac{1}{\Delta T_{jst}}\right] q_{kj} + \frac{1}{\Delta T_j} q_{k,j+1} = 3\left[\frac{R_{kj} - R_{k-1,j}}{\Delta T_{st(j-1)}^{\ 2}} + \frac{R_{k+1,j} - R_{k,j}}{\Delta T_{stj}^{\ 2}}\right], j = 2, \cdots, M-1$$

(3.8)

For j=1 and j=M, then

$$\frac{1}{\Delta t_{k-1}} r_{k-1,j} + 2\left[\frac{1}{\Delta t_{k-1}} + \frac{1}{\Delta t_k}\right] r_{kj} + \frac{1}{\Delta t_k} r_{k+1,j} = 3\left[\frac{q_{kj} - q_{k-1,j}}{\Delta t_{k-1}^{\ 2}} + \frac{q_{k+1,j} - q_{kj}}{\Delta t_k^{\ 2}}\right], k = 2, \cdots, N-1 \tag{3.9}$$

For k=1, …, N, then

$$\frac{1}{\Delta T_{st(j-1)}} r_{k,j-1} + 2\left[\frac{1}{\Delta T_{st(j-1)}} + \frac{1}{\Delta T_{stj}}\right] r_{kj} + \frac{1}{\Delta T_{stj}} r_{k,j+1} = 3\left[\frac{p_{kj} - p_{k,j-1}}{\Delta T_{st(j-1)}{}^{2}} + \frac{p_{k,j+1} - p_{kj}}{\Delta T_{stj}{}^{2}}\right], j = 2, \cdots, M-1$$
(3.10)

All the coefficients of the spline interpolation functions can be computed iteratively through the equations from (3.2)-(3.10). The interpolation methods are conducted by Matlab.

3.4 Simulation and System Analysis

In the simulation model, the main circuit is shown in Fig. 3.4.

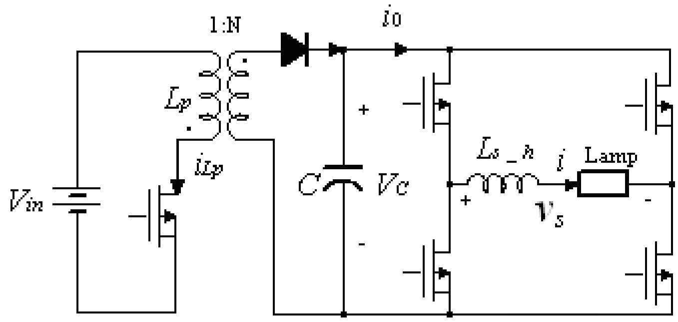

Fig. 3.4 The main circuit of the whole system

In the circuit, L_p is the primary inductance, N is the turns ratio of main transformer. V_C is the capacitor voltage and it is also the input DC voltage of the full-bridge. i_0 is the input current of the full-bridge. i is the lamp current.

Before the lamp is ignited, the flyback converter works in DCM (Discontinuous Current Mode), the lamp resistance is infinitely large, that is, the flyback converter works in a light load mode. When the lamp is ignited, the system can be expressed as the following equations

$$\begin{aligned} \frac{di_{L_p}}{dt} &= \frac{-(1-D)}{NL_p} V_C + \frac{D}{L_p} V_{in} \\ \frac{dV_C}{dt} &= \frac{1-D}{NC} i_{L_p} - \frac{i_0}{C} \end{aligned} \tag{3.11}$$

where D is the duty ratio of the transistor in the flyback converter. In Fig. 3.1, L_{s_h} is the inductor of the secondary transformer, R_{lamp} is the resistance of the lamp and V_{in} is the input power supply of whole circuit. This ballast circuit is used as the lamp is ignited and v_s is the power supply given by the full-bridge inverter, So:

$$v_s(t) = L_{s\_h}\frac{di}{dt} + Ri \tag{3.12}$$

The expression of the $i(t)$ and $v_s(t)$ for full-bridge respectively are (3.13) given by Fourier analysis [126-128], where f is the frequency of the full-bridge. The larger the n is, the more accurate the value. Here, n=7 is adopted as a compromise between the accuracy and computing time.

$$\begin{aligned} i(t) &= \sum_{n=1}^{\infty}\frac{2i_0}{n\pi}(1-\cos n\pi)\sin(2n\pi ft) \\ v_s(t) &= \sum_{n=1}^{\infty}\frac{2V_C}{n\pi}(1-\cos n\pi)\sin(2n\pi ft) \end{aligned} \tag{3.13}$$

Using the above spline interpolation model and circuit analysis, an HID ballast system is simulated. The parameters used in the experimental ballast and HID lamps are shown as follows:

1) HID Lamp: Philips 35W MH lamp (D2S) with a cylindrical arc tube.
2) Primary Inductance and turns ratio of transformer in flyback converter: L_p=10μH, N=7. Output capacitor in flyback converter: C=5.6μH. The secondary self-inductance of high voltage transformer: L_{s_h}=0.6mH. Power Supply: V_{in}=12V.
3) The maximum operating temperature: 442°C; Room temperature: 24.6 °C.

Before the lamp is ignited, the lamp resistance is assumed to be 1080Ω (which can be defined arbitrary in order to show in the figure). Fig. 3.5 shows the limited amount of input data that describe the relationship between lamp resistance and start temperature. All of these data are obtained from the experiment. There are 7 different start temperature and 63 time data of each type and the total number of lamp resistance data pairs is 441. The selected number is a compromise between the computing speed and precision. For more than 7 sets of temperature, the accuracy has no substantial improvement. Fig. 3.6 shows the spline interpolation result.

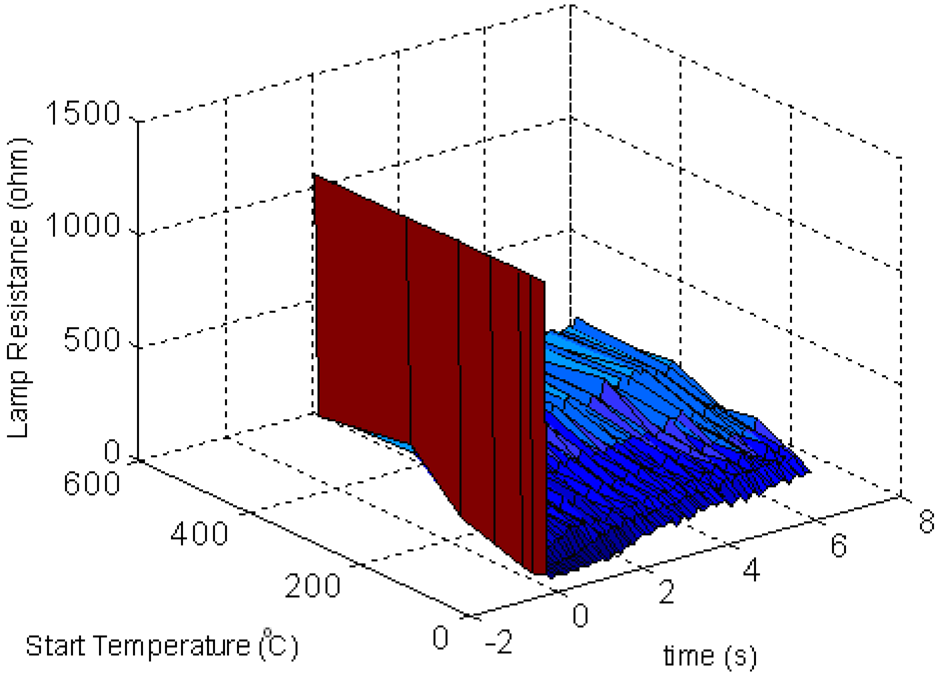

Fig. 3.5 Known nonlinear characteristics of lamp resistance

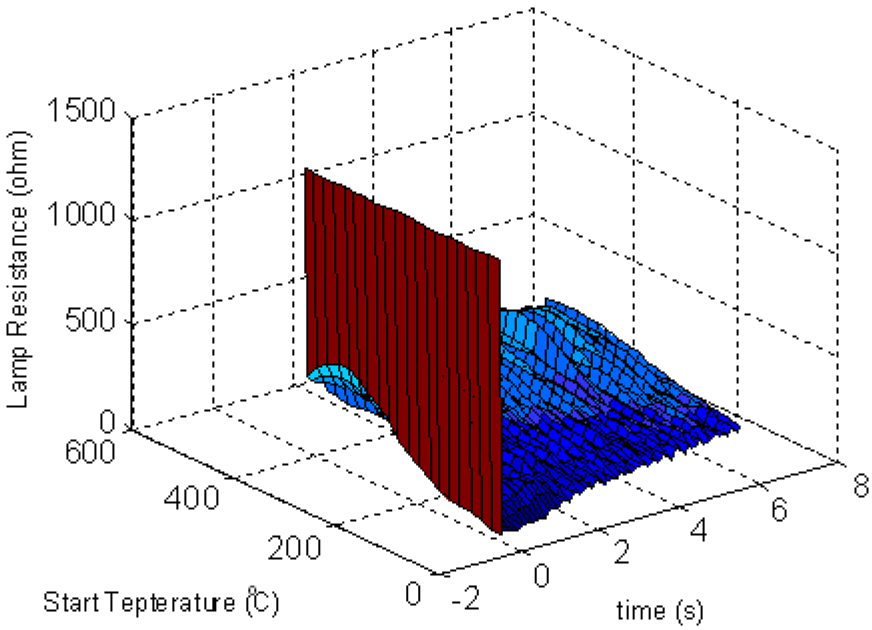

Fig. 3.6 Interpolation result of the input characteristics

Fig. 3.7 shows the comparison at the start temperature of 24.6 °C, 120 °C and 274 °C between experimental values and interpolation values. It is seen that the interpolation values are virtually identical with the experimental values.

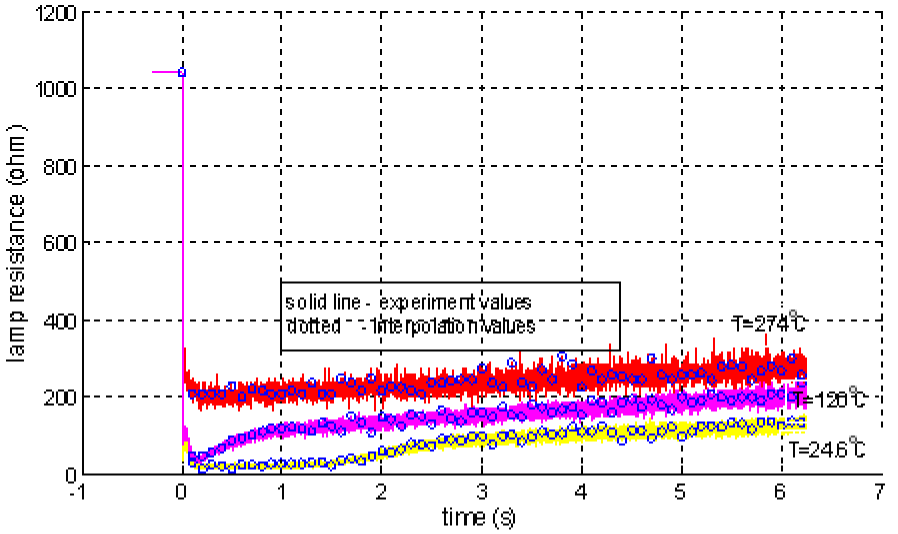

Fig. 3.7 Comparison between the interpolation values and experimental values

Fig. 3.8 shows the block diagram of the system simulation which is divided into three parts, that is, the HID ballast, the lamp model and the controller. This simulation model can tell the dynamic state and steady state of the system. In addition, from ignition of the lamp to its steady state, there are different control modes required in the controller. They are the constant voltage control (CVC) mode, the constant current control (CCC) mode, the decrease power control (DPC) mode and constant power control (CPC) mode. In this simulation study, the following definition is used:

Constant Voltage Control (CVC): Control Mode=0;

Constant Current Control (CCC): Control Mode=1;

Decrease Power Control (DPC): Control Mode=2;

Constant Power Control (CPC): Control Mode=3;

The control mode is to show the control state of the system which is good for the parameter design of the controller. The Display block can show the control mode in the simulation. For example, when 0 is shown in dispaly, it means that CVC is used.

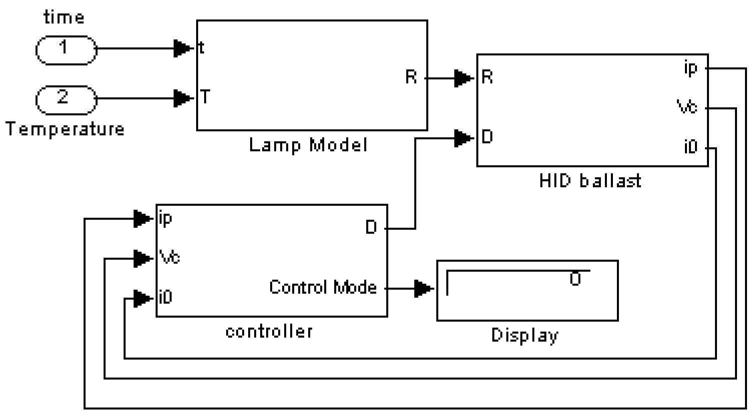

Fig. 3.8 The simulation block

Fig. 3.9 (a) and (b) show the simulation values and experimental values of the output voltage of the flyback converter $V_s(t)$ at a start temperature of 24.6 ^oC. Before the lamp ignites, the output voltage of the flyback converter is equal to 400V in simulation. After a voltage doubler, the voltage is raised to 800V. The typical voltage of SG to breakdown is 600V. Therefore the voltage is sufficient to ignite the lamp. The lamp could also be ignited if the output voltage of flyback is more than 300V. Fig. 3.9 (a) shows the simulation results of the output voltage of flyback and the start-up voltage is 400V, but it is less than 400V as shown in the experimental results in Fig. 3.9(b). This is one difference between the simulation result and experimental result.

Interestingly, in the cold start, the lamp current rises to a large value (around 2A) to meet the SAE standard (to the maximum output power-75W). The current change in the inductor L_{s_h} is large and it will be coupled to the capacitor C, so a large ripple will appear in the output voltage of the flyback. The simulation result has fewer ripples during the transient warm-up state whereas the experimental results have a large ripple. Fig. 3.9 (c) and (d) show the simulation and experimental results of lamp current at the same start temperature.

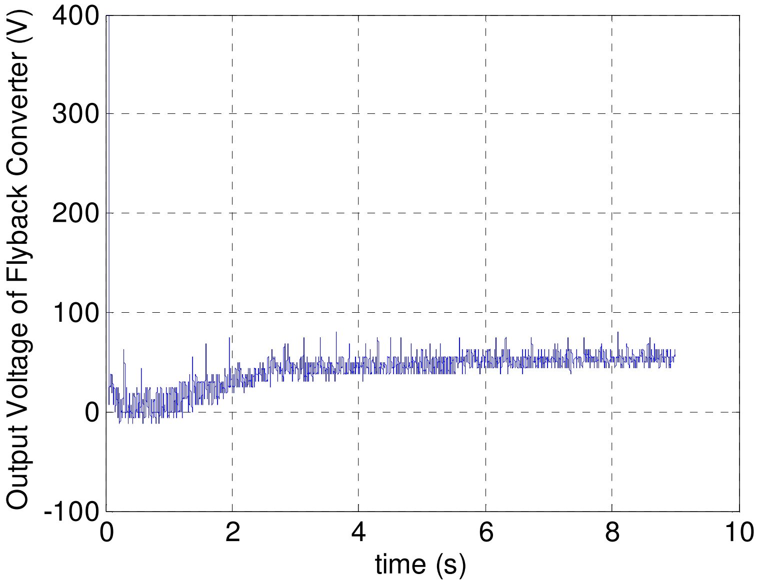

(a)

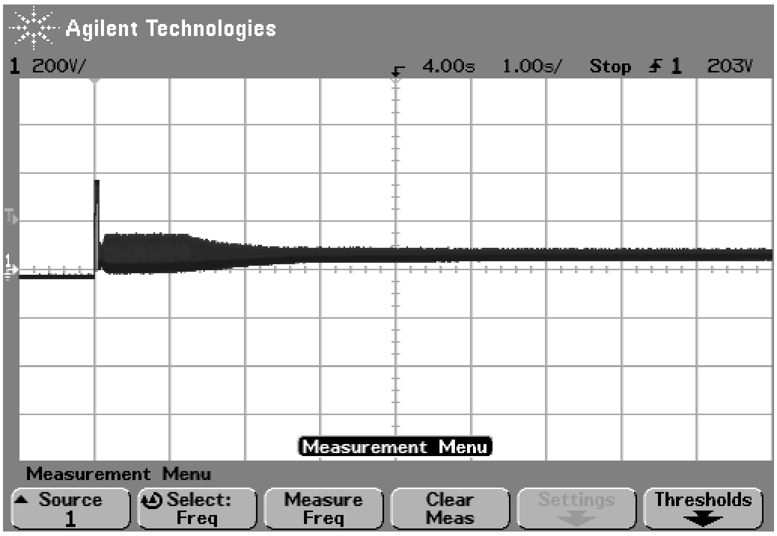

(b)

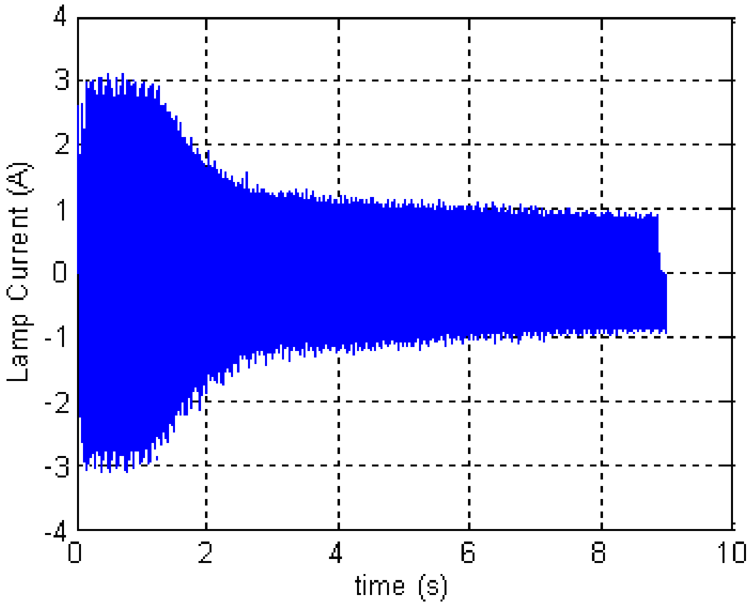

(c)

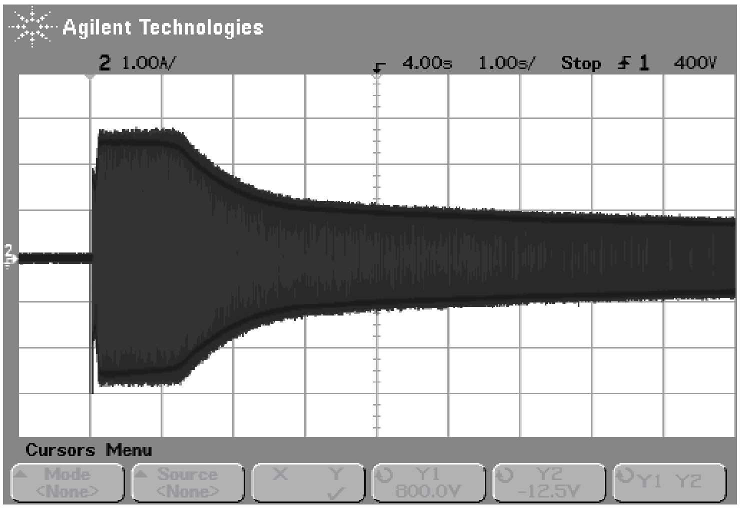

(d)

Fig. 3.9 Start temperature 24.6 °C (a)Simulation result of output voltage of flyback converter (b) Experimental values of output voltage of flyback converter(voltage: 200V/div time: 1s/div) (c)Simulation result of lamp current (d) Experimental values of lamp current (current: 1A/div time: 1s/div)

Fig. 3.10 (a) and (b) show the simulation values and experimental values of the output voltage of the flyback converter at a start temperature of 120°C. Fig. 3.11 shows values at a start temperature of 440°C. Compared to Fig. 3.9(b), Fig. 3.10(b) has a small voltage ripple. The reason is that the lamp temperature here is 120°C and the current change is smaller than that in the cold start. With the lamp temperature increases, the current change decreases and the ripple in the capacitor decreases.

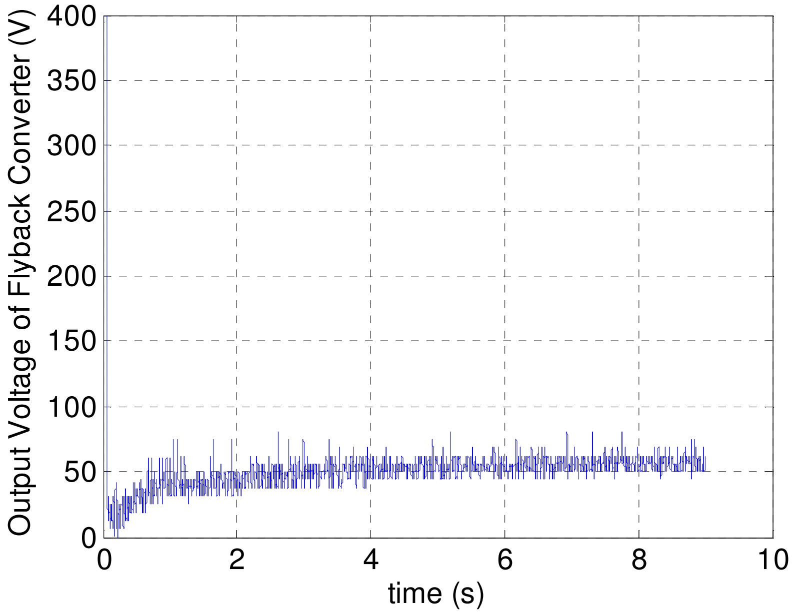

(a)

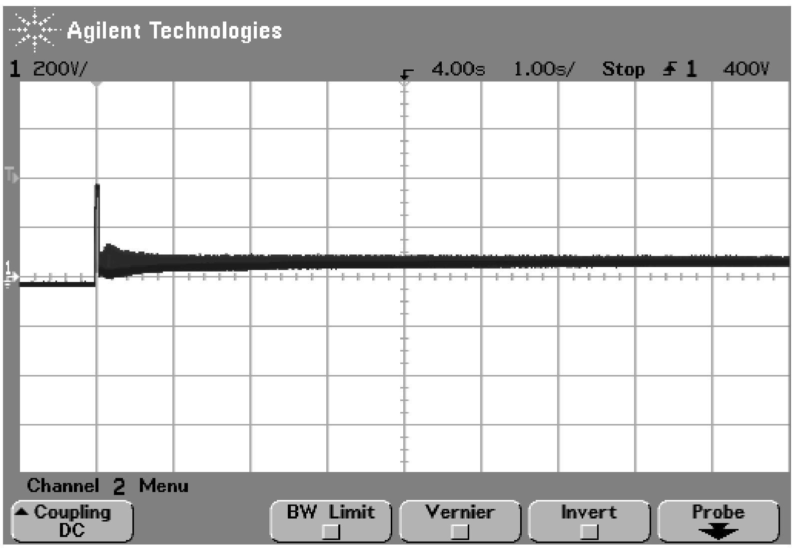

(b)

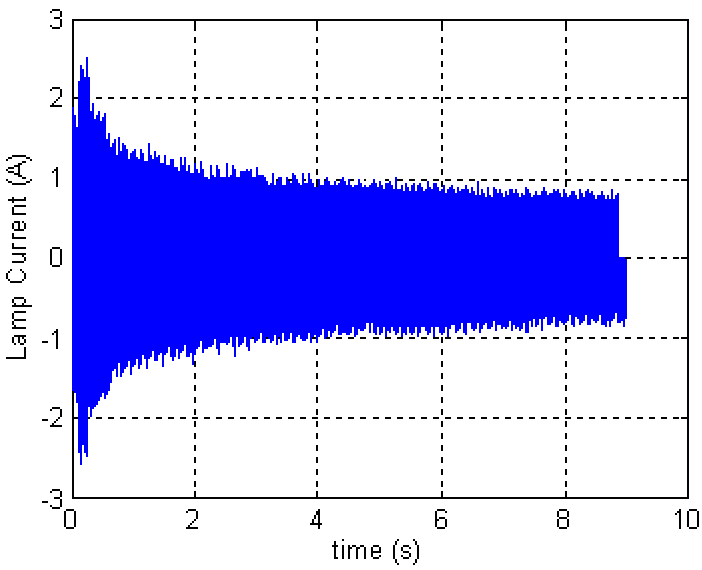

(c)

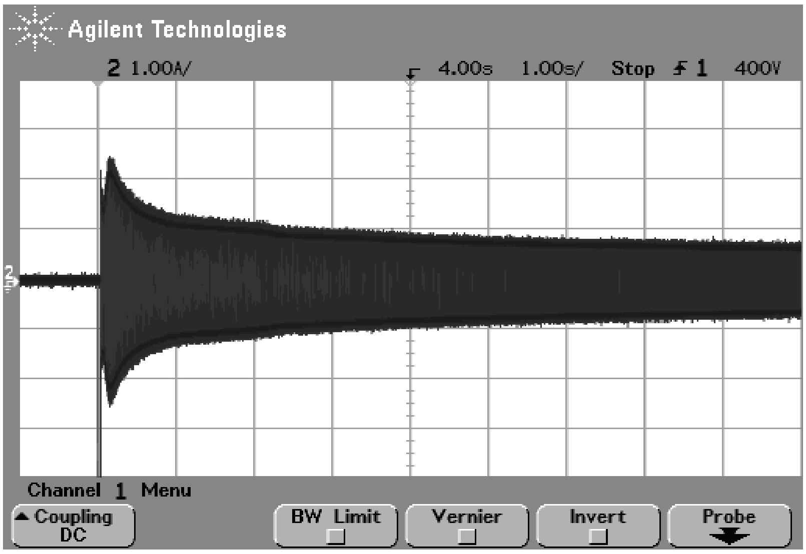

(d)

Fig. 3.10 Start temperature 120^{o}C (a)Simulation result of output voltage of Flyback converter (b) Experimental values of output voltage of flyback converter(voltage: 200V/div time: 1s/div) (c)Simulation result of lamp current (d) Experimental values of lamp current (current: 1A/div time: 1s/div)

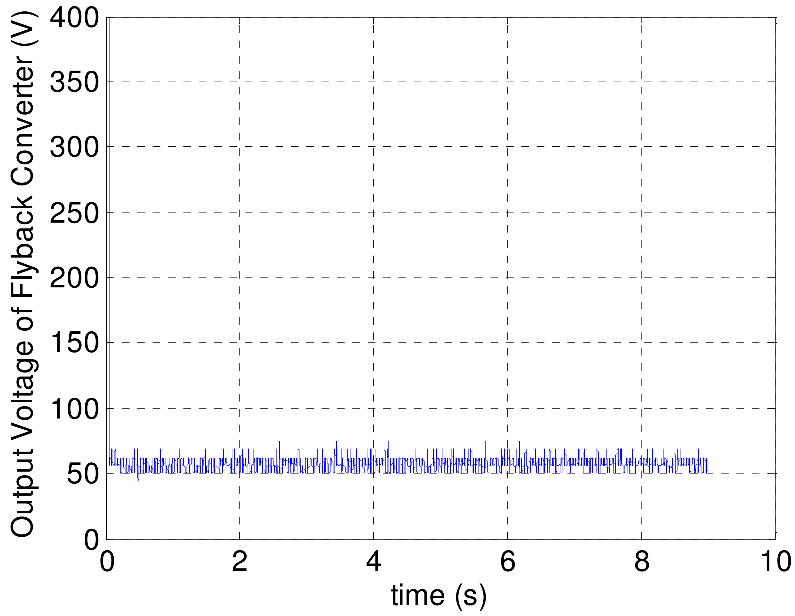
Output Voltage of Flyback Converter (V)
400
350
300
250
200
150
100
50
0
0
2
4
6
8
10
time (s)

(a)

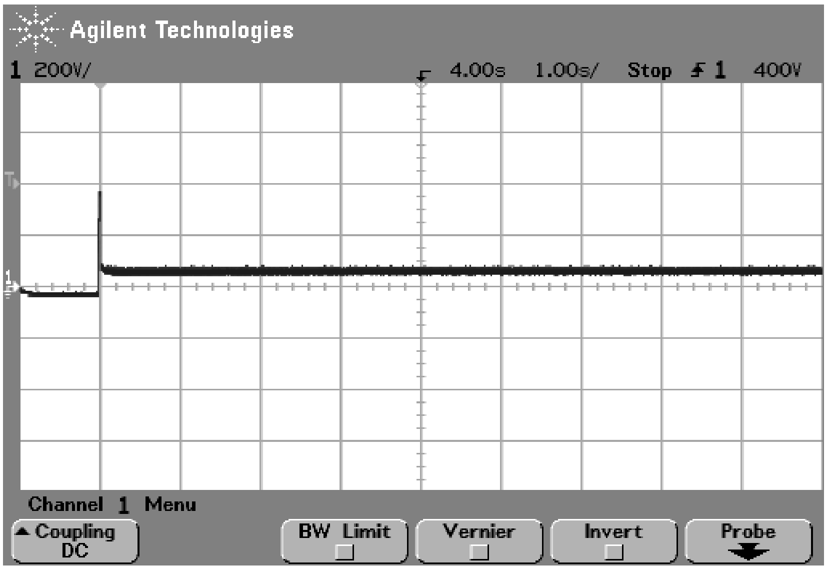
Agilent Technologies
1 200V/
4.00s 1.00s/ Stop 1 400V
Channel 1 Menu
Coupling DC
BW Limit
Vernier
Invert
Probe

(b)

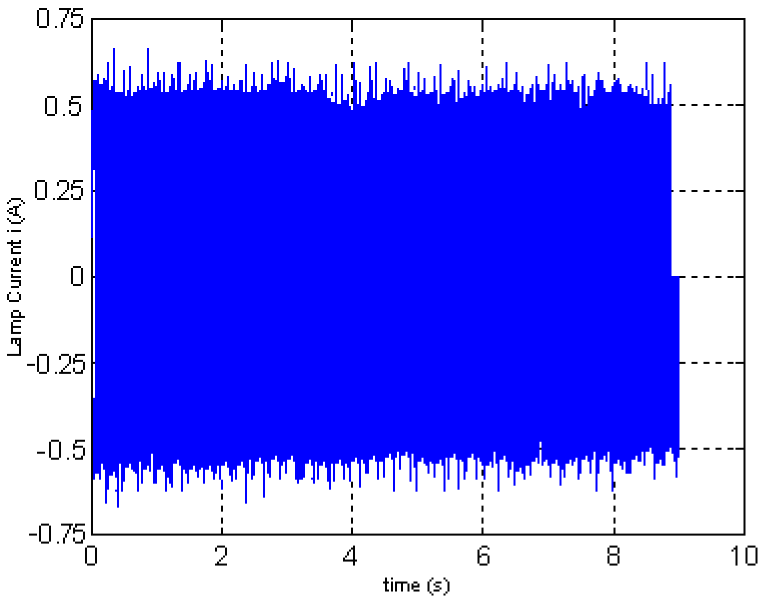

(c)

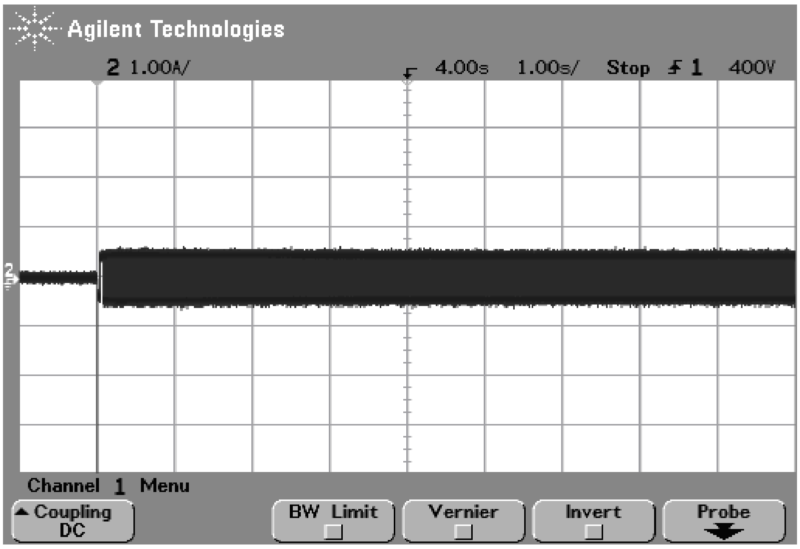

(d)

Fig. 3.11 Start temperature 440^{o}C (a)Simulation result of output voltage of flyback converter (b) Experimental values of output Voltage of flyback converter(voltage: 200V/div time: 1s/div) (c)Simulation result of lamp current (d) Experimental values of lamp current (current: 1A/div time: 1s/div)

3.5 Summary

This chapter presents a novel method of modeling of Xenon lamp for use in automotive application. The circuit under examination is an H-bridge inverter to drive the HID lamp. The DC supply is derived from 12V through a flyback converter. Due to the temperature property of the lamp, the 2-D spline interpolation has been developed to model the lamp characteristics. The simulation has been conducted in various temperature settings from start up to steady state. The method only requires limited number of data. The comparison of simulation and experimental measurement has confirmed that the model can precisely represent the model characteristics. The model provides a platform using the spline to develop other HID lamp models using limited data. The study of warm lamp has also been carried out. The temperature at 440^{o}C has been examined for high start-up temperature. Very good agreement has been obtained. It is confirmed that both cold start and warm start can be accurately represented by the proposed method.

The model developed and the simulation system can be used to design the parameter of the front-end converter and overall system control.

Chapter 4

Development and DSP Implementation of New Electronic Ballast Based on Unified Controller

4.1 Introduction

In chapter 2, two different electronic ballasts (EBs) are compared and developed. The design method of EB is presented. Due to the complexity of the characteristic of the lamp, although some optimizations, such as using the devices with lower rated power [78], less windings [79] and improving the lamp efficiency [80] are used to reduce the cost of ballast, there are also many other aspects needed to be considered in the ballast design. The most important and complex part is the controller which controls and dictates the mode of operation depending on the stages from start-up to steady state. There are many different hardware realizations of the controller in the market, such as special IC (UCC2305, 3305) [65], microprocessor [67, 81] and DSP. In addition, microprocessor and DSP can realize the digital control and have the advantages, such as less susceptible to ageing and environmental variations, less sensitive to noise and easy to control by changing software. In order to examine the control method, a DSP control unit-DS1104 research & development (R&D) controller board developed by dSPACE Corp is used to develop a new EB. The DS1104 R&D Controller Board is a new piece of hardware that upgrades our PC to a powerful development system for rapid control prototyping. The real-time hardware based on PowerPC technology and its set of I/O interfaces makes the board an ideal solution for developing controllers in various industrial fields.

In hardware design, almost the same structure (see Fig. 2.1) is used in the electronic ballast, that is, a structure with a high frequency DC-to-DC converter followed by a low frequency DC-to-AC inverter. The DC voltage source is a battery which varies between 9V and 16V. The DC-to-DC converter is used to boost the voltage of the power supply to 350V level which can strike the lamp at start period and boost the voltage to 85V level at steady state. Here the flyback converter is used. DC-to-AC inverter converts the DC output voltage of flyback converter to square wave voltage which is used to keep the voltage of two electrodes of the HID lamp balance and to avoid the acoustic resonance [62]. Igniter is used in the lamp ignition stage to make the spark gap break down and ignite the HID lamp. Except for the controller, the rest of the parts of the ballasts are almost the same with the microprocessor based EB. Due to the simple structure, the classical PI controller is realized by the analogue circuit in the integrated circuit (IC) based EB. The microprocessor based EB is realized by UC3843.

In this chapter, the structure of DSP based EB is first described. The controller design based on Prototype DS1104 Controller board is then presented. A new control concept, called unified controller, is then analyzed and realized by two control methods. One is the two-loop PI controller and the other is the adaptive controller.

4.2 Proposed HID Electronic Ballast

4.2.1 Proposed Structure

This section shows the design and optimization of the proposed ballast. The requirements of the automotive HID ballast are the same as the traditional ballast: (1) battery input voltage: 9-16V. (2) Power output at steady state: 35W. (3) Light output: specified by SAE J2009. A Philips 35W MH lamp (D2S) with a cylindrical arc tube is used in this application. The nominal steady state voltage is 85V. The steady state power is 35W, and the transient power is needed to meet the SAE standard, that is, 75W.

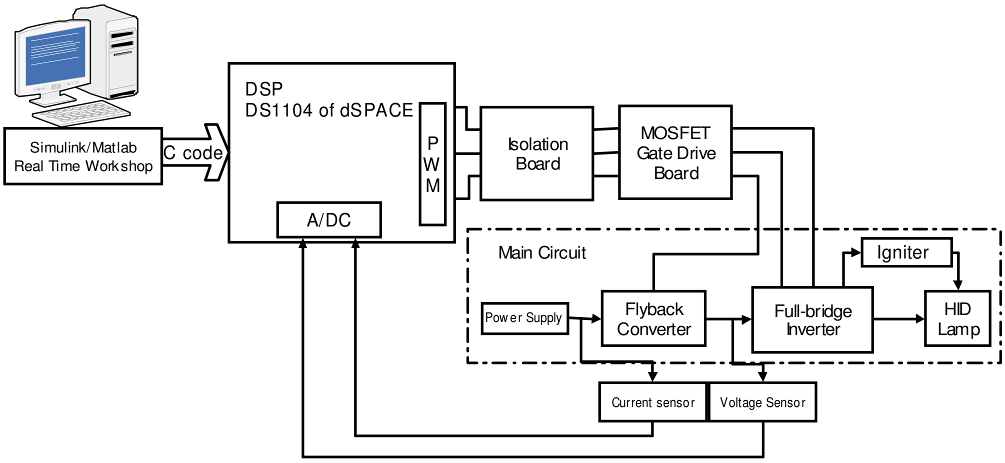

Fig. 4.1 Schematic block diagram of the DSP based EB system

The schematic block diagram of the proposed ballast with DS1104 is shown Fig. 4.1. Two 16-bit ADCs and three PWM channels, one for flyback and the other for the full-bridge, are used in our system. Real-time control codes can be generated with a Simulink diagram through Matlab real-time workshop.

4.2.2 Main Circuit

The main circuit used here is similar to the microprocessor based EB. The operation principle of this ballast has been shown in chapter 2. The main circuit based on DS1104 is given as Fig. 4.2.

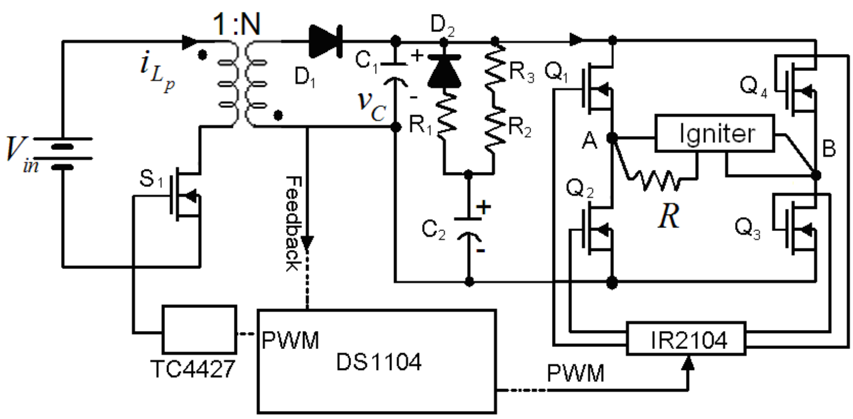

Fig. 4.2 Main circuit used in DSP based ballast

This designed ballast is developed according to the input and output data presented in Table 4.1. Table 4.2 summarizes the parameters used in the implementation of the main circuit. It must be pointed out that the circuit is made up of components, D_2, R_1, R_2 and R_3. The components form a fast discharge mechanism. It is used in the HID lamp for run up stage and to give enough current to the HID lamp. They make sure that the lamp is ignited and not extinguished.

Table 4.1 Input and output Data of the proposed EB

Electrical/Physical Data	Value
Input voltage	12V
Switching frequency of Flyback Converter	100kHz
rms value of dc link	85V
Switching frequency of full bridge inverter	400Hz
Nominal output power	35W

Table 4.2 Parameters employed in the main circuit

Designation	Value
Turns ratio of main transformer	1:7 (EE core)
Diode: D_1, D_2	MUR860, MUR160
Capacitor: C_1, C_2	0.47µF/630V, 4.7µF/400V
Resistance: R_1, R_2, R_3	1kΩ/1W, 100Ω/1W,100Ω/1W
Power switch: S_1	IRF370
Switch: Q_1, Q_2, Q_3, Q_4	IRF830

The igniter between points A and B of the full bridge inverter is shown in Fig. 4.3. This is the voltage doubler circuit, in which the breakdown voltage of SG is 600V. The igniter parameters are shown in Table 4.3.

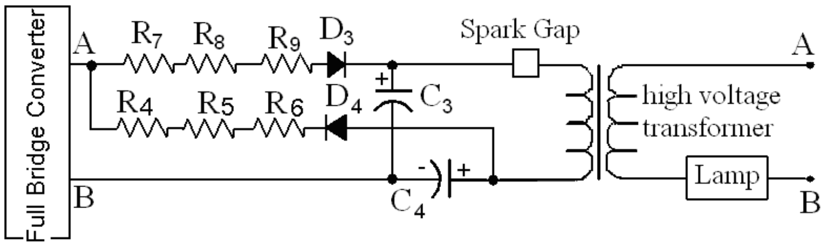

Fig. 4.3 Voltage doubler igniter circuit

Table 4.3 Parameters in the igniter circuit

Designation	Value
Resistance: R_4, R_5, … , R_9	1.8kΩ/1W
Diode: D_3, D_4	UF4006
Turns ratio of High voltage transformer	1:100 (R core)
Capacitor: C_3, C_4	0.68μF/400V
SG	SG-600V

4.2.3 MOSFET Gate Drive Board

The PWM signal is provided by DS1104 whose supply voltage is 5V. The voltage required by MOSFET is around 15V. Level shift gate drive ICs are needed. They are TC4427CPA and IR2104.

TC4427CPA is a 1.5A dual high-speed power MOSFET driver. It does not distort the PWM signal, and provides good driving current signal [82]. Fig. 4.4 shows the PWM signal of flyback converter given by DS1104 (ch1) and the drive signal of MOSFET is given after TC4427CPA (ch2). The PWM signal is of frequency 100 kHz.

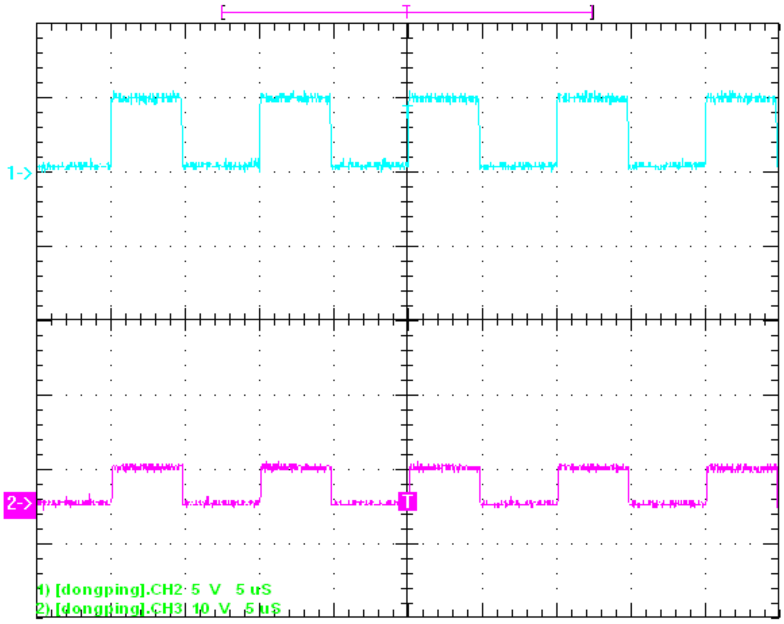

Fig. 4.4 PWM signal of DS1104 and TC4427 (ch1: DS1104, 5V/div, 5μs/div; ch2: TC4427, 10V/div, 5μs/div)

IR2104 is high voltage, high speed power MOSFET driver with dependent high and low side referenced output channels [83]. This IC is used to give high current signal to the full bridge converter and the schematic diagram of this IC is shown in Fig. 4.5. The points A, Q_1, Q_2 are connected to the associated points in Fig. 4.2. The external parameters of this IC are shown in Table 4.4.

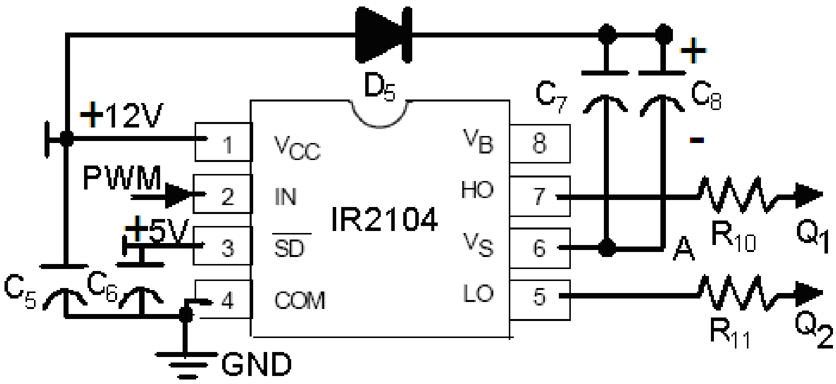

Fig. 4.5 Schematic diagram of the IC- IR2104

Table 4.4 External parameters of IC IR2104

Designation	Value
Resistance: R_{10}, R_{11}	68Ω
Diode: D_5	FR107
Capacitor: C_5, C_6, C_7	0.1μF
Capacitor: C_8	22μF/25V

Fig. 4.6 shows the PWM signals for the top and bottom drives at frequency 400 Hz provided by IR2104 (ch2, ch3). The PWM signal of flyback converter with switching frequency 100 kHz is shown in ch1.

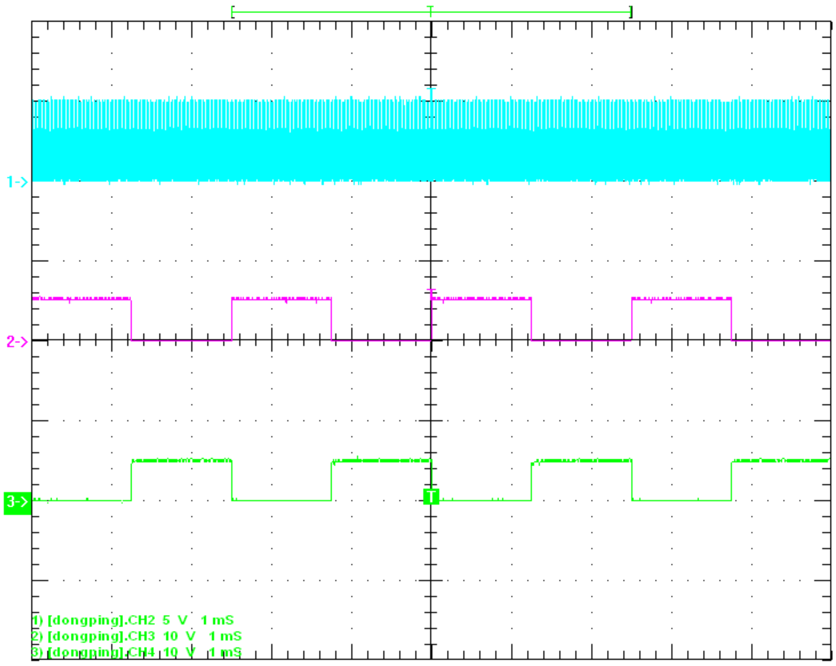

Fig. 4.6 PWM signals (V_{GS}) (ch1: switch S_1 of flyback converter given by DS1104, 100 kHz, 5V/div, 1ms/div; ch2: switch Q_1 of full bridge given by IR2104, 400Hz, 10V/div, 1ms/div; ch3: switch Q_2 of full bridge given by IR2104, 400 Hz, 10V/div, 1ms/div)

4.2.4 Isolation Board and Hall-effect Sensors

In order to protect the DS1104 card, isolation board IC- 6N137 is used. This IC- 6N137 is built in with optocouplers which consist of a light emitting diode and a high gain integrated photo detector to provide electrical isolation between input and output [84]. Similar to TC4427, 6N137 does not distort the PWM signal, and the external circuit is simple.

The Hall-effect sensor is selected because it has the internal isolation function. The current sensor and the voltage sensor are selected as LA25-NP and LV25-P, respectively [85]. The parameters of the external circuit connected to the main circuit and Hall-effect sensor are shown in Table 4.5.

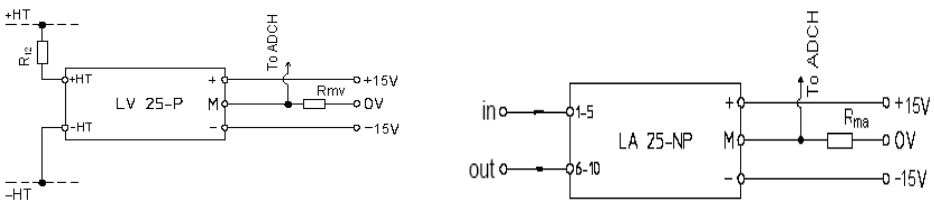

(a) (b)

Fig. 4.7 Connection circuit of Hall-effect sensor (a) LV25-P (b) LA25-NP

Table 4.5 External parameters of Hall-effect sensor

Designation	Value
Resistance in LA25-NP: R_{ma}	300Ω
Resistance in LV25-P: R_{mv}	150Ω
Resistance in LV25-P: R_{12}	40kΩ

The DS1104 based EB is expensive and is about HK$38,000. It can be replaced by an economic DSP and this will decrease the total cost. If a DSP such as D434TSC is used, the cost of components will be reduced significantly and the programming work is the same. For information, the price of this chip is about HK$120.

4.2.5 Digital Signal Processor Control Unit

The DS1104 is a sound development system for industry and equally good for academic research. It gives us all the benefits of a dSPACE Prototype system: full graphical configuration, easy programming in SIMULINK/Stateflow from The MathWorks and simple experimental control with state-of-the-art software tools. The board can be installed virtually in any PC with a free PCI slot. Many hardware sources such as A/D, D/A, and I/O are available in the board. Fig. 4.8 shows a DS1104 controller board.

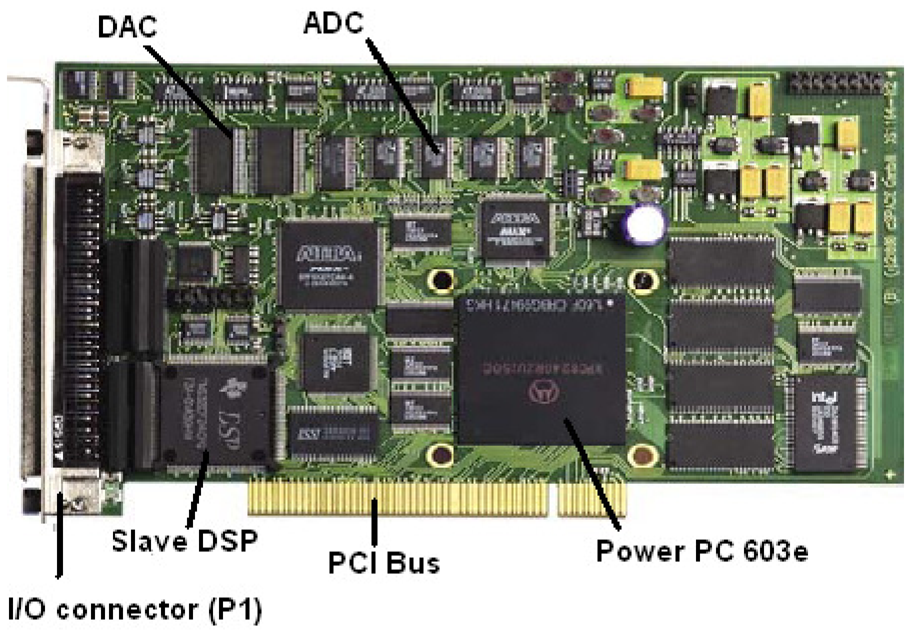

Fig. 4.8 Prototype of DS1104 controller board

SIMULINK is a software package for modelling, simulating and analyzing dynamic systems. It supports linear and nonlinear systems, modelled in continuous time, sampled time or a combination of the two. The associated software, simulink/RTW, includes two main parts, the SIMULINK /Real Time Workshop (RTW) and ControlDesk.

The RTW enables a SIMULINK model to be run in real-time on a remote processor. It is possible to design a control system using MATLAB/ SIMULINK, generate code from a block diagram model, and then compile and download it directly to the target hardware. It provides an easy-to-use and integrated environment to design quickly without lengthy hand coding and debugging. It is ideal for real-time control, real-time signal processing, rapid prototyping, hardware-in-the-loop testing and other applications. The principle of RTW is illustrated in Fig. 4.9 [86].

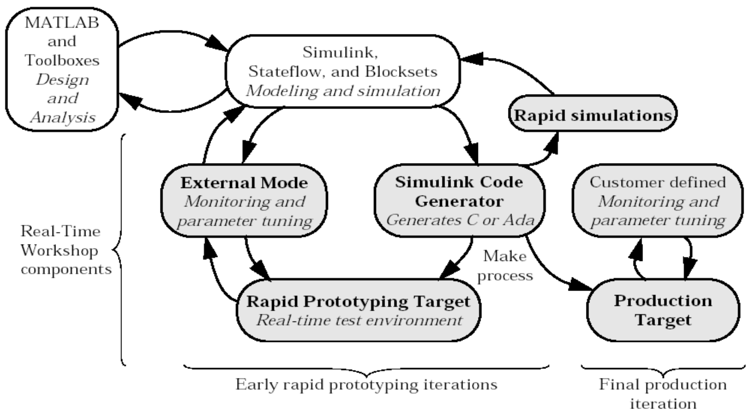

Fig. 4.9 Principal diagram of SIMULINK /RTW

The ControlDesk is dSPACE's well-established experiment software that provides all the functions to control, monitor and automate experiments and makes the development of controllers more efficient. It is user friendly and combines an integrated technical computing environment with numeric computation, advanced graphics and visualization, and a high-level programming language. Fig. 4.10 is a graphical user interface of the ControlDesk.

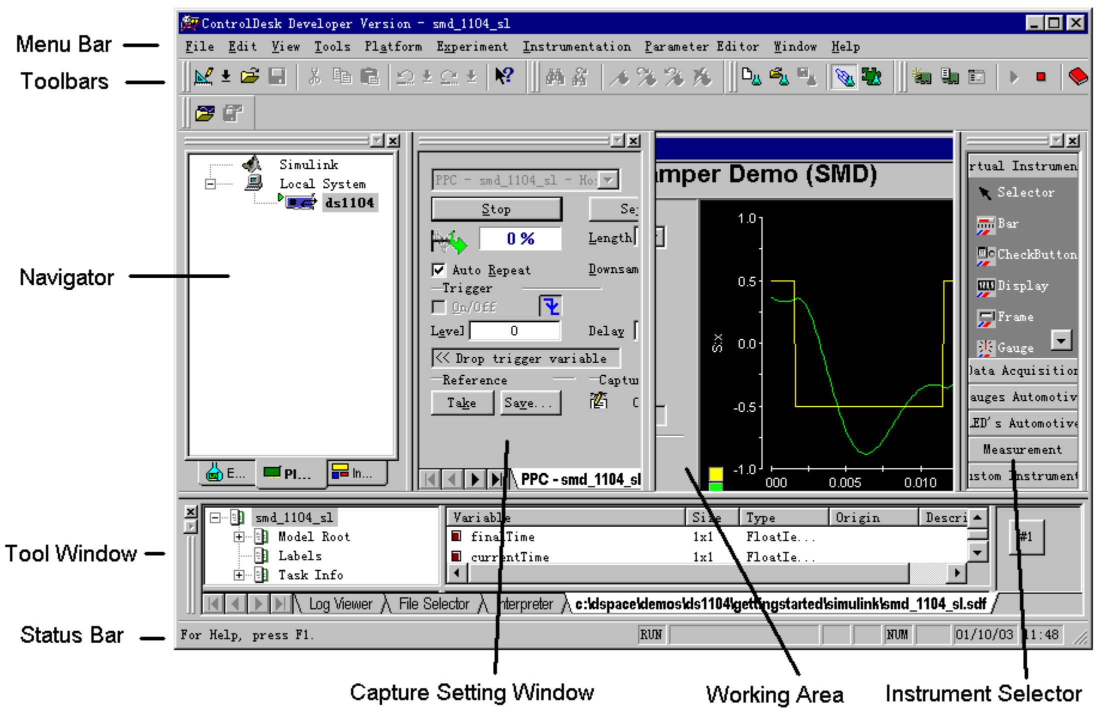

Fig 4.10 A GUI of the ControlDesk.

4.3 Design of Unified Controller

The controller used in the electronic ballast is designed to give sufficient voltage to ignite the lamp, to supply sufficient current for developing 75W, and to keep the constant power control in the steady state to extend the life of the HID lamp. During this process, the control parameters are changed from the voltage and current to the power. From the control point of view, to program different control parameters in different stages makes the programming complex. How to use one parameter to realize all the control functions is the problem to be resolved in this section.

The performance of the EB is decided by the flyback converter because the full-bridge inverter is an unregulated low frequency converter without magnetic components. The circuit being analyzed is shown in Fig. 4.11. The flyback converter is a non-minimum phase system [78] and the direct feedback control of voltage is not feasible [79]. Meanwhile, the lamp power is not measured from the output of the H-bridge circuit. So, the third variable or intermediate variable is considered to do the indirect regulation.

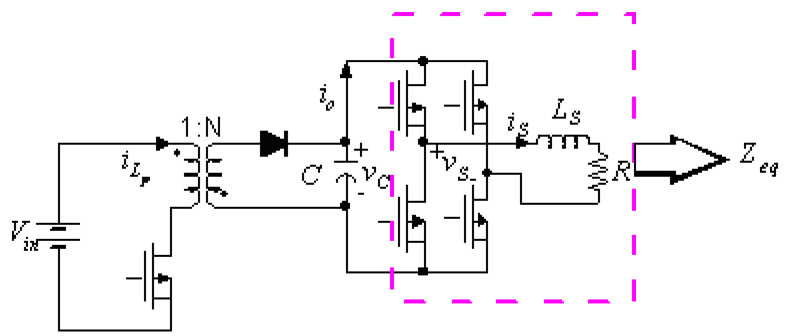

Fig. 4.11 Schematic circuit of real control stage for the electronic ballast

Fig. 4.11 shows the annotation of the current and voltage of the circuit. The current i_{L_p} is chosen as the control variable. The constant voltage, constant current and constant power control can be realized by keeping the inductor current i_{L_p} constant [78]. The model deriving from Fig. 4.11 of the system is given as follows and the model is used for the implementation of the control algorithms:

$$\begin{aligned}\frac{di_{L_p}(t)}{dt} &= \frac{-(1-u(t))}{NL_p}v_C(t)+\frac{u(t)}{L_p}V_{in}\\ \frac{dv_C(t)}{dt} &= \frac{1-u(t)}{NC}i_{L_p}(t)-\frac{1}{Z_{eq}C}v_C(t)\end{aligned} \tag{4.1}$$

where i_{L_p}, v_C denote the inductor current and capacitor voltage in the flyback converter respectively and the current directions are shown in Fig.4.11. u describes the state of the switches taking values in the discrete set {0, 1}. i_S and v_S are current of the inductor L_S and the output voltage of full-bridge inverter, respectively. L_S is the magnetising inductance of the secondary side of the high voltage transformer used in the electronic ballast. R is the equivalent resistance of the lamp. Z_{eq} is the equivalent load impedance of flyback converter. ω_1, d_1 are the switching frequency and duty ratio of H-bridge inverter respectively and ω_1=400Hz, d_1=0.5. The impedance of the inductance L_s is much smaller than the lamp resistance R, and the voltage conversion of the H-bridge inverter is unity. Therefore the input impedance $Z_{eq} \approx R$.

Here, the inductor current i_{L_p} is used as the control variable to do the indirect regulation. The control objective is to regulate the current, voltage and output power to a desired constant value by the same controller in different operational stages. In order to do the comparison, two different control algorithms are examined in detail below.

4.3.1 Linear PI controller

The current mode control used is a two-loop structure. The inner loop senses the inductor current to provide protection against line and load disturbances. The outer loop senses the voltage(current) and uses a PI controller to make it equal to the desired values.

The inner current-loop is designed in the first step. The current signal i is then taken as a virtual control input i_{ref}, and a PI controller is designed to ensure voltage regulation in the sense that $v_C(t) \rightarrow v_{C\,ref}$ asymptotically. This control mode is also called current control mode which is well-known and documented [87-89]. The schematic diagram of the unified controller which can realize the current mode, voltage mode and power mode control is shown in Fig. 4.12 where LUT, the look-up table, is the means to facilitate the constant power control. If constant voltage control is used, the reference voltage V_{ref} is used. If constant current control is used, it is referenced as $i_{o_{ref}}$. The change from constant power control to constant current control has been examined in LUT method [81].

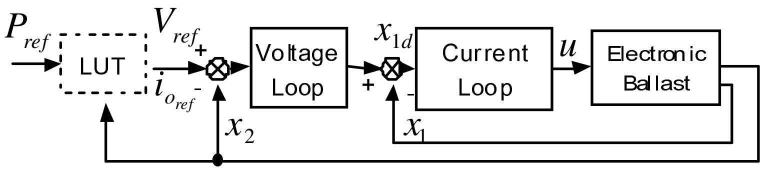

Fig. 4.12 Block diagram of unified controller with two-loop control

The state vector x is chosen as $x = [i_{L_p}, v_C]^T$. Equation (4.1) could be expressed as:

$$\dot{x} = \begin{bmatrix} \dot{x}_1 \\ \dot{x}_2 \end{bmatrix} = \begin{bmatrix} 0 & \dfrac{-(1-u)}{NL_p} \\ \dfrac{1-u}{NC} & -\dfrac{1}{Z_{eq}C} \end{bmatrix} \begin{bmatrix} x_1 \\ x_2 \end{bmatrix} + \begin{bmatrix} \dfrac{u}{L_p} \\ 0 \end{bmatrix} V_{in} \tag{4.2}$$

(1) Current Loop

The function of this loop is to give the control signal for the switch of the flyback converter u and to make the current converge asymptotically. Let us define $x_{1d} = i_{L_p ref}$, $e = x_{1d} - x_1$. The Lyapunov function chosen is: $V = \frac{1}{2}e^2$, and the controller of the current loop is:

$$u = \frac{NL_p}{x_2 + NV_{in}} \left[\dot{x}_{1d} + \alpha\left(x_{1d} - x_1\right) + \frac{1}{NL_p} x_2 \right] \tag{4.3}$$

where α>0 is a user defined parameter.

(2) Voltage Loop

Define the desired voltage to be $V_{ref} = x_{2d}$. The classical PI controller used in the voltage loop is,

$$x_{1d} = K_P\left(x_{2d} - x_2\right) + K_i \int_0^t \left(x_{2d} - x_2\right) dt \tag{4.4}$$

where the proportional and the integral gain K_P and K_i are the parameters of the controller. If the maximum current of the inductor is $x_{1\max}$, the output of (4.4) must meet the need of the limitation, $x_{1d} = \begin{cases} x_{1\max} & x_{1d} > x_{1\max} \\ x_{1d} & x_{1d} < x_{1\max} \end{cases}$.

Combining (4.3), (4.4) and after some algebraic manipulation, the last controller of the current loop is given as (4.5).

$$u = \frac{NL_pC}{C(x_2 + NV_{in}) - K_P L_p x_1} \left[-\frac{K_P}{NC} x_1 + \frac{K_P}{RC} x_2 + K_i\left(x_{2d} - x_2\right) + \alpha\left(x_{1d} - x_1\right) + \frac{1}{NL_p} x_2 \right]$$

(4.5)

If the constant voltage control mode is used, the wanted voltage value is directly given as V_{ref}. If the constant current reference value is i_{oref} control, the value of the wanted voltage is expressed as $x_{2d} = i_{oref} R$ (R is the lamp resistance). The LUT method is used in the constant power control mode shown in Fig. 4.13.

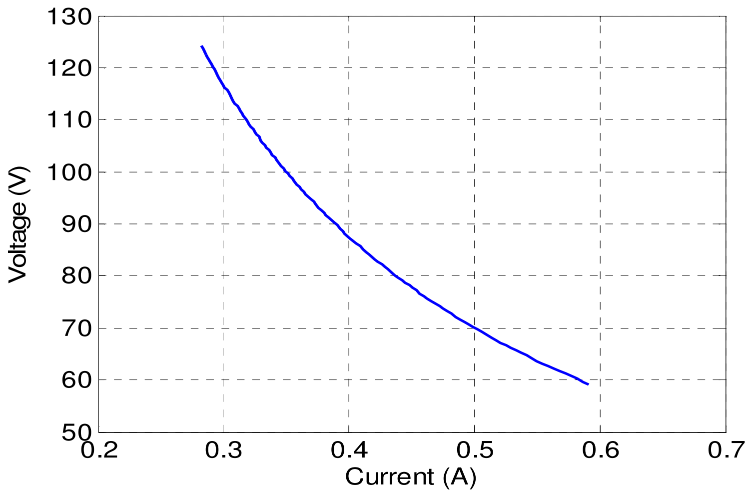

Fig. 4.13 The LUT used in the constant power control mode

According to PWM-controller law, the values of u could be specified as duty ratio function μ with a bound of [0, 1], i.e. $\mu \in [0 \quad 1]$. The average state vector z is chosen, and the average state variable could be obtained by a low pass filter. The methods for selecting the control parameters, K_p, K_i, are based on an empirical mechanism and trial-and-error. Other example of selection can also be refereed to reference [129].

4.3.2 Nonlinear Adaptive controller

In this section, the adaptive feedback regulation scheme for PWM controlled system is proposed with average model. For the same reasons as mentioned above, the control variable used here is also the inductor current z_1. The state vector z is chosen as $z = [i_{L_p}\sqrt{L_p}, v_C\sqrt{C}]^T$. The equation (4.1) can be rewritten as [90]:

$$
\begin{aligned}
\dot{z}_1 &= -\frac{1-\mu}{N}\omega_0 z_2 + ub \\
\dot{z}_2 &= \frac{1-\mu}{N}\omega_0 z_1 - \omega_1 z_2
\end{aligned}
\tag{4.6}
$$

where $\omega_0 = 1/\sqrt{L_p C}$, $\omega_1 = 1/(RC)$, $b = V_{in}/\sqrt{L_p}$

Fig. 4.14 shows the control scheme of this controller.

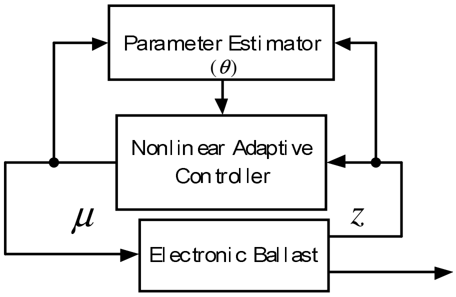

Fig. 4.14 The adaptive controller scheme

The ballast system equations can be expressed as:

$$\dot{z} = \theta_1^{\ 1} f_1(z) + \theta_2^{\ 1} f_2(z) + \mu[\theta_1^{\ 2} g_1(z) + \theta_2^{\ 2} g_2(z)] \tag{4.7}$$

where: $\omega_0 / N = \theta_1^{\ 1}$, $\omega_1 = \theta_2^{\ 1}$, $\theta_1^{\ 2} = \omega_0 / N$, $\theta_2^{\ 2} = b$, $f_1(z) = \begin{bmatrix} -z_2 \\ z_1 \end{bmatrix}$, $f_2(z) = \begin{bmatrix} 0 \\ -z_2 \end{bmatrix}$,

$g_1(z) = \begin{bmatrix} z_2 \\ -z_1 \end{bmatrix}$, $g_2(z) = \begin{bmatrix} 1 \\ 0 \end{bmatrix}$.

If the wanted voltage value is Z^* and duty ratio $\mu=U$, according to (4.6), the indirect regulation is obtained as: $z_{1d} = \dfrac{U\theta_2^{\ 1}\theta_2^{\ 2}}{\left(\theta_1^{\ 1} - U\theta_1^{\ 2}\right)^2}$, $z_{2d} = Z^* = \dfrac{U\theta_2^{\ 2}}{\theta_1^{\ 1} - U\theta_1^{\ 2}}$. Define the error to be:

$$e = h(z) = z_1 - z_{1d} = z_1 - \theta_1^{\ 3} z_{2d} - \theta_2^{\ 3} z_{2d}^{\ 2} \tag{4.8}$$

where $\theta_1^{\ 3} = \dfrac{\theta_2^{\ 1}}{\theta_1^{\ 1}}$, $\theta_2^{\ 3} = \dfrac{\theta_2^{\ 1}\theta_1^{\ 2}}{\theta_1^{\ 1}\theta_2^{\ 2}}$. Then the input current state equation could be obtained from an asymptotically stable behaviour:

$$\dot{z}_1 = -\alpha[z_1 - z_{1d}] = -\alpha\left[z_1 - \theta_1^{\ 3} z_{2d} - \theta_2^{\ 3} z_{2d}^{\ 2}\right] \tag{4.9}$$

with $\alpha > 0$ which is a user selected value. The average adaptive controller can be obtained by the estimated values of the actual parameters:

$$\mu = \frac{\hat{\theta}_1^{\ 1} z_2 - \alpha\left[z_1 - \hat{\theta}_1^{\ 3} z_{2d} - \hat{\theta}_2^{\ 3} z_{2d}^{\ 2}\right]}{\hat{\theta}_1^{\ 2} z_2 + \hat{\theta}_2^{\ 2}} \tag{4.10}$$

where $\dot{\hat{\theta}}_1^{\,1} = -z_2 e$, $\dot{\hat{\theta}}_2^{\,1} = 0$, $\dot{\hat{\theta}}_1^{\,2} = \mu z_2 e$, $\dot{\hat{\theta}}_2^{\,2} = \mu e$, $\dot{\hat{\theta}}_1^{\,3} = -\alpha z_{2d} e$, $\dot{\hat{\theta}}_2^{\,3} = -\alpha z_{2d}{}^2 e$.

If the constant control mode is used, the wanted voltage Z^* is equal to the V_{ref}. The controller could be used in the constant voltage control stage directly. If the system comes to the constant current stage whose wanted current is z_{1d}, then: $Z^* = z_{1d} R$. If the system comes to the constant power stage whose desired power is P^*, then: $Z^* = \sqrt{P^* R}$. This adaptive controller could be used and the parameter of the controller could be adjusted automatically. So, the different stages of the system can be controlled by using just one controller.

The two-loop PI controller is used to verify the feasibility of the proposed electronic ballast. Here the controller is realized by digital control method (but in microprocessor based EB, the PI controller is realized by the drive chip using the analogue circuit). The nonlinear adaptive controller is an improved method which is also realized by digital control method.

4.4 Simulation results of Unified Controllers

The parameters of the system are given in Table 4.6. The switching frequency of the flyback converter is 100 kHz.

Table 4.6 Electronic ballast and lamp profile

	Notation	Values	Unit
Inductance of primary winding in Flyback converter	L_p	10	μH
Capacitance in Flyback converter	C	5.6	μF
Inductance of secondary winding in Full-bridge converter	L_S	0.6	mH
Turns ratio	N	7	-
Input voltage	V_{in}	12	V
Switching frequency of Full-bridge converter	f_l	400	Hz

4.4.1 Response of Control mode change

The different control modes are tested to verify the unified controller. The constant voltage control is the first stage. The wanted voltage is 350V in order to ignite the lamp; then comes to the constant current stage, and the required output current of the flyback converter is 1.5A. The last one is the constant power control stage, with 35W wanted power.

Figs. 4.15 and 4.16 show the simulation results of the two-loop PI controller (control parameters K_p=10, K_i=0.1, α=1) and adaptive controller. In these figures, Constant Voltage Control is abbreviated as CVC; Constant Current Control as CCC and Constant Power Control as CPC. It is clear that the two controllers can realize the control and reach required values after a short transient.

The output voltage of the lamp is around 300V during the CCC mode because the lamp resistance is 200Ω; but in real experiment, the output voltage is far less than this value because the lamp resistance is around several tens of ohms. In simulation, the average state of EB system using the two-loop PI controller can be realized by using discrete filter arithmetic: $\begin{matrix} z_1(i) = (1-\gamma)z_1(i-1) + \gamma x_1(i) \\ z_2(i) = (1-\gamma)z_2(i-1) + \gamma x_2(i) \end{matrix}$ and $\gamma = 1 - e^{-T/T_f}$, $i = 0,1,\cdots$. T is the sampling period and T_f is the time constant of low pass filter. The value γ=0.1 is selected.

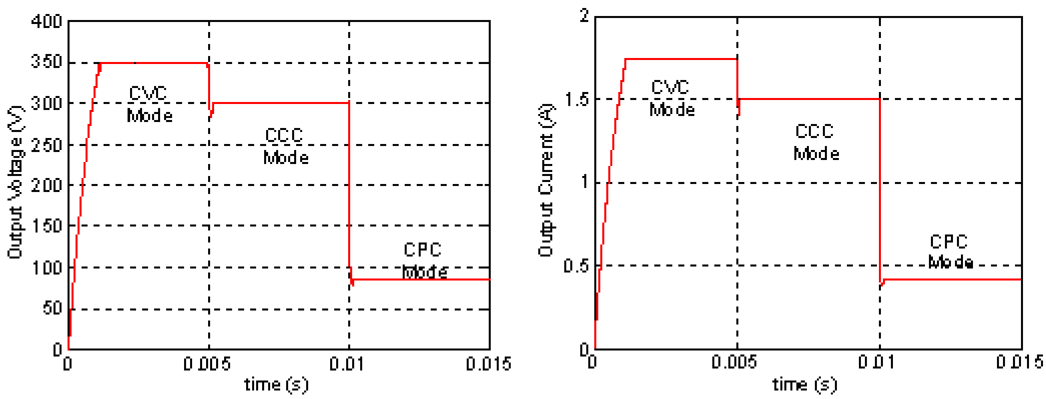

(a) (b)

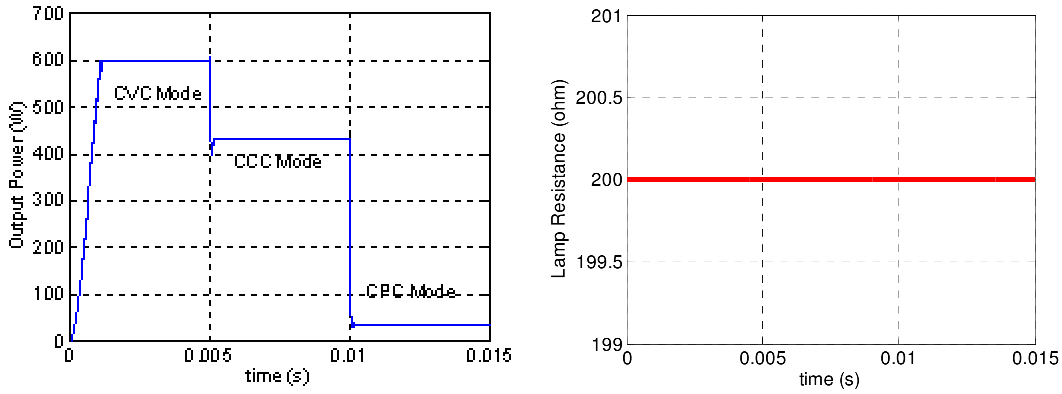

(c) (d)

Fig. 4.15 Simulation results of two-loop PI controller for control mode change (a) output voltage (b) output current (c) output power (d) lamp resistance

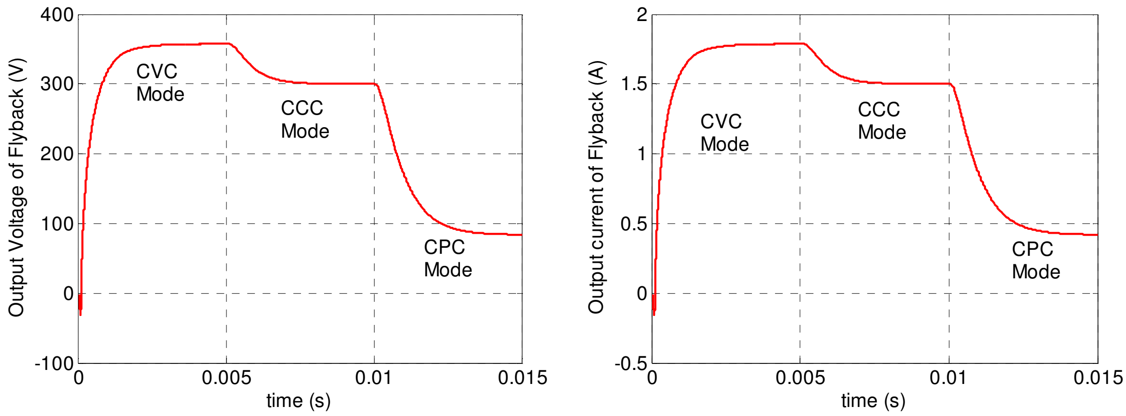

(a) (b)

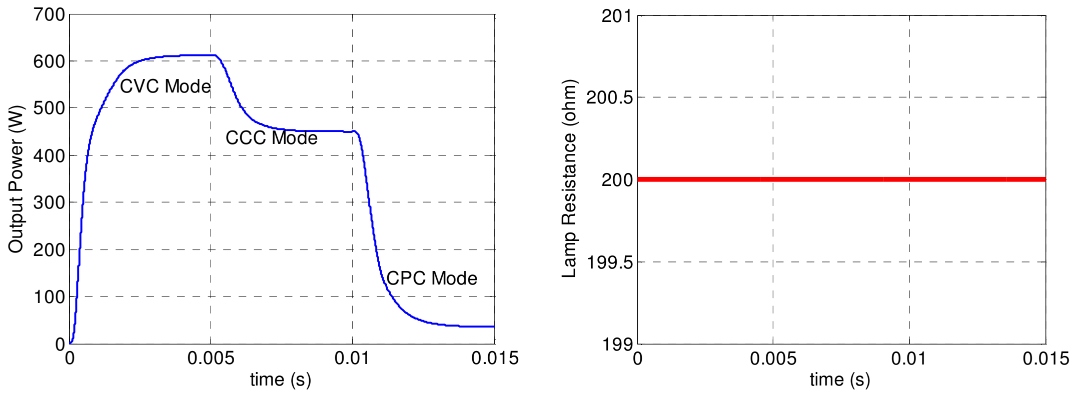

(c) (d)

Fig. 4.16 Simulation results of adaptive controller for control mode change (a) output voltage (b) output current (c) output power (d) lamp resistance

4.4.2 Response of Lamp Resistance Change

When the lamp resistance changes from 200Ω to 400Ω, the adaptive controller can realize the control of CVC mode, CCC mode and CPC mode(as seen from Fig. 4.18). Except the overshoot and ripple in the simulation results (shown in Fig. 4.17), the parameters of two-loop PI controller will be adjusted in order to get a good control effect. When lamp resistance R=200Ω, K_p=10 and K_i=0.1. When R=400Ω, K_p=5 and K_i=0.4. If the lamp resistance changes to 400Ω, the adaptive controller could realize different control modes which just need a long (around 10ms) adjusting time.

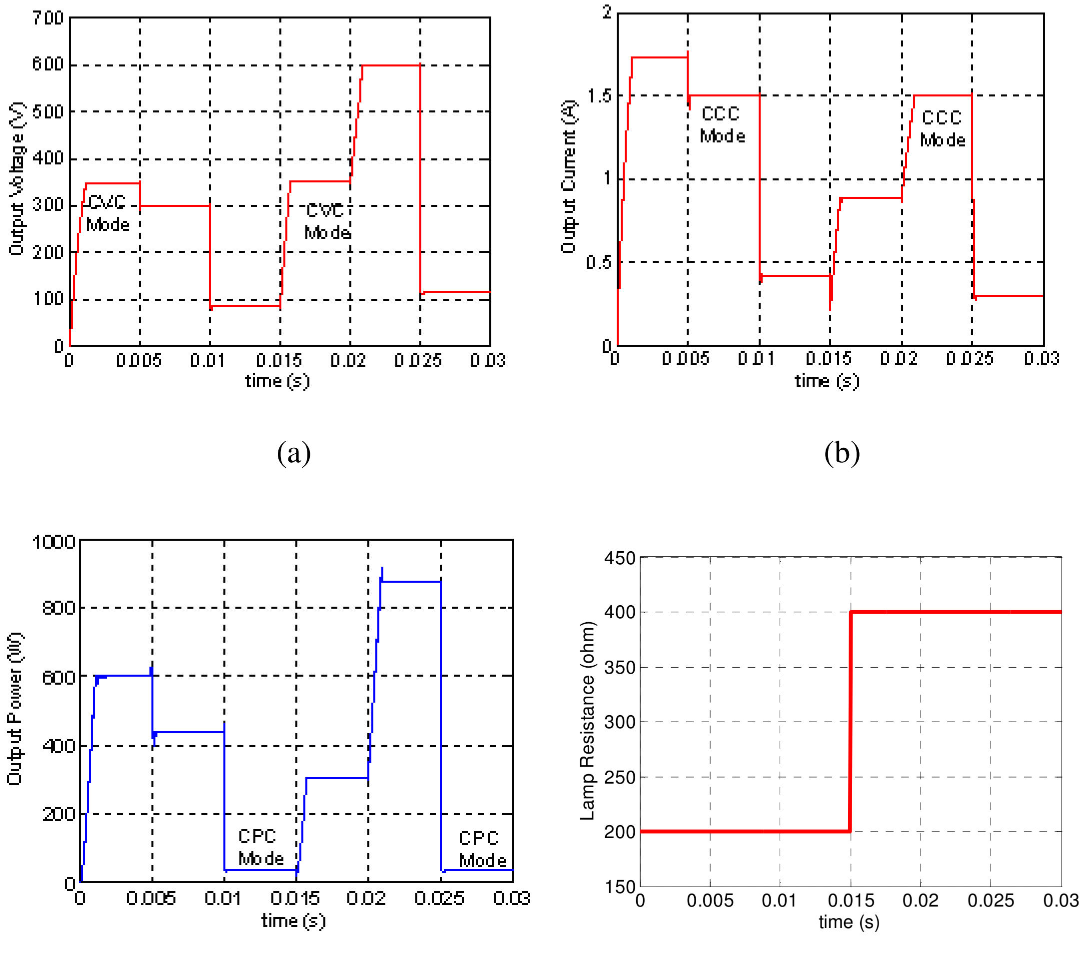

(a) (b) (c) (d)

Fig. 4.17 Simulation results of two-loop PI controller for lamp resistance variations of 100% (a) output voltage (b) output current (c) output power (d) lamp resistance

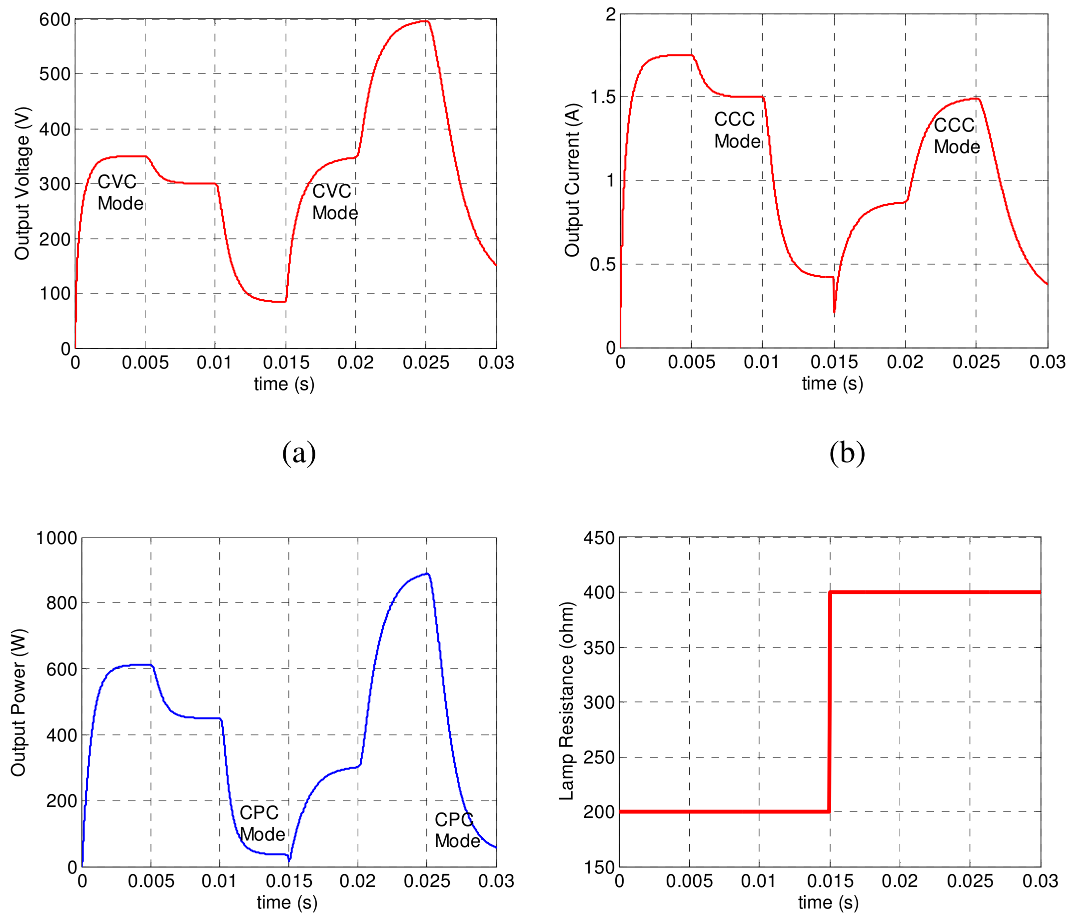

(a) (b)

(c) (d)

Fig. 4.18 Simulation results of adaptive controller for lamp resistance variations of 100%

(a) output voltage (b) output current (c) output power (d) lamp resistance

4.4.3 Response of System parameter Change

(1) Change of Capacitor Value

When the value of the capacitor changes from 5.6μF to 2.8μF and the lamp resistance is 200Ω, the adaptive controller can follow the control mode change of the system, but the adjusting time of the system will be affected (as seen from Fig. 4.20). As in the case of the lamp resistance change, if the control parameters change to K_p=5, K_i=0.3 and the capacitor value is changed, the performance of two-loop PI controller is not affected (as seen from Fig.4.19).

In addition, the voltage ripple and current ripple are increased, so does the ripple of lamp power. Fig. 4.21 shows the change of the ripple of lamp voltage and lamp current using the two-loop PI controller. The corresponding simulation results for the adaptive controller are not shown because they are similar.

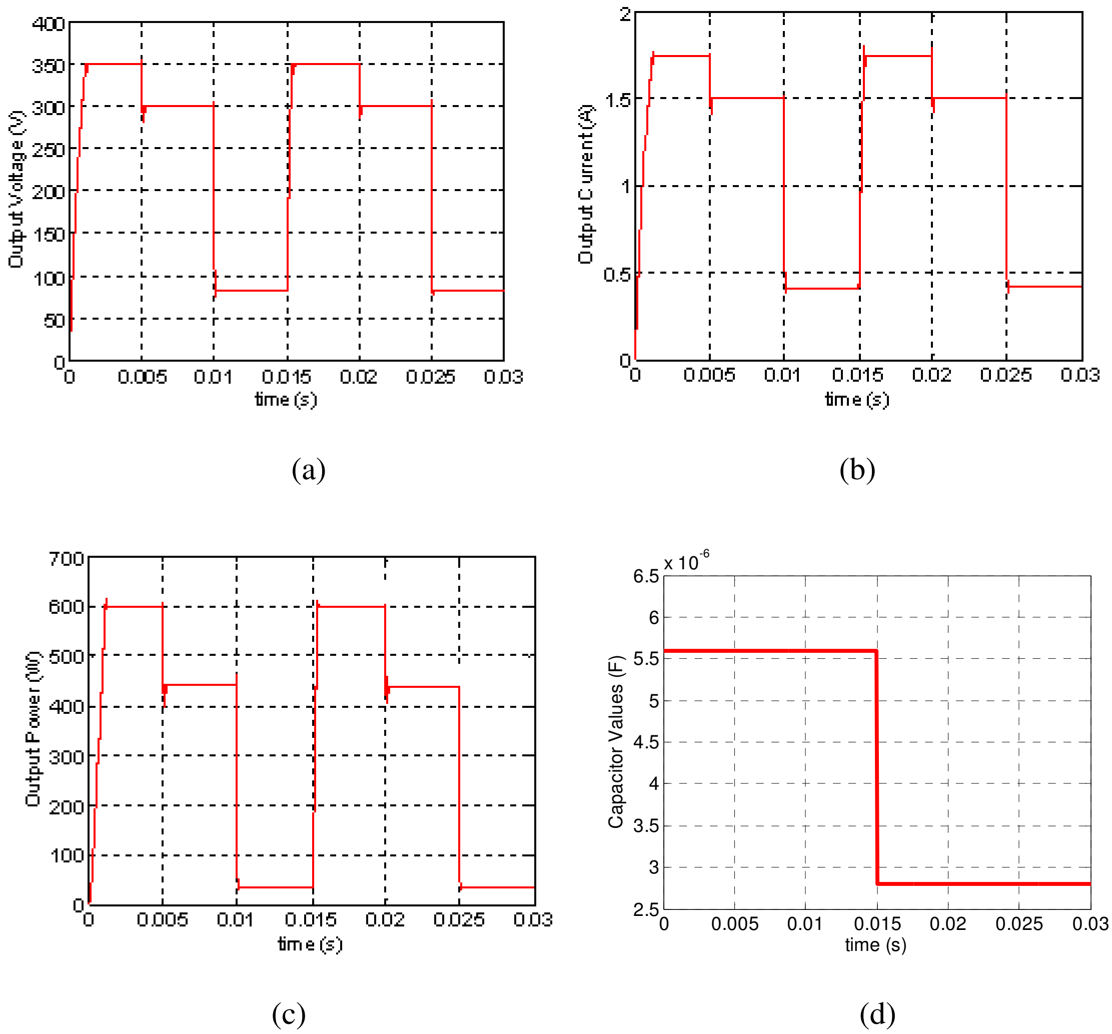

Fig. 4.19 Simulation results of two-loop PI controller for capacitor value variations of 100% (a) output voltage (b) output current (c) output power (d) capacitor value

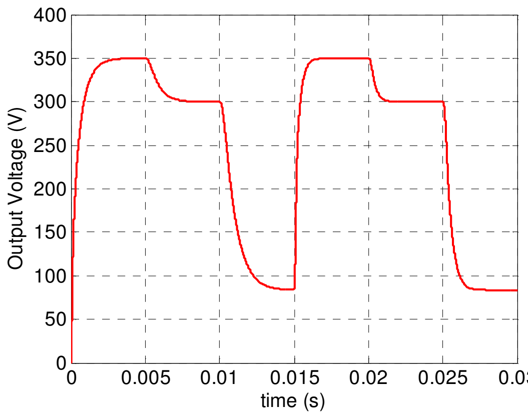

(a)

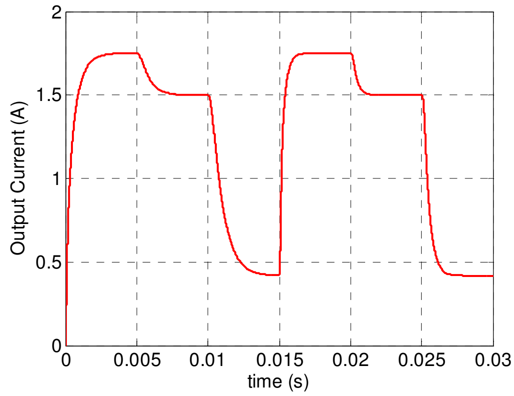

(b)

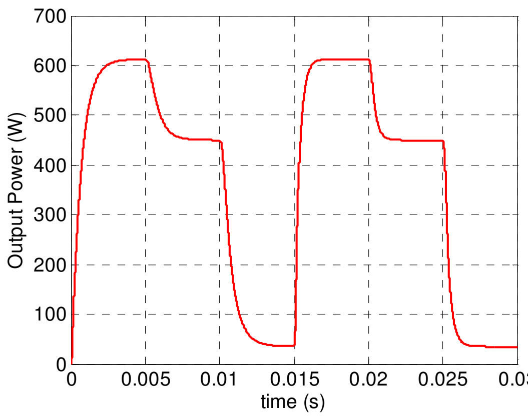

(c)

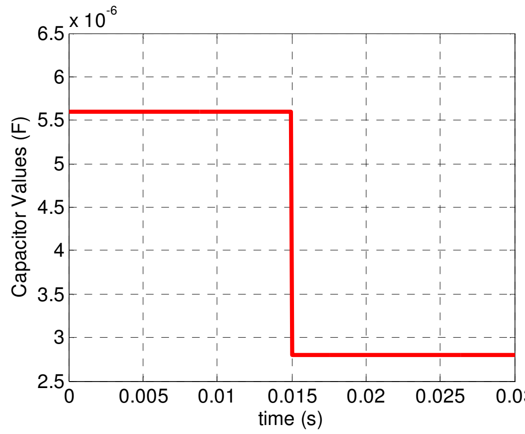

(d)

Fig. 4.20 Simulation results of adaptive controller for capacitor value variations of 100% (a) output voltage (b) output current (c) output power (d) capacitor value

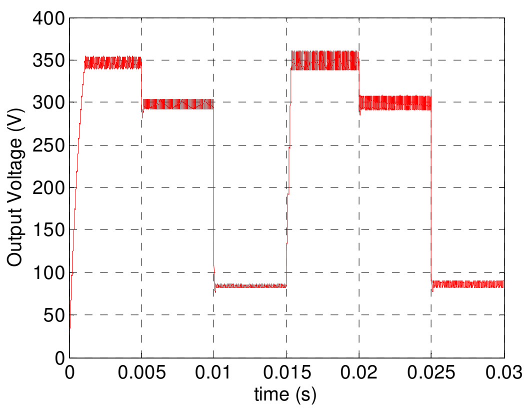

(a)

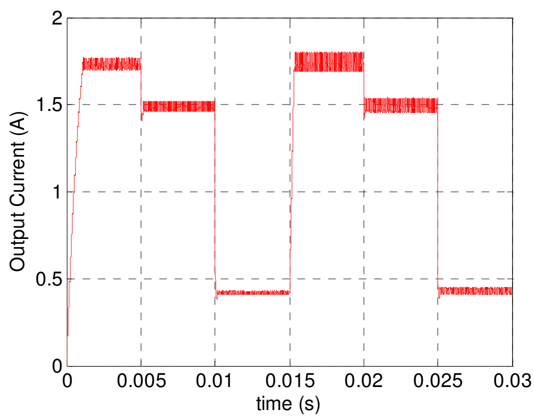

(b)

Fig. 4.21 Simulation results for ripple change (a) output voltage (b) output current

(2) Change of Inductor Value

When the value of the capacitor changes from 2.5μH to 1.25μH and the lamp resistance is unchanged at 200Ω, there is no change in the performance of the system in terms of voltage, current and power in the adaptive controller (as seen in Fig. 4.23). The control parameters used in two-loop PI controller change to K_p=8, K_i =0.5 and good simulation results are obtained (as seen from Fig. 4.22).

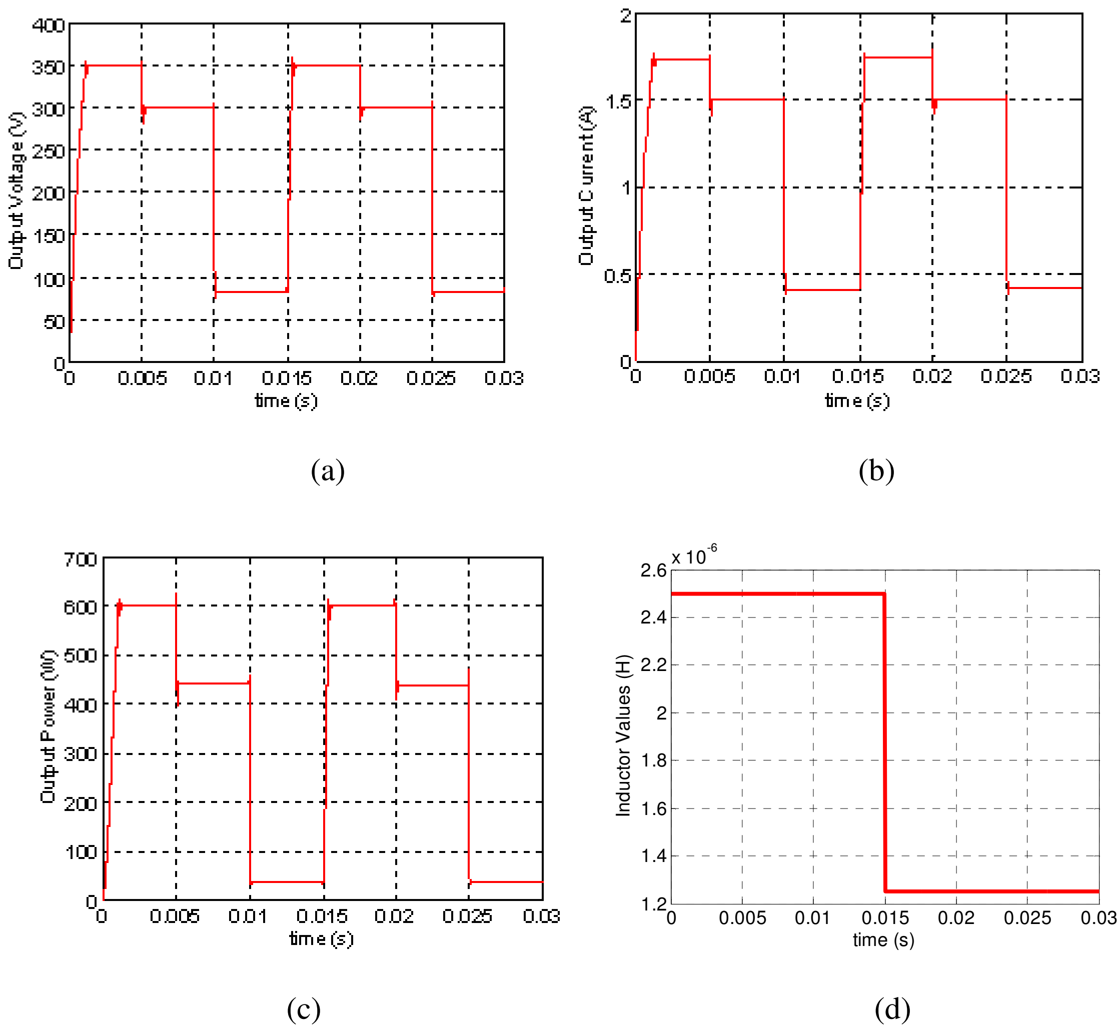

(a) (b) (c) (d)

Fig. 4.22 Simulation results of two-loop PI controller for inductor value variations of 100%

(a) output voltage (b) output current (c) output power (d) inductor value

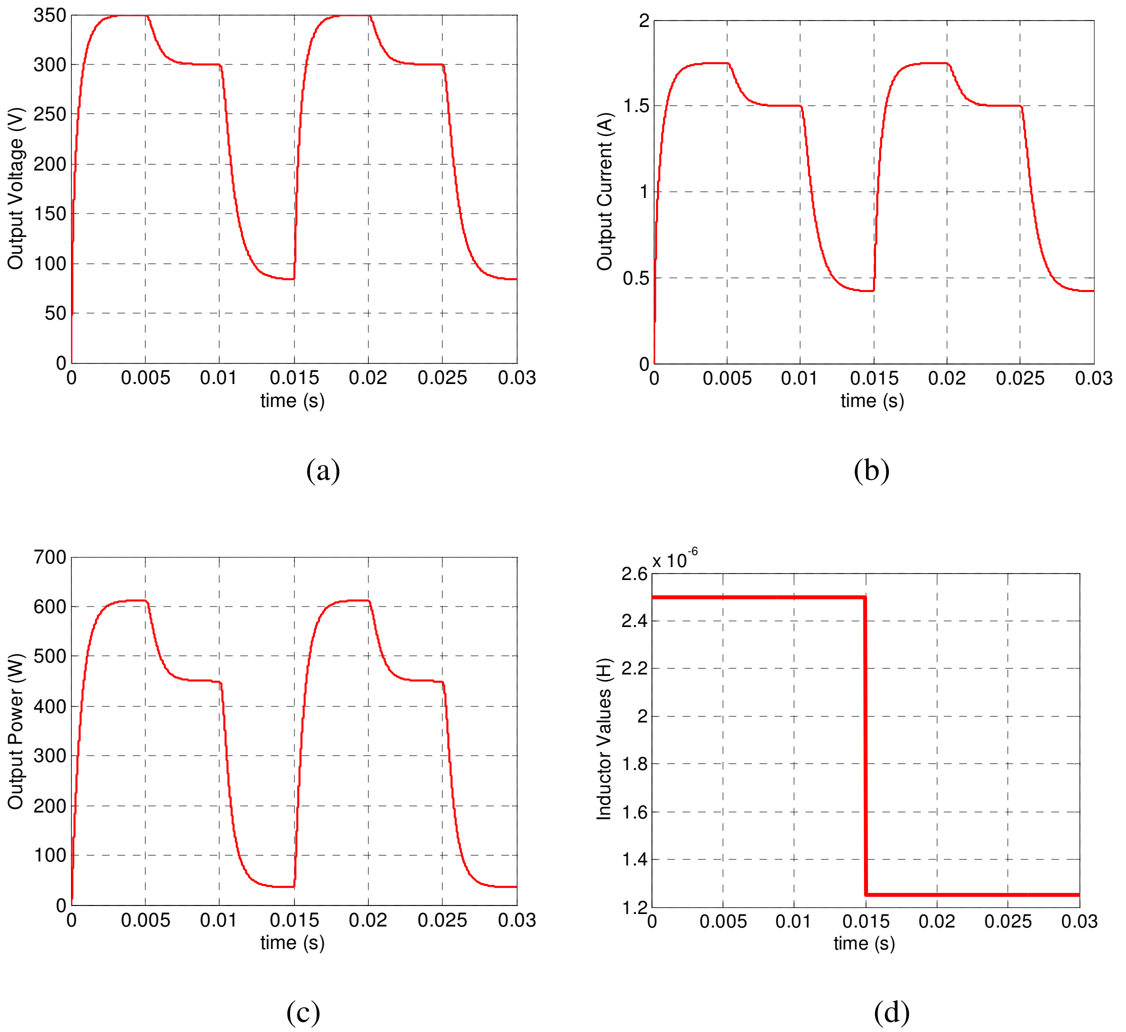

Fig. 4.23 Simulation results of adaptive controller for inductor value variations of 100% (a) output voltage (b) output current (c) output power (d) inductor value

(3) Change of Input Voltage

The robustness to the change of input voltage is tested here. If the input voltage changes from 9V to 16V and the lamp resistance is 200Ω in this time, both controllers could realize all the functions (as shown in Fig. 4.24 and 4.25).

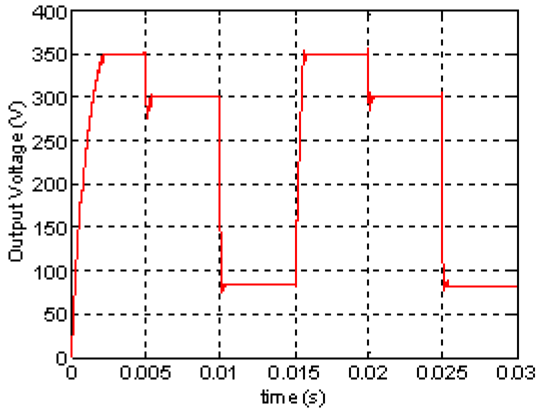

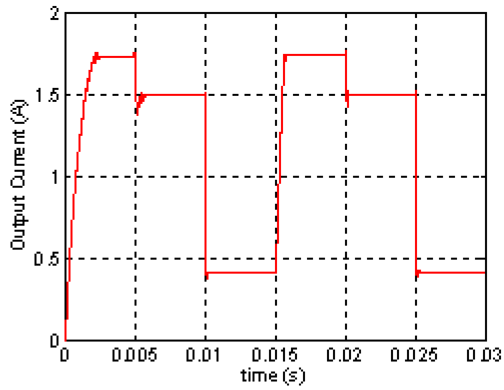

(a) (b)

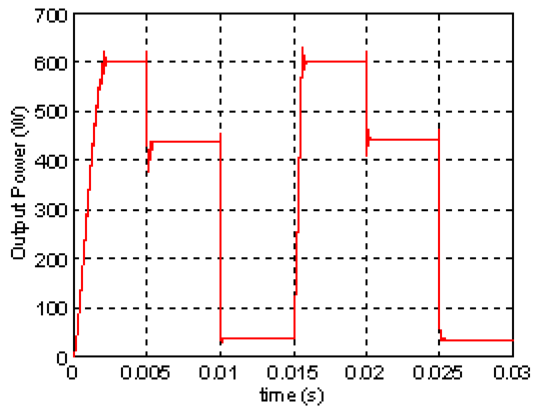

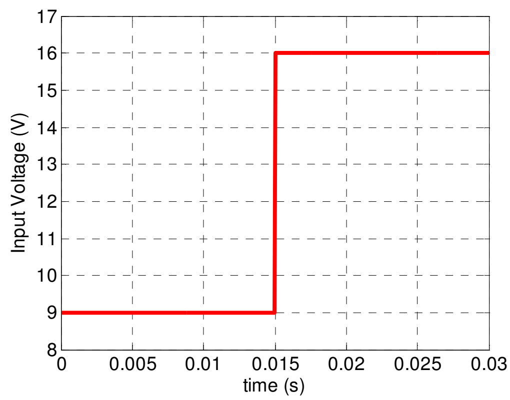

(c) (d)

Fig. 4.24 Simulation results of two-loop PI controller for input voltage variations from 9V to 16V (a) output voltage (b) output current (c) output power (d) input voltage

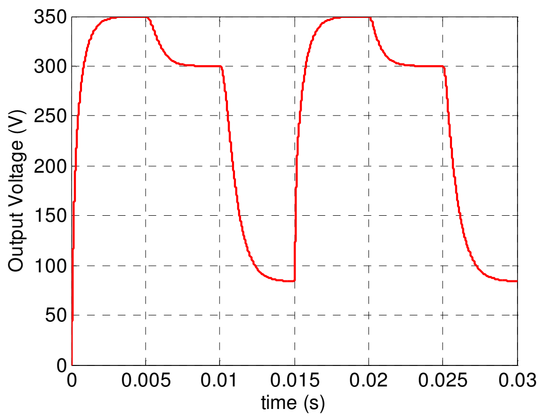

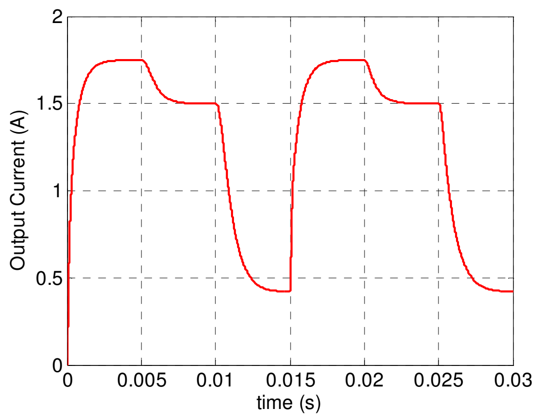

(a) (b)

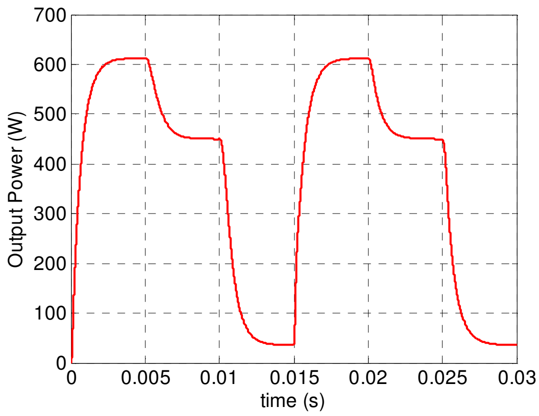

(c)

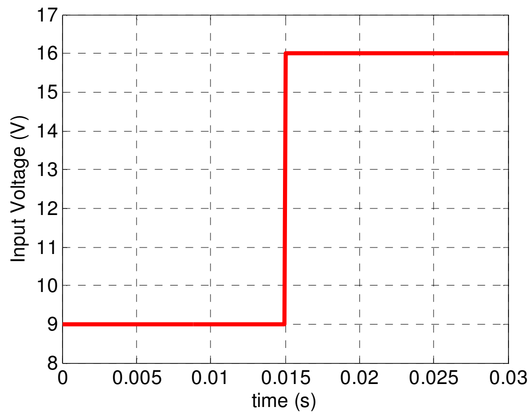

(d)

Fig. 4.25 Simulation results of adaptive controller for input voltage variations from 9V to 16V (a) output voltage (b) output current (c) output power (d) input voltage

4.5 Experimental Results

The simulation results show that the unified controller is feasible under the condition that the equivalent lamp resistance is 200Ω for a new lamp and 400Ω for an old lamp.

But for a real lamp, the equivalent lamp resistance change from several ohms to hundred ohms (given in chapter 3), the software design in DS1104 is not simple as a unified controller used in the simulation. The flow chart of DS1104 based controller is given in Fig. 4.26.

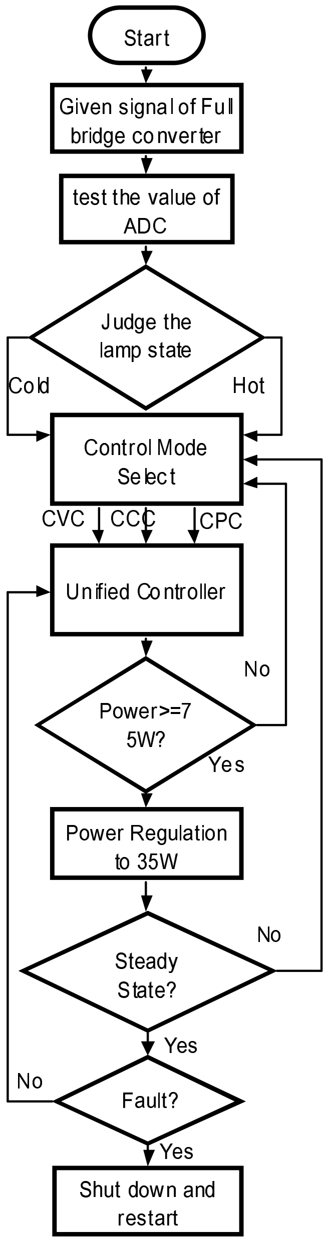

Fig. 4.26 Flow chart of DS1104 based controller

There are four different stages in the operation of an HID lamp: voltage control mode, current control mode, power control mode and constant power mode. At start-up, the voltage of the DC converter builds up to 300V (the breakdown voltage of SG is 600V) and the converter is said to be in the voltage control mode. After the lamp is ignited, the lamp is supplied with a steady current of about 2A to satisfy the SAE standard and this mode is the current mode control. The lamp then enters into variable power mode when the power of the lamp is about 75W and is gradually reduced to the steady state value of 35W. The ballast reaches its last stage when the lamp power is maintained at a steady value of 35W resulting in constant power mode. The software detects all the transitions by sensing the lamp current and voltage, and precisely generates the control signal to all the switches in the circuit. Due to the complex flow chart, the S-function of Matlab is used in the experiment.

4.5.1 Comparison between PI controller and adaptive controller

The two-loop PID controller and nonlinear adaptive controller are used in the electronic ballast. The HID lamp used in this application is a 35W D2S (Philips). Fig. 4.27 shows the experimental result using the two-loop PID controller and Fig. 4.28 is the experimental result of adaptive controller. These two controllers could ignite the lamp and it is feasible to use them in the electronic ballast. Furthermore, with the lamp ageing (the equivalent lamp resistance increases), the time for the lamp to go to the steady state increases. Table 4.7 shows the different time for the new lamp or old lamp based on the two-loop PI controller and the adaptive controller. It is clear that the transient time of the EB based on adaptive controller is shorter than that of the EB based on the two-loop PI controller. The waveforms of the EB based on adaptive controller are presented in the following sections, and the waveforms based on PI controller are not shown because of similarity.

Table 4.7 Time needed from the lamp start to its steady state

	New lamp	Old lamp
Two-loop PI Controller	109s	178s
Adaptive Controller	90s	118s

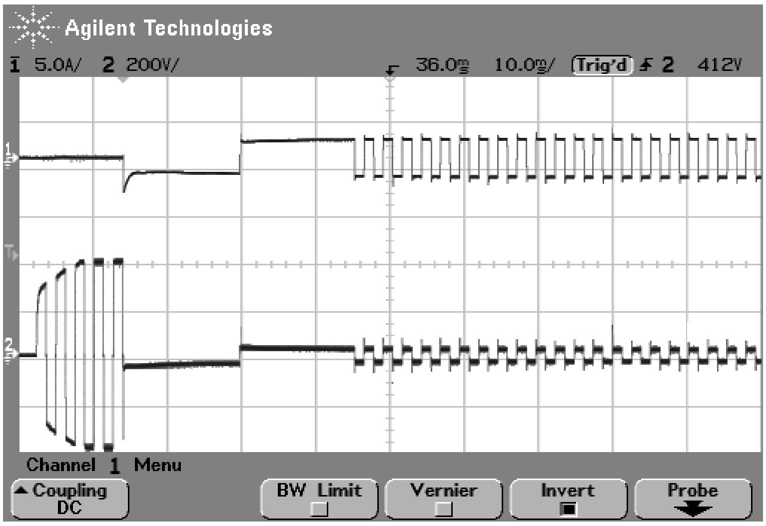

Fig. 4.27 Lamp voltage and current waveform using PI controller (ch2: lamp current, 5A/div, 10ms/div; ch1: lamp voltage, 200V/div, 10ms/div)

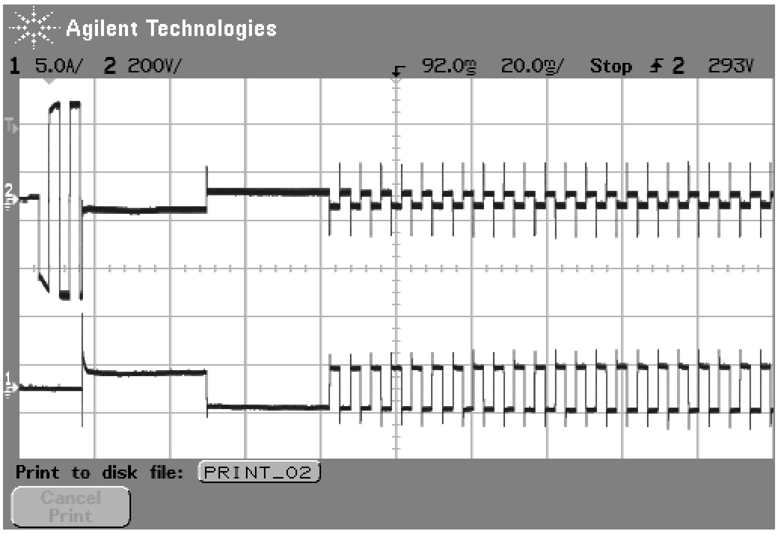

Fig. 4.28 Lamp voltage and current waveform using adaptive controller (ch1: lamp current, 5A/div, 10ms/div; ch2: lamp voltage, 200V/div, 10ms/div)

4.5.2 Waveforms of the EB based on adaptive controller

A test is then performed to measure the system performance of the EB in cold and hot start. Fig. 4.29 gives the lamp current and voltage waveforms when the lamp is in cold start. Fig. 4.30 shows the waveforms when the lamp is in hot start. The adaptive controller based EB could work well in different required conditions.

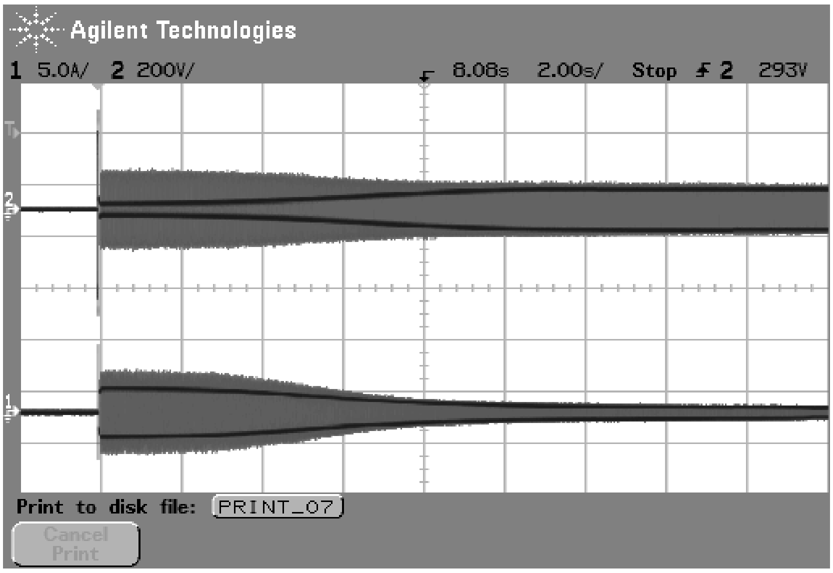

Fig. 4.29 lamp voltage and current waveform in cold start (ch1: lamp current, 5A/div, 10ms/div; ch2: lamp voltage, 200V/div, 10ms/div)

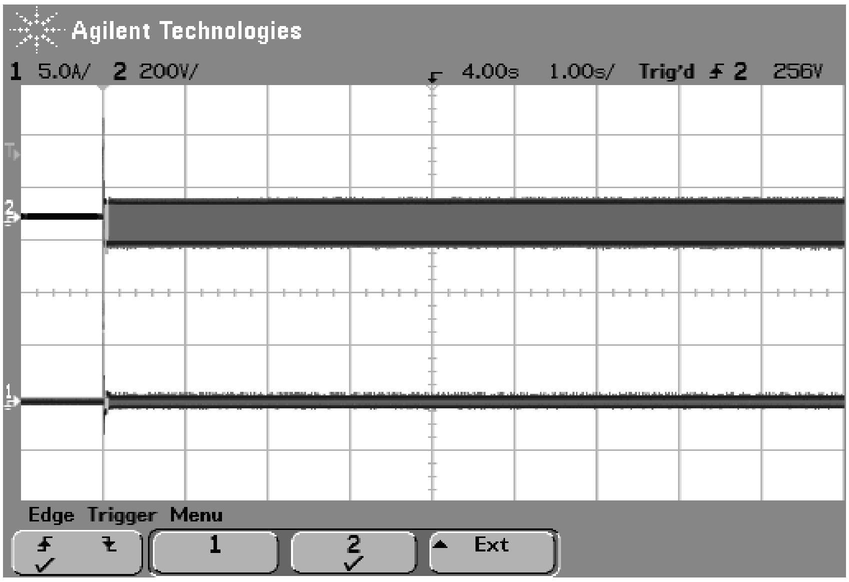

Fig. 4.30 Lamp voltage and current waveform in hot start (ch1: lamp current, 5A/div, 10ms/div; ch2: lamp voltage, 200V/div, 10ms/div)

The waveforms from Fig. 4.31 to Fig. 4.33 show the system robustness of the EB. The capacitor value, inductance value and the input voltage are changed respectively. The experimental results show that the performance of the system would not be deteriorated, even if the value of parameter, the output capacitor or the inductor is changed. Fig. 4.31 shows the waveforms when the capacitor value is 2.8μF. Fig. 4.32 shows the waveforms when the inductor value is 1.25μH. If the input voltage changed from 12V to 16V, the electronic ballast based on adaptive controller could work in good condition. Fig. 4.33 shows the waveforms when the input voltage is 16V.

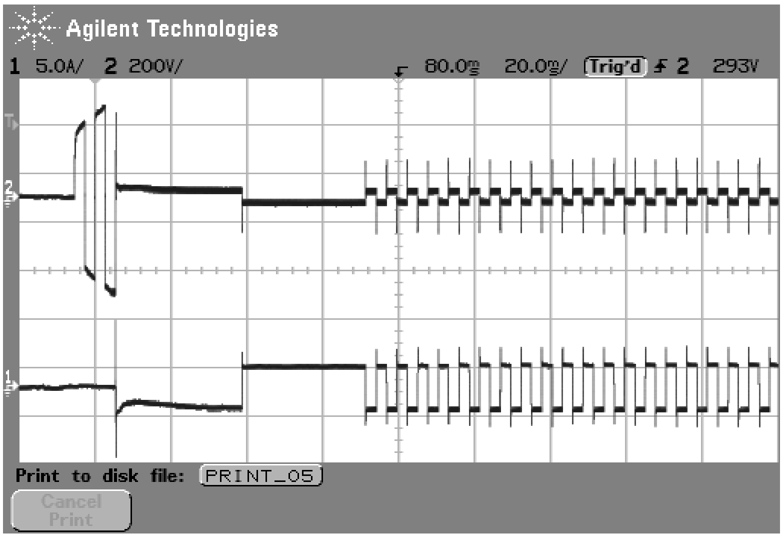

Fig. 4.31 Lamp voltage and current waveform using adaptive controller when capacitor value increased to twice of the initial system (ch1: lamp current, 5A/div, 10ms/div; ch2: lamp voltage, 200V/div, 10ms/div)

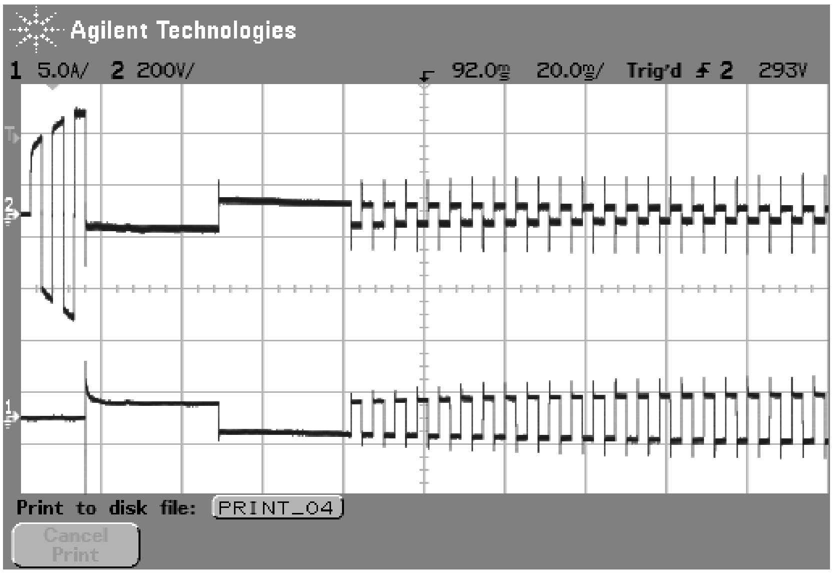

Fig. 4.32 Lamp voltage and current waveform using adaptive controller when inductor value increased to twice of the initial system (ch1: lamp current, 5A/div, 10ms/div; ch2: lamp voltage, 200V/div, 10ms/div)

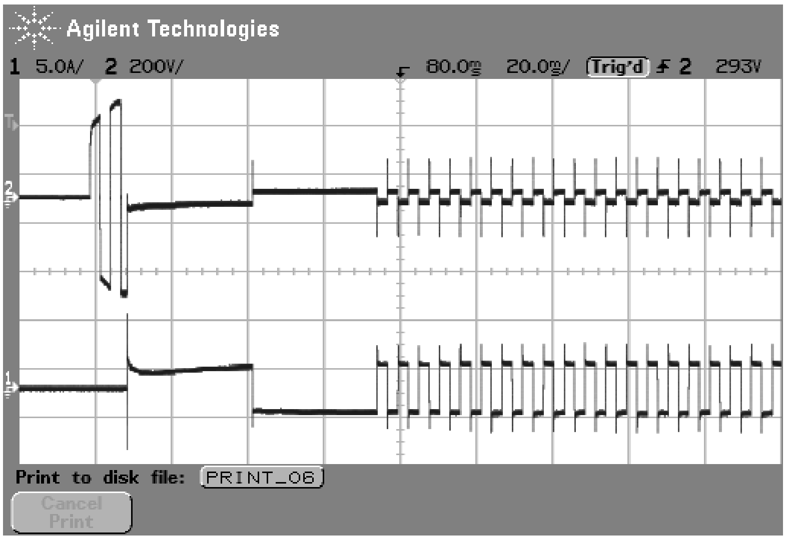

Fig. 4.33 Lamp voltage and current waveform using adaptive controller when input voltage is 16V (ch1: lamp current, 5A/div, 10ms/div; ch2: lamp voltage, 200V/div, 10ms/div)

4.6 Summary

In this chapter, the dSPACE card- DS1104 is used to develop a new electronic ballast and a unified indirect controller is designed to regulate the voltage, current and power of the electronic ballast of HID lamp used in the automotive headlight system. The hardware realization of the proposed electronic ballast is first presented. In order to give a unified controller used in this system, the system is analyzed by using two different controllers, the two-loop PI controller and nonlinear robust controller. The simulation and experimental results show that the proposed unified controller is a good solution under the variation of the voltage, current and power control in electronic ballast system. This controller has better performance in the response and the proposed electronic ballast is effective in performance.

The unified controller is robust which would not vary with the variation of system parameters and lamp resistance in different control modes. If the PI controller with fixed control parameters is used in an HID lamp, the time for the lamp to go to the steady state is longer than that in the adaptive controller. In addition, with the lamp ageing, the time for the lamp to go to the steady state in the PI controller based EB also longer than that in the adaptive based EB. The above study has confirmed that adaptive control is feasible and is a better method for EB implementation.

Chapter 5

Research on Adaptive Passivity-based Indirect Constant Power Controller

5.1 Introduction

With the exception of the difficulty of hot re-strike [73, 91] and low efficiency, the constant power control is also one of the needs in designing of the electronic ballast as it can extend the lamp life. The output power is not available for measurement that makes the problem complicated. Further, the lamp resistance is unknown and it would change with lamp ageing.

PBC (Passivity-based Control) is a controller design approach with “energy shaping” and “damping injection” [78]. When a PBC controller is designed, a desired energy function is first selected. According to the properties of passive physical systems, the energy of the system is clearly non-increasing, thus the convergence of the energy function can be increased by increasing the system damping through control methods. The models presented in PCH (port-controlled Hamiltonian) [92] equations or EL (Euler-Lagrange) equations [93], which encompass very large classes of physical nonlinear systems, are easily used to establish the PBC controller. PBC methods have been applied successfully in UPS [78] and DC-to-DC converter [94] in power electronics. All these application results show that the PBC could make the system more robust. In this chapter, the PBC is used to explore the regulation of the constant output power.

5.2 Review of Constant Power Control used in HID Lamp System

There are two objectives to use constant power control in steady state of the HID lamp. The first one is to keep the illumination output of the lamp constant. The difference in lamp power will cause a change in the illumination. The second one is to extend the lamp life span. The ageing of the lamp will cause the increase of lamp voltage which would damage the lamp.

To achieve constant power control, one simple method to consider first is the DPR (Direct Power Regulation), as seen from Fig. 5.1. The output power is used as the feedback parameter, but a multiplier must be used. The multiplier is difficult to use because of its large computation time, hence it is not accepted in the products. Both the lamp voltage and the lamp current could be taken as the feedback parameters [95-97]. The two loop structure, shown in Fig. 5.2 is based on the power curve and the relationships between the lamp voltage and lamp current, but it is too complicated with high cost. The easiest control method is to use LUT (Lookup Tables), as shown in Fig. 5.3. This method can increase the feedback speed, but it needs large memory storage.

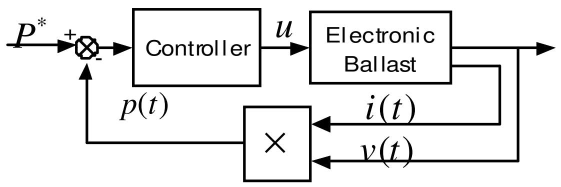

Fig. 5.1 Direct power regulation

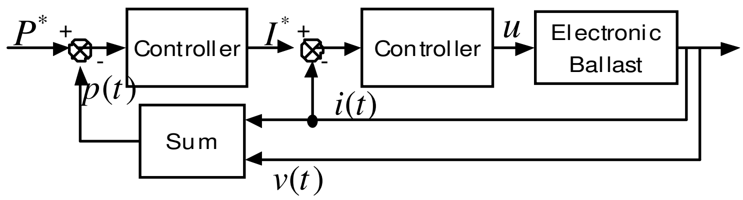

Fig. 5.2 Block diagram of two loop structure

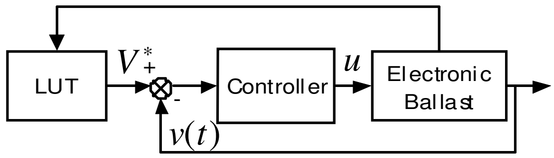

Fig. 5.3 LUT control method

The PLL (phase-locked loop) is also used for constant power control [98] in Metal Halide (MH) lamp system. Due to the characteristic of the non-minimum phase system, the electronic ballast is easy to be unstable. The controller based on the linearization model [99] will deviate from the operation point with the ageing of the lamp (it means the classical PI controller is valid only for region near to operation point), which also makes the system prolong the transient into steady state. These are all the problems to be solved by the controller designer. In the next section, a PBC controller based on the energy functions will be introduced, in order to guarantee the global stability of the system.

5.3 Passivity and average model of EL system

5.3.1 Passivity and dissipativity

The concept of energy is one of the most important ones in science and engineering. The property of the dynamic systems of dissipating energy is known as dissipativity. Passivity is a special case of the dissipativity. Passive systems are a class of dynamical system which cannot store more energy than are supplied to them from the outside, with the difference being the dissipated energy. Passivity has been used for controllers design. The methodology is called passivity based control (PBC). The detail can be referred to reference [78] and [100]. Passivity means the exchange of energy of the system with its environment. From a different perspective, the energy interpretation of passivity can be related to system stability. So, the system robustness could be improved by PBC.

Consider a system:

$$\text{G:}\begin{cases} \dot{X} = f(X) + g(X)\text{U}(t) \\ \text{Y} = h(X) \end{cases} \tag{5.1}$$

where $\text{G}: \quad \text{U}(t) \rightarrow \text{Y}$, U(t) is the input signal and Y is the output; *X* is the state variable.

Definition 1 **(*Dissipativity*):** [100] The system G: is dissipative in *X* with the consume rate *w*(U, Y), if there exists a function *S*(*x*), with *S*(0) = 0, such that for all $x \in X$: $S(x) \geq 0$ and

$$\int_0^T w(\text{U}, \text{Y})dt \geq S(x(T)) - S(x(0)) \tag{5.2}$$

for all U and all $T > 0$, such that $x \in X$ for all $t \in [0, T]$.

***Definition 2 (Passivity)*:** [100] System G: is said to be passive if it is dissipative with supply rate $w(\text{U}, \text{Y}) = \text{U}^{\text{T}}\text{Y}$.

The general theory of dissipative dynamical systems relates the functions *w*(U, Y) and *S*(*x*) to the physical notion of applied power and total energy stored, respectively [96]. Thus, (5.2) says that the total energy cannot exceed the externally applied energy to the system at any time. The definition of passivity constrains the supply rate function to be symmetric, and positive semidefinite bilinear form. Moreover, if the entries of *w* (that is, U and Y) have units such that their product is given in terms of unit of power (for the case of electrical systems, currents and voltages), then system G defines a passive system with port variables (U, Y) and storage function *S*(*x*) related with the total energy of the system.

5.3.2 The average Euler-Lagrange Equations

The EL parameters of the circuits could be established by considering the topologies which replace the two possible positions of regulating switch [99, 101]. Consider a nonlinear system of the form,

$$\dot{x} = f(x) + g(x)u \tag{5.3}$$

where u is a switch position function taking values in the discrete set {0, 1}. x is the state vector of the system. According to Sira-Ramirez [102] and the PWM-controller law, the values of u are specified as:

$$u = \begin{cases} 1 & t_k \le t < t_k + \mu T \\ 0 & t_k + \mu T \le t < t_k + T \end{cases} \qquad t_k + T = t_{k+1}; \quad k = 0,1,2,\cdots \tag{5.4}$$

where the mapping μ represents the duty ratio function, which is usually regarded as a state dependent quantity and which specifies, at each sampling instant t_k, the state dependent width μT of the control input pulse during the upcoming inter-sampling interval of fixed duration T (known also as the duty cycle, or, simply, the sampling period). It is easy to see, from (5.4), that the duty ratio function is evidently limited to non-negative values, which do not exceed the upper bound of 1, i.e. $\mu \in [0 \quad 1]$. It has been shown that a piecewise smooth average model of (5.3) can be obtained by assuming an infinitely large sampling frequency. This assumption results in a model of (5.3) in which the discrete-valued control input function u is replaced by the limited piecewise smooth duty ratio function μ, i.e.:

$$\dot{z} = f(z) + g(z)\mu \tag{5.5}$$

where z is the average vector of the system.

The average EL equations are obtained in the same method using the smooth duty ratio function μ to replace the switching position signal. For sufficiently high sampling frequencies, controllers designed on the basis of average models can indeed be used to regulate the actual switched converters [100]. These average states can be approximately obtained by low pass filtering the real circuit states, x. The relationship between the state vector x and average vector z is shown in Fig. 5.4.

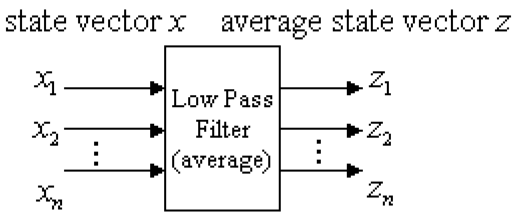

Fig. 5.4 Relationship between *x* and *z*

5.4 Modeling of HID Electronic Ballast and HID Lamp

5.4.1 HID Lamp Model

Much effort has been devoted to the development of sophisticated high intensity discharge lamp models [26-29]. From a plasma physics point of view, Xenon lamps are extremely complex devices, which include many physical processes and chemical species. In transient state, the lamp resistance is a nonlinear time-variant function [103], but, after it goes into the steady state, the resistance could be thought as a constant value which varies in a tiny small scope. As it can be seen from Fig.5.5 (a), (b), the waveform profiles of lamp voltage and current are both square wave. Fig. 5.6 shows the lamp resistance in steady state of a new lamp. In addition, with the lamp ageing, the lamp resistance would be increased. Fig. 5.5 and Fig.5.6 are obtained from the experiment.

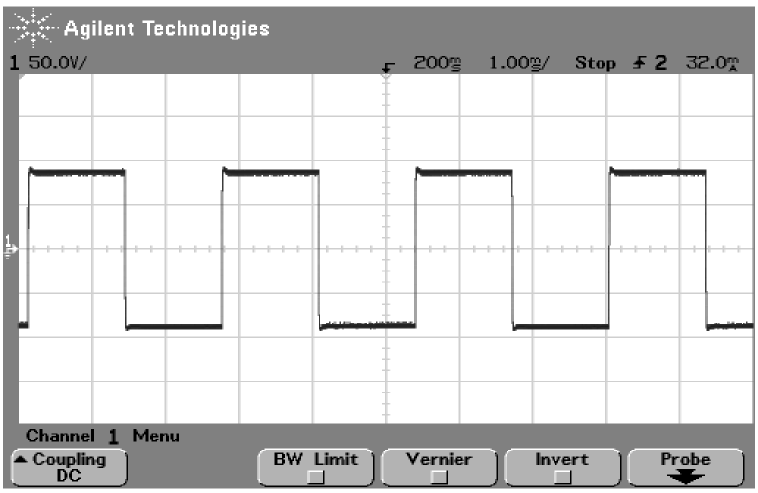

(a)

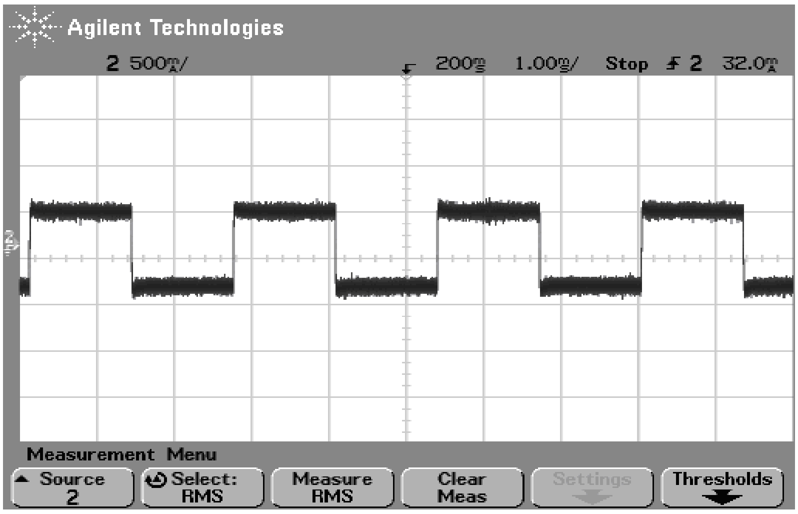

(b)

Fig. 5.5 (a) Lamp voltage waveform in steady state (b) Lamp current waveform in steady state

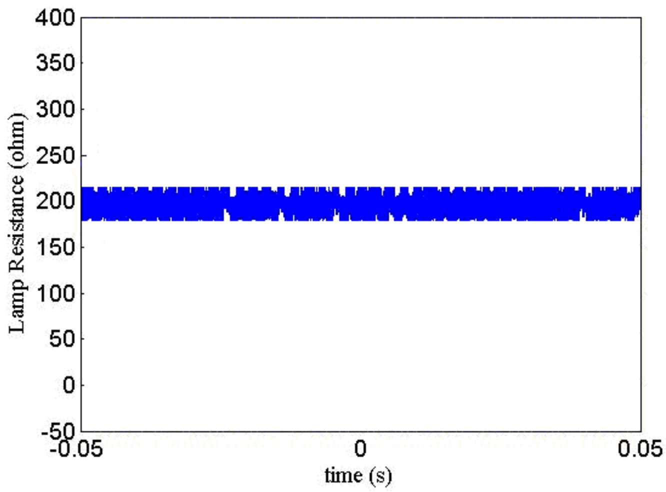

Fig. 5.6 Calculated equivalent resistance of new HID lamp in steady state

5.4.2 Electronic Ballast Model

When the HID lamp works in the steady state, the electronic ballast circuit is as shown in Fig. 5.7. In order to get the system model, the following considerations are given: a) The components are ideal. b) The control signal ranges for the transistors are in {0, 1}. c) The state vector is in $\Re^2 > 0$. d) The lamp resistance R is unknown.

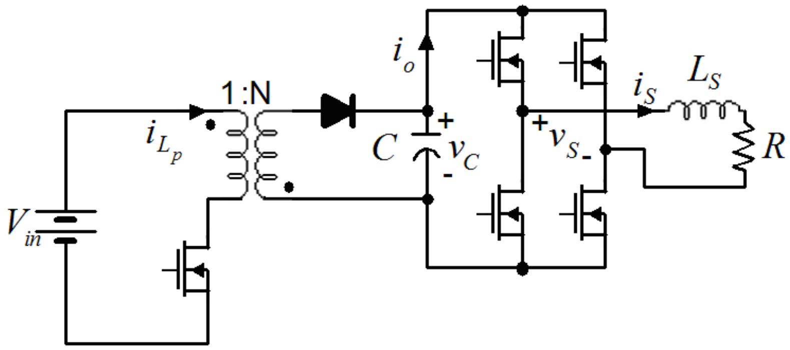

Fig. 5.7 Circuit schematic of the electronic ballast in the steady state

The circuit is actually a cascade connection of two subsystems. The first one, the DC-DC flyback converter with an unstable right hand-plane zero, is fed with modulation signal. Equation (5.6) shows the system dynamic:

$$
\begin{aligned}
\frac{di_{L_p}(t)}{dt} &= \frac{-(1-u(t))}{NL_p} v_C(t) + \frac{u(t)}{L_p} V_{in} \\
\frac{dv_C(t)}{dt} &= \frac{1-u(t)}{NC} i_{L_p}(t) - \frac{1}{Z_{eq}C} v_C(t)
\end{aligned} \tag{5.6}
$$

where i_{L_p}, v_C denote the inductor current and capacitor voltage in the flyback converter and the directions are shown in Fig. 5.7. u describes the position of the switches taking values in the discrete set {0, 1}. Z_{eq} is the equivalent load impedance of flyback which is equal to the input impedance of the full-bridge inverter, which will be described in the following.

The second one acts as an AC power supply to the HID lamp in order to give the balance to the two lamp electrodes. The switching frequency ω_1 and duty ratio d_1 of the four switches in the inverter are fixed, and the inductor L_S is the secondary magnetising inductor of high voltage transformer used in the electronic ballast. R is the equivalent resistance of the lamp.

$$
\frac{di_S(t)}{dt} = \frac{R}{L_S} i_S(t) + \frac{1}{L_S} v_S(t) \tag{5.7}
$$

where i_S and v_S are current of the inductor L_S and the output voltage of full-bridge inverter, respectively. The relationship between output voltage v_C of flyback converter and v_S of full-bridge is (5.8) given by Fourier analysis.

$$v_S(t) = \sum_{n=1}^{\infty} \frac{2v_C}{n\pi}(1 - \cos n\pi)\sin(n\omega_1 t) \tag{5.8}$$

The performance of the electronic ballast is decided by the flyback converter because the full-bridge inverter is an unregulated low frequency converter without magnetic components.

Because the switching frequency and the duty ratio of the inverter are fixed, the switching frequency ω_1, and duty ratio d_1 of the four switches in the inverter are unchanged. The inductor impedance of the system high voltage transformer, $Z_{L_S} = 2\pi f_1 L_S = \omega_1 L_S << R$, so the equivalent load impedance $Z_{eq} \approx R$. The cascade connection of two subsystems could be simplified into a flyback converter, that is, in steady state, the lamp constant power control can be considered as the flyback output power constant control.

The state vector x is chosen as $x = [i_{L_p}, v_C]^T$. The total energy function, $H(x)$ can be defined as the sum of the energy stored in the inductor and capacitor, that is: $H(x) = \frac{1}{2L_p} i_{L_p}{}^2 + \frac{1}{2C} v_C{}^2$. With this energy function, the model of the electronic ballast could be rearranged as the equation of EL model [100]:

$$D\dot{x} + g(u)x + R_g x = \varepsilon \tag{5.9}$$

where x is a vector, D is diagonal and positive element, $g(u)$ is a skew symmetric matrix, R_g is a positive element matrix, ε is the input voltage vector. R_g represents the dissipative elements and must be positively defined. Using (5.6) and the selected state vector, x, the dynamic model in EL format can be represented as:

$$D_B\dot{x}+J_Bx+R_Bx=\varepsilon_B \tag{5.10}$$

where $D_B=\begin{bmatrix} L_p & 0 \\ 0 & C\end{bmatrix}$, $J_B=\begin{bmatrix} 0 & \frac{1-u}{N} \\ -\frac{1-u}{N} & 0\end{bmatrix}$, $R_B=\begin{bmatrix} 0 & 0 \\ 0 & \frac{1}{R}\end{bmatrix}$ and $\varepsilon_B=\begin{bmatrix} u(t)V_{in} \\ 0\end{bmatrix}$.

Taking the time derivative of $H(x)$ along the trajectories of (5.6) and integrating from 0 to t gives the following energy balance equation:

$$H(t)-H(0)+\frac{1}{Z_{eq}}\int_0^t {v_C}^2(\tau)d\tau=\int_0^t V_{in}i_{L_p}(\tau)d\tau \tag{5.11}$$

Since the system dynamic satisfies (5.11), it follows from reference [78] that the system is passive.

In addition, the relationship between the equilibrium of the average output voltage and the average inductor current of the flyback converter can be given by (5.6), that is, the constant equilibrium values x_1 and x_2 for a constant duty ratio $u=u^*$ are given by:

$$x_1^*=\left[\frac{u^*}{(1-u^*)^2}\right]\frac{N^2V_{in}}{R},\ x_2^*=(\frac{u^*}{1-u^*})NV_{in} \tag{5.12}$$

5.4.3 An average model for Electronic Ballast

In equation (5.6), the control input variable u takes values in the discrete set $\{0,\ 1\}$, representing the values of a switch position function. Using the duty ratio function μ, it has been shown that a piecewise smooth average model of the electronic ballast (5.6) can be obtained by assuming an infinitely large sampling frequency, i.e.:

$$D_B\dot{z}+J_Bz+R_Bz=\varepsilon_B \tag{5.13}$$

where $D_B=\begin{bmatrix} L_p & 0 \\ 0 & C\end{bmatrix}$, $J_B=\begin{bmatrix} 0 & \frac{1-\mu}{N} \\ -\frac{1-\mu}{N} & 0\end{bmatrix}$, $R_B=\begin{bmatrix} 0 & 0 \\ 0 & \frac{1}{R}\end{bmatrix}$ and $\varepsilon_B=\begin{bmatrix} \mu V_{in} \\ 0\end{bmatrix}$. z denotes the averaged state vector of electronic ballast.

5.5 Controller Design

5.5.1 Control objectives

The control objective is to regulate the output power to a desired constant value P^*, and verifying the assumptions a)-d) as shown in section 5.4.2.

5.5.2 Indirect Output Power Regulation

Because the output power is not available for measurement in our system, a substitute is using the output voltage or output current as the controller parameter. It is easy to think to use the output voltage of the flyback. The output power of lamp could be obtained as:

$$P = \frac{1}{R} v_C{}^2 \tag{5.14}$$

In order to keep the output power constant, the value of the square of output voltage v_C divided by the lamp resistance must be constant. If the HID lamp resistance could be estimated, we can get the reference voltage through (5.14) and use the voltage tracking method to get the constant power. A direct regulation policy of the output voltage is unfeasible because the flyback converter is the same type of non-minimum phase system as the buck-boost converter [78]. Indirect output voltage regulation achieved by the regulation of the input current. The indirect power regulation scheme is given in Fig. 5.8.

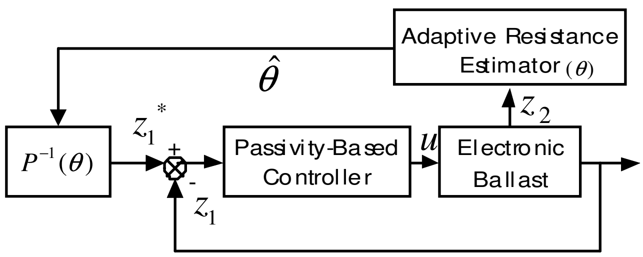

Fig. 5.8 Indirect power regulation scheme

In Fig.5.8, θ is the estimated value of HID lamp resistance. $P^{-1}(\theta)$, which can be called a power function, is the function of HID lamp resistance θ and the wanted inductor current z_1^* . The passivity-based controller, adaptive resistance estimator and power function will be given in the next section.

5.5.3 Passivity-based Controller

The state error can be defined as $e = z - z_d$, where $z_d = [\begin{matrix} z_{1d} \\ z_{2d} \end{matrix}]$ is the "wanted" state vector, which defines the desired system performance. With the natural dissipative elements of the actual plant, the system damping will be small, reducing the closed-loop system performance. So, additional damping injection is given as:

$$R_{1B} = \begin{bmatrix} K_1 & 0 \\ 0 & 0 \end{bmatrix};\ K_1 > 0 \tag{5.15}$$

The parameter K_1 is a designer chosen constant with the only restriction of being strictly positive. According to (5.10), (5.15) and substituting e, the model of the state error becomes:

$$D_B\dot{e} + J_B e + \mathrm{R}'\mathrm{e} = \Phi \tag{5.16}$$

where $\Phi = \varepsilon_B - \left(D_B\dot{z}_d + J_B z_d + R_B z_d - R_{1B}e\right)$, $R' = \begin{bmatrix} K_1 & 0 \\ 0 & \dfrac{1}{R} \end{bmatrix}$. This control problem is defined as a trajectory problem. The system energy function can be defined as:

$$H_d(z) = \frac{1}{2}e^T D_B e \tag{5.17}$$

where e is the trajectory error. So,

$$\dot{H}_d(z) = e^T J_B e - e^T\,\mathrm{R}'\mathrm{e} + e^T\Phi \tag{5.18}$$

Because the matrix J_B is skew symmetric, the term $e^T J_B e$ is zero. The term is also called as "workless force". Combining to the Lyapunov stability theory and (5.18), $\dot{H}_d \le 0$, if the system is stable, that is, $-e^T R'e < 0$ and Φ needs to be zero through suitable control effect. The controller dynamic is obtained from (5.10) and (5.16) by setting $\Phi = 0$, that is:

$$L_p \dot{z}_{1d} - K_1(z_1 - z_{1d}) + \frac{1-\mu}{N} z_{2d} = \mu V_{in} \tag{5.19}$$

$$C\dot{z}_{2d} - \frac{1-\mu}{N} z_{1d} + \frac{1}{R} z_{2d} = 0 \tag{5.20}$$

The first step is to let the HID lamp resistance be known, the constant output power control could be realized by regulating the inductor current z_1 to be a constant. Substituting $z_{1d} = z_1^*$ into (5.19), (5.20), the duty ratio function becomes:

$$\dot{\mu} = \frac{1-\mu}{NC[V_{in} + K_1(z_1 - z_1^*)]} \left\{ \frac{(1-\mu)^2}{N} z_1^* - \frac{\mu N V_{in} + NK_1(z_1 - z_1^*)}{R} + \frac{K_1 C\left[-\mu N V_{in} + (1-\mu) z_2\right]}{L} \right\} \tag{5.21}$$

5.5.4 Adaptive Resistance Estimator

With the ageing of the HID lamp, the lamp resistance will change slowly during the long working period. It can be estimated using the adaptation method.

Define $\theta = \frac{1}{R}$, its estimation value is $\hat{\theta}$, and the error is θ_e which is satisfied with the equation $\theta = \hat{\theta} - \theta_e$. Then, $R_{2B} = \begin{bmatrix} 0 & 0 \\ 0 & \hat{\theta} \end{bmatrix}$, $R_{3B} = \begin{bmatrix} 0 & 0 \\ 0 & \theta_e \end{bmatrix}$. Substituting $R_B = R_{2B} - R_{3B}$ into (5.16), then:

$$D_B \dot{e} + J_B e + R_B e + R_{1B} e = \varepsilon_B - D_B \dot{z}_d - J_B z_d - R_{2B} z_d + R_{3B} z_d + R_{1B} e \tag{5.22}$$

From (5.19, 5.20) and combining with e, we can obtain:

$$D_B \dot{e} + J_B e + R_B e - R_{3B} z_d = -R_{1B} e \tag{5.23}$$

$$\varepsilon_B - D_B \dot{z}_d - J_B z_d - R_{2B} z_d = -R_{1B} e \tag{5.24}$$

Here, the Lyapunov function is proposed as: $H_{AD} = \frac{1}{2}\left(e^T D_B e + \frac{\theta_e^{\,2}}{\gamma}\right)$. where $\gamma > 0$. Also, we can obtain:

$$\dot{H}_{AD} = e^T D_B \dot{e} + \frac{1}{\gamma}\theta_e \dot{\theta}_e = -e^T J_B e - e^T\left(R_B + R_{1B}\right)e + \theta_e\left[z_{2d}(z_2 - z_{2d}) + \frac{1}{\gamma}\dot{\theta}_e\right] \tag{5.25}$$

Combining with the Lyapunov stability theory, the term $-e^T J_B e = 0$ and $-e^T\left(R_B + R_{1B}\right)e < 0$, in order to make $\dot{H}_{AD} < 0$, the adaptive law of the system is:

$$\dot{\hat{\theta}} = -\gamma z_{2d}(z_2 - z_{2d}) \tag{5.26}$$

5.5.5 Power Function and the last Controller

If the desired output power is P^*, and let us define the z_{1d}, the relationship of these two values is derived and coincided with (5.14), (5.15) and (5.18), that is,

$$z_{1d} = \frac{P^*}{V_{in}} + (N\sqrt{\hat{\theta}P^*}) \tag{5.27}$$

The equation (5.27) is called power function, and also, z_{1d} and z_1 coincide at the equilibrium point, that is, if the estimator of lamp resistance is known, the wanted current of the inductor is known.

Combining (5.27), (5.26) and (5.21), an adaptive nonlinear average state feedback controller is given after some algebraic and derivative manipulations:

$$\begin{aligned}
\dot{z}_{2d} &= -\frac{1}{C}\left\{\begin{aligned}&\hat{\theta}z_{2d} - \frac{P^* + NV_{in}(P^*\hat{\theta})^{\frac{1}{2}}}{z_{2d}V_{in}} + \frac{P^* + NV_{in}(P^*\hat{\theta})^{\frac{1}{2}}}{V_{in}(NV_{in} + z_{2d})} * \\ &\left[\left[\frac{1}{N}z_{2d} - K_1\left(z_1 - \frac{P^*}{V_{in}} - N(P^*\hat{\theta})^{\frac{1}{2}}\right) + \frac{NL_p(P^*/\hat{\theta})^{\frac{1}{2}}}{2}\right]\right]\end{aligned}\right\} \\
\mu &= \frac{N}{z_{2d} + NV_{in}}\left[\frac{NL_p}{2}\left(\frac{P^*}{\hat{\theta}}\right)^{\frac{1}{2}} - K_1\left(z_1 - \frac{P^*}{V_{in}} - N(P^*\hat{\theta})^{\frac{1}{2}}\right) + \frac{z_{2d}}{N}\right] \\
\dot{\hat{\theta}} &= -\gamma z_{2d}(z_2 - z_{2d})
\end{aligned} \tag{5.28}$$

5.6 Simulation

The parameters of the system are given in Table 5.1. The switching frequency of the flyback converter is 100 kHz. Besides the simulation results of PBC controller, in order to do the comparisons, the simulation results of LUT method are given. The LUT which has no relationship with the lamp resistance is shown in Fig. 5.9. With this lookup table, constant power control could be achieved with a PI controller. Also, the indirect constant power control is used, that is the inductor current becomes the control parameter. Simulation is carried out with *MATLAB SIMULINK* and its block diagram is shown in Fig. 5.10. The wanted constant power is 35W. The control parameter γ is selected in the range $\gamma>0$, here γ is selected as 6. The choice of γ is based on empirical decision. The actual range of γ between 10 and 1 also provide good performance in this application.

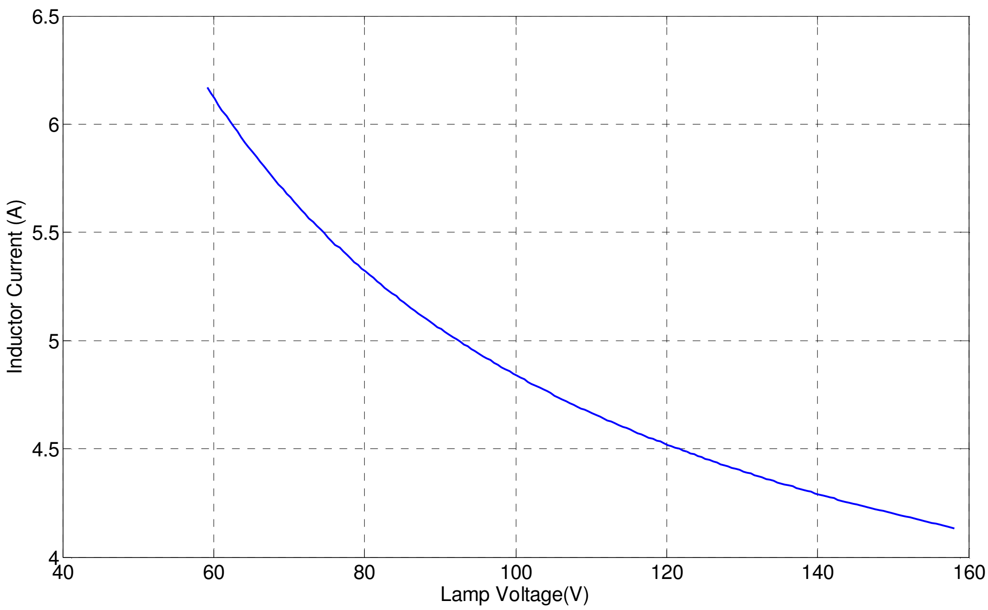

Fig. 5.9 Lookup tables used in simulation

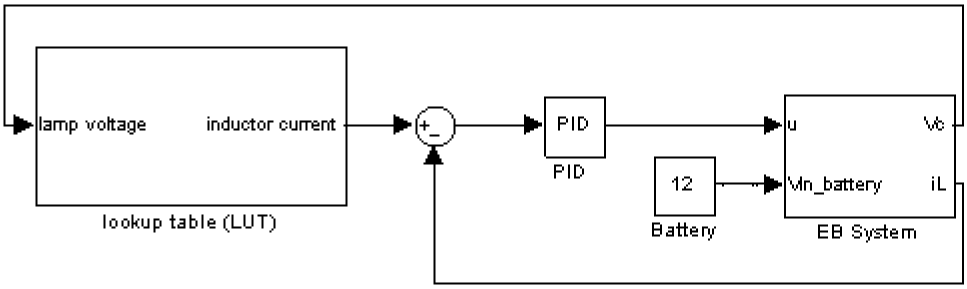

Fig. 5.10 Simulation block diagram for lookup table method of constant power control

Table 5.1 Electronic Ballast and Lamp Profile

	Notation	Values	Unit
Inductance of primary winding in Flyback	L_p	10	μH
Capacitance in Flyback	C	5.6	μF
Inductance of secondary winding in Full-bridge	L_S	0.6	mH
Turns ratio	N	7	
Input voltage	V_{in}	12	V
Switching frequency of Full-bridge	f_l	400	Hz
Lamp resistance	R	200	Ω

Three different conditions are studied in the simulation, namely, the response of lamp resistance change, the performance of the load estimator and the power trajectory response. The lookup table method does not have the function of load estimator.

5.6.1 Lamp Resistance Change Response

The response test for the lamp resistance changing from 200Ω to 400Ω has been conducted and the simulation results between the PBC controller and LUT control method are given in Fig.5.11 and Fig.5.12, respectively. It is clearly shown that, for the PBC controller, response to the changes of lamp resistance is very fast. The LUT method can also achieve constant power. There is no major difference between these two methods, but there is a small overshoot in the input voltage of the lamp at the instant of step change of the lamp resistance using LUT control method.

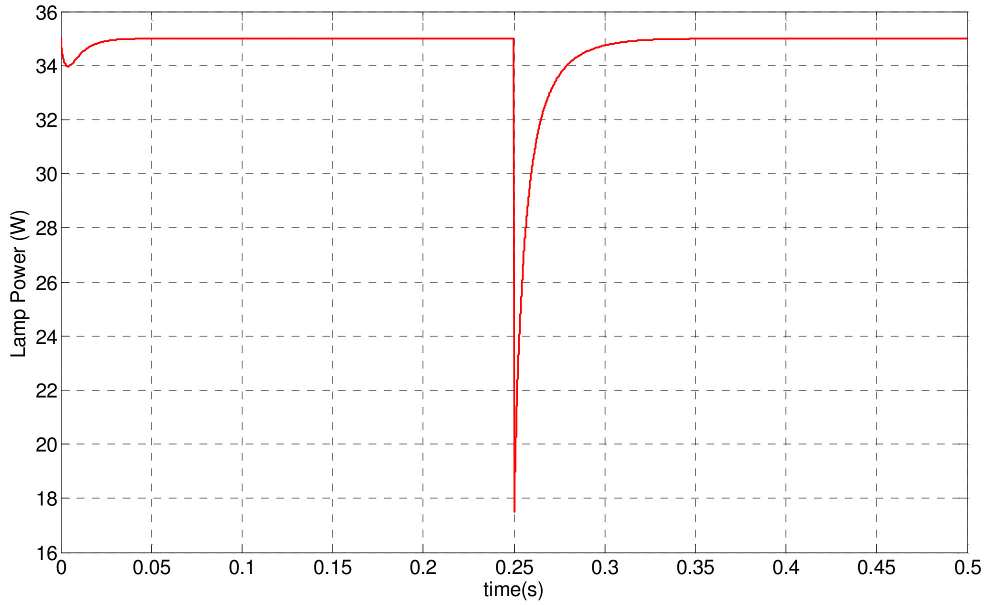
Lamp Power (W)
36
34
32
30
28
26
24
22
20
18
16
0
0.05
0.1
0.15
0.2
0.25
0.3
0.35
0.4
0.45
0.5
time(s)

(a)

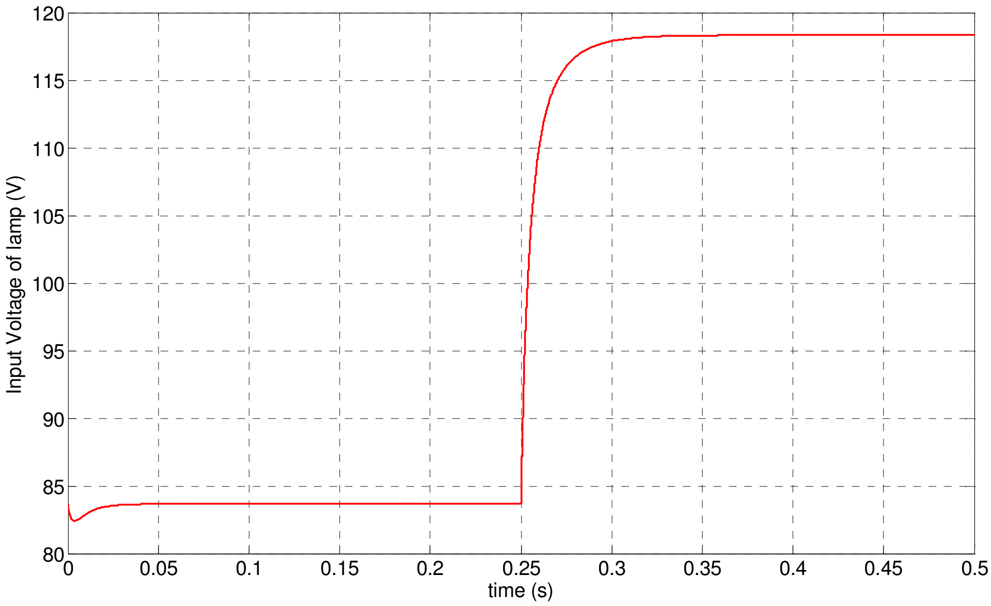
Input Voltage of lamp (V)
120
115
110
105
100
95
90
85
80
0
0.05
0.1
0.15
0.2
0.25
0.3
0.35
0.4
0.45
0.5
time (s)

(b)

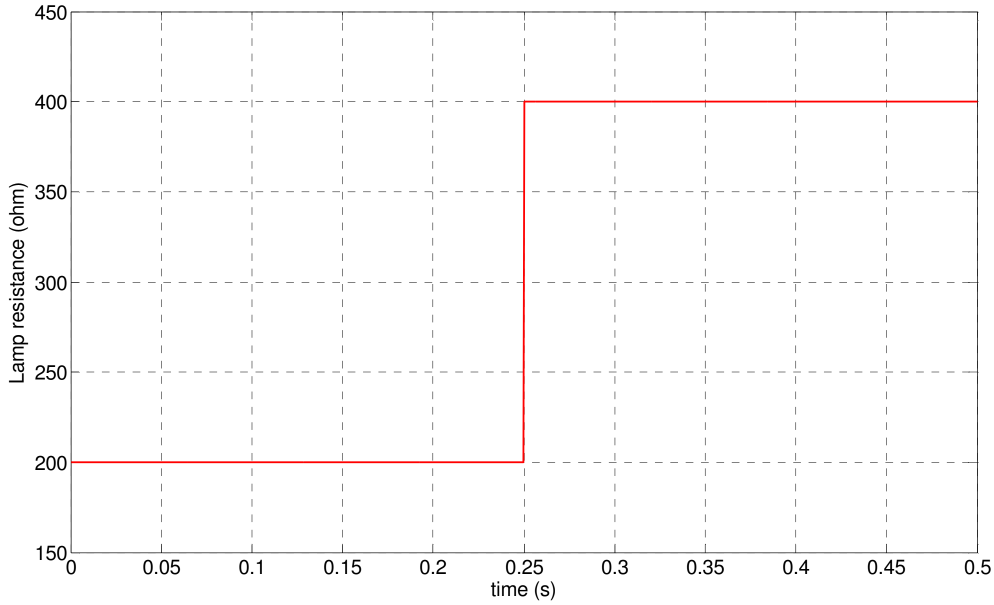

(c)

Fig. 5.11 Simulation results of PBC controller (a) lamp power (b) input voltage of lamp (c) lamp resistance

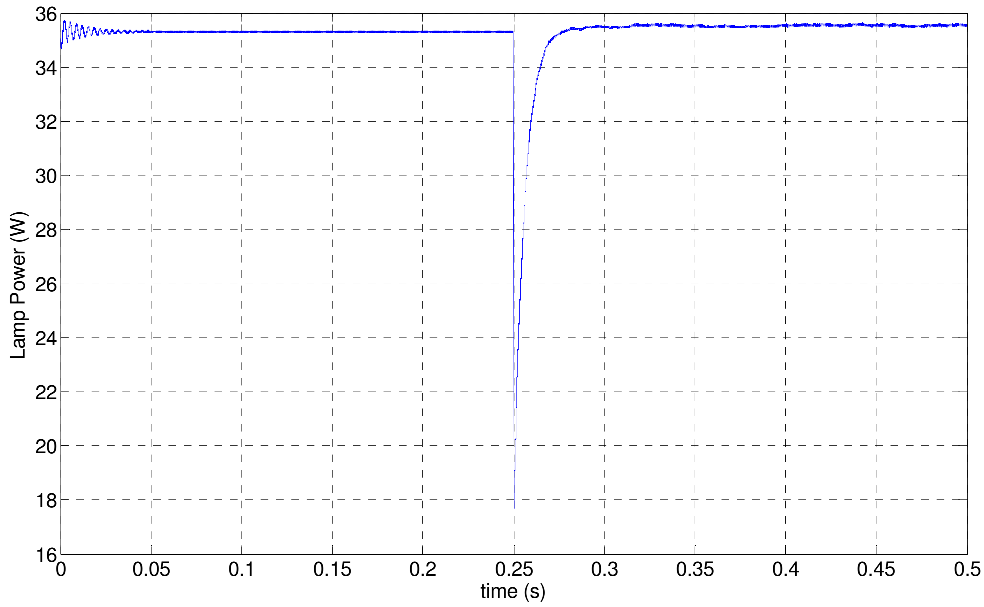

(a)

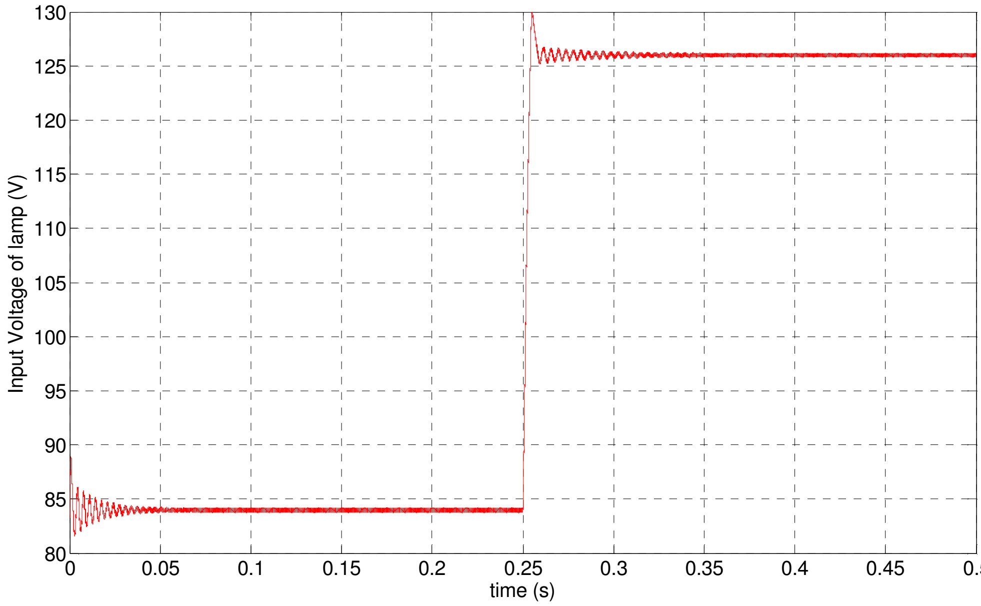

(b)

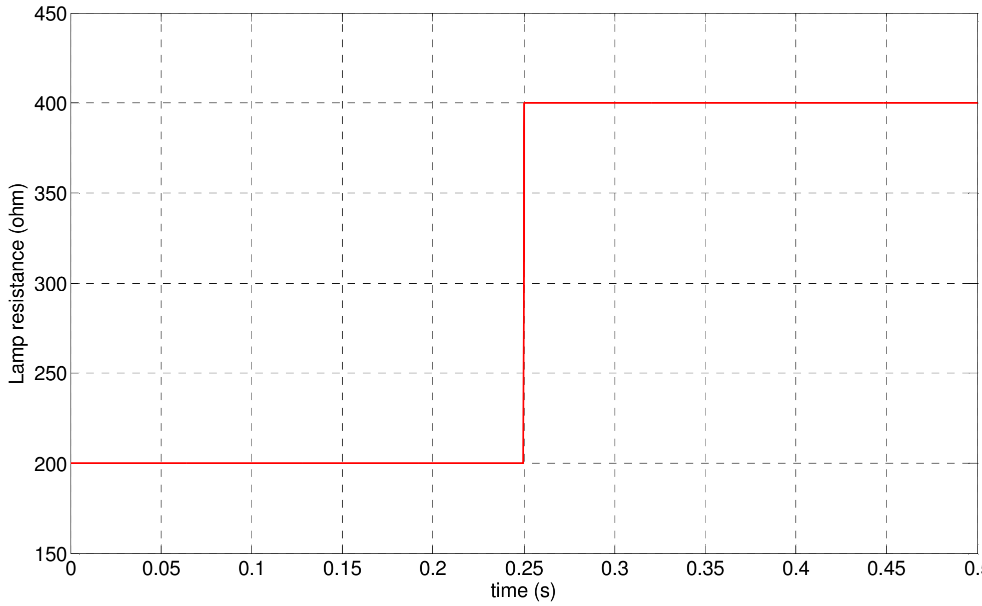

(c)

Fig. 5.12 Simulation results of LUT control method (a) lamp power (b) input voltage of lamp (c) lamp resistance

5.6.2 Load Estimation Performance

The value of the load estimation is determined by the system lamp. If the values of the lamp current and lamp voltage are known, the load estimator can give the value of lamp resistance of the system. Fig. 5.13 and Fig. 5.14 show that at different states with different HID lamp resistances, the PBC controller can make the system run in stable state with constant power, and the estimator can obtain the real value of the system.

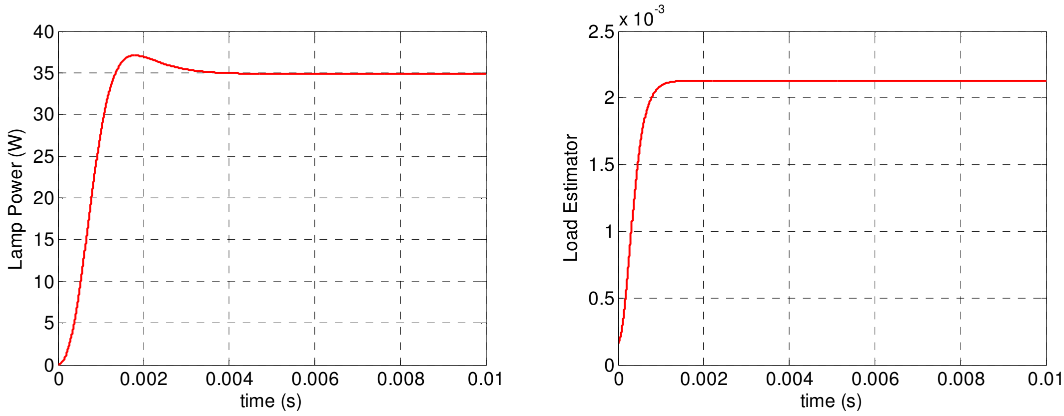

(a) (b)

Fig. 5.13 (a) The lamp power with 125 Ω load (b) load estimator

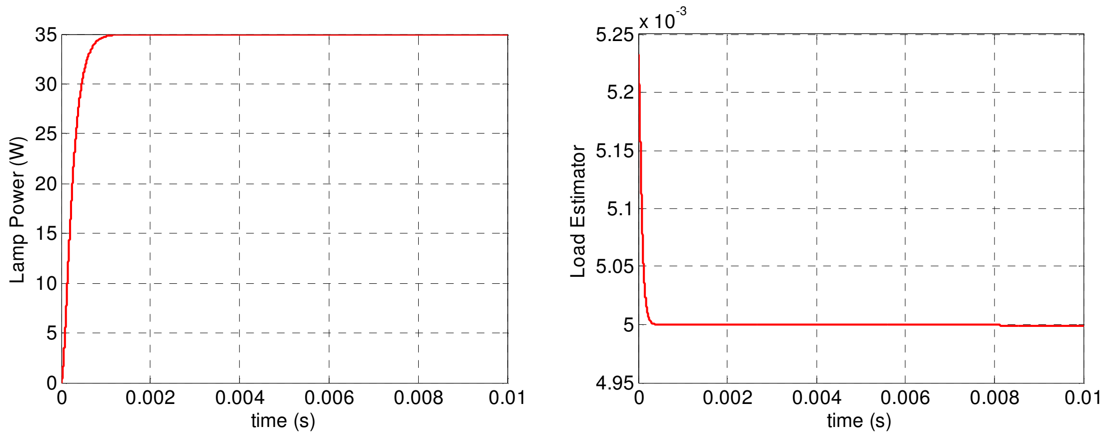

(a) (b)

Fig. 5.14 (a) The lamp power with 200 Ω load (b) load estimator

5.6.3 Power Tracking Performance

When the lamp resistance and the desired power have changed, the PBC controller can track the desired power to achieve the constant power control. In the simulation, no matter which the parameters (lamp resistance or desired power) are changed, the damping injection factor (K_1) of PBC controller is the same. In order to do the comparison, the controller factors of PID (K_p, K_i and K_d) are unchanged in different modes, too. Figs.5.15 and 5.16 show the power tracking performance under the variation of lamp resistance. It is clear that the adjusting time is getting longer in PBC controller but it can still track the desired power. But the steady state error is large and cannot follow the desired power in LUT method. LUT is non-adaptive hence the steady state error is large indeed. The PBC method gives a much better performance.

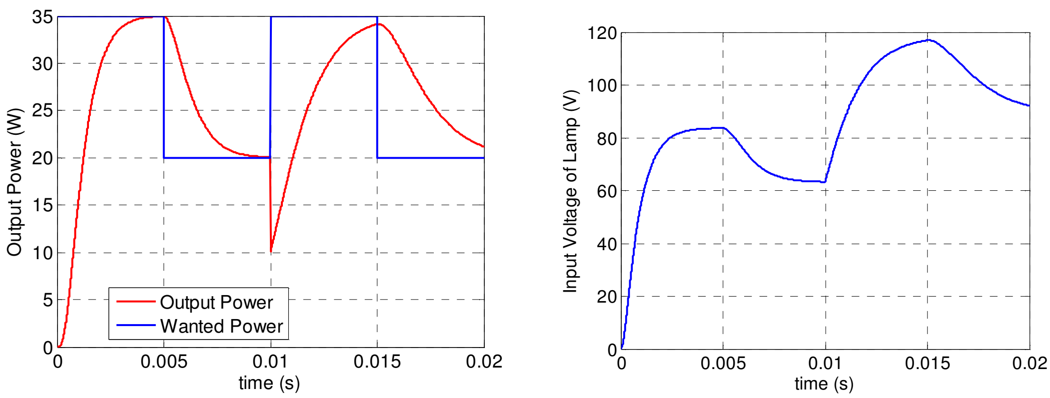

(a) (b)

Fig. 5.15 Simulation results of power tracking performance using PBC controller (a) lamp output power (b) Input voltage of lamp

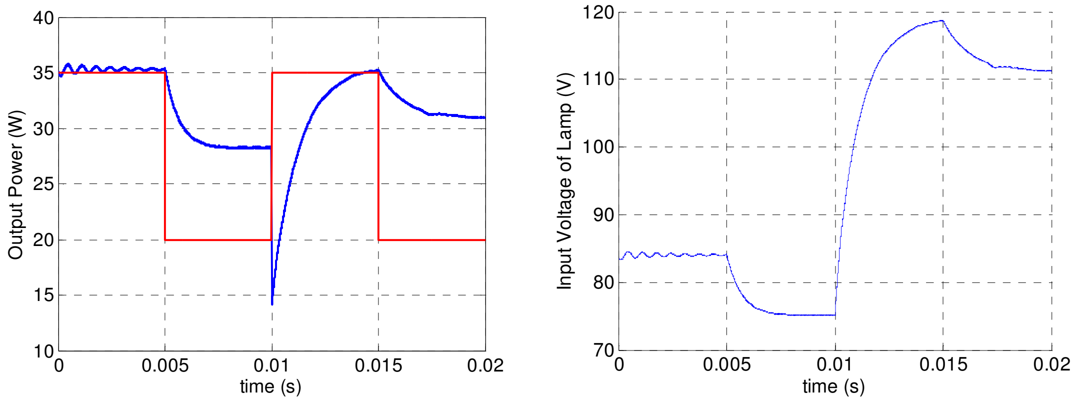

(a) (b)

Fig. 5.16 Simulation results of power tracking performance using LUT method (a) lamp output power (b) input voltage of lamp

5.7 Experimental Results

The simulation results show that the PBC controller is more robust and can estimate the lamp resistance successfully.

As seen from the experimental and simulation results, the difference between the PID controller and PBC controller can be concluded as: in real PI controller, the analogue circuit is used and the resistance and capacitor are used to realize the controller's function. Due to the PID controller is based on the linearization model, the operation is limited. If the parameters of the system change, a large adjusting time is needed. Fig. 5.17 (a) shows the ripple when the lamp resistance changes. In the meantime, if the reference power is changed from 35W to 20W, the PID controller is unstable (the simulation result shown in Fig. 5.16 (a)) which is also verified by the experiment. When the lamp power changes from 35W to 20W, the HID lamp extinguishes.

Fig. 5.17 (a) and (b) shows the measured lamp power for both PID and PBC controllers. The PBC controller can respond to the lamp resistance rapidly whereas there is considerable transient in the LUT controller. The PBC controller enjoys a faster response than its counterpart.

Fig. 5.18 shows the experimental results of the lamp power when the lamp resistance changes from 200Ω to 400Ω. For this case, when the lamp resistance changes, the lamp output power is maintained constant at 35W. In order to compare with the simulation results in Fig. 5.9, the input voltage of the HID lamp is measured by an oscilloscope. The magnitude of the lamp voltage is equal to the input voltage if the power loss is not considered. So, lamp voltage will be increased with the lamp resistance change in order to keep the lamp power constant. The results show that the response time is very short and the error is small.

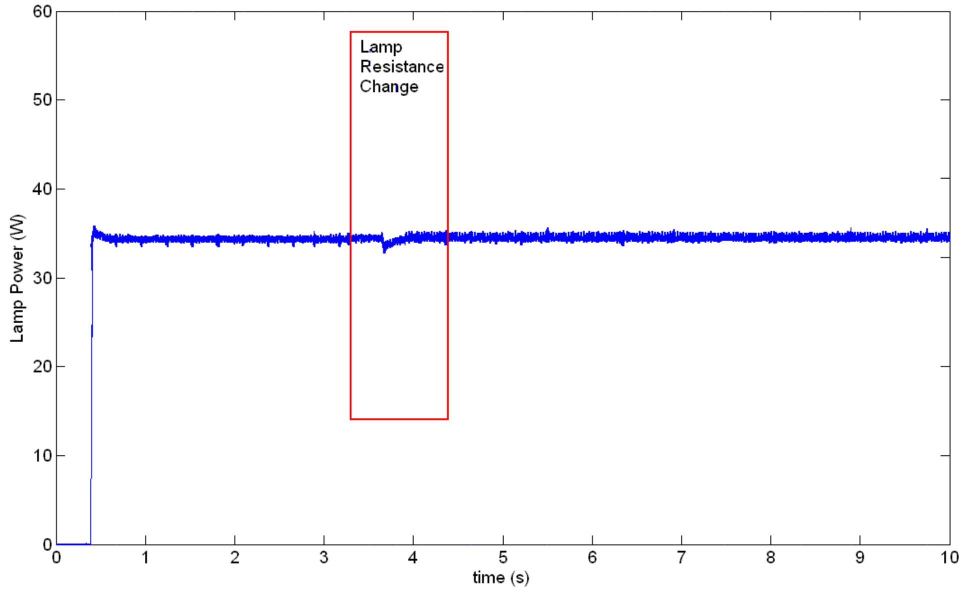
Lamp
Resistance
Change
Lamp Power (W)
time (s)
0
10
20
30
40
50
60
0
1
2
3
4
5
6
7
8
9
10

(a)

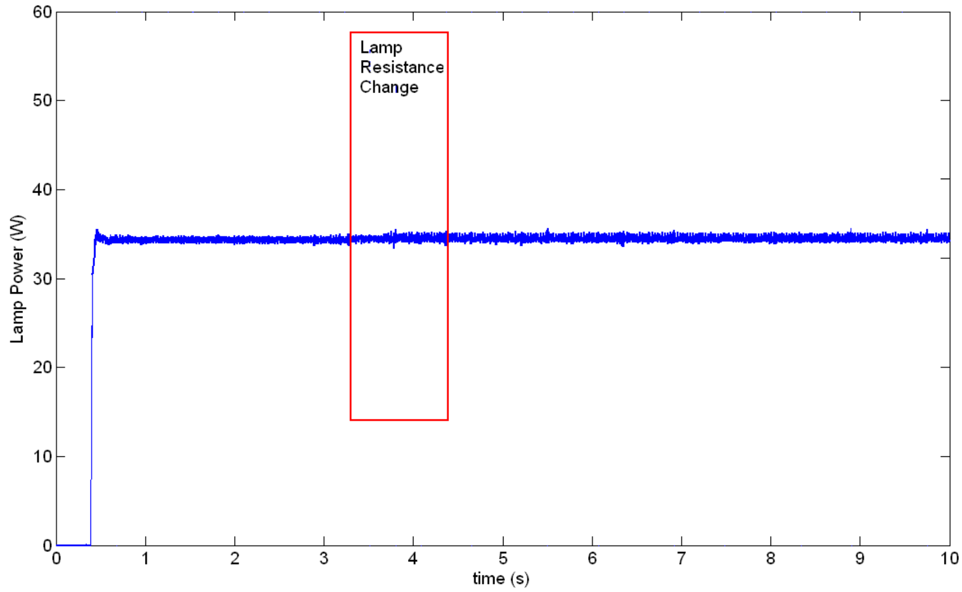
Lamp
Resistance
Change
Lamp Power (W)
time (s)
0
10
20
30
40
50
60
0
1
2
3
4
5
6
7
8
9
10

(b)

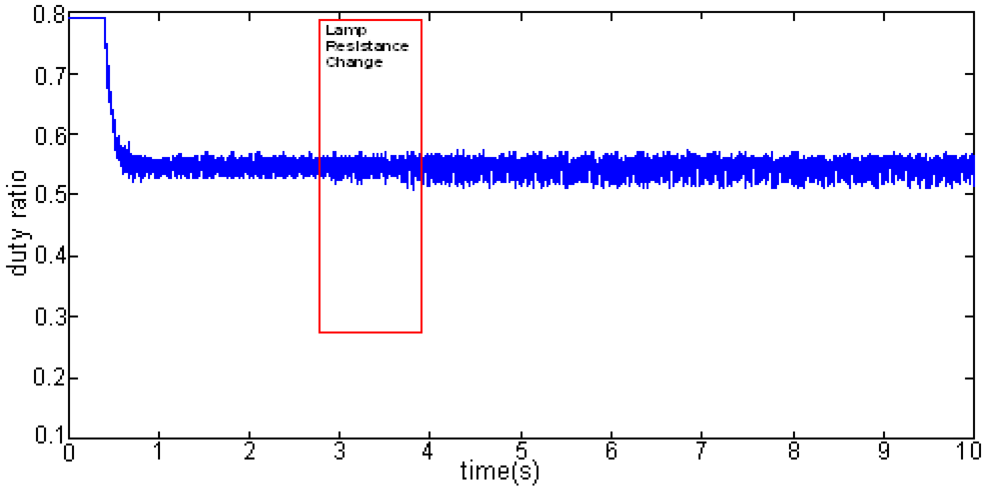

(c)

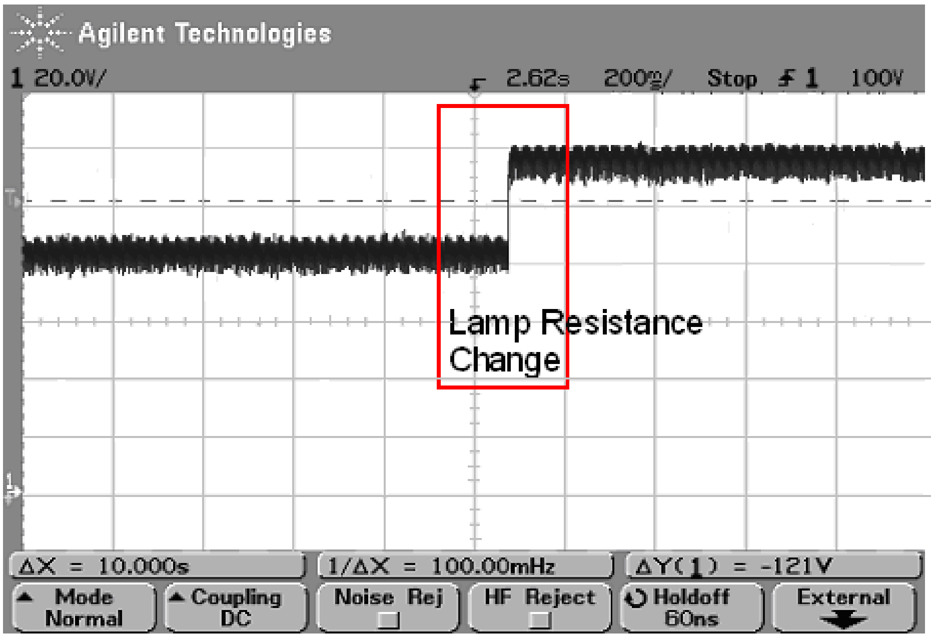

(d)

Fig. 5.17 Experimental results of EB with the lamp resistance change from 200Ω to 400Ω (a) lamp power with PID controller (b) lamp power with PBC controller (c) duty ratio (d) Amplitude of input voltage of H-bridge inverter (voltage: 20V/div, time: 200ms/div)

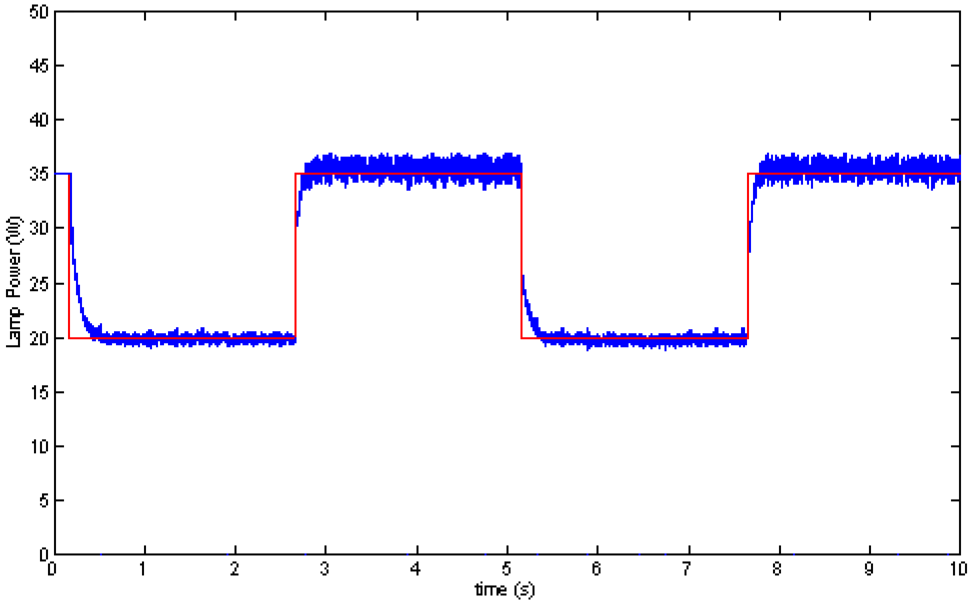

(a)

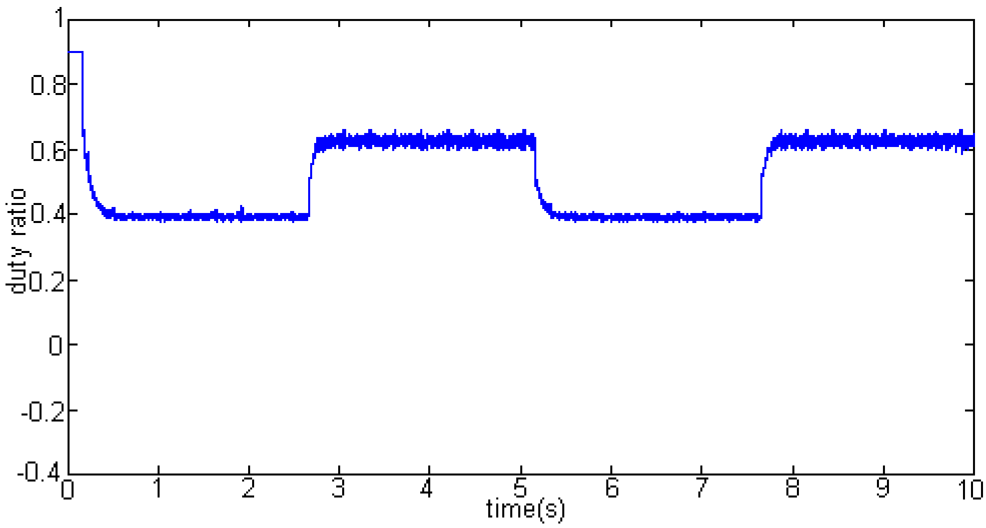

(b)

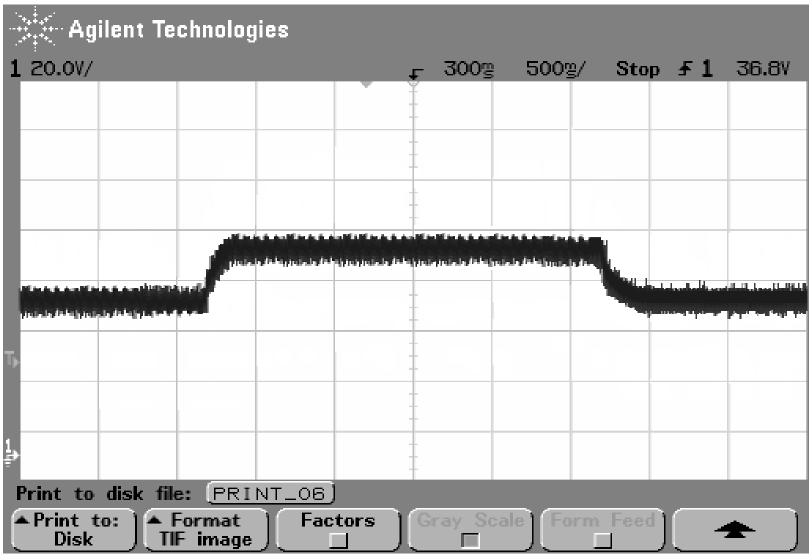

(c)

Fig. 5.18 Experimental results of EB with the lamp power change from 35W to 20W (a) lamp power (b) duty ratio (c) Amplitude of input voltage of H-bridge inverter (voltage: 20V/div, time: 500ms/div)

5.8 Summary

A detailed controller design, simulation and experimental implementation of an adaptive PBC controller for indirect constant power regulation of HID electronic ballast are described. This controller uses the nonlinear equations of the system which can avoid the shortcomings of linear controller based on the linear model of the system and enhance the system robustness. Besides, the indirect regulation and PBC method guarantee the global stability and the asymptotic convergence of all state errors.

After analysis and simplification, the system based on the EL equation has been constructed. Using a power function, this indirect PBC controller is realized by reshaping the system energy and injecting the required damping. The adaptive load estimator has been derived that insures that the controller is effective under large load disturbance and can adapt to changes due to lamp ageing.

The simulation and experimental results verified the model and the nonlinear controller. This constant power control method is very simple in structure and is very easy to use.

Chapter 6

Analysis and Comparison of Dimming Control Method for Electronic Ballast

6.1 Introduction

Due to energy saving and to meet the needs of different users' requirements in various environmental conditions, dimmable electronic ballasts are already widely adopted for fluorescent lamps [104-106]. To the automotive headlight system, HID lamps are being fitted in high beam and low beam. The low-beam position could use lower intensity; a dimmer should be implemented for this purpose. In addition, the other motivating factor for this work is to include some flexibility in the control of the HID lamp to suit the various driving environments in the modern cities and country roads.

The dimming control in steady state is to keep the system stable, and the equivalent circuit of the system is the same as that in chapter 5 which is redrawn in Fig. 6.1. The DC-DC converter (here is the flyback converter) works in fixed high frequency mode, and the full-bridge inverter works in a fixed low frequency mode. The inductor L_p is the primary inductance of the transformer, i_0 and v_C are the output current and voltage of the flyback converter, respectively. According to the system structure, there is no resonant circuit in the system. It is feasible to use the variable duty-ratio control and variable bus voltage control in the dimming control of this system.

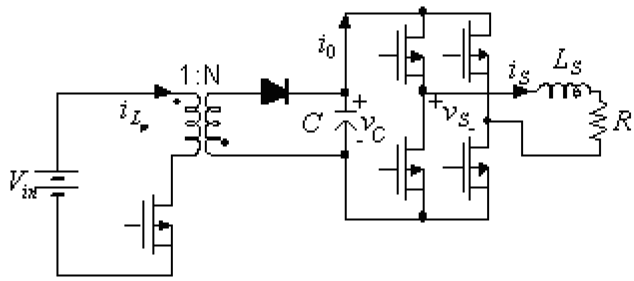

Fig. 6.1 Circuit schematic of the electronic ballast in the steady state

It is the purpose of this chapter to explore the problem of dimming the HID lamp used in the automotive headlight system. To investigate the relationship between the lamp power and control parameters, a power-dependent HID lamp model is established. The two methods, variable duty-ratio control and variable bus voltage control, are analyzed and applied in the system. The variable duty-ratio control is realized by changing the referenced dimmed power in the software of the controller, whereas the variable bus voltage control is realized by changing the value of the current sensor or voltage sensor. The simulation is used to study the comparison among three different dimming control methods, i.e. power tracking method, constant voltage power tracking method and constant current power tracking method. The 2nd and 3rd methods are later proved to be not very promising and the power tracking method is then examined in detail. The experimental results are used to verify and compare these two methods.

6.2 Review of the Dimming Control used in Discharge Lamp

Many methods have been used in dimming control and it can be divided into three different categories, i.e., variable switching frequency control, variable duty-ratio control and variable bus voltage control.

6.2.1 Variable Switching Frequency Control

The variable switching frequency control is popularly used in practical implementation because of its simplicity [58,107-113]. When the switching frequency is located further away from the resonant frequency of the tank, less energy is coupled to the lamps, which makes them dim. Although the lamp is dimmed when the switching frequency is fixed further away from the resonant frequency of the tank, an inherent unstable region exists due to the interaction between the negative impedance of the lamps. Fig. 6.2 shows the variable switching frequency control used in fluorescent and HPS lamps.

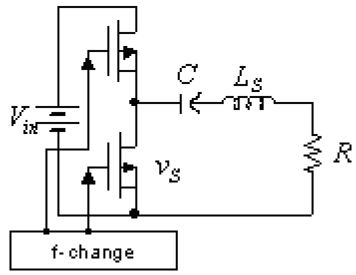

Fig. 6.2 Equivalent of variable switching frequency control

The dimming ballast with variable switching frequency control can only be realized in a limited range, typically 3:1 [58]. The stable dimming range could be extended by using DC-link voltage control [114, 115]. By selecting a switching frequency close to the un-damped natural frequency, the electronic ballasts behave as a current source controlled by the bus voltage.

6.2.2 Variable Duty-ratio control/Variable Bus Voltage Control

Controlling the duty cycle of the switches can control the load power. Duty-ratio control can achieve a level of performance similar to that of DC-link voltage control. Actually, with the asymmetrical duty-ratio control, a small DC-biased lamp current is formed [116-118]. But in half-bridge inverter, the maximal duty-ratio is 0.5. Using variable duty-ratio control, operation will change from ZVS to ZCS if the duty-ratio is small [119].

6.3 Lamps for Dimming Operation

6.3.1 Physical Characteristic of HID Lamp in dimming condition

To establish the lamp model in dimming operation, a Philips 35W MH lamp (D2S) with a cylindrical arc tube has been selected to be used in the analysis and experiment. Fig. 6.3 shows a typical experimental *V-I* characteristic of an HID lamp under dimming condition. There are two equivalent lamp resistances, the positive resistance and negative resistance. A positive-resistive *V-I* curve will appear at the beginning of dimming process. Then a negative resistance appears. The reason of these two equivalent resistances is given in reference [120] by using the thermal ionization processes of the whole ionization processes.

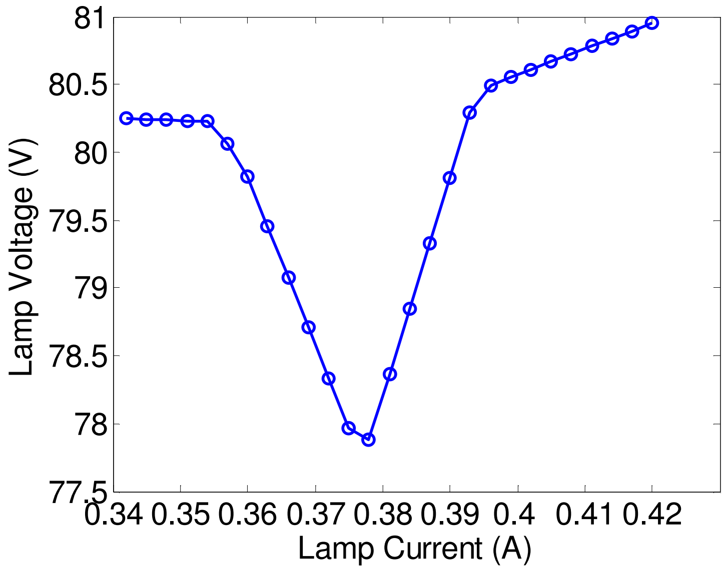

Fig. 6.3 Lamp voltage versus lamp current

6.3.2 Modeling of HID Lamps for Dimming Operation

The physical characteristic of this type of HID lamp under a dimming condition is the same as that given in reference [120]. The lamp model employed to analyze the system is a function of lamp mean power [121], as follows:

$$V_{lamp} = aP_{lamp} + b \tag{6.1}$$

$$R(P_{lamp}) = \frac{V_{lamp}^{\ \ 2}}{P_{lamp}} \tag{6.2}$$

where V_{lamp} is the lamp voltage, P_{lamp} is the lamp power and $R(P_{lamp})$ is the equivalent lamp resistance. According to the experimental data the values of a and b could be obtained by linear regression. This is just a simple method and the interpolation method is used here to improve the veracity. The interpolation method has been shown in chapter 3.

Fig.6.4 shows the simulation result and the experimental result using this interpolation method.

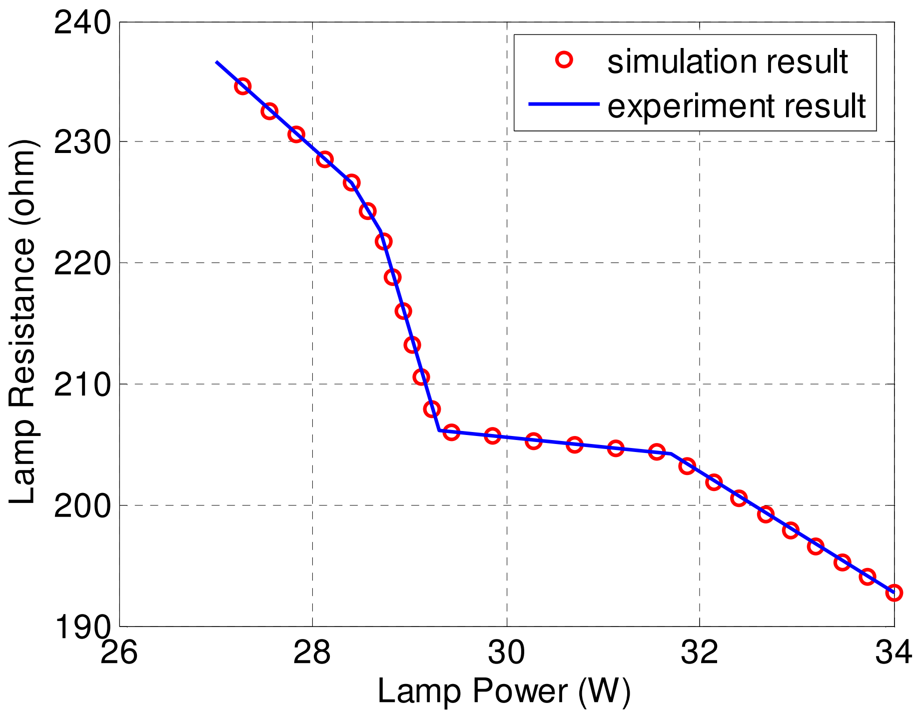

Fig. 6.4 Lamp resistance under dimming condition

6.4 Study of Dimmable Electronic Ballast with Different Methods

6.4.1 Dimming Operation with Variable Duty-ratio Control

The duty ratio control in dimming operation is called the power tracking control. The dimmed power tracks the change of reference lamp power by changing the duty ratio.

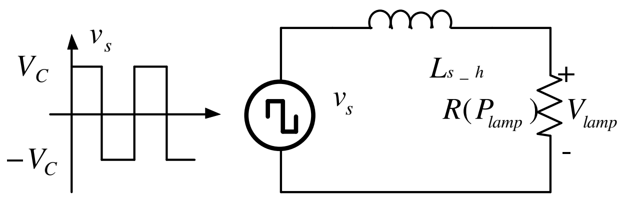

Fig. 6.5 Equivalent circuit of the full-bridge stage

The inverter stage being studied is shown in Fig. 6.5. By symmetrically driving four MOSFETs, a square-wave voltage source with amplitude of $\pm V_C$ is applied to the HID lamp. The switching frequency ω_1 and duty ratio D of the four switches in the inverter are fixed, and the L_{S_h} is the inductance referred to the secondary side of high voltage step-up transformer used in the electronic ballast. $R(P_{lamp})$ is the equivalent resistance of the lamp.

$$v_S(t) = \sum_{n=1}^{\infty} \frac{2v_C}{n\pi}(1-\cos n\pi)\sin(n\omega_1 t) \tag{6.3}$$

The relationship between v_s and the output voltage of flyback converter is given in (6.3), and from Fig. 6.5 the lamp voltage can be expressed as:

$$V_{lamp} = V_S\left|\frac{R(P_{lamp})}{Z_s + R(P_{lamp})}\right| = V_C\left|\frac{R(P_{lamp})}{Z_s + R(P_{lamp})}\right| \tag{6.4}$$

where $Z_S = j\omega_1 L_{s\_h}$. $V_C = \dfrac{ND}{1-D}V_{battery}$

According to the HID lamp model under dimming condition and the output voltage of the flyback converter, equation (6.4) can be simplified into

$$V_{lamp} = \frac{NDV_{battery}}{(1-D)}\left|\frac{R(P_{lamp})}{Z_s + R(P_{lamp})}\right| \tag{6.5}$$

From (6.5), the duty ratio that gives the lamp power P_{lamp} is determined by

$$D(P_{lamp}) = \frac{V_{lamp}}{V_{lamp} + NV_{battery}\left|\dfrac{R(P_{lamp})}{Z_s + R(P_{lamp})}\right|} \tag{6.6}$$

Therefore, using the lamp model under dimming operation developed in (6.2), the relationship between the lamp power and the control parameter D can be obtained from (6.6) for a given battery voltage and secondary inductance value Z_S of the high voltage transformer. Fig. 6.6 shows the calculated P_{lamp}-D curves with different Z_S values. For example with $V_{battery}$=12V, the turns ratio of main transformer of flyback converter is 5.5.

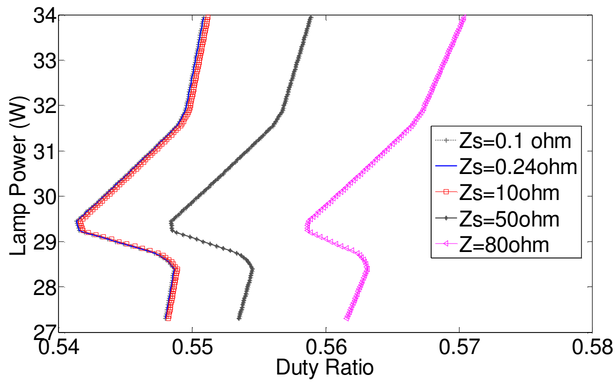

Fig. 6.6 Lamp power versus duty ratio

Fig. 6.6 shows that the range of duty ratio varies with the inductance of high voltage transformer. For high inductance impedance, the required duty ratio is also high. It is noted that the lamp voltage and lamp current do not vary with the inductance. In addition, the duty ratio varies with the required dimmed power. The variable duty ratio dimming methods are dependent on the constant power control methods.

6.4.2 Dimming Operation with Variable Bus Voltage Control

The variable bus voltage control is realized by changing the values of current or voltage sensor, which will change the input voltage of HID lamp directly. Two methods are examined in the constant power control circuit study. They are the summation method (which has been used in UCC2305 chip) and a multiplier method (proposed and used in the microprocessor or DSP chip) and are shown in Figs. 6.7 and 6.8. The voltage gain is named to be k_v and current gain is named to be k_i. Normally, the peak current comparison method is used to obtain the switching signal. The duty ratio is adjusted by the comparison of the power control signal v_{level} with the power reference signal v_{ref} . The power reference signal v_{ref} is a constant level that is used to control the output power. If v_{ref} is fixed to a fixed power, the values of current sensor and voltage sensor are fixed. Different power is obtained by changing the values of current sensor and voltage sensor to get the variable bus voltage.

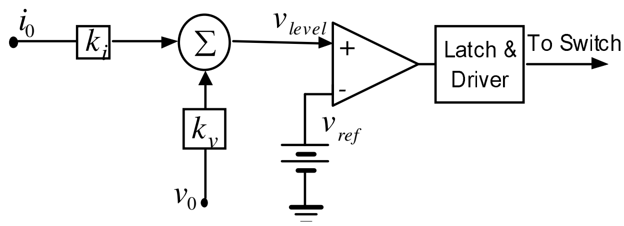

Fig.6.7 Summation method to obtain constant power

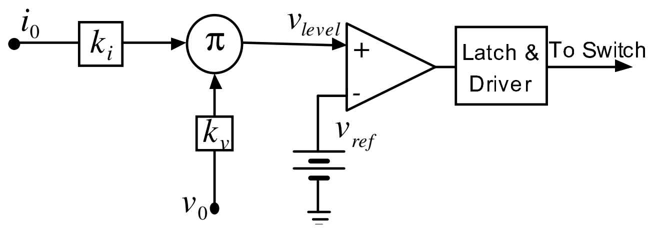

Fig. 6.8 Multiplier method to obtain constant power

(1) Summation Method

From the scheme of Fig. 6.7, the power control signal v_{level} can be expressed as

$$v_{level} = k_i \cdot i_0 + k_v \cdot v_0 \tag{6.7}$$

According to peak current modulation method, the peak current of the lamp can be written as

$$i_{0p}(v_0) = -\frac{k_v}{k_i} v_0 + \frac{v_{ref}}{k_i} \tag{6.8}$$

From Fig. 6.1, the output power of the flyback is the lamp power if the power loss is neglected, that is,

$$P_0 = \frac{V_{in} N i_{0p} \cdot (v_0 - N i_{0p} L_p N f_s)}{v_0} \tag{6.9}$$

Fig. 6.9 gives the operating range of the HID lamp. Define the slope to be $m = \frac{I_{0\max} - I_{0\min}}{V_{0\max} - V_{0\min}}$, then the current gain and voltage gain are obtained as

$$\begin{aligned} k_i &= \frac{v_{ref}}{I_{0\max} - mV_{0\min}} \\ k_v &= -m \cdot k_i \end{aligned} \tag{6.10}$$

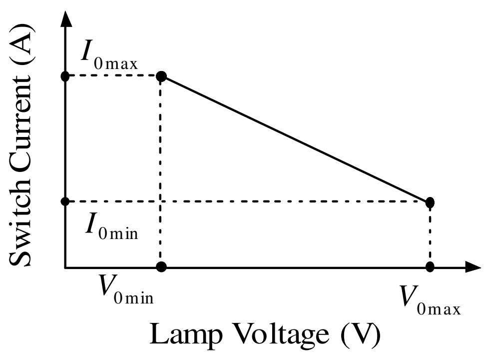

Fig. 6.9 Operating range of HID lamp

The range of lamp operating voltage for the 35W HID lamp is 60 to 110V. If the power reference signal $v_{ref} = 2.5$ V and input battery voltage is 12V, the relationship among the current gain, voltage gain and power are shown in Fig. 6.10 and Fig. 6.11.

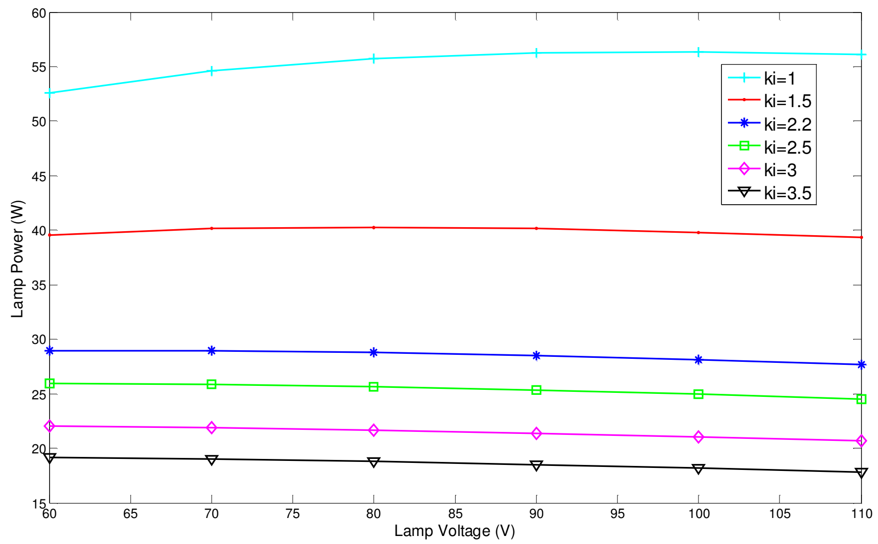

Fig. 6.10 Lamp power versus lamp voltage: effect of current gain ($k_v = 0.00485$)

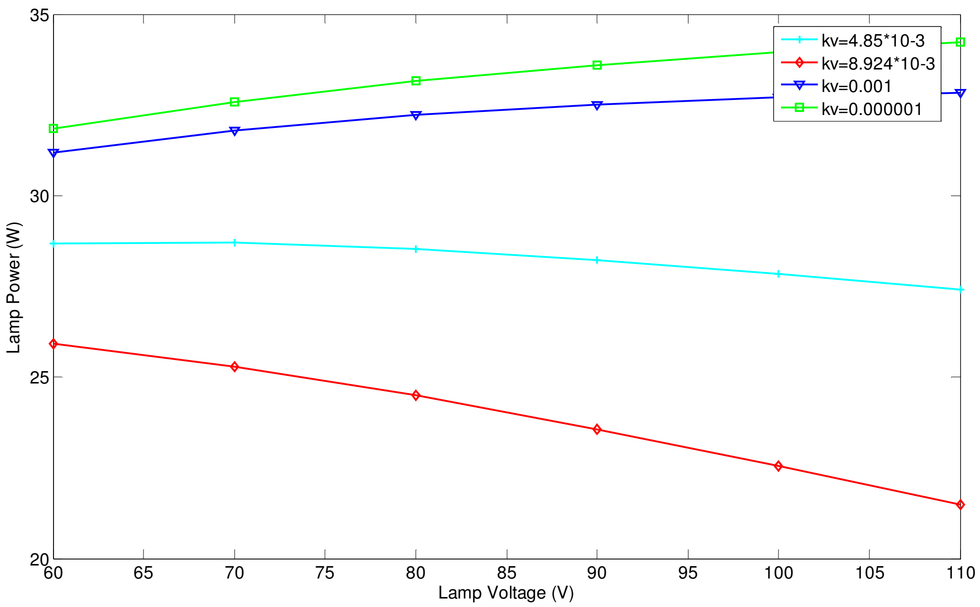

Fig. 6.11 Lamp power versus lamp voltage: effect of voltage gain ($k_i = 2.224$)

Two points can be concluded from Fig. 6.11 and 6.12: (i) The lamp output power can be changed by varying the current gain or voltage gain. (ii) In dimming operation, the current gain is used to change the lamp power, because it can keep the lamp power constant over a wide range of lamp voltage.

(2) Multiplier Method

From the scheme of Fig. 6.8, the power control signal v_{level} can be expressed as

$$v_{level} = k_i \cdot i_0 * k_v \cdot v_0 \tag{6.11}$$

According to peak current modulation method, the peak current of the lamp can be written as:

$$i_{0p}(v_0) = \frac{v_{ref}}{k_v k_i v_0} \tag{6.12}$$

The current gain and voltage gain are obtained as:

$$\begin{aligned} k_i &= \frac{v_{ref}}{k_v \cdot v_0 \cdot (mv_0 + I_{0\max} - mV_{0\min})} \\ k_v &= \frac{v_{ref}}{k_i \cdot v_0 \cdot (mv_0 + I_{0\max} - mV_{0\min})} \end{aligned} \tag{6.13}$$

Combining (6.10), the power reference signal $v_{ref} = 2.5$ V and input battery voltage is 12V. The relationship between the current gain, voltage gain and power is derived and are shown in Fig. 6.12 and Fig. 6.13.

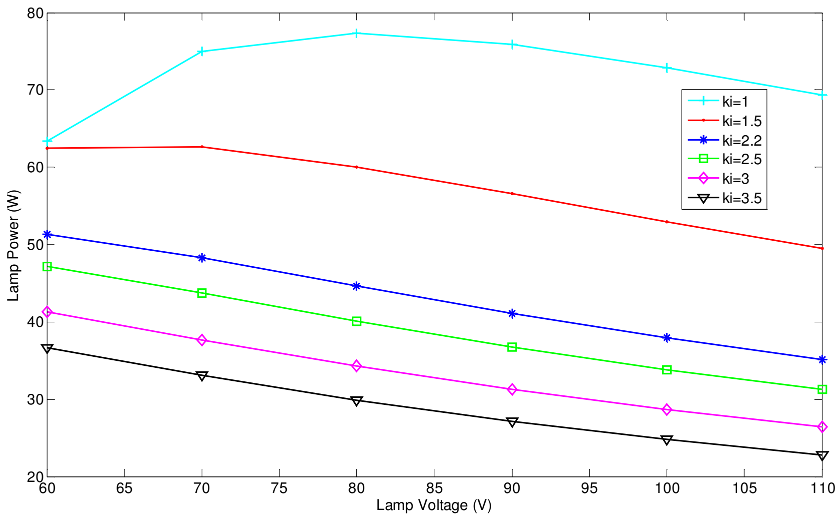

Fig. 6.12 Lamp power versus lamp voltage: effect of current gain ($k_v = 0.008924$)

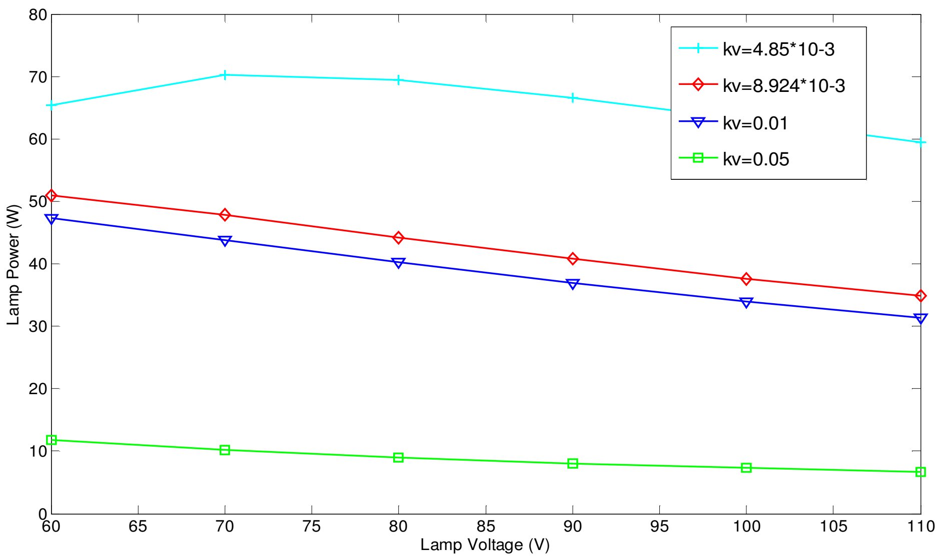

Fig. 6.13 Lamp power versus lamp voltage: effect of voltage gain ($k_i = 2.224$)

From Figs. 6.12 and 6.13, the both current gain and voltage gain can be used to control the lamp power, but the former is recommended due to small power variation with large voltage scope. Comparing the two methods, it could be concluded that: a) If the current gains of both methods are the same ($k_i = 2.224$), larger voltage gain is needed in the multiplier method. b) A larger power variation appears in the multiplier method when the lamp voltage is changed from 60V to 110V, but a small power variation appears in the summation method.

6.5 Application of variable duty ratio dimming methods

The simulation parameters which are the same as those in chapters 3-5 are given in Table. 6.1. The desired dimming power is 34W, 30.625W, 30W, 29.167W, 28W.

Table 6.1 Electronic Ballast and Lamp Profile

	Notation	Values	Unit
Inductance of primary winding in Flyback converter	L_p	10	μH
Capacitance in Flyback converter	C	5.6	μF
Inductance of secondary winding in Full-bridge converter	L_S	0.6	mH
Turns ratio	N	7	
Input voltage	V_{in}	12	V
Switching frequency of Full-bridge converter	f_1	400	Hz

6.5.1 Power tracking duty ratio control method

Here, the reference power setting is changed with the required dimmed power, and the constant power control method is used to track the reference power. Under this condition, the lamp current and lamp voltage will change, but the product of them is equal to the required dimmed power. The indirect two-loop constant power controller used in Chapter 4 is used here, and the controller is rewritten as

(1) Current Loop:

$$u = \frac{NL_p}{x_2 + NV_{in}}\left[\dot{x}_{1d} + \alpha\left(x_{1d} - x_1\right) + \frac{1}{NL_p}x_2\right] \tag{6.14}$$

where α>0 is a user defined parameter. The function of this loop is to give the control signal for the switch of the flyback converter u and make the current converge.

(2) Voltage Loop: A PI controller is used here, that is,

$$x_{1d} = K_p\left(x_{2d} - x_2\right) + K_i\int_0^t\left(x_{2d} - x_2\right)dt \tag{6.15}$$

where the proportional gain K_p and the integral gain K_i are the parameters of the controller. $x = [i_{L_p}, v_C]^T$, x_{1d} and x_{2d} are the inductor current and output voltage, respectively. The dimming lamp model established in Section 6.3 is used.

The simulation of power tracking duty ratio dimming control method is shown in Fig. 6.14. The lamp voltage varies slightly, but the variation of lamp current is larger. This power tracking duty ratio control can give the desired dimming power. This should be a feasible method for the dimming control.

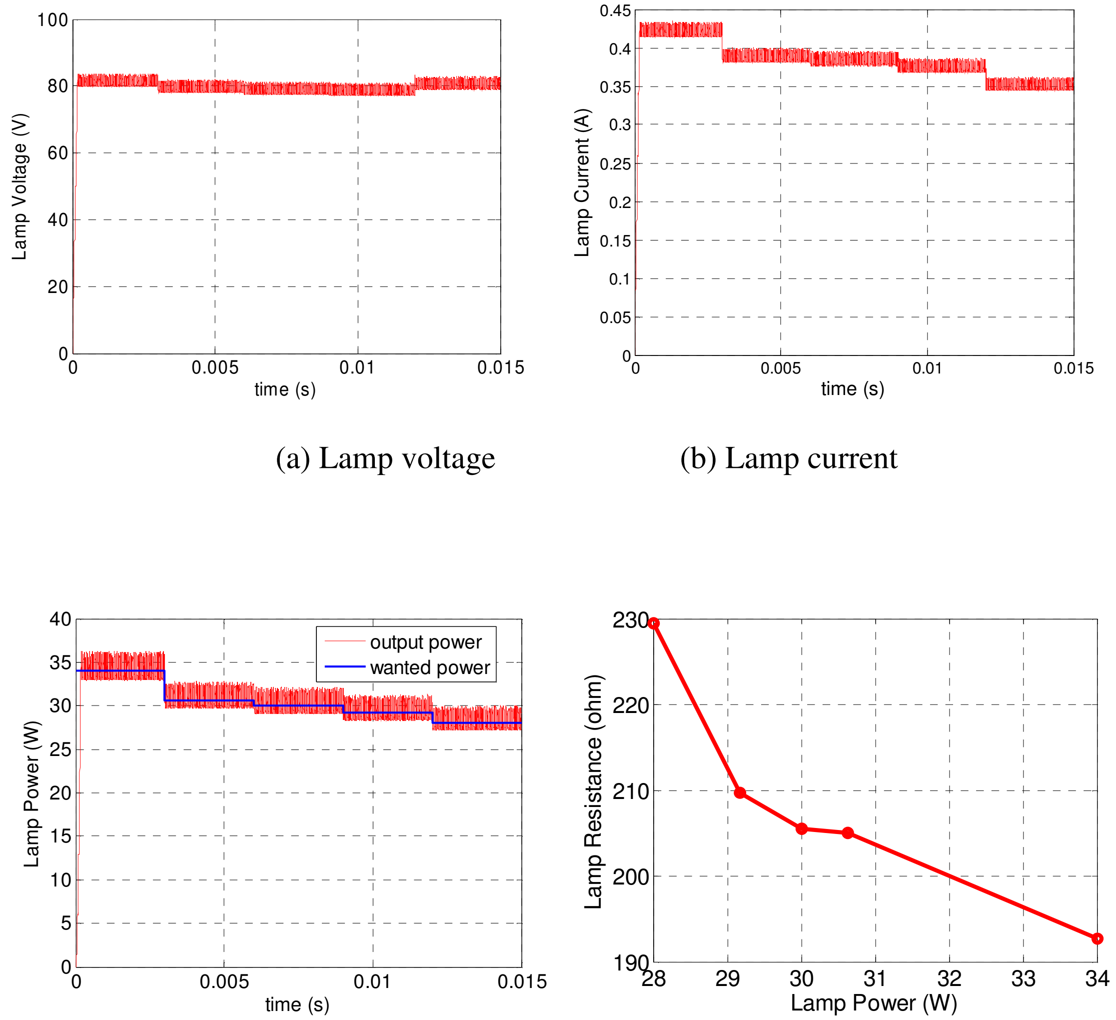

(a) Lamp voltage (b) Lamp current

(c) Lamp power (d) Lamp resistance

Fig. 6.14 Power tracking method using constant power control

6.5.2 Constant Voltage Power tracking duty ratio control method

In this situation, the lamp voltage is constant during the whole dimming operation; otherwise the lamp current would be changed with the reference power and the lamp resistance. The voltage loop is omitted and the desired voltage is defined as 85V, $x_{2d} = v_{0ref}$ =80.952V. $\dot{x}_{2d} = 0$. The controller is just given by using equations (6.14), (6.15) and (4.2) as:

$$u=\frac{NL_pC}{C(x_2+NV_{in})-K_PL_px_1}\left[-\frac{K_P}{NC}x_1+\frac{K_P}{RC}x_2+K_i(x_{2d}-x_2)+\alpha(x_{1d}-x_1)+\frac{1}{NL_p}x_2\right] \tag{6.16}$$

The simulation of constant voltage power tracking duty ratio dimming control method is shown in Fig. 6.15. The lamp voltage is fixed, and the lamp current varies with the reference power. But the desired power could not be tracked as shown in Fig. 6.15(c), so this method could not be used in the dimming operation.

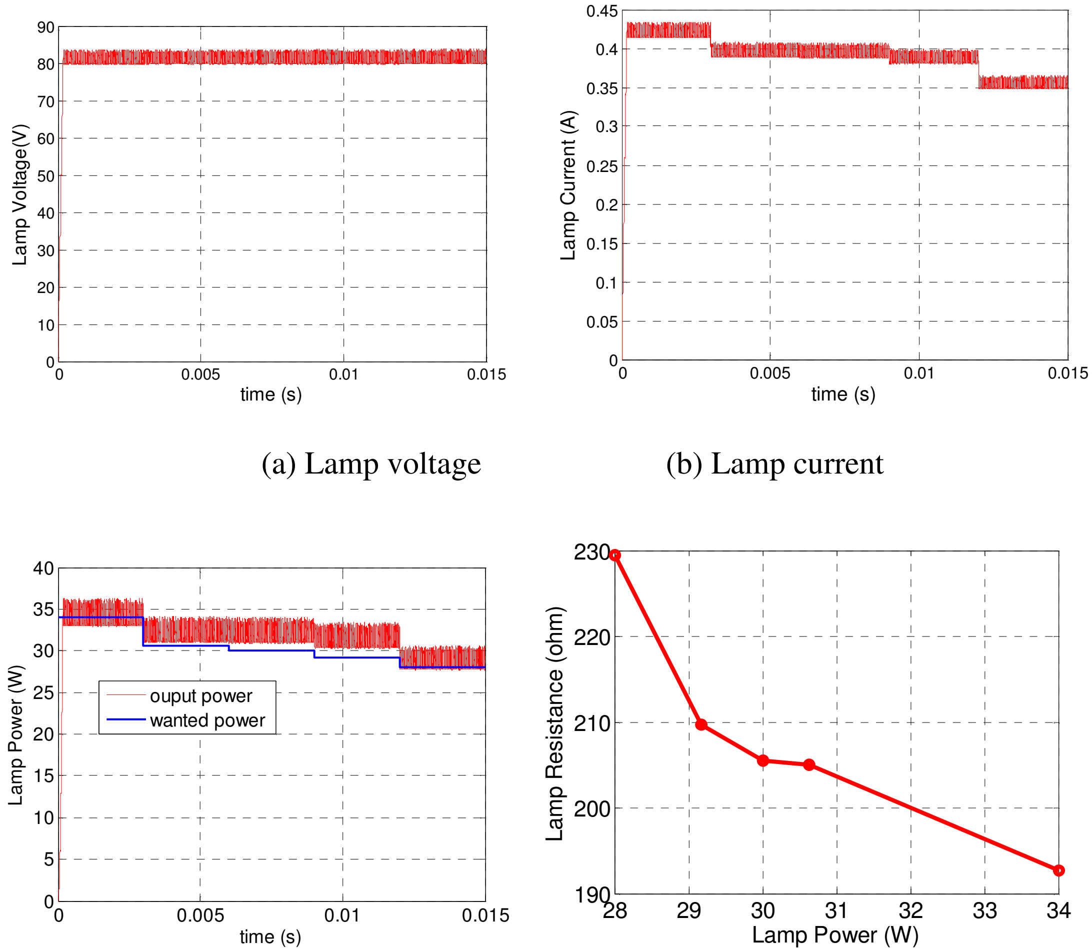

(a) Lamp voltage (b) Lamp current

(c) Lamp power (d) Lamp resistance

Fig. 6.15 Power tracking method using constant voltage control

6.5.3 Constant Current Power tracking duty ratio control method

The lamp current is constant but the lamp voltage is allowed to change with the reference power and the lamp resistance. Here x_{1d}=constant, then $\dot{x}_{1d} = 0$. According to equation (6.15), the wanted value x_{2d} varies as:

$$\dot{x}_{2d} + \frac{K_i}{K_p} x_{2d} - \frac{1}{K_p}[K_i x_2 + K_p(\frac{1-u}{NC} x_1 - \frac{1}{RC} x_2)] = 0 \qquad (6.17)$$

The controller is the same as equation (6.16) with the changed wanted value x_{2d}.

The simulation of constant current duty ratio dimming control method is shown in Fig. 6.16. The lamp current is fixed, and the lamp voltage varies with the desired power. The deviation of the desired power from the real output power is more severe than that of the constant voltage power tracking duty ratio control method.

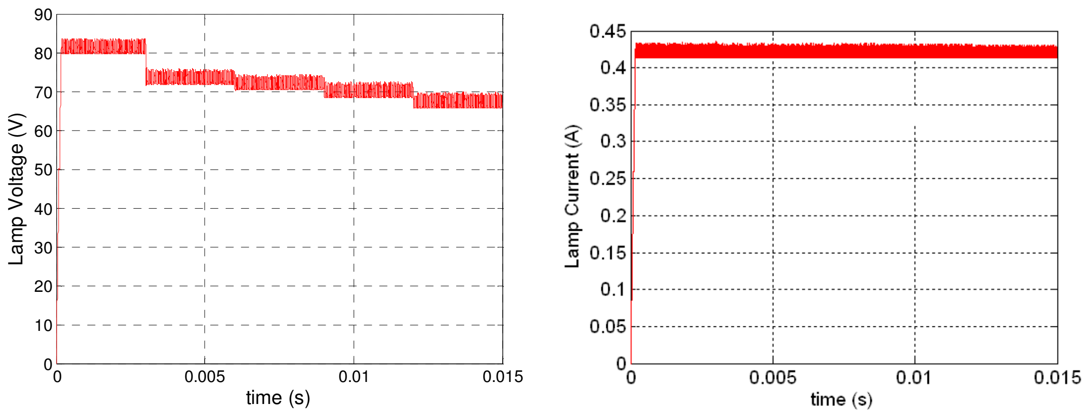

(a) Lamp voltage (b) Lamp current

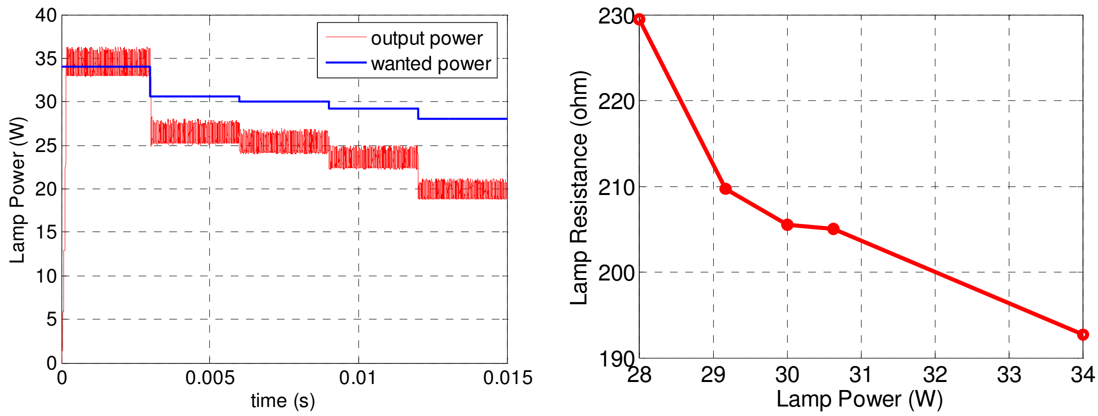

(c) Lamp power (d) Lamp resistance

Fig. 6.16 Power tracking method using constant current control

6.5.4 Summary of variable duty ratio dimming methods

The above study shows that the two dimming control methods, constant voltage power tracking method and constant current power tracking method, are not able to track the wanted dimming power. The reason is that: the lamp equivalent resistance which varies and is decided by the current or temperature of the lamp but is not controlled by the controller. If the lamp voltage or current is fixed, the lamp current or voltage respectively is fixed due to the constant power condition (the product of current and voltage is constant). But the equivalent lamp resistance is not fixed by that value equal to the ratio of voltage/current. So, just the power tracking duty ratio control method is used in the dimming control to get the desired power.

6.6 Experimental results

The dimming control was carried out in the steady state and the experimental results were obtained. The PI controller was used in the experiment in order to verify the simulation results. The Philip D2S lamp was used in the experiment. The desired dimming powers, 30W, 29.2W and 26.25W, were obtained in the experiment. The two dimming methods, namely variable duty ratio method and variable bus voltage method, are compared in this section.

6.6.1 Variable Duty ratio Dimming Method

Figs. 6.18-20 show the experimental results of lamp current and lamp voltage in dimming condition under different output power. Fig. 6.17 gives the lamp current and lamp voltage waveforms without dimming control whose output power is 35W. Fig. 6.21 shows the dimming process of lamp current and lamp voltage when the lamp power is dimmed from 35W to 26.25W. Using the power tracking dimming control method, the output power varies with the lamp current. Noticeably, the output light has reduced and energy has been saved. The minimum dimming power is 26.25W. In this dimming process, the lamp voltage changes in a tiny small range as shown in Fig. 6.21.

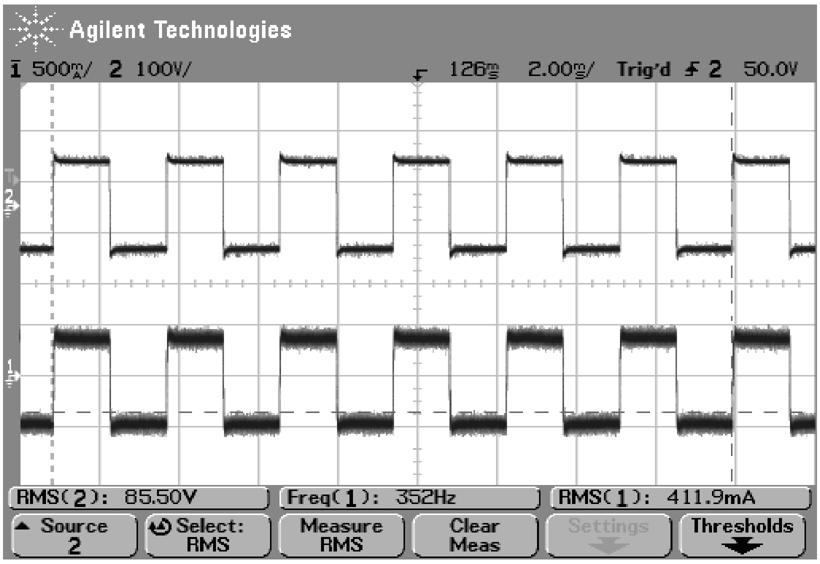

Fig.6.17 Lamp voltage and current at 35W (voltage: 85.50V, current: 0.411A) (ch1: lamp current, 500mA/div, 2ms/div; ch2: lamp voltage, 100V/div, 2ms/div)

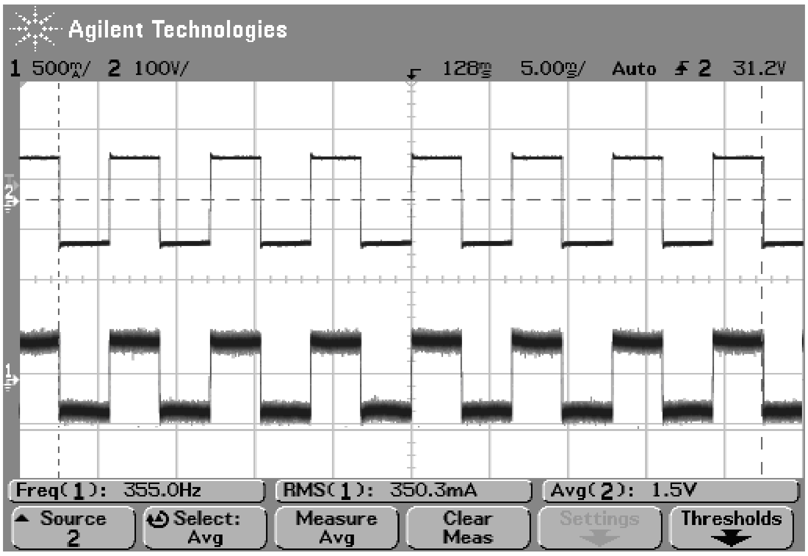

Fig.6.18 Lamp voltage and current at 30W (voltage: 85.51V, current: 0.350A) (ch1: lamp current, 500mA/div, 2ms/div; ch2: lamp voltage, 100V/div, 2ms/div

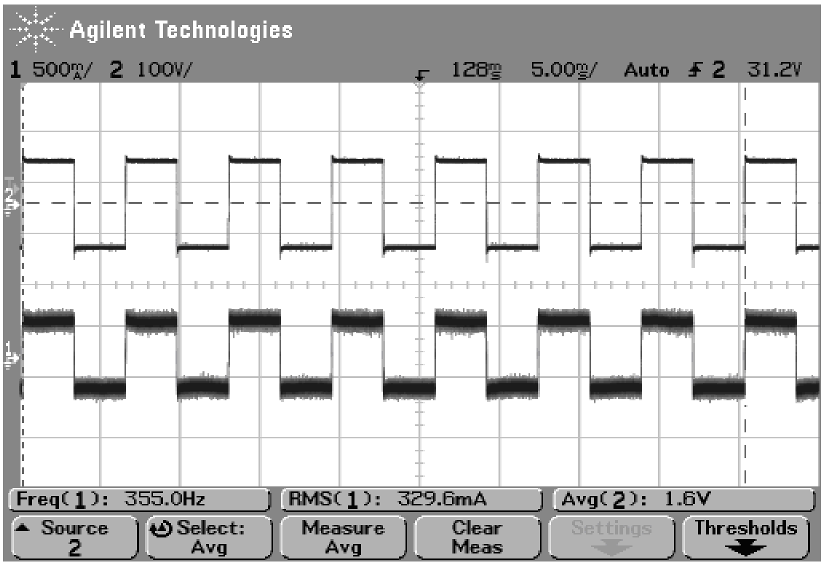

Fig.6.19 Lamp voltage and current at 29.2W (voltage: 85.56V, current: 0.329A) (ch1: lamp current, 500mA/div, 2ms/div; ch2: lamp voltage, 100V/div, 2ms/div)

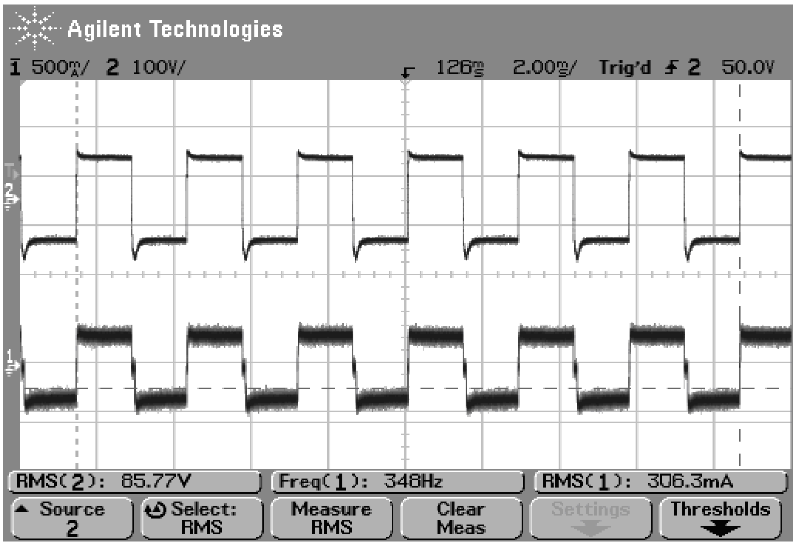

Fig.6.20 Lamp voltage and current at 26.25W (voltage: 85.77V, current: 0.306A) (ch1: lamp current, 500mA/div, 2ms/div; ch2: lamp voltage, 100V/div, 2ms/div)

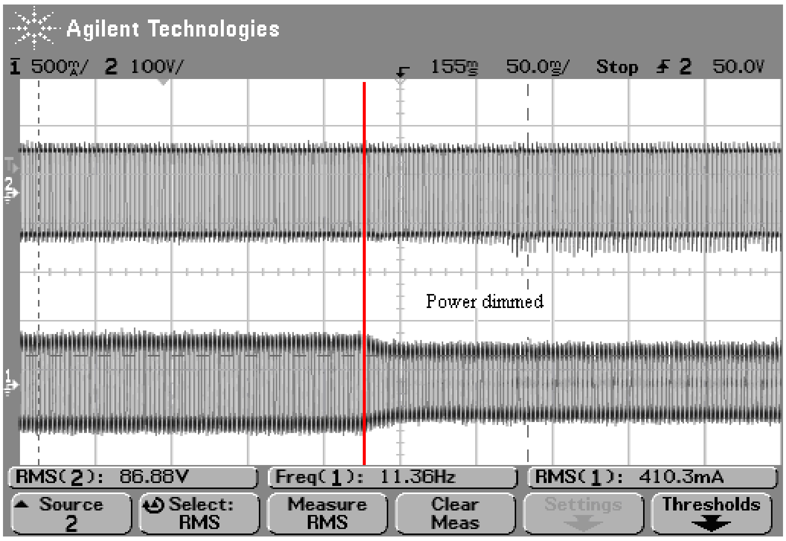

Fig.6.21 Lamp voltage and current from 35W to 26.25W (ch1: lamp current, 500mA/div, 50ms/div; ch2: lamp voltage, 100V/div, 50ms/div)

6.6.2 Variable Bus Voltage Control

This dimming method is now realized by the UCC2305 based ballast system. In this controller, the summation method is used, so a larger dimming range can be obtained.

Fig. 6.22 shows the lamp current and lamp voltage under 28W output power. Fig. 6.23 gives the lamp current and lamp voltage under 23.1W output power. The minimum dimming power is 23.1W for successful illumination. Using variable bus voltage control, the lamp current and lamp voltage would be changed with reduced power. If the desired power decreases, the lamp voltage decreases, too. But using variable duty-ratio control method, the lamp voltage could not be changed. A larger dimming scope is obtained by the variable bus voltage control and this conclusion has been verified by the experimental result. Using the variable bus voltage method, the power of a 35W-HID lamp can be reduced by 34%. Using the variable duty-ratio control method, the power of a 35W-HID lamp can be reduced by 23%.

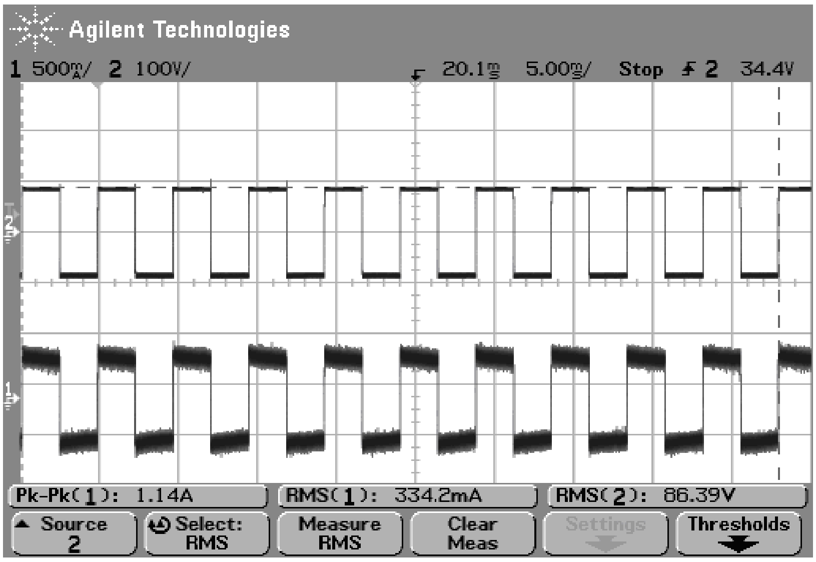

Fig.6.22 Lamp voltage and current at 28W (voltage: 86.39V, current: 0.334A) (ch1: lamp current, 500mA/div, 2ms/div; ch2: lamp voltage, 100V/div, 2ms/div)

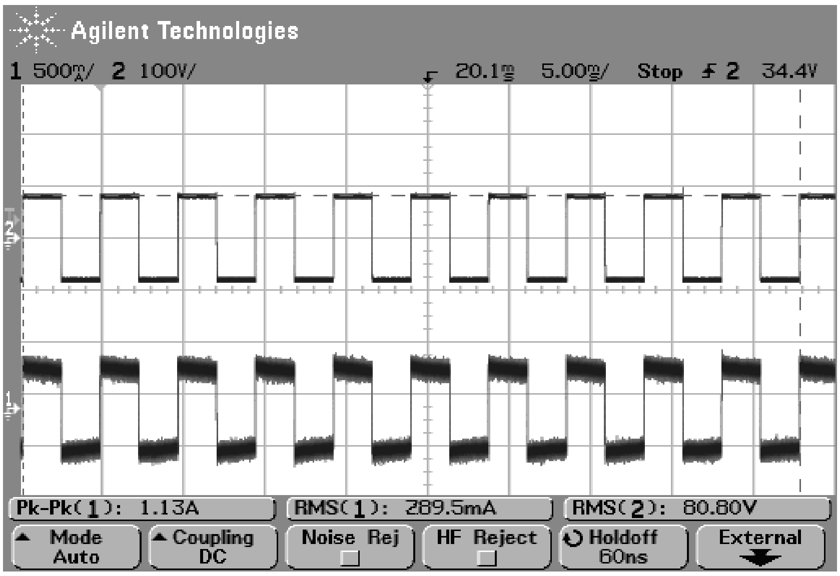

Fig.6.23 Lamp voltage and current at 23.1W (voltage: 80.80V, current: 0.289A) (ch1: lamp current, 500mA/div, 2ms/div; ch2: lamp voltage, 100V/div, 2ms/div)

6.6.3 Light Output

Dimming control using the microprocessor based power tracking method has been conducted and their spectra have been measured using the Integrated Sphere. Fig.6.24 and 6.25 show the optical results of the HID lamp at output power 35W and 26.25W. It is clear that the light output changes from 2462 *lm* to 1672 *lm* respectively. When the lamp power is reduced, the light output is also reduced. Further, the efficacy is 56.49*lm*/W at 35W and it decreases to 47.03*lm*/W at 26.25W.

In addition, the integrated sphere measures efficacy using Light-output/P_{in} and since light output is proportional to P_{out}, it is fair to say that the trend (not the absolute value) of the efficiency of the ballast can be tracked by the change in the efficacy of the lamp. As long as the same ballast is used for recording the data under normal and dimming condition, we can surely say that there is a drop in the efficiency of the circuit under dimming condition as the circuit is working at a different power level.

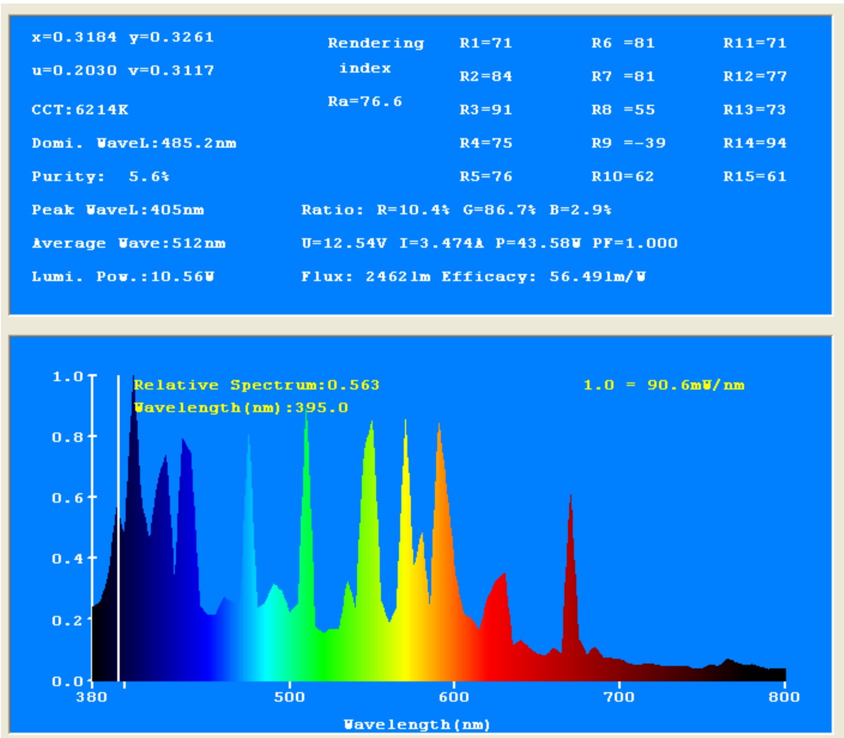

Fig.6.24 Spectrum map under output power is 35W

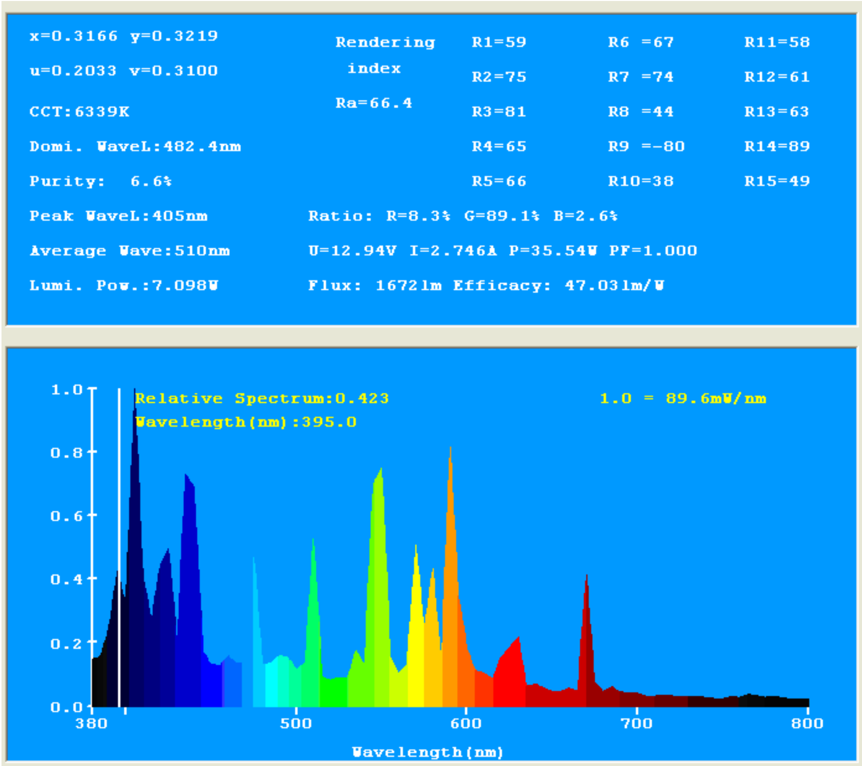

Fig.6.25 Spectrum map under output power is 26.25W

6.7 Summary

The research and implementation of the dimming control is presented in this chapter. Variable duty ratio dimming method (VDRDM) and variable bus voltage dimming method (VBVDM) are described. Mathematical analysis, simulation and experiments are conducted. These two methods are used in the dimming control.

In VBVDM, the advantage of changing current gain is to regulate constant power with large voltage change that is better than the changing voltage gain method. In VDRDM, the power tracking duty ratio control method is preferred because it can track the desired power variation very well. Contrasting the VDRDM and VBVDM, a larger dimming range can be realized by the VBVDM.

Lastly, it is reported that the ballast achieves a reduction of 32% light output.

Chapter 7

Ageing Analysis of Electronic Ballast

7.1 Introduction

The HID lamp ballast is under the operation of constant power control to examine the ageing of the lamp. Under such condition, the equivalent lamp resistance will increase at the same time the excitation voltage of the lamp will increase from 85V to 104V, even to 140V. In addition, the distance between the electrodes will be enlarged, that is, the voltage drop of the electrodes increases. For a new Xenon lamp, the distance of the electrodes is short and it is around 4.2mm.

According to the standard – SAEJ2009, the accurate rated luminous flux and the rated average life are shown in Table 7.1. The D2S lamp type is usually used in the car headlight system. In this table, it is clear that the HID lamps have good luminous flux and lamp life.

Table 7.1 Luminous Flux Requirements of Standard

Designation	Accurate Rated Luminous Flux	Rated Average Life
	(*lm*)	(hours)
D1R	2800±150	2000
D2R	2800±150	2000
D2S	3200±150	2000
D3R	2800±150	2000
D3S	3200±150	2000
D4R	2800±150	2000
D4S	3200±150	2000

The purpose of this chapter is to find out the alternative method to compensate a Xenon lamp near the end of its life time. In the past, the lamp will be disposed if an effective intensity cannot be obtained. The proposed study is to provide a compensation method that, based on the measured characteristics of general Xenon lamps, and to calculate the required compensation power and to extend the constant illumination time.

The study below is first to conduct the life time measurement of a number of lamps. Two test groups, whose burning cycles are 100 hours and 25 hours, have been conducted under the continuous lighting condition. The generalized characteristic of lamp resistance is obtained. The required power for maintaining constant lumen output is made and to compensate for the correct lamp output.

This chapter is not to investigate a high level research of compensation technique, but to provide a simple solution to compensate a Xenon lamp for constant illumination and it is a chapter to describe the practical application of HID lamps. The method has been proposed to automotive parts manufacturers.

7.2 Ageing Test Experiment Setup

7.2.1 Methods

Lamp life was studied in this chapter with a lamp life test. Lamps were burned in open surroundings. Due to the high value of the starting input current of each lamp, each lamp is turned on in sequence with a delay of 5 seconds to avoid the large start up current which may trip the power supply. A sequence controller as shown in Fig. 7.1 is needed in the lighting group. It is noted that the input current of HID lamp has a large transient current whose value is almost to 26A, as shown in Fig. 7.2.

The supply voltage was 12V. The rated voltage was declared by the manufacturer were 9-16V. The temperature of the test room was +15˚C- 220˚C.

The two test groups were:

Group 1: 100 hour burning cycle, 99 hours on and 1 hour off

Group 2: 25 hour burning cycle, 24 hours on and 1 hour off

In each test group there were 5 lamps which came from 5 different manufacturers. Wattage of each lamp was 35W. The controller used here had two functions: one was the timer and the other was the delay. The controller was realized by a microprocessor and the prototype of the system is shown in Appendix IV. The ballasts used in the two testing groups were the same.

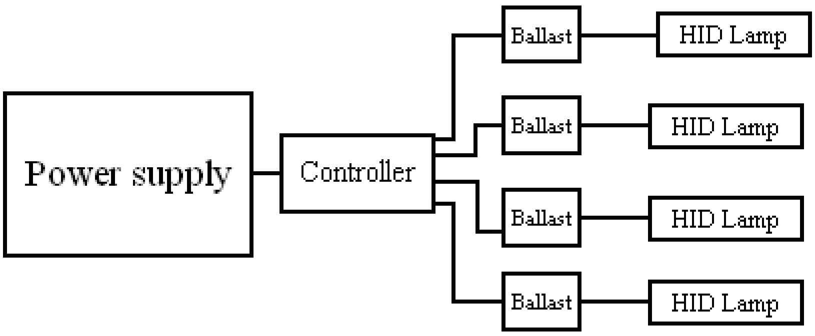

Fig. 7.1 Test set up and controller

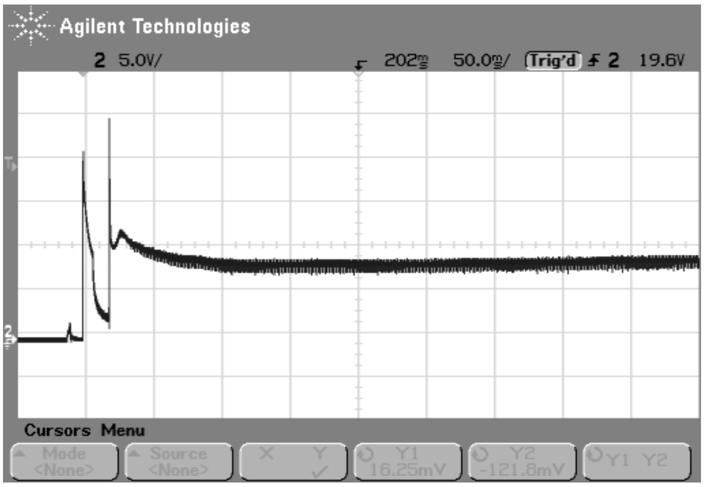

Fig. 7.2 Input current of Philips D2S lamp (input peak current: 26.35A, 5A/div)

7.2.2 Testing Devices and electrical measurements

Both photometric and electrical measurements were made during the off time of each burning cycle.

Lamps were burned in the integrated sphere (Fig. 7.3) and the stabilization period was 10 minutes. The diameter of the sphere is 1m. The spectrometer is connected to a PC, which then calculates the luminous flux and color properties of the test lamp.

The electrical measurements included the lamp voltage, current, peak power and steady state power.

Supply voltage was 12V. The measured quantities were:

V_{lamp}	Lamp voltage in steady state
I_{lamp}	Lamp current in steady state
P_{lamp}	Lamp power in steady state
Φ	Luminous flux measured
η	Luminous efficacy $\Phi / Plot$
CCT	correlated color temperature

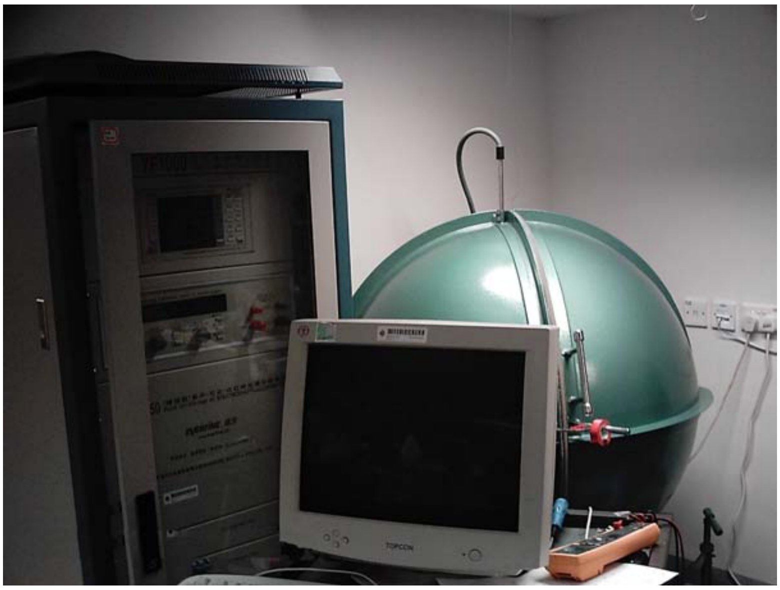

Fig. 7.3 Spectrum analyzer and integrating sphere

7.3 Ageing Results

The output luminous flux of a normal HID lamp is 2800lm and it is used as the reference here. Generally speaking, the output luminous flux of the HID lamp which is burned 1000 hours is not less than 70% of that of a new lamp. In this section, the ageing results include the lamp voltage analysis, lamp current analysis, lamp power analysis, lumen maintenance and mortality. Here, five different lamps use A, B, C, D and E as their names.

7.3.1 Lamp Voltage Analysis

The rated lamp voltage in steady state is 85V which is used as the reference voltage value. The lamp voltage is the voltage value of the lamps during operation. A parameter called voltage maintenance is defined to present the aging level of the lamp.

$$R_{Vm\_a} = \frac{v_{lamp}}{V_{rated}} \times 100\% \tag{7.1}$$

where V_{rated} is rated lamp voltage in steady state. v_{lamp} is the lamp voltage in real burning time and R_{Vm_a} is the voltage maintenance.

Table 7.2 shows values of the voltage maintenance of the two groups after 100, 2000 and 3700 burning hours. In this table, the higher the values of the voltage maintenance, the higher is the lamp voltage. If the value of the voltage maintenance is N/A, it means the lamp burns out.

Table 7.2 Voltage maintenance (R_{Vm_a}) between different manufactures after 100, 2000 and 3700 burning hours

		Burning time (h)		
		100	2000	3700
Group 1	A	96.94%	115.06%	N/A
	B	88.47%	90.94%	117.88%
	C	93.53%	107.41%	N/A
	D	94.82%	107.41%	109.06%
	E	99.06%	104.94%	105.35%
Group 2	A	125.53%	126%	N/A
	B	112%	113.65%	112%
	C	98.56%	N/A	N/A
	D	99.88%	108.18%	110.01%
	E	100.71%	110.82%	111.29%

There were variations between different test groups and also between different manufacturers. When compared with different test groups, the voltage maintenance was higher on small burning cycle (group 2, cycle is 25 hours). C is the first lamp which burned out.

(1) Same brand with different burning cycles

If the burning hour is the same with different burning cycles, the increasing rate of lamp voltage is different. In general, the burning cycle is shorter, the rising rate is faster. Fig. 7.4 gives the comparison results in the same burning time of same brand lamp with different burning cycles. It shows that the lamp voltage in burning cycle 25 hours is bigger than that of burning cycle 100 hours in the same burning time.

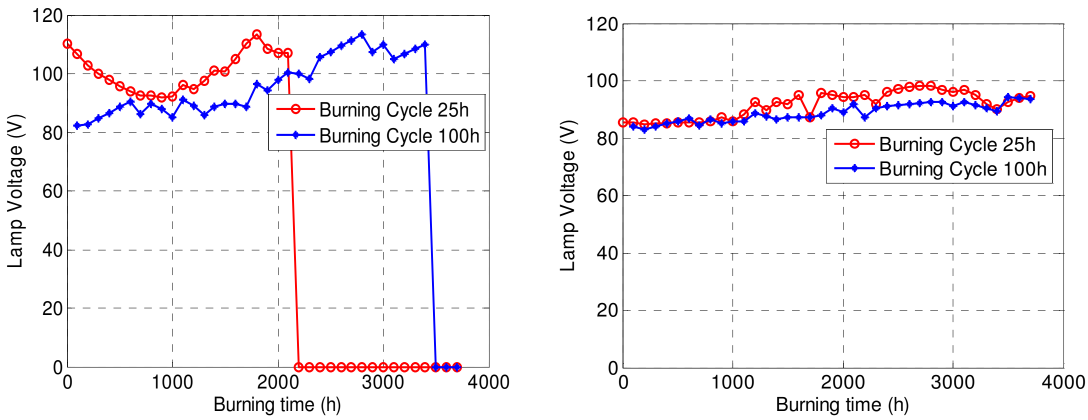

(a)Brand name is A (b) Brand name is E

Fig. 7.4 The voltage comparison between the two groups with the same brand

(2) Different brands with the same burning cycles

If the burning cycle is the same, different HID lamp with different brand has different lamp voltage in steady state. If the reference voltage of the HID lamp is 85V, the lamp with the brand name E has a better performance in keeping the lamp voltage constant. With the increasing of the burning time, the lamp voltage is increased that is similar for all the HID lamps. Fig. 7.5 shows the comparison results of different HID lamps in the same test group.

In the diagram, those lines dropping rapidly to zero refer to the cases that the lamps were burnt out at that instant.

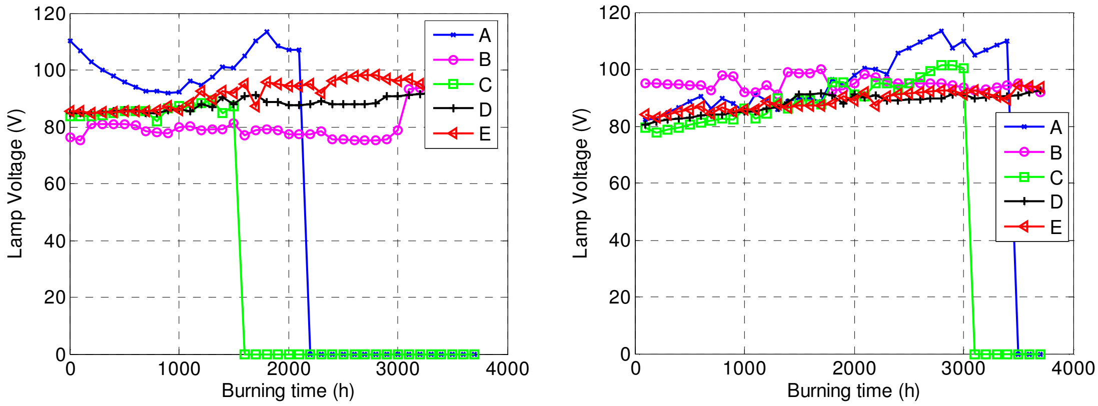

(a)Burning cycle is 25 hours (b) Burning cycle is 100 hours

Fig. 7.5 The voltage comparison between the different brand lamps with the same group in the same burning time

Summary: a) There were variations between different manufacturers in one test group. The lamp voltage would increase with the ageing hours of the HID lamp. b) The same HID lamp ages faster with a shorter turn on and off cycle.

7.3.2 Lamp Current Analysis

The rated lamp current in steady state is 0.412A which is used as the reference current value. A parameter called current maintenance is defined to present the aging level of the lamp.

$$R_{Am\_a} = \frac{i_{lamp}}{I_{rated}} \times 100\% \tag{7.2}$$

where I_{rated} is rated lamp current in steady state. i_{lamp} is the lamp current in real burning time and R_{Am_a} is the current maintenance.

In Table 7.3, there are the values of the current maintenance of two groups after 100, 2000 and 3700 burning hours. In this table, the lower the values of the current maintenance are, the lower the lamp current decrease. Again, if the value of current maintenance is N/A, it means the lamp is burned out.

Table 7.3 Current maintenance (R_{Am_a}) between different manufactures after 100, 2000 and 3700 burning hours

		Burning time (h)		
		100	2000	3700
Group 1	A	101.76%	87.19%	N/A
	B	110.5%	108.07%	90.83%
	C	106.86%	93.26%	N/A
	D	102.97%	92.04%	89.61%
	E	102.97%	98.11%	93.26%
Group 2	A	81.11%	81.11%	N/A
	B	87.43%	88.4%	107.1%
	C	106.86%	N/A	N/A
	D	99.33%	95.69%	92.04%
	E	100.54%	90.83%	88.4%

(1) Same brand with different burning cycles

The lamp current decreases with the burning time. In general, the shorter the burning cycle, the faster the lamp current decreases in the steady state. Fig. 7.6 gives the comparison results in the same burning time of same brand lamp with different burning cycles. The figure shows that the decreasing rate of the lamp current is large when burning cycle is 25 hours and the rate is smaller in burning cycle 25 hours than that of burning cycle 100 hours in the same burning time.

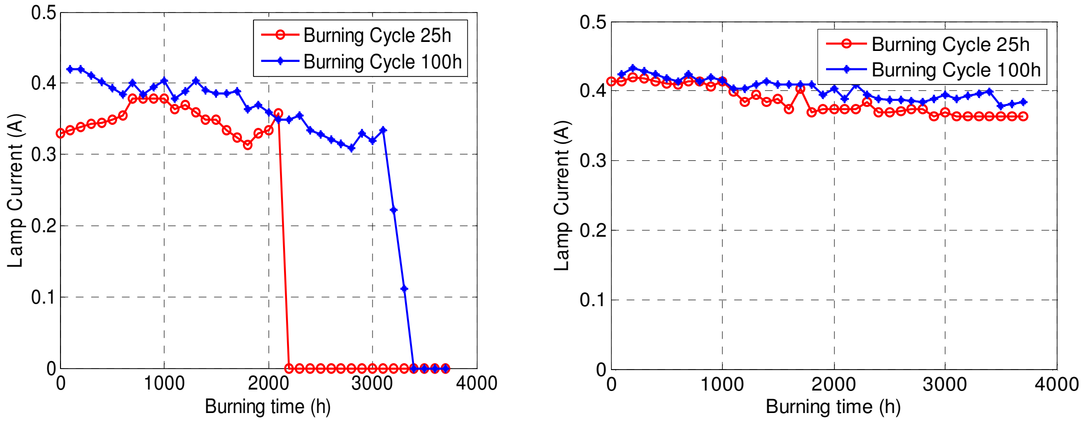

(a)Brand name is A (b) Brand name is E

Fig. 7.6 The current comparison between the two groups in the same brand

(2) Different brands with the same burning cycles

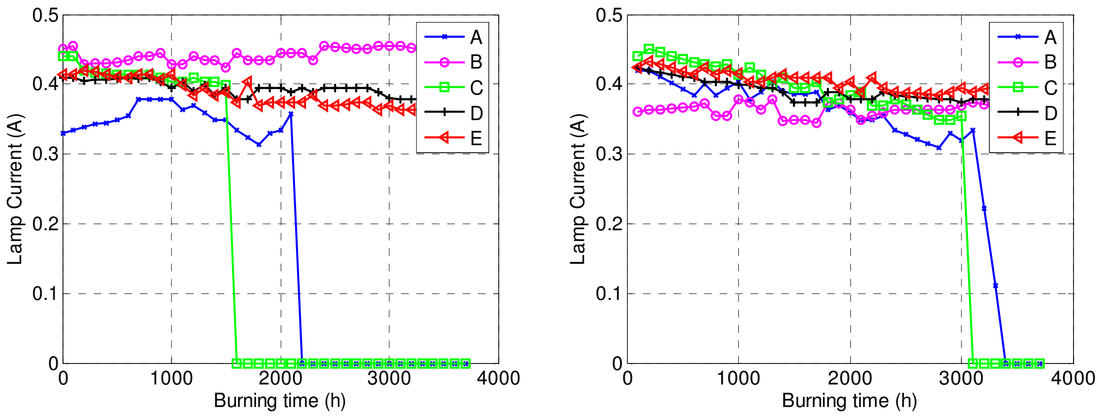

(a)Burning cycle is 25 hours (b) Burning cycle is 100 hours

Fig. 7.7 The current comparison between the different brand lamps with the same group in the same burning time

The tendency of the lamp current is decreasing with time whereas the tendency of the lamp voltage as shown in section 7.3.1 is increasing with time.

7.3.3 Lamp Power Analysis

In steady state, the constant power control is used to make the lamp life longer. In general, the power is 35W in steady state. A parameter called power maintenance is defined to present the aging level of the lamp.

$$R_{Pm\_a} = \frac{p_{lamp}}{P_{rated}} \times 100\% \tag{7.3}$$

where P_{rated} is rated lamp power in steady state. p_{lamp} is the lamp power in real burning time and R_{Pm_a} is the power maintenance.

Generally speaking, if the lamp power is constant, the power maintenance is constant. In Table 7.4, there are the values of the power maintenance of two groups after 100, 2000 and 3700 burning hours. The output power would increase before the HID lamp is burned out.

Table 7.4 Power maintenance (R_{Pm_a}) between different manufactures after 100, 2000 and 3700 burning hours

		Burning time (h)		
		100	2000	3700
Group 1	A	97.14%	97.14%	N/A
	B	97.14%	97.14%	97.14%
	C	97.14%	100.57%	N/A
	D	97.14%	97.14%	97.14%
	E	102.29%	103.14%	103.41%
Group 2	A	97.14%	97.14%	N/A
	B	97.14%	97.14%	97.14%
	C	97.14%	N/A	N/A
	D	97.14%	97.14%	97.14%
	E	101.43%	102%	103.14%

(1) Same brand with different burning cycles

Fig. 7.8 gives the comparison results in the same burning time of same brand lamp with different burning cycles. It is interesting to see that the lamp with shorter burning cycle is easier to burn out. Again the line dropping to zero rapidly refers to the lamp burn out at that instant.

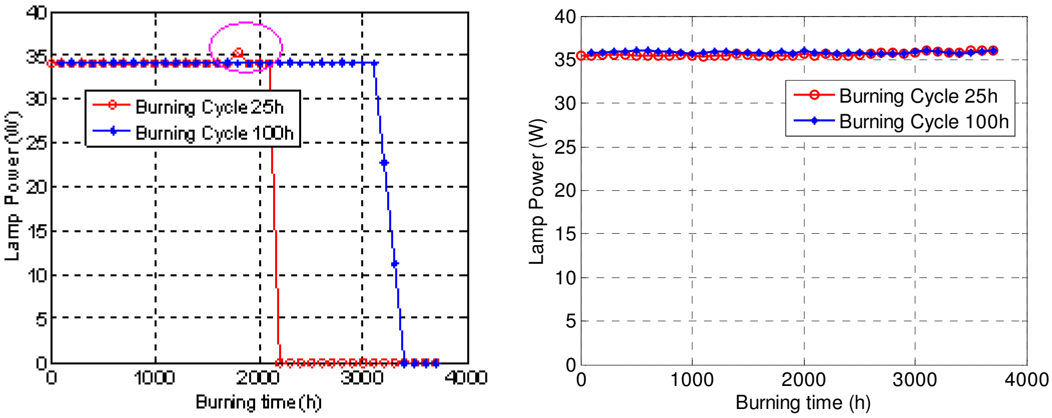

(a)Brand name is A (b) Brand name is E

Fig. 7.8 The power comparison between the two groups in the same brand

(2) Different brands with the same burning cycles

The comparison of lamp powers of different brand lamps in the burning cycle 25 hours and 100 hours is shown in Fig. 7.9(a) and Fig. 7.9(b), respectively.

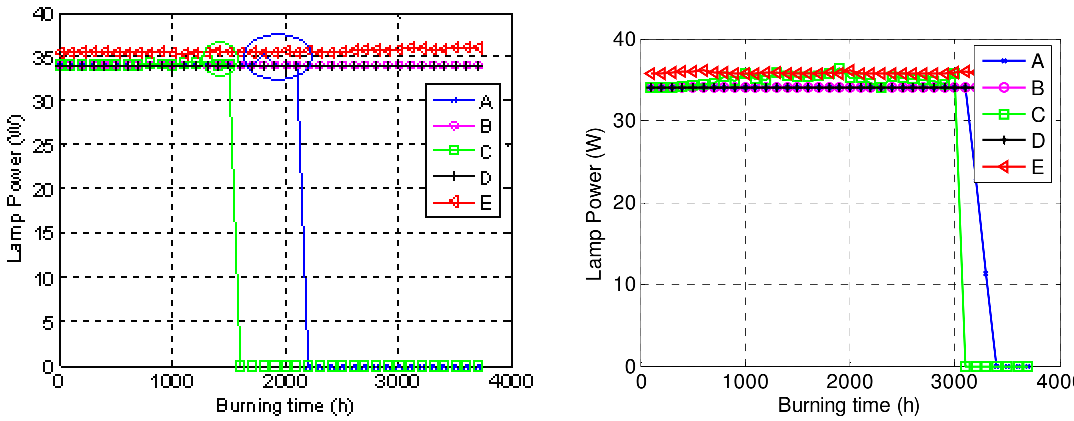

(a)Burning cycle is 25 hours (b) Burning cycle is 100 hours

Fig. 7.9 The power comparison between the different brand lamps with the same group in the same burning time

Summary: a) In our experiment, the lamp power will increase with the burning hour. Just before a lamp burns out, the lamp power increases slightly as shown in the highlighted circle in Fig. 7.8(a) and Fig. 7.9(a). b) The shorter the burning cycle, the easier it is for the HID lamp to burn out.

7.3.4 Lumen flux Maintenance

With the lamp ageing, the lumen flux will decrease. A parameter called lumen flux maintenance is defined to present the aging level of the lamp.

$$R_{\Phi m\_a} = \frac{\varphi_{lamp}}{\Phi_{rated}} \times 100\% \tag{7.4}$$

where Φ_{rated} is reference lumen flux in steady state. φ_{lamp} is the lumen flux in real burning time and $R_{\Phi m\_a}$ is the lumen flux maintenance.

Table 7.5 gives the values of the lumen flux maintenance of two groups after 100, 2000 and 3700 burning hours. The reference lumen here is 2800*lm* which is the accurate rated luminous flux requirement in the HID lamp.

Table 7.5 Lumen maintenance ($R_{\Phi m\_a}$) between different manufactures after 100, 2000 and 3700 burning hours

		Burning time (h)		
		100	2000	3700
Group 1	A	79.68%	54.32%	N/A
	B	72.32%	63.93%	50.07%
	C	77.96%	50.25%	N/A
	D	108.14%	84.04%	67.79%
	E	113.32%	78.86%	58.46%
Group 2	A	69.89%	34.81%	N/A
	B	76.39%	44.25%	31.91%
	C	69.79%	N/A	N/A
	D	96.82%	73.09%	53.19%
	E	99.61%	62.97%	49.66%

(1) Same brand with different burning cycles

Fig. 7.10 gives the comparison results in the same burning time of same brand lamp with different burning cycles. The figure shows that the lamp with shorter burning cycle is easier to have lumen flux decreased.

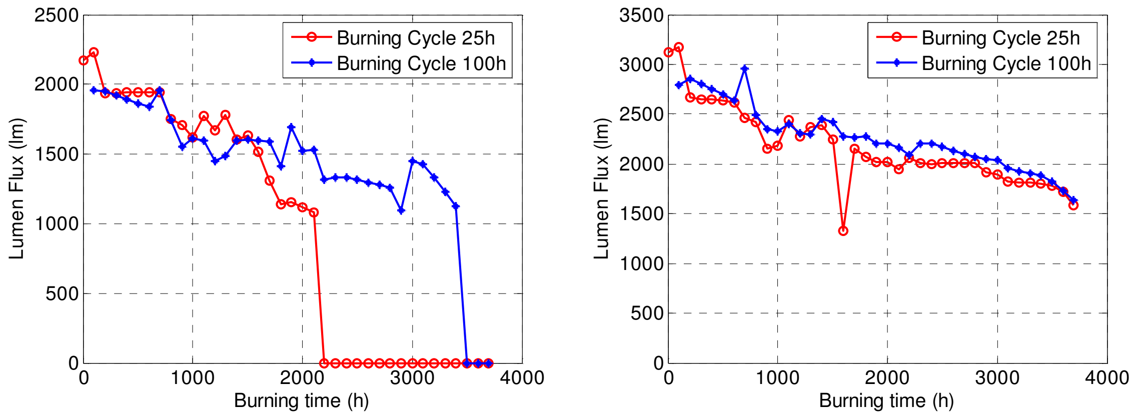

(a)Brand name is A (b) Brand name is E

Fig. 7.10 The lumen comparison between the two groups in the same brand

(2) Different brands with the same burning cycles

The comparison of lumen flux of different brand lamps in the burning cycle 25 hours and 100 hours are shown in Fig. 7.11(a) and Fig. 7.11(b), respectively

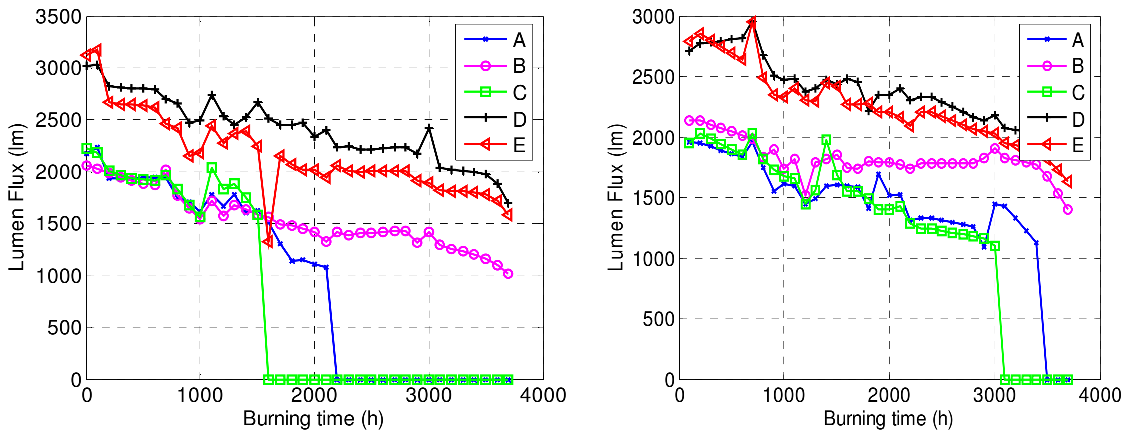

(a)Burning cycle is 25 hours (b) Burning cycle is 100 hours

Fig. 7.11 The lumen comparison between the different brand lamps with the same group in the same burning time

Summary: a) In our experiment, the lamp lumen flux will be decreased with the burning hours, and before one lamp burns out, the lamp lumen flux decreased evidently. b) The shorter burning cycle is easier to make the HID lamp burn out.

7.3.5 Mortality

The mortality is defined as:

$$M_{ag} = \frac{N_{bo}}{N_{all}} \times 100\% \tag{7.5}$$

where N_{bo} is the number of the burned-out lamp. N_{all} is the lamp numbers in different test groups and M_{ag} is the morality of the lamp. The survival is calculated by 1- M_{ag}.

The comparison of mortality between two test groups is shown in Fig. 7.12. It shows that the shorter burning cycle will shorten the lamp life.

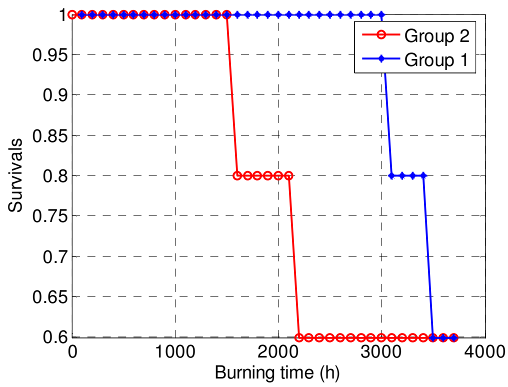

Fig. 7.12 Mortality curves of different test groups

7.4 Compensation and Lamp life model

With the lamp ageing, the output of lumen flux decreases continuously. When the output has declined to a point where an effective intensity cannot be obtained, the lamp still lights, but it is called to reach the end of its 'usable life'. In order to ensure the safety of the car driver, compensation of the lumen flux is needed. The HID lamp has a negative-resistance characteristic so that constant power control is needed in steady state.

7.4.1 Equivalent Resistance of ageing lamp

Lamp lifetime is a measure of ageing and the lamp life model means the ageing model of the lamp. The ageing level of the lamp is affected by the following factors: 1) The burning cycles. The shorter the burning cycle is, the shorter the lamp life. (as shown in test results in section 7.3.) 2) The type of ballast used to operate the lamps. 3) The surroundings, such as, the temperature, the sunlight and the lamp locations. The lifetime calculation of a pulse lamp is [124]:

$$Lifetime = (\frac{E_0}{E_x})^{-8.5} \tag{7.6}$$

where E_0 is the pulse energy and E_x is the corresponding explosion energy at a specific pulse duration.

An approximate lamp life model used to estimate total cost of light with different incandescent and compact fluorescent lamps was developed by Sullivan [125].

In order to apply easily, the equivalent lamp resistance model is used to do as the lamp life model for the compensation. The burning cycle is 100 hours and the data used here are given in group 2. The resistance of 5 different brands lamps are shown in Fig. 7.13. If the lamp ages, the lamp equivalent resistance and the lamp voltage increase; however, the lamp current decreases.

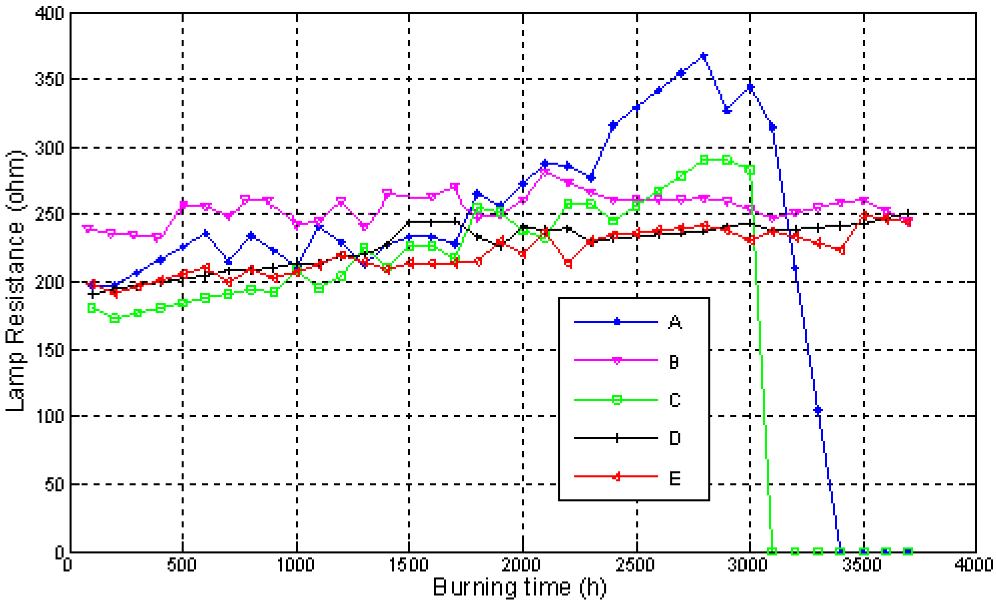

Fig. 7.13 Lamp resistance vs burning time

The equivalent lamp resistance R_{ageing} could be seen as a function of burning time t_o:

$$R_{ageing} = C_1 t_o + C_2 \tag{7.7}$$

where C_1 and C_2 are the constants obtained from the experimental data. The fitting values of C_1 and C_2 in different brand lamps are shown in Table 7.6.

Table 7.6 Fitting Values of the lamp resistance

Brand	C_1	C_2
A	0.0501	175.9469
B	0.0019	165.4634
C	0.0407	162.8149
D	0.0141	201.9560
E	0.0134	195.5795

The average resistance value of the five lamps could be obtained from:

$$R_{ageing\_av} = C_{1\_av} t_o + C_{2\_av} \tag{7.8}$$

According to Table 7.1, the rated average life of HID lamp in standard is 2000 hours. The lumen flux maintenance $R_{\Phi m\_a}$ is around 60% when the lamps burn at 3000 hour (from the data of the lamps in group 2) where the compensation method could be used.

7.4.2 Compensation Method

The cost would be high if a calculagraph is used in the ballast. In order to know the time for the compensation, the parameters of lamp voltage, current and resistance are needed. According to (7.8), the average resistance is 272Ω at 3000 hours. In the normal operation, the lamp works at 35W constant power control in steady state. Hence, the lamp voltage is 97V and lamp current is 0.359A. The lamp voltage is measured in the control process and it is used as a signal for the compensation. If the power loss is accounted for, and the lamp voltage is over 95V three times, the compensation is used in the HID lamp. When the lamp comes to the compensation state, the lamp voltage needs not to be measured again to avoid the error operation.

The light output is affected by the lamp current. In compensation process, the lamp current is fixed as 0.4A (as the nominal current in the requirement in chapter 2) and the compensation power is calculated by

$$P_{com} = {i_{lamp}}^2 * R_{ageing\_tr} \tag{7.9}$$

where R_{agein_tr} is the lamp resistance at the time of compensation. P_{com} is the lamp power in compensation process. If the lamp resistance in equation (7.9) is known, the power for compensation could be obtained. The values of R_{ageing_tr} could be calculated by the lamp voltages measured as compensation signal. Because the constant power is 35W if the compensation is not used, then:

$$R_{ageing\_tr} = \frac{|v_{lamp}|^2}{35W} \tag{7.10}$$

where v_{lamp} is the lamp voltage measured at the time of compensation. The relationship between the lamp voltage and compensation power is shown in Fig. 7.14.

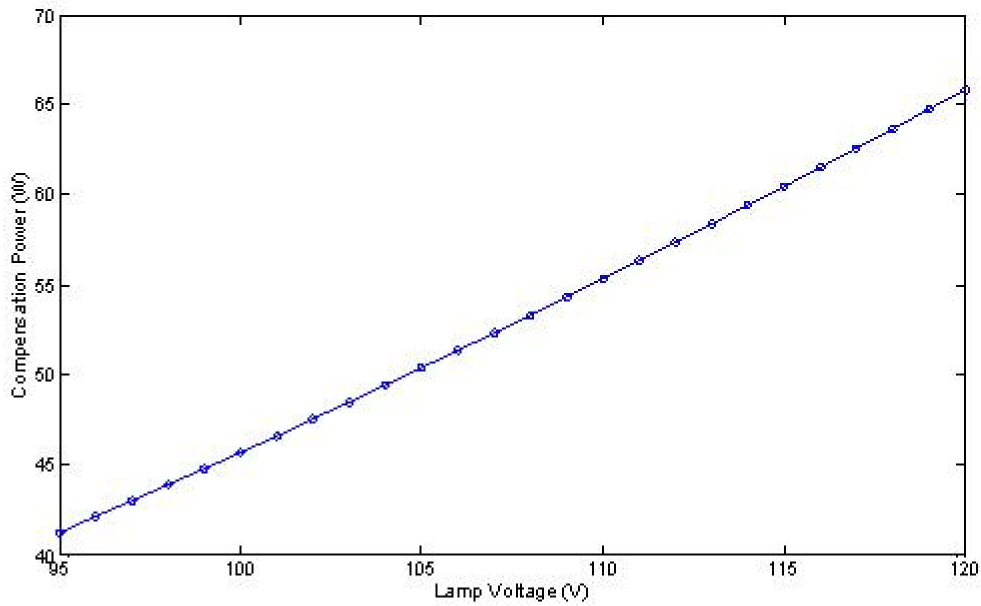

Fig. 7.14 Compensation power and lamp voltage

In order to conduct the test, a manual switch is used. Fig. 7.15 shows that a switch (SW_1) and an RC combination is integrated with the usual ballast. The software monitors the status of the switch. The compensation request is initiated when the switch is ON and cancelled when OFF. The software is designed to accept the compensation request only after the lamp has attained the steady state.

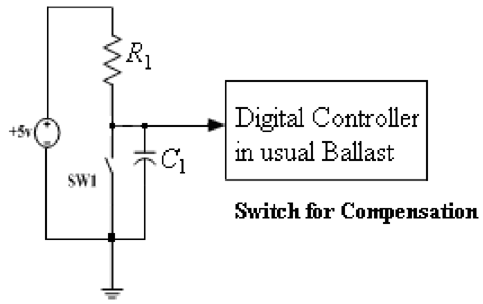

Fig. 7.15 Manual Switch for compensation

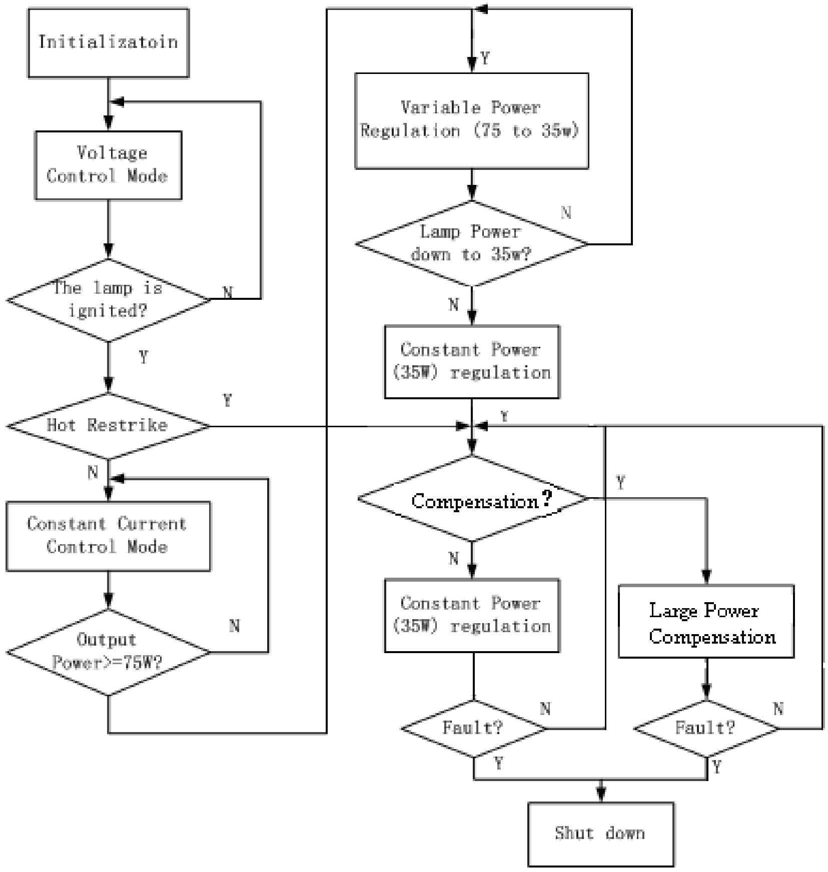

Fig. 7.16 Flow chart of compensation

The experimental results for new lamp, aged lamp and compensation installed aged lamp are as shown in figures 7.17, 7.18 and 7.19 respectively. The output luminous flux of aged lamp is 1823*lm*. The ballast is able to compensate the lamp luminous flux from

1823*lm* to 2208*lm*. But the compensation method would increase the ageing speed of the HID lamp due to the large power used in the steady state.

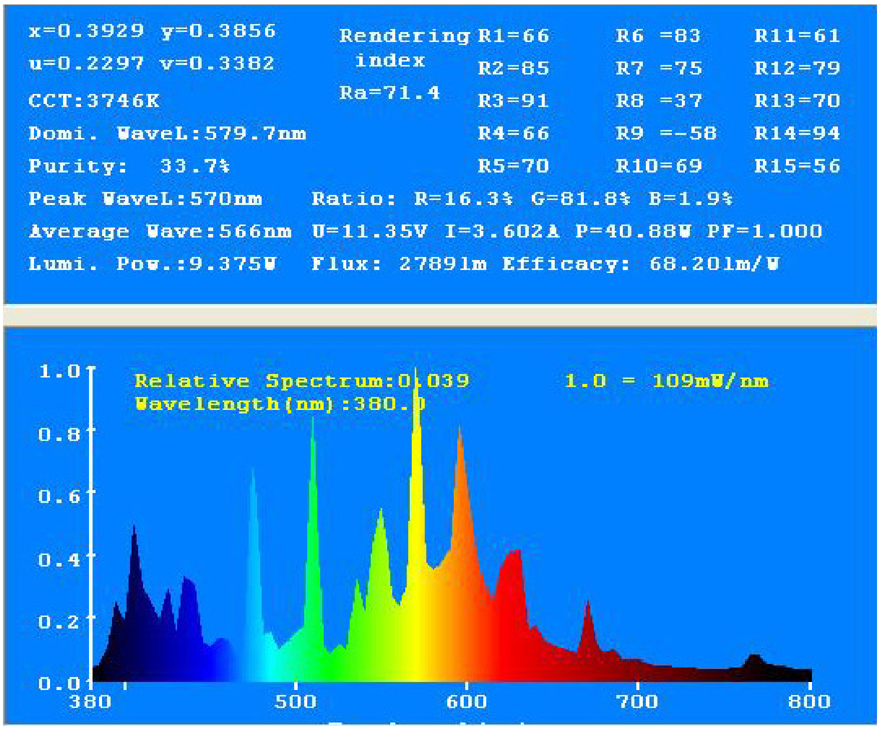

Fig. 7.17 Spectrum map of the new lamp (Flux: 2789*lm*)

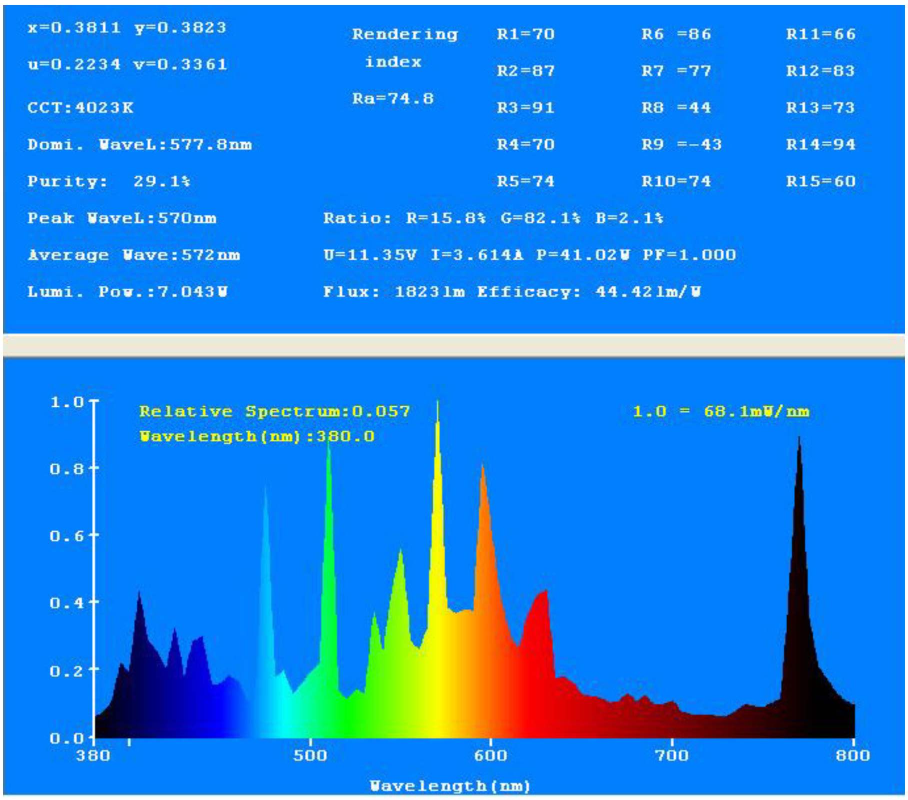

Fig. 7.18 Spectrum map of the aged lamp (Flux: 1823*lm*)

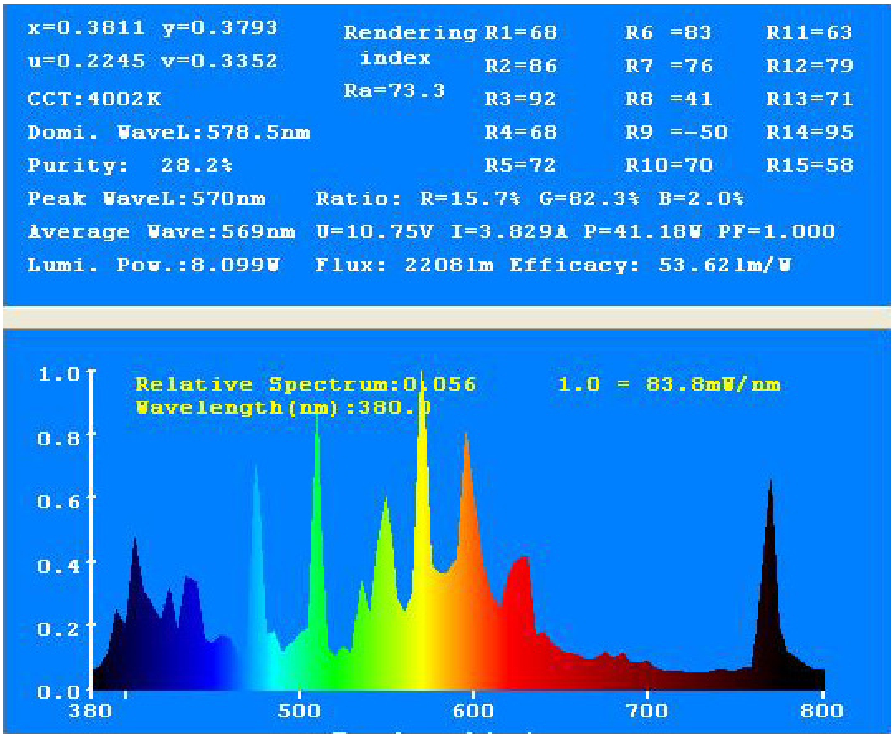

Fig. 7.19 Spectrum map of the aged lamp with compensation (Flux: 2208*lm*)

7.5 Summary

A number of experiments have been carried out on two groups of HID lamps to monitor the change in the characteristics of lamps as they age. It is evident from the study that frequent switching makes the lamps age more quickly. From above analysis, the following conclusions can be drawn:

(1) The burning cycle will affect the lamp ageing, such as the lamp current and lamp voltage. The shorter the burning cycle is, the larger the ageing effect.

(2) The mortality will be increased with the shorter burning cycles.

The compensation method has been developed in this chapter. According to the lamp life model of the HID lamp, the lumen maintenance is around 60% when the lamps burn for 3000 hours. Compensation is activated when the lamp voltage is increased to 95V which is the suitable level following the study for a number of lamps. In order to supply enough lamp current to the lamp, the compensation power is calculated by using the lamp resistance. Then the compensation power serves as the reference power in steady state. This compensation method can extend the constant illumination life time and the experimental results show that it is feasible for a simple consistent illumination driving method.

Chapter 8

CONCLUSIONS AND SUGGESTIONS FOR FUTURE RESEARCH

The HID lamp is widely used in the automotive headlight system due to its high luminous output and long life. Although automotive and electronics companies are devoted to this type of lamp, detailed analysis of high performance electronic ballast does not catch up with the market trend. The modelling of HID lamp, application of more stable control method, ageing analysis and dimming control are all hot topics for research. The main purpose of this thesis is to explore the development and optimization of the automotive headlight system.

8.1 Main Contributions

In this thesis, three different electronic ballasts (EB) have been examined and developed. A novel HID lamp model has also been developed to assist the understanding and design of EB. Furthermore, new application and optimization technique have been analyzed and verified in this thesis. They are described briefly as follows:

(1) Development of two electronic ballasts with traditional structure

Two traditional HID ballasts that have the same electrical circuit topology have been analyzed, but their controllers are realized differently by a microprocessor and a special chip (UCC2305). The ballast circuits are based on a 100 kHz DC-DC converter, a voltage doubler igniter and a 100-400Hz operated square-wave inverter.

Precise design criteria and specification have been presented to meet the need of the requirements and complex ignition condition of HID lamps. Most components used in these two EBs are the same and the acoustic resonance is avoided. The difference in design is: a) The IC based EB is more expensive and more sensitive to noise than the microprocessor based EB. b) The microprocessor based EB has less components. c) In microprocessor based EB, a DC operation time is needed to improve the igniting reliability of HID lamp under a high switch frequency operation.

The magnetic design for the EB has also been undertaken. R core and EE core are compared and R core is finally selected because of its better performance in the high voltage design. It is more difficult to saturate and less bulky.

(2) Development of new electronic ballast based on DS1104

The DSP DS1104 controller system has been used for the control of the HID lamp ballast. A unified indirect controller is purposely designed to regulate the voltage, current and power of HID lamp. The controller has been analyzed by two controllers, two-loop PI controller and nonlinear adaptive controller. Both of them have better performance in response to the variation of system parameters and lamp resistances under different conditions. The PI control uses fixed control parameters, whereas control parameters of the adaptive controller vary with system parameters. Experimental results have confirmed that the adaptive control is successful in different stages of operation for ageing lamp under temperature variation.

(3) Modelling of HID lamp based on Bicubic Spline Interpolation

A new model of Xenon lamp has been developed based on 2-D spline interpolation. The simulation has been conducted under various temperature settings from start up to steady state. The comparison of simulation and experimental measurement confirms that the model precisely represents the lamp characteristics. The model can provide a platform using the spline to develop other HID lamp models with limited data. The study of warm lamp has also been conducted. The temperature at 440^{o}C has been examined at high start-up temperature. Very good agreement has been obtained. The 2D spline model developed and the simulation system can be used to design the parameters of the front-end converter (in this case the flyback converter) and overall system control.

(4) Indirect Constant Power Control with PBC Controller

The EB system has been analyzed and simplified, and a model based on the EL equation has been constructed. Using power function, this indirect PBC controller is realized by reshaping the total energy of system and injecting the required damping. The adaptive load estimator has been derived and insures that the controller is effective in large load disturbance. The simulation and experimental results have verified the model and the nonlinear controller. This constant power control method is very simple in structure and it is very easy to use.

(5) Dimming Control mathematic Analysis

Variable bus voltage dimming method and variable duty ratio dimming method have been analyzed. For the variable bus voltage dimming method, there are two application cases. One is by changing the current gain and the other is by changing the voltage gain. The summation method and multiplier method are classified according to the structure of the controller, and they have different dimming effects in using the variable bus voltage dimming method. The changing current gain has a better dimming performance because a small power variation in large voltage variation could be obtained. If the same current gain is used ($k_i = 2.224$), the EB based on summation method has a better dimming performance due to the large voltage variable scope with small power change.

For the variable duty ratio dimming method, the power tracking duty ratio control method is used. Because the lamp resistance could not be controlled by the controller, the constant voltage power tracking method and constant current power tracking method are not feasible.

The experimental results show that 34% lamp power can be reduced by using the variable bus voltage dimming method and 23% lamp power can be reduced by using the variable duty ratio dimming method. The ballast achieves a reduction of 32% light output in the dimming control.

Lastly, an engineering approach for open loop life time compensation for constant illumination output is presented. This method can automatically compensate by judging the lamp resistance, and the lamp voltage is selected as an operation signal as there is no online illumination feedback. The constant illumination life time is extended by this compensation method.

8.2 Future Research

The future work should concentrate on the front-lighting system (AFS). AFS has been promoted widely in the automotive industry. The critical element is to use dimmable lamp with position control. The work conducted in the thesis can be extended to AFS. A high performance 2D actuator is integrated with the dimmable EB system to realise the intelligent AFS control.

REFERENCES

[1] B. Schoettle, M. Sivak, M.J. Flannagan & G. Adachi, "*The Illuminated surface areas of HID and tungsten-halogen headlamps in the U.S.*" (Report No. UMTRI-2002-32). Ann Arbor, MI. The University of Michigan Transportation Research Institute.

[2] David W. Moore. "*Headlamp History and Harmonization*" (Report No. UMTRI-98-21). Ann Arbor, MI. The University of Michigan Transportation Research Institute.

[3] Information of HID-D2R bulbs. http.//www.hidbulbsource.com/HID-D2R_Bulbs.html.

[4] OSRAM, Technical Information for HTI.S 35/12, 1998.

[5] PHILIPS, Product Information sheet for micro power Xenon light D2S, 1996.

[6] J. F. Waymouth and F. Bitter, "*Analysis of the plasma of fluorescent lamps*". J. Appl. Phys., Vol. 27, 1956, pp.122.

[7] V. Francis, "*Fundamentals of Discharge Tube Circuits*". London, U.K.. Methuen & Co. Ltd., 1948.

[8] C. Kenty, "Production of 2537 radiation and the role of metastable atoms in an argon-mercury discharge". J. Appl. Phys., Vol. 21, 1950, pp. 1309.

[9] M. A. Cayless, "*Theory of low pressure mercury rare-gas discharges*", in Proc. 5th International Conf. Phenomena in Ionized Gases, Vol. 1, 1961, pp. 262.

[10] -, "Excitation and ionization rates of mercury in discharge plasmas". British J. Appl. Phys., Vol. 10, 1959, pp. 186.

[11] -, "Theory of the positive column in mercury rare-gas discharges". British J. Appl. Phys., Vol. 14, 1963, pp. 863.

[12] L. Cifentes, "*High-pressure discharge lamps. Approaches to Modelling*". Light. Res. Technol., 1991, 23, (4), pp. 161-165.

[13] J. J. Lowke, R. J. Zollweg and R.W. Liebermann, "*Theoretical description of ac arcs in mercury and argon*". J. Appl. Phys., 1975, 46, (2), pp. 650-660.

[14] H. P. Stromberg and R. Schafer, "*Time-dependent behaviour of high-pressure mercury discharges*". J. Appl. Phys., 1983, 54, (8), pp. 4338-4347.

[15] G. Lister, "*Principles of high intensity discharge lamp operation*". Presented at IEEE Industry applications society annual meeting (IAS), Rome, Italy, 2000.

[16] M. S. Benilov, "*Near-Cathode Phenomena in HID lamps*". IEEE Trans. On Industry Applications, Vol. 37(4), Jul. 2001, pp. 986-993.

[17] E. Fischer, "Modelling of low-power high-pressure discharge lamps". Philips J. Res, 1987, 42, pp. 58-85.

[18] E. Pfender, "*Electric arcs and arc gas heater*", in Hirsh, M.N., and Oskan H.J. Gaseous Electronics.

[19] M. S. Kettlitz, "Lowering of the cathode fall voltage by laser exposure of the cathode in a high-pressure mercury discharge". J. Phys. D., Appl. Phys., Vol. 38, (17), pp. 3175-3181.

[20] O. L. Dabringhaused, and J. Mentel. "*Different modes of arc attachment at HID cathodes. Simulation and comparison with measurements*". J. Phys. D, Appl. Phys., Vol. 38, (17), 2005, pp. 3128-3124.

[21] P. Y. Chang and W. Shyy, "A study of three-dimensional natural convection in high pressure mercury lamps, Part I. Parametric variations with horizontal mounting", Int. J. Heat Mass Transf., Vol. 33(3), 1990, pp. 483-493.

[22] W. Shyy and P.Y. Chang, "A study of three-dimensional natural convection in high pressure mercury lamps, Part II. Wall temperature profiles and inclination angles". Int. J. Heat Mass Transf., Vol. 33(3), 1990, pp. 495-506.

[23] P. Y. Chang and W. Shyy, "A study of three-dimensional natural convection in high pressure mercury lamps, Part III. arc centering by magnetic field". Int. J. Heat Mass Transf., Vol. 35(8), 1992, pp. 1857-1864.

[24] C. P. Khokan, "Development of a Robust 3-D Model for HID lamps and Comparison of Predicted and Measured Electrode Temperatures". IEEE Trans. on Plasma Science, Vol. 35 (2), 2007, pp. 188-196.

[25] Y. Wei, "Nonlinear high-intensity discharge lamp model including a dynamic electrode voltage drop", IEE Proc. Sci. Meas. Technol., Vol. 150, (4), 2003, pp. 161-167.

[26] Y. Wei, "*A Universal PSpice Model for HID lamps*", IEEE Trans. on Industry Applications, Vol. 41 (6), 2005, pp. 1594-1602.

[27] M. Janos, "*Ballast curves for HPS lamps operating on high frequency*". Proc. IEEE Industry applications society Annual Meeting, Vol.2, 1992, pp. 1908-1914.

[28] E. Rasch, "Behavior of metal halide lamps with conventional and electronic ballasts", J. Illum. Eng. Soc., 1991, pp. 88-96.

[29] E. L. Laskowski, J. F. S. Donghua, "*Model of a Mercury Arc Lamp's Terminal V-I behavior*". IEEE Transactions on Industry Applications, Vol. 17, No.4, July-Aug. 1981. pp. 419-429.

[30] Zhang Weiping, Zhang Yinru, et al. "*Study of the Model for MH Lamps and the Controlling Approaches for Its Electronic Ballasts*", ACTA ELECTRONICA SINICA, Vol. 27, No.8, Aug. 1999. pp. 142-143. (In Chinese)

[31] U. Mader, "*A dynamic model for the electrical characteristics of fluorescent lamps*", in Proc. IEEE Industry Applications Society Annual Meeting, Vol. 2, 1992, pp. 1928.

[32] N. Sun, B. Hensterman, "*PSpice high frequency dynamic fluorescent lamp model*", in Proc. 11^{th} Annual Applied Power Electronics Conf. and Exposition (APEC'96), Vol.2, 1996, pp.641.

[33] T.F. Wu, "A PSpice circuit model for low-pressure gaseous discharge lamps operating at high frequency". IEEE Trans. Ind. Electron., Vol. 44, 1997, pp. 428.

[34] M. Gulko, "*Current-sourcing parallel-resonance inverter: theory and application as a fluorescent lamp driver*", in Proc. 8^{th} Annual Applied Power Electronics Conf. and Exposition (APEC'93), pp. 411.

[35] K. H. Loo, "A dynamic Collisional-Radiative model of a low-pressure Mercury-argon discharge lamp: a physical approach to modeling Fluorescent lamps for circuit simulations", IEEE Trans. on Power Electronics, Vol. 19 (4), 2004, pp. 1117-1129.

[36] K. H. Loo, "A dynamic Conductance model of Fluorescent lamp for electronic ballast design simulation", IEEE Trans. on Power Electronics, Vol. 20 (5), 2005, pp. 1178-1185.

[37] W. Alling, "*Important Design Parameters for solid-state ballasts*", IEEE Trans. on Industry Applications, Vol.25 (2). 1989, pp. 203-207.

[38] Unitrode, Products & Applications Handbook, 1995-96.

[39] H. Endo, T. Yamashita, "*A high power factor buck converter*", conference record of IEEE-PESC 1992, pp. 1071-1076.

[40] L. H. D. Jr, "*High power factor pre-regulator for off-line power suppliers*", Unitrode switching regulator power supply design seminar manual, SEM-700, 1990.

[41] M.M. Jovanovic, “*A novel active snubber for high-power boost converters”*, IEEE Trans. on Power Electronics, Vol. 15 (2), 2000, pp. 278-284.

[42] M. T. Madigan, “*Integrated high-quality rectifier-regulators”*, IEEE Trans. on Industrial Electronics, Vol. 46 (4), 1999, pp. 749-758.

[43] A. M. Cross, and A. J. Forsyth, *“Simulation and Evaluation of High-Voltage Power Systems for Civil Aircraft”*, SAE 2004 Transactions - Journal of Aerospace, 2005.

[44] C. C. Chan and K. T. Chau, *“A new zero-voltage-switching dc/dc boost converter,”* IEEE Trans. on Aerospace and Electronic Systems (TAES), Vol. 29, No. 1, January 1993, pp. 125-134.

[45] W. Alling, “The Integration of microcomputers and controllable output ballasts- a new dimension in lighting control”, IEEE Trans. on Industry Applications, Vol.IA-20, (5), 1984, pp. 1198-1205.

[46] W. Alling, “*Important design parameters for solid-state ballasts”*, IEEE Trans. on Industry Applications, Vol. 25 (2), 1989, pp. 203-207.

[47] R. R. Verderber, “Performance of Electronic ballast and controls with 34- and 40-Watt F40 Fluorescent lamps”, IEEE Trans. on Industry Applications, Vol. 25(6), 1989, pp. 1049-1059.

[48] M. Gulko and S. Ben-Yaakov, “Current-source push-pull parallel-resonance inverter: theory and application as a fluorescent lamp driver”, IEEE Trans. on Industrial Electronics, Vol. 41(3), 1994, pp. 285-291.

[49] M. Jordan and J. A. O’Connor, “*Resonant Fluorescent lamp converter provides efficient and compact solution”*, Conference Record of IEEE-APEC 1993, pp. 424-431.

[50] Y. L. Lin and A. F. Witulski, “Analysis and design of current-fed push-pull resonant inverters- cold cathode fluorescent lamp drivers”, Conference Record of IEEE-IAS, 1996, pp. 2149-2152.

[51] M. Gulko, “*A MHz Electronic ballast for automotive-type HID lamps”*, Conference Record of IEEE-PECS, 1997, pp. 39-45.

[52] J. A. Sierra and W. Kaiser, “*Comparison of fluorescent lamp stabilization methods in the current-fed push-pull inverter”*, IEEE Trans. on Industry Applications, Vol. 36(1), 2000, pp. 105-110.

[53] R. Redl and K. Arakawa, “A low-cost control IC for single-transistor ZVS cold-cathode fluorescent lamp inverters and DC/DC converters”, Conference Record of IEEE-APEC, 1997, pp. 1042-1049.

[54] M. M. Hernando, "Fluorescent lamps supplied with DC current and controlled in current mode", Proceedings of EPE 1991, pp. 499-503.

[55] E. L. Corominas, "Optimizing lamp-power regulation in low-voltage-supplied electronic ballasts by using non-resonant inverters", Conference Record of IEEE-IAS, 1998, pp. 2060-2067.

[56] A. S. Simoes, "*A boost-type converter for DC-supply of fluorescent lamps*", IEEE Trans. on Industrial Electronics, Vol. 41 (2), 1994, pp. 251-255.

[57] H. J. Boswinkel, "*A buck-type converter for DC-supply of fluorescent lamps*", Conference Record of IEEE-IAS1998, pp. 2089-2093.

[58] C. S. Moo, H. L. Chung, et al. "*Design Dimmable Electronic Ballast with frequency control*". Conference Record of IEEE-APEC 1999, pp. 727-733.

[59] R. Redl and J.D. Paul, "A new high-frequency and high-efficiency electronic ballast for HID lamps. topology, analysis, design, and experimental results". Applied Power Electronics Conference and Exposition-APEC '99. Vol.1, 14-18, pp .486 – 492.

[60] H. Kakehasi, M. Habu, T. Ninomiya, et al. "*A high-frequency electronic ballast for HID lamps based on a λ/4-long distributed constant line*". IEEE Trans. on Power Electron., Vol. 13, No. 3, Nov. 1998, pp. 1023-1029.

[61] Yongxuan Hu. "*Analysis and Design of High-intensity-discharge Lamp Ballast for Automotive Headlight*", Master thesis, November 19, 2001, Virginia Polytechnic Institute and State University.

[62] Y. Wei, S. Y. Hui, "*An adaptive acoustic resonance free electronic ballast for HID lamps*", IEEE Trans on Industry Applications, 2003, pp. 1020-1024.

[63] Information of UCC3305. http.//focus.ti.com/docs/prod/folders/print/ucc3305.html.

[64] Y. F. Jiang, Qiukai Huang; Min Chen; Zhaoming Qian; "*Analysis and design of a new hot-striking igniter for HID lamp*", Industry Applications Conference- IAS'04, Conference Record of the 2004 IEEE, Vol. 1, 3-7 Oct. 2004.

[65] R. Fiorello, "Driving a 35W AC mental halide high intensity discharge lamp with the UCC3305 HID lamp controller". Unitrode Application Note U_162.

[66] B. Y. N. AOIKE, M. HOSHINO & A. IWABUCHI. "*Automotive HID headlamps",* IEEE Industry Applications Magazine, 2002, pp. 37-40.

[67] Kyu-Chan Lee; Bo Hyung Cho; "*Design and analysis of automotive high intensity discharge lamp ballast using micro controller unit*". IEEE Trans. on Power Electronics, Vol. 18, Issue 6, Nov. 2003, pp.1356 – 1364.

[68] Jiaxing Lee. “High-frequency dimmable electronic ballast for driving HID lamps”, Master Thesis, ZhongYuan University, Taiwan.

[69] M. Ponce, E. Flores and R. Osorio, “*Analysis and design of igniters for HID lamps fed with square waveforms”,* Power Electronics Specialists Conference, PESC’04, Vol.1, pp. 396 - 400.

[70] W. D. Greason, Z. Kucerovsky, S. Bulach and M. W. Flatley. “*Investigation of the Optical and Electrical Characteristics of a Spark Gap”,* IEEE Trans. on Industry Applications, Vol.33, No. 6, Nov./Dec. 1997, pp. 1519-1526.

[71] J. Rozenboom. “*The electronic ballast circuit and low pressure lamps”*, Int. Journal Electronics, Vol. 82, No.3, 1997, pp. 269-294.

[72] J. Garcia-Garcia, et al. “Using solid-state Over-voltage Protection Devices for High Intensity Discharge Lamps Ignition”. Conference record of IEEE-IAS’02, Vol.1, pp. 363-368.

[73] P. Dong, K. W. Cheng, et al; *“Study of Distributing Parameters in High Voltage Transformer for HID Ballast”*, IEEE International Magnetics Conference 2006, CD-03. San Diego, California, May 8-12, 2006.

[74] J. F. Waymouth, Electric Discharge Lamps, M. I. T. Press, Cambridge, 1978.

[75] E. Deng, S. Cuk, Deng. “*Negative Incremental impedance and stability of Fluorescent Lamps”*, Applied Power Electronics Conference and Exposition, APEC '97 Vol. 2, pp. 1050 – 1056.

[76] T. Liu, K. J. Tseng, et al. *“Pspice model for the electrical characteristics of fluorescent lamps”*, Conference record on IEEE PESC’98, pp. 1749-1754.

[77] X. D. Xue, K. W. E. Cheng, S. L. Ho, “*Simulation of switched reluctance motor drives using two-dimensional bicubic spline”*, IEEE Trans. on Energy Conversion, Vol. 19, Issue 3, Sept. 2004, pp. 649 – 650.

[78] R. Ortega, A. Loria, P. Nicklasson, “*Passivity-based Control of Euler-Lagrange Systems”*. London, U.K.: Springer, 1998.

[79] Byungcho Choi, “*Step load response of a current-mode-controlled DC-to-DC converter”*. IEEE Transactions on Aerospace and Electronic Systems, Vol. 33, no. 4, Oct. 1997, pp. 1115-1121.

[80] R. B. Ridley, “*A new continuous-time model for current-mode control”,* IEEE transactions on power and Electronics 1991, Vol. 6, pp. 271-280.

[81] D. H. Wang, K. W. E.Cheng, et al. "*Development of an automotive HID Electronic Ballast based on Microprocessor*", 2nd International Conference on Power Electronics Systems and Applications, 2006, Hong Kong, pp. 229-233.

[82] Data sheet.http.//www.datasheetcatalog.com/datasheets_pdf/T/C/4/4/TC4427.shtml

[83] Data sheet. http.//www.datasheetcatalog.com/datasheets_pdf/I/R/2/1/IR2104.shtml.

[84] Data sheet. http.//www.datasheetcatalog.com/datasheets_pdf/6/N/1/3/6N137.shtml

[85] Data sheet.http.//www.datasheetcatalog.com/datasheets_pdf/L/V/2/5/LV25-P.shtml

[86] Data sheet of DS1104. http.//www.dspaceinc.com/ww/en/inc/home/medien.cfm?nv=n1.

[87] J. Alvarez-Ramirez, G. Espinosa-Perez, et al. "C*urrent-mode control of DC-DC power converters. a backstepping approach",* International Journal of Robust and Nonlinear control 2003, Vol. 13, pp. 421-442.

[88] R. D. Middlebrook, "*Topics in multi-loop regulators and current-mode programming",* IEEE Transactions on Power Electronics, 1987, Vol.2, No. 2, pp. 109-124.

[89] Z. Wu, H. Li, et al. "*Cascade Control of DC/DC Boost Converters*", Proceedings of the CSEE, Vol.22, No. 1, Jan. 2002, pp. 110-115. (In Chinese)

[90] H. Sira-Ramirez, "*Sliding motions in bilinear switched networks*", IEEE Transactions on Circuits and Systems, Vol. CAS-34, no. 8, Aug. 1987, pp. 919-33.

[91] W. S. Kim, B. H. Cho, K. C. Lee, *"Design and analysis of high-voltage transformer for HID lamp igniter"*, Applied Power Electronics Conference and Exposition-APEC'05. Vol 2, pp. 1043 – 1047.

[92] R. Ortega, and A. Van Der Schaft, *"Putting energy back in control",* IEEE Control System, Mag., 2001, 21(2), pp. 18-33.

[93] R. Ortega, A. Schaft, B. Maschke, and G. Escobar, *"Energy-shaping of port-controlled Hamiltonian systems by interconnection"*, Proc. Conf. on Decision and Control, Phoenix, Arizona, USA, 1999, pp. 1646-1651.

[94] G. Escobar, D. Chevreau, R. Ortega, *"An adaptive passivity-based controller for a unity power factor rectifier",* IEEE Trans. Control System Technol. 2001, 9(4), pp. 637-644.

[95] A. M., Stankovic, D. J., Perreault, *"Analysis and experimentation with dissipative nonlinear controllers for serious resonant DC/DC converters"*. In Proc. 28th Annual IEEE Power Electronics Specialist Conf. (PESC 97), St. Louis, MI, May, Vol. 1, pp. 679-685.

[96] Zhang Weiqiang, and Xu dianguo. *"Novel Constant power control of electronic ballast for HPS lamps",* In Conf. Rec. IEEE ICIT'02, Vol.1, pp. 129-132.

[97] Yan Jiang, Jinghai Zhou, Zhaoming Qian. *"A Novel single stage single switch PFC converter with Constant Power control for Ballast for Medium HID lamps",* Conference Record of the IEEE Industry Applications Conference-IAS'2000, Vol.5, pp. 3415-18.

[98] Chang-Hua Lin, Chung-Lun Ou, Tien-Shuo Liu. *"A Novel Constant Power Control of High Frequency Electronic Ballast Applying the PLL Technique for a Metal halide Lamp".* IEEE 5th International.Power Electronics and Motion Control Conference- IPEMC '06. Vol. 3, pp. 1-5.

[99] Robert W. Erickson, Dragan Maksimovic. *"Fundamentals of Power Electronics"*, Springer, 1st Edition, 1997.

[100] G. Escobar, A. J.van der Schaft, and R. Ortega. "A Hamiltonian viewpoint in the modeling of switching power converters". Automatica, 1998.

[101] B. M. Maschke, A. J. van der Schaft, and P.C. Breedveld. *"An intrinsic hamiltonian formulation of the dynamics of LC circuits",* IEEE Trans. On Circ. Syst., Vol. 42, no. 2, 1995, pp. 73-82.

[102] H. Sira-Ramirez, P. Lischinsky-Arenas, *"Dynamical discontinuous feedback control of nonlinear systems",* IEEE Transactions on Automatic Control 35, 1373-1378; 1991

[103] P. Dong, K. W. E. Cheng, et al. "Simplified Model and Simulation Validation Used in Xenon Automotive Lamp". APSCOM'06, Hong Kong.

[104] T. J. Ribarich and J. J. Ribarich, *"A new control method for dimmable high-frequency electronic ballasts."* IEEE Industry Applications Society IAS Annual Meeting 1998.

[105] C. S. Moo, Y. C. Chuang, Y. H. Huang, and H. N. Chen, *"Modeling of fluorescent lamps for dimmable electronic ballasts,"* IEEE Industry Applications Society IAS Annual Meeting 1996, pp. 2231-2236.

[106] R. Severns, *"Topologies for three-element resonant converter,"* IEEE Trans. on Power Electronics, Vol. 7. No. 1, Jan. 1992, pp.89-98.

[107] J. Rozenboom. *"The electronic ballast circuit and low pressure lamps",* Int. Journal Electronics, Vol. 82, No.3, 1997, pp. 269-294.

[108] J. Ribas, J. M. Alonso, E. L. Corominas, et al. "Design Considerations for Optimum Ignition and Dimming of Fluorescent Lamps Using a Resonant Inverter Operating Open Loop". Conference Record of IEEE-IAS 1998, pp. 2068-2075.

[109] T. F. Wu, T. H. Yu, et al. "Single-stage Electronic ballast with dimming feature and Unity Power Factor. IEEE Trans. on Power Electronics". Vol.13, No.3, May 1998. pp. 586-597.

[110] T. F. Wu, T. H. Yu, et al. *"Analysis and Design of a High power Factor, Single-Stage Electronic Dimming ballast"*. IEEE Trans. on Industry Applications. Vol. 34, No. 3, May 1998, pp. 606-615.

[111] T. F. Wu, Y. C. Wu, et al. *"Design Consideration for Optimum Dimming in Single-stage Electronic Ballasts"*. Conference Record of IEEE-IAS 2000, pp. 3374-3381.

[112] C. Branas, F. J. Azcondo, et al. "Electronic Ballast for HPS Lamps with Dimming Control by Variation of the switching frequency. soft start-up method for HPS and Fluorescent lamps". Conference Record of IEEE-IECON 1998, pp. 953-958.

[113] T. J. Ribarich and J. J. Ribarich. *"A new Control Method for Dimmable High frequency Electronic Ballasts"*, Conference Record of IEEE-IAS 1998, pp. 2038-2043.

[114] C. S. Moo, H. L. Cheng, et al. *"A new Control Method for Dimmable High-frequency Electronic Ballasts"*, Conference Record of IEEE-ISIE 1999, pp. 786-791.

[115] S. Y. R. Hui, L. M. Lee, et al. *"Electronic Ballast with wide Dimming Range, High PF, and low EMI"*. IEEE Trans. on Power Electronics, Vol. 16, No. 4, July 2001, pp. 465-472.

[116] J. H. Reijnaerts. "Circuit Arrangement for Reducing Striations in a low-pressure Mercury Discharge Lamp". US Patent No. 5,369,339, Nov. 29, 1994.

[117] R.L. Steigerward and L. D. Stevanovic. "Elimination of Striations in Fluorescent Lamps driven by High-frequency Ballast". US Patent No. 5,701,059, Dec. 23, 1997.

[118] C. R. Sullivan. *"Control System for Proving Power to a Gas Charge Lamp"*. US Patent No. 5,864,212, Jan. 26, 1999.

[119] C. Branas, *"Fluorescent lamps. Introduction to Quasi-Optimum control"*, Conference record of IEEE-IAS 1998, pp. 970-975.

[120] Y. Wei, S. Y. Hui. *"An analysis into the dimming control and characteristic of Discharge Lamps"*. IEEE Trans. on Power Electronics, Vol. 20, No.6, Nov. 2005, pp. 1432-1440.

[121] Y. K. E. Ho, S. T. S. Lee, H.S.H. Chung, and S.Y. Hui, *"A comparative study on dimming control methods for electronic ballasts"*. IEEE Trans. Power Electronics, 2001, 16, (6), pp. 828-836.

[122] H. L. Chan, K. W. E. Cheng, D. Sutanto, *"Calculation of inductances of high frequency air-core transformers with superconductor windings for DC-DC converters",* IEE Proceedings- Electric Power Applications, Vol. 150, Issue 4, pp. 447 – 454.

[123] K. W. E. Cheng, P. D. Evans, *"Calculation of winding losses in high-frequency tropical inductors using single strand conductors",* IEE Proceedings-Electric Power Applications, Vol. 141, Issue 2, pp. 52 – 62.

[124] Lamp life data, www.noblelight.net.

[125] C. R. Sullivan and A. C. Drescher. "*Influence of On-Time and Use-Frequency on Cost-Effectiveness of Compact Fluorescent Lamps*", IEEE Industry Applications Society Annual Meeting, October 1993, Toronto, pp. 2283-2290.

[126] K. T. Chau, *"Nonlinear modelling of switching dc-dc converters operating in discontinuous conduction mode,"* International Journal of Electronics (IJE), Vol. 83, No. 2, August 1997, pp. 271-286.

[127] A. J. Forsyth, G. A. Ward, and S. V. Mollov. *"Extended fundamental frequency analysis of the LCC resonant converter"*, IEEE Trans. Power Electronics, Vol. 18-6, 2003.

[128] A. J. Forsyth, S. Y. Yang, P. A. Mawby and V. X. Igic. *"Measurement and modelling of power electronic devices at cryogenic temperatures"*, IEE Proc, CDS, Vol. 153-5, 2006.

[129] Selected control parameters. http://www.iacmall.com/news-3-154.html.

APPENDICES

Appendix I. Schematic Diagrams of the electronic ballast based on DS1104

1.1 Main Circuit

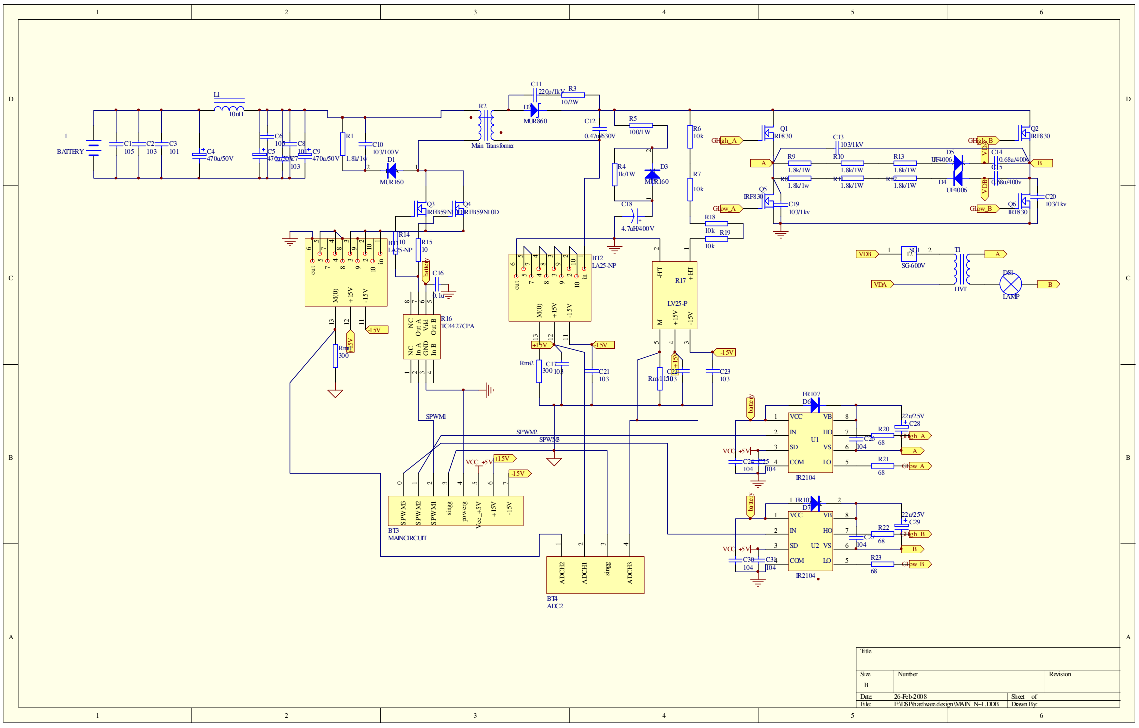

1.2 Control Circuit

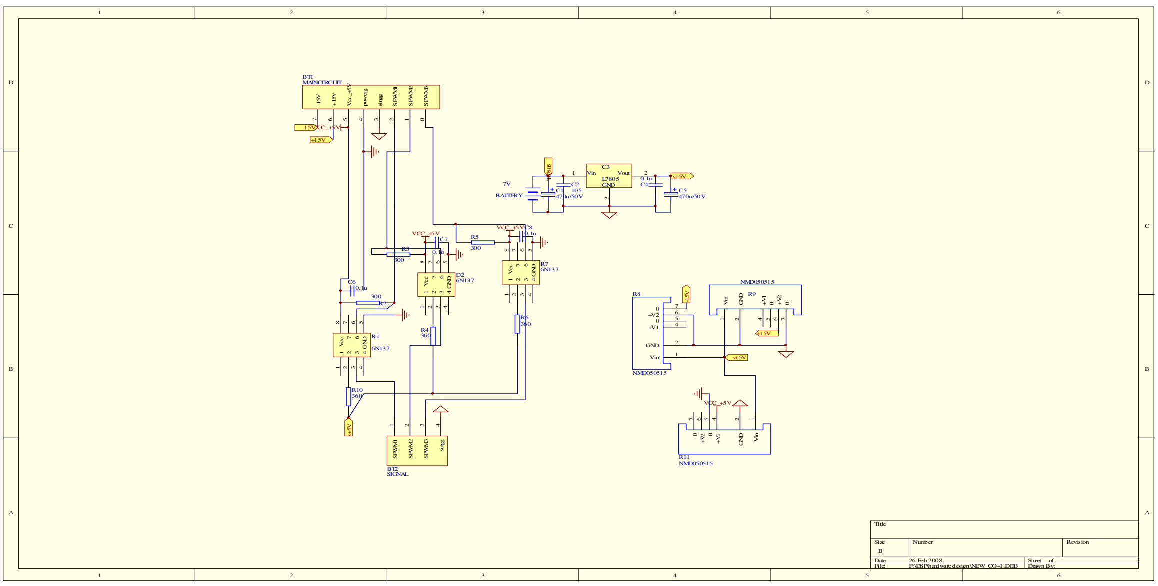

Appendix II. Electronic Ballast based on DS1104

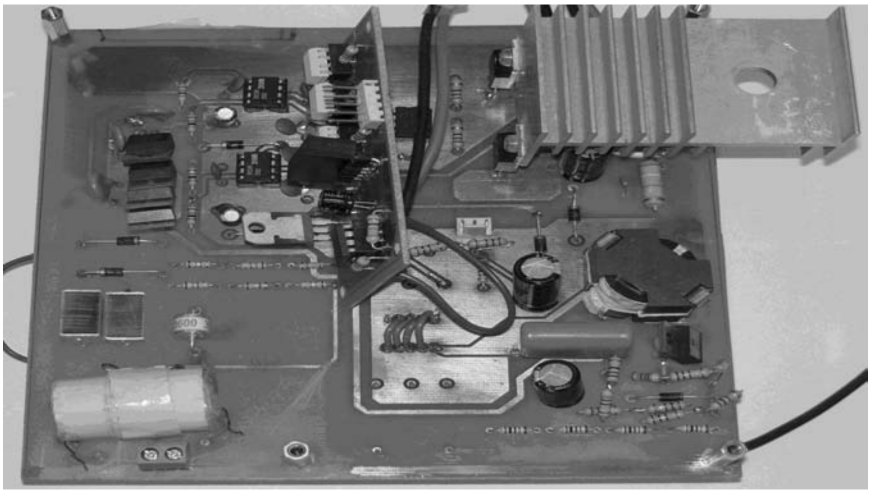

Appendix III. Prototype of two electronic ballasts based on UCC2305 and Microprocessor

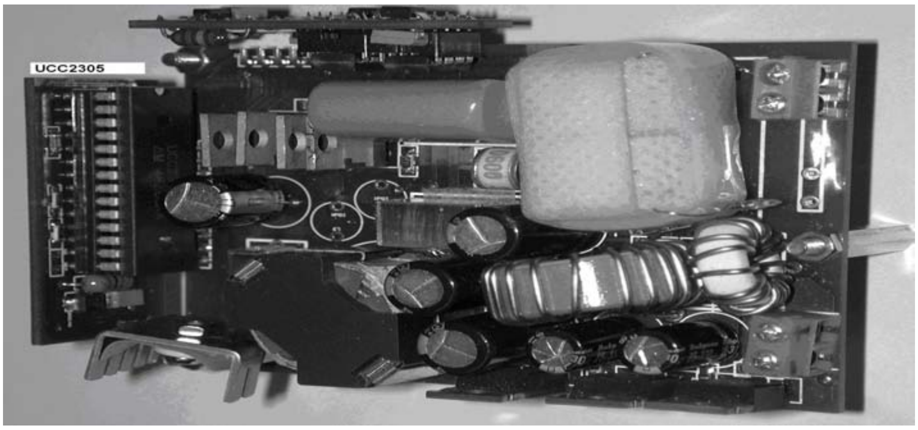

EB based on UCC2305

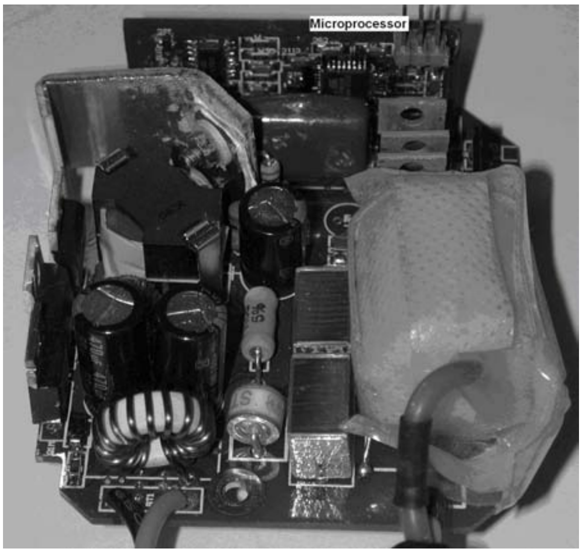

EB based on Microprocessor

Appendix IV. Prototype of the ageing Circuit